2021

Linker Histone Medicated Regulation of Mitotic Chromosome Compaction and Individualization

Pavan Choppakatla

LINKER HISTONE MEDIATED REGULATION OF MITOTIC CHROMOSOME COMPACTION AND INDIVIDUALIZATION

A Thesis Presented to the Faculty of

The Rockefeller University

in Partial Fulfilment of the Requirements for

the degree of Doctor of Philosophy

by

Pavan Choppakatla

June 2021

LINKER HISTONE MEDIATED REGULATION OF MITOTIC CHROMOSOME COMPACTION AND INDIVIDUALIZATION

Pavan Choppakatla, Ph.D.

The Rockefeller University 2021

Mitotic chromosomes are scaled to the cell size to ensure effective chromosome segregation. Recent studies have shown how condensins and DNA topoisomerase II organize the mitotic chromosome. However, the regulation of these factors in maintaining proper chromosome size in different cell types remains a mystery.

Here, I investigated the role of the linker histone variant H1.8 in regulating mitotic chromosome structure. I showed that H1.8 suppresses binding of condensins and topo II to mitotic chromatin in *Xenopus* egg extracts. Using an *in vitro* reconstitution system, I showed that H1.8 inhibits binding of purified condensins and topo II to nucleosome arrays. I also showed that condensin binding to nucleosome arrays is sensitive to magnesium dependent chromatin compaction. By using direct measurement of chromosome length, I then showed that H1.8 suppresses chromosome length solely through condensin I enrichment on chromatin.

I then investigated the organization of *Xenopus* egg extract chromosomes using chromosome conformation capture technique Hi-C. Using Hi-C analysis, I showed that condensin I organizes both mitotic loops and loop layers of mitotic chromosomes and that H1.8 mediated suppression of condensin I increases both mitotic loop and layer sizes. This analysis also corroborates direct measurements of chromosome length. I also showed that nucleosome depletion results in further reduction in loop and layer sizes over H1.8 depletion. This suggests

that chromosome length can be regulated by condensin I binding through competitive inhibition by both nucleosomes and linker histones.

Mitotic chromosomes are organized in a rod to increase both physical rigidity of chromosomes and to ensure effective resolution. Using Hi-C data, I observed that both condensins play a role in maintaining chromosome rigidity and subsequently in maintaining chromosome individualization. I then showed that, like sister chromatid resolution, condensin activity drives topo II activity to continuously resolve interchromosomal links in mitosis. Since H1.8 suppresses both condensin and topo II, it suppresses chromosome individualization. I then go on to show that this suppression of chromosome individualization is necessary to maintain spindle integrity.

Based on these data, I propose a model where mitotic chromosome length and individualization can be regulated by using linker histone stoichiometry on chromatin as a rheostat. As linker histones are a dynamic component of chromatin that have been shown to have extensive cell cycle dependent phosphorylation, I discuss the possibility that titrating linker histone stoichiometry on chromatin may be used as a mechanism to control the binding of DNA binding proteins in both interphase and mitosis and thus regulate cellular functions.

ACKNOWLEDGMENTS

I would like to first thank Dr. Hironori Funabiki for his patient mentorship throughout all my time in his lab. He allowed me the freedom to make my mistakes and the time to learn from them.

And I would also like to thank all the current members of the Funabiki lab for all the help and great discussions. Dr. Christopher Jenness and Dr. Christian Zierhut, past members of the Funabiki lab, were great mentors and friends both then and now.

This work was helped immensely by two collaborations. Bastiaan Dekker and Dr. Job Dekker helped with performing and analyzing Hi-C data on these tricky frog genomes. Dr. Erin E. Cutts and Dr. Alessandro Vannini generously provided me with purified human condensins for the biochemistry experiments and helped me think of my project in a new light.

Dr. Javier F. Martinez provided great help in purifying topo II and Dr. Michael Rout was generous in letting me use his lab's facilities for the same.

Dr. Alison North, Dr. Carlos Rico and Dr. Kate Cialowicz at Bioimaging resource center (BIRC) for maintaining the great microscopes that I spent years on.

My faculty advisory committee members, Dr. Sanford Simon, Dr. Agata Smogorzewska and Dr. Shixin Liu who agreed to serve on my committee and were very patient during my committee meetings and made themselves available for discussions outside the committee meetings graciously and I would like to thank them for that.

Dr. Rebecca Heald and Dr. Coral Zhou were great sounding boards for ideas and help with setting up collaborations.

I would like to thank Dr. Susannah Rankin, Dr. Tatsuya Hirano, Dr. Yoshiaki Azuma, Dr. Hiroshi Kimura for providing valuable reagents that helped move my project along.

Table of Contents

List of Figures

List of Tables

Chapter 1: Introduction

Defining the DNA compaction regimes

Nucleosomes and nucleosome fibers

All living cells store genetic information in long chains of deoxyribonucleic acids (DNA). DNA chains are organized in the double-helix structure where two complementary strands of nuclei acids wrap around each other. This configuration of DNA helps cells to efficiently store and copy the genetic information (Alberts et al., 2015). The end-to-end length of the genomic DNA is much longer than the cells that the genome encodes. The average diploid human cell contains 6 billion nucleic acid basepairs (International Human Genome Sequencing Consortium, 2004). Stretched out end-to-end, this DNA would be around 2 m in length. This is 20,000 times the size of the average human cell. The DNA in all eukaryotic cells is further constrained into a membrane bound section of the cell known as the nucleus, thus required even more packaging of the DNA (Belmont, 2006). The process of packing the cellular DNA in order to fit into the cell and enable it to perform its functions is known as DNA compaction.

To effectively pack the DNA into such a small cell, the DNA undergoes several steps of compaction. In all eukaryotic and at least some archaeal cells, most of the DNA is packaged into a characteristic DNA-protein complex known as the nucleosome (Luger et al., 1997). The canonical eukaryotic nucleosome is generally composed of 147 bp of DNA wrapped around an octameric protein complex comprised of two copies each of histones H2A, H2B, H3 and H4. Since the size of the nucleosome is ~ 10 nm (Luger et al., 1997), the linear compaction achieved in this step is ~ 7-fold (Swedlow and Hirano, 2003)(**Figure 1-1**). There have been several reported non-canonical nucleosome variants (Kurumizaka et al., 2020). Most of the commonly reported variants result in similar linear compaction, however, some proposed variants such as the H2A.Bbd nucleosome may result in lower linear compaction at the nucleosome level as

less DNA is wrapped around the nucleosome (Bao et al., 2004; Luger et al., 2012). Nucleosome level compaction can be controlled by changing the nucleosome spacing or the occupancy of nucleosomes themselves on a given piece of DNA.

A stretch of closely positioned nucleosomes on DNA can organize into a higher order structure known as the nucleosome fiber. These higher order nucleosome fiber structures can be organized through a mixture of direct nucleosome-nucleosome interactions and indirect interactions through other nucleosome binding proteins. Several factors including solvent conditions such as salt concentration and molecular crowding can modulate these interactions. Thus, this level of organization is highly variable within even a single cell and can achieve up to ~5-fold linear compaction over that of a single nucleosome (Swedlow and Hirano, 2003). These two levels of DNA compaction, the nucleosome and the nucleosome fiber, together result in a ~30-fold compaction of DNA and will be referred to as the local compaction regime.

Global compaction

Since the linear compaction of DNA in a cell is in the order of 10,000-fold, this implies that the nucleosome fibers need to be compacted by several orders of magnitude. Although there may be several mechanisms to achieve this compaction, a combination of recently developed experimental techniques and previous work on polymers have elucidated some of these mechanisms. One set of widely conserved processes that are beginning to be characterized recently involves the formation of DNA loops. In both prokaryotes and eukaryotes, DNA loops formed by proteins that can bind two distant sites on a single DNA molecule simultaneously, thus creating cross-linking different parts of the DNA, can severely compact the DNA (Shukron and Holcman, 2017; Yatskevich et al., 2019). Modulating the size, number and position of these loops can generate the desired level of compaction.

Figure 1-1 DNA undergoes several steps of compaction to fit into a cell

The relative compaction (left) of the stages of DNA compaction in a mitotic chromosome (right). Eukaryotic genomic DNA is compacted into nucleosomes to achieve a 6-7-fold compaction to generate a 10 nm fiber. This fiber may also fold into higher-order structures known as the 30 nm fiber that achieve up to a 30-fold compaction. Both the 10 nm and 30 nm fibers are then compacted into loops which contains from 10 kb to 1 Mb of DNA depending on the organism and cell type. These loops are then arranged to generate the ~20, 000-fold compaction achieved in a rod-like mitotic chromosome.

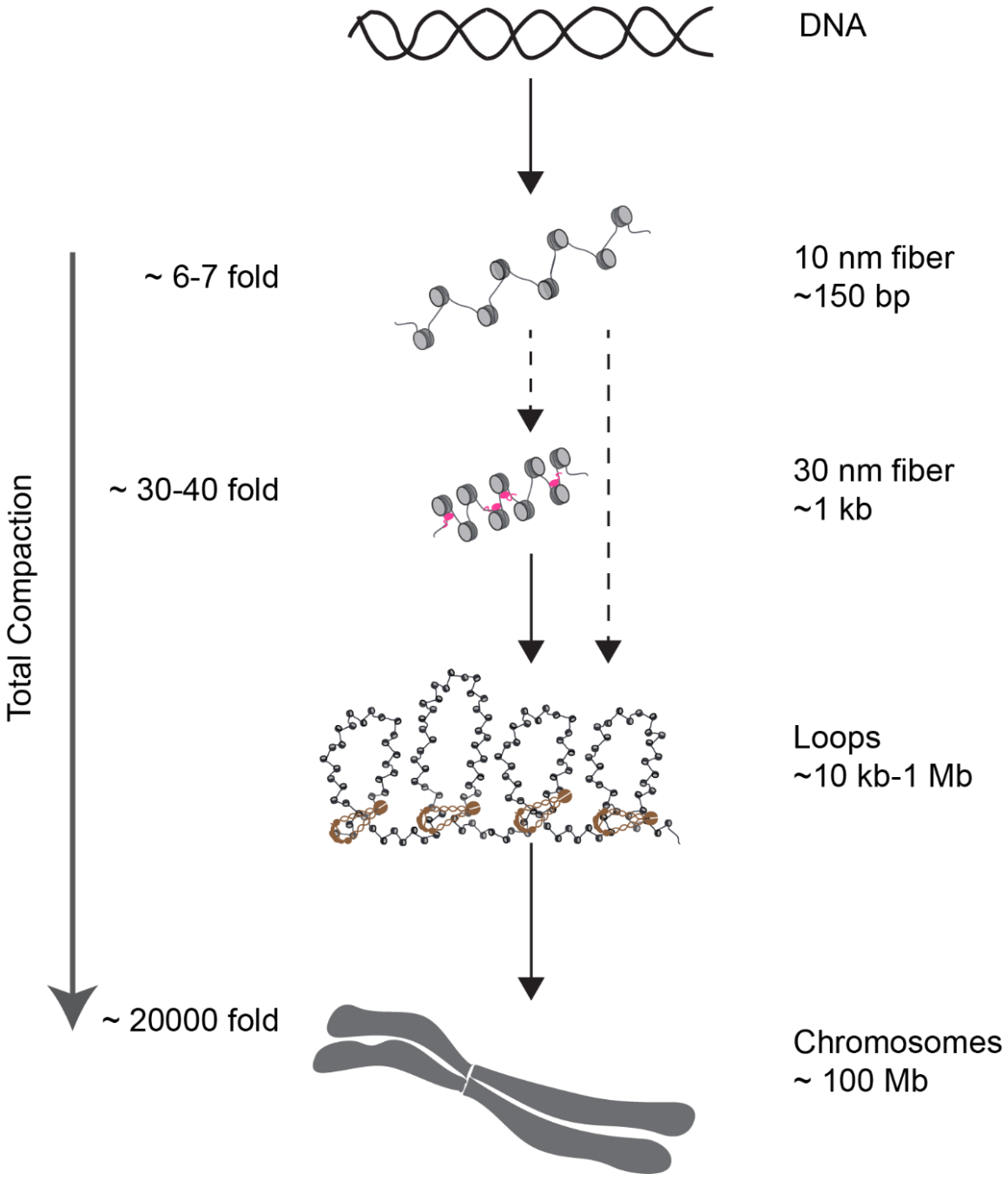
DNA
10 nm fiber
~150 bp
~ 6-7 fold
30 nm fiber
~1 kb
~ 30-40 fold
Loops
~10 kb-1 Mb
Total Compaction
~ 20000 fold
Chromosomes
~ 100 Mb

Structure and Function

DNA encodes the genetic information of cell, serving as a substrate for several processes such as transcription, replication and karyokinesis. DNA compaction needs to be able to accommodate these processes. For example, transcription and replication necessitate accessible open DNA structure, whereas DNA adopts a compact and mechanically stable form during mitosis (Gerlich et al., 2006). This implies that the DNA packaging needs to be actively regulated at various time scales from seconds to years and at various spatial length scales ranging from a few basepairs to thousands of megabases of DNA. The structure of the DNA is thus finely tuned to serve its specific purpose.

Condensation vs compaction

The most common metric used to measure changes in DNA packing is usually DNA volume. Although passively packaging the DNA, which is referred to as condensation, can effectively reduce the DNA volume, it can affect DNA accessibility for DNA-binding proteins. This suggests that condensation may not be useful as a general principle for organizing DNA in actively growing cells. However, condensation, and a related phenomenon known as phase separation, may play a role in organizing certain regions of the genome in eukaryotic cells that are more passively packaged. Even these condensed regions in cells are usually more accessible to DNA-binding proteins than passive DNA aggregates, suggesting a more dynamic set of interactions in the condensate (Strom et al., 2017). As most of the DNA in eukaryotic cells is packaged by nucleosomes (Lee et al., 2007), it is likely regulated by nucleosome or nucleosome fiber level processes.

Mitosis

The functional requirements of mitotic chromosome compaction are very different from those of interphase compaction. Mitotic chromosomes need to be packaged in order to enable

efficient segregation of the genetic material equally into the daughter cells. The conspicuous condensation of chromatin in eukaryotic cells during mitosis in animal and plant cells were some of the most striking observations from the early cytological studies of cells (Flemming, 1882; Kuwada, 1939). However, these studies also noted the distinct rod like nature of chromosomes in mitosis as opposed to the more diffuse chromosomes in interphase. Since this rod like appearance of mitotic chromosomes are common in vertebrates and many other eukaryotes, the shape of the mitotic chromosome appears to play a role in its function.

After replication is finished, the sister chromatids are intertwined topologically and also linked together by cohesin rings (Losada et al., 1998; Michaelis et al., 1997; Sundin and Varshavsky, 1981). Since each sister chromatid needs to be segregated to a different daughter cell, one role of mitotic compaction processes is to resolve these links and individualize the chromatids. The second function of mitotic compaction is to enable efficient segregation of the separated chromatids by the mitotic spindle. To ensure that one copy each of the genome goes to the dividing cells, the spindle checkpoint pathway stops mitosis until all the chromosomes are aligned at metaphase plate (Funabiki, 2019; Hoyt et al., 1991; Minshull et al., 1994). Mitotic compaction is required to ensure that the chromosomes can physically survive the forces of the mitotic spindle and satisfy the spindle checkpoint (Gerlich et al., 2006; Houlard et al., 2015; Sun et al., 2018). The rod-like structure of the mitotic chromosome plays a role in both these roles of mitotic chromosomes. Rod like chromosomes enable efficient decatenation by reducing the overlap between the chromatids and chromosomes (Brahmachari and Marko, 2019) and they are a consequence of mitotic loop extrusion which is essential for chromosome rigidity (Sun et al., 2018). Here below, I will discuss how mitotic local and global compaction processes discussed earlier play a role in satisfying the two roles of mitotic compaction.

Building a DNA packaging system in a nucleus requires processes that involve an active interplay between compaction at the nucleosome and nucleosome fiber level (local) and higher

order processes up to the nuclear level (global). Since our studies on DNA compaction have been historically done using microscopy, it is convenient to understand the compaction process from the highest level of compaction to the lowest.

Global compaction-mechanisms and regulation

Chromosome conformation assays

DNA compaction has been studied since the late 19th century using light microscopy (Boveri, 1909; Flemming, 1882) and many advancements in understanding the proteins required for the regulation of large nuclear features were made using light microscopy (Mora-Bermúdez and Ellenberg, 2007). However, conventional microscopy techniques were insufficient to interrogate the finer organization of the genomic DNA. In the last two decades, much progress has been made in understanding these features due to two classes of techniques. One of them was the development of imaging techniques combining iterative fluorescence *in situ* hybridization and single molecule localization microscopy. The recent advances in these techniques and the data obtained from them has been reviewed in Boettiger and Murphy, 2020.

The second class of techniques involves using sequencing to interrogate the proximity of loci. The most commonly used of these techniques are adaptions of the chromosomal conformation capture (3C) method (Dekker et al., 2002). The basic principle of the technique is to first preserve the nuclear structure by crosslinking using formaldehyde. The crosslinked chromatin is then digested using restriction enzymes (3C, 4C, Hi-C, 5C) or micrococcal nuclease (micro-C) to yield small DNA-protein complexes that contain two or more DNA fragments crosslinked to each other directly or indirectly through other proteins. The sticky ends of the digested DNA are filled in with biotinylated nucleotides and a ligation reaction is then performed, where two pieces of DNA loci in a DNA-protein crosslinked complex can

ligate to form a single molecule. These DNA fragments are treated with proteases, purified using the biotin handles and sequenced to identify the two ligated DNA loci (Belton et al., 2012). The likelihood of two DNA loci being ligated in a single molecule is anti-correlated to their physical proximity in the nucleus at the point of crosslinking (Finn et al., 2019).

The data produced from these genome wide conformation capture experiments (Hi-C, micro-C) has been reproduced using orthogonal techniques that do not rely on formaldehyde fixation (Beagrie et al., 2017; Redolfi et al., 2019) and imaging based methods (Bintu et al., 2018; Mateo et al., 2019). The principles of the 3C family have been adapted for other adaptations to address other questions about the nuclear architecture (McCord et al., 2020). The interaction probability data that is obtained in genome wide assays such as Hi-C is then plotted as a pairwise interaction probability matrix known as the Hi-C map (Belton et al., 2012; Lieberman-Aiden et al., 2009). Loci specific interactions, such as centromere-centromere contacts in yeast, show up as hotspots in the Hi-C map (Mizuguchi et al., 2014). To learn more about the general organization of the genome, the DNA polymer can be simulated at a variety of length scales, and the data can then be fitted to the experimental Hi-C data (Imakaev et al., 2015; Naumova et al., 2013; Sanborn et al., 2015).

SMC complexes

Structure and composition

SMC and SMC-like protein complexes have been identified in prokaryotes, eukaryotes and archaea (Nasmyth and Haering, 2005; Takemata et al., 2019). Many of the early members in bacteria and eukaryotes were identified through genetic screens for proteins involved in enabling efficient DNA segregation (Larionov et al., 1985; Niki et al., 1991). Although some of the members of this super-family do not show much sequence homology, they all have similar subunit and domain architecture (**Figure 1-2**) (Hassler et al., 2018).The core SMC

family complexes contain a ring like architecture containing an SMC dimer and one kleisin subunit. The two SMC domain proteins in bacteria is a homodimer, whereas eukaryotic SMC family proteins have two different SMC subunits. These SMC subunits contain a large-coiled coil domain flanked by the hinge dimerization domain on one side and a head domain on the other side. The head domains of the two SMC monomers dimerizes to generate two ATPase sites at the dimerization interface. The kleisin subunit binds both the head domains and generates a closed ring that can topologically entrap DNA (Cuylen-Haering et al., 2011; Farcas et al., 2011). SMC complexes also contain additional accessory subunits (HEAT repeat subunits and/or KITE domain proteins) that regulate DNA binding and other properties of the complexes (Hassler et al., 2018). These accessory subunits also play a role in regulating the activity of these complexes through post-translational modifications (Kschonsak and Haering, 2015).

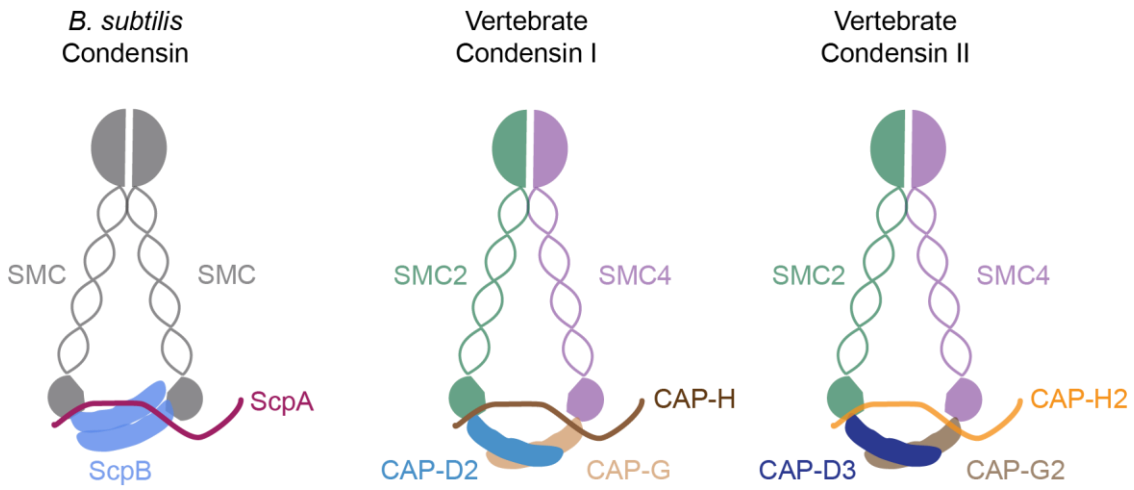

Figure 1-2 Condensins from bacteria share general architecture with vertebrate condensins

Condensins across kingdoms of life share common architecture. Bacterial condensins are composed of a homodimer of SMC subunits, kleisin ScpA and a homodimer of accessory subunits ScpB. Vertebrate condensins both consist of the SMC2-SMC4 heterodimer and different kleisin (CAP-H or CAP-H2) and HEAT repeat accessory subunits (CAP-G/CAP-D2 or CAP-G2/CAP-D3).

Most bacteria have a single member of the SMC family such as SMC-ScpAB of *B. subtilis* (Nasmyth and Haering, 2005). Eukaryotes have at least three different flavors of the SMC family, condensins, cohesins and the SMC5-SMC6 complex. Some eukaryotes also contain the closely related dosage compensation complex and the MRN complex (Jans et al., 2009; Kanaar and Wyman, 2008). All eukaryotic condensins are derived from ancestral condensin complex from the last eukaryotic common ancestor (LECA) and share the same two SMC subunits SMC2 and SMC4 (Hirano, 2016). Vertebrates express two forms of the condensin complex, which differ in the kleisin subunit and the two HEAT repeat subunits (**Figure 1-2**). Cohesin complexes among all eukaryotes are all composed of the Smc1-Smc3 heterodimer, the kleisin Scc1 (Rad21) and two unique HEAT repeat subunits Scc2 (SA2) and Pds5 (STAG1). SMC5/6 complexes are composed of the two SMC subunits SMC5 and SMC6, the kleisin Nse4 and two **k**leisin **i**nteracting **t**andem winged-helix elements (KITE) domain proteins Nse1 and Nse3. The cohesin and SMC5/6 complexes also require other accessory subunits for their functionality such as the NIPBL-Mau2 complex or the Nse5-Nse6 complex respectively (Davidson et al., 2019; Kim et al., 2019).

Localization

All three members of the SMC family are DNA binding proteins (Gutierrez-Escribano et al., 2020; Kim and Loparo, 2016; Kong et al., 2020; Losada et al., 2000; Serrano et al., 2020; Terakawa et al., 2017). However, these complexes do not show pan-genome localization in cells. *B. subtilis* condensin is loaded onto the circular chromosome at the centromeric parS site, after which it can move along the DNA to perform its function (Wang et al., 2015). Budding yeast condensin is localized primarily at the centromeres and the rDNA loci until chromosome biorientation is achieved in metaphase, when it is redistributed to the chromosome arms to resolve sister chromatid intertwines (Leonard et al., 2015; Renshaw et al., 2010; St-Pierre et al., 2009). Fission yeast and vertebrate condensin I show similar behaviour. They are both

enriched on mitotic chromosomes and accumulate near the centromere and at some transcription start sites of highly expressed genes (Hirota et al., 2004; Kim et al., 2013; Ono et al., 2004; Sutani et al., 1999, 2015). Vertebrate condensin II complex remains in the nucleus during interphase and is enriched along with TFIIIC and H3K4me$_3$ at some TAD boundaries (Yuen et al., 2017). In mitosis, Cdk1 phosphorylation leads to its activation and it is also enriched near the centromeres but stains closer to the chromosome axis by super-resolution microscopy (Abe et al., 2011; Walther et al., 2018).

Cohesin loading on chromatin is a much more complicated process, than that of condensins, that involves the interplay of several factors that change in significance depending on the cell cycle stage and cell type (reviewed in Yatskevich et al., 2019). Cohesin binding to chromatin *in vivo* requires the cohesin loader complex Scc2-Scc4 (NIPBL-Mau2) (Ciosk et al., 2000). Cohesin dissociation from DNA is promoted by the WAPL and Pds5A/B complex (Ciosk et al., 2000; Wutz et al., 2017). This dissociation is protected by Sororin on the chromosome arms in vertebrates (Lafont et al., 2010; Mitter et al., 2020) and Shugoshin at the centromeres (Hara et al., 2014). Most of the cohesin on the chromosome arms is removed upon entry into mitosis by WAPL and Plk1-mediated phosphorylation of cohesin subunit SA2 (Giménez-Abián et al., 2004; Shintomi and Hirano, 2009). Centromeric cohesin, which represents the majority of mitotic cohesin in vertebrates and fission yeast, is protected until anaphase by the Shugoshin-PP2A complex (Hara et al., 2014; Kitajima et al., 2006) and is released from the chromosomes upon entry into anaphase by proteolysis (Ciosk et al., 1998; Funabiki et al., 1996a, 1996b; Uhlmann et al., 2000). In interphase nuclei of vertebrates, apart from the centromeres, cohesin is enriched at CTCF binding sites due to CTCF acting as a loop extrusion barrier and protecting it from eviction by WAPL (Li et al., 2020; Parelho et al., 2008; Wendt et al., 2008). In budding yeast and fission yeast interphase, in the absence of an insulator

protein like CTCF, cohesins are moved to the 3' ends of convergent genes by transcription (Lengronne et al., 2004).

The SMC5/6 complexes are the least well characterized of the three classes discussed here. SMC5/6 complexes can bind single stranded DNA, DNA-RNA hybrids and Holliday junctions with high affinity (Roy et al., 2015; Serrano et al., 2020). Human SMC5/6 complex also prefers to bind and stabilize supercoiled DNA (Gutierrez-Escribano et al., 2020; Serrano et al., 2020). SMC5/6 complexes have also been reported to localize to mitotic axes during early stages of mitosis (Chu et al., 2020). SMC5/6 complexes localize to the chromosome arms during interphase at cohesin binding sites in yeast and vertebrates (Jeppsson et al., 2014) and are also evicted during prophase (Gallego-Paez et al., 2014). It is unclear if this recruitment is related to the DNA substrate preference discussed earlier. SMC5/6 complexes are also recruited to telomeres in yeast and mammalian cells (Potts and Yu, 2007; Zhao and Blobel, 2005). The mechanisms underlying this dynamic recruitment are still unclear (Aragón, 2018).

SMC family functions

Members of all three classes of the above described SMC family have been shown to possess ATP-dependent DNA compacting ability *in vitro* (Davidson et al., 2019; Ganji et al., 2018; Gutierrez-Escribano et al., 2020; Kim and Loparo, 2016; Kim et al., 2019; Kong et al., 2020; Serrano et al., 2020). Both condensins and cohesins are essential for proper segregation of genetic material. Cohesins maintain sister chromatid cohesion by encircling two different DNA molecules (Gutierrez-Escribano et al., 2019; Haering et al., 2002). This activity is separate from its role in organizing the chromosome through *cis* loops (Rao et al., 2017).

SMC5/6 complexes were first identified in a screen for increased radiation sensitivity in fission yeast (Nasim and Smith, 1975). They are also involved in maintaining cohesion and proper mitotic chromosome axis formation (Gallego-Paez et al., 2014). The role of SMC5/6

complexes in maintaining cohesion also results in their importance for efficient homologous repair (HR) in yeast, vertebrates and plant cells (Potts and Yu, 2005; Stephan et al., 2011; Watanabe et al., 2009). SMC5/6 complexes also localize to and are required for telomere maintenance in yeast and human ALT cancer cells (Potts and Yu, 2007; Zhao and Blobel, 2005). SMC5/6 complexes also play a role in stabilizing stalled replication forks and thus play a role in ensuring efficient replication (Aragón, 2018).

B. subtilis condensin zips the circular bacteria chromosome to individualize the replication origins and is essential for efficient segregation of the nucleoids to the daughter cells (Wang et al., 2015, 2017). Condensins in fission yeast and vertebrates are essential for mitotic chromosome organization (Hirano and Mitchison, 1994; Sutani et al., 1999). Budding yeast condensins organize the rDNA repeats throughout mitosis (Lavoie et al., 2004; Schalbetter et al., 2017) and in anaphase, condensin redistributed from the centromere, compacts chromosome arms to mediate resolution of sister chromatid intertwines (Leonard et al., 2015; St-Pierre et al., 2009). Eukaryotic condensins also appear to be able to induce positive supercoiling on some substrates (Baxter et al., 2011; Kimura and Hirano, 1997). Bacterial chromosomes are packaged at least partially by negative supercoiling (Wang et al., 2013). It is yet unclear if this supercoiling activity of condensins is important for its role in chromosome segregation other than in budding yeast (Baxter et al., 2011; Hirano, 2014). Current models for chromosome organization by condensins is thought to occur at least partially through their ability to form loops (discussed later).

Mechanisms of loop formation

Cis loops formed by cohesins and condensins have been shown to be the backbone of chromosome organization in interphase and mitosis respectively (Gibcus et al., 2018; Kakui et al., 2017; Rao et al., 2017). Two mechanisms to generate such loops have been described, the

diffusion capture model (Cheng et al., 2015) and the loop extrusion model (Nasmyth, 2001; Riggs, 1990). In the diffusion capture model, loops are formed by sequential binding of two DNA loci by the loop forming protein. Since the second DNA binding may be constrained by both 2D and 3D diffusion, this results in a distribution of loop sizes. This diffusive mechanism also implies that loops may be formed between non-consecutive loop anchors and also that the compaction process may be energy independent (Cheng et al., 2015). The loop extrusion model, which is more widely accepted, postulates that a loop forming protein binds a DNA chain at one site and progressively pulls (extrudes) the DNA polymer through the protein molecule. This results in a growing loop size. The size of the loops can be tuned by changing the half-life of the loop extruding molecule, extrusion rate and introducing obstacles to loop extrusion (Alipour and Marko, 2012; Goloborodko et al., 2016a; Marko et al., 2019). As the molecule is performing a motor like function by pulling DNA through the molecule, this is also an energy dependent process.

Loop extrusion has been observed *in vitro* by purified budding yeast condensin, human condensins and human cohesins (Davidson et al., 2019; Ganji et al., 2018; Kim et al., 2019; Kong et al., 2020). It was also observed in *Xenopus* egg extracts which is a more physiological system (Golfier et al., 2020). With one exception. these experiments were performed on lambda DNA substrates, which is unrepresentative of chromatin in cells. Yeast cohesin complex translocation on DNA was blocked by nucleosomes or other large barriers (Stigler et al., 2016), suggesting that nucleosomes may block loop extrusion. However, purified human condensin complexes showed the ability to extrude unhindered through sparsely deposited nucleosomes on lambda DNA (Kong et al., 2020). Yeast condensin complexes were also able to continue loop extrusion through another condensin molecule (Kim et al., 2020).

The molecular details of loop extrusion by condensins and cohesins are still unclear. Due to the long coiled-coil domains in the SMC subunits, all the SMC family complexes are large

complexes which can fit multiple DNA strands through the closed ring formed between the SMC and kleisin subunits (Datta et al., 2020). Loop extrusion by human and *Xenopus* cohesins is symmetric, i.e. it pulls DNA from both sides of the molecule, and loop extrusion by yeast and vertebrate condensins is asymmetric (Davidson et al., 2019; Ganji et al., 2018; Golfier et al., 2020; Kim et al., 2019; Kong et al., 2020). The differences in the SMC molecular machinery that results in such a disparity is not well understood. The step size of human and yeast condensins, *i.e* the DNA extruded per ATP hydrolyzed is also very large (50 nm) (Ganji et al., 2018; Kong et al., 2020). This requires an unusual motor mechanism where large scale conformational changes occur during the ATP hydrolysis cycle (Cutts and Vannini, 2020; Datta et al., 2020).

Direct observations of loop formation *in vivo* are difficult due to the technical difficulty of imaging such dynamic processes at the high resolution needed. A gradual increase in loop size was observed in *B. subtilis* by the SMC-ScpAB complex, consistent with the loop extrusion model (Wang et al., 2017). Polymer simulations of vertebrate mitotic chromosomes are also more consistent with a consecutive loop array which is suggestive of loop extrusion as well (Gibcus et al., 2018; Naumova et al., 2013). Hi-C 'stripes' emanating from sites of stable cohesin binding in a manner dependent on ATP indicate loop size increases progressively (Vian et al., 2018). This also supports the loop extrusion model for cohesin complexes in cells.

Chromosomes and chromosome territories

The size of the genome ranges from just over a hundred kilobases in symbiotic bacteria (Bennett and Moran, 2013) to thousands of megabases in plants (Pellicer et al., 2010). The cells that contain these genomes occupy a smaller physical size range. Small bacterial cells contain all their genetic information in one single DNA molecule, whereas cells containing larger

genomes split the genome into multiple chromosomes as the cell size limits the maximum chromosome size (Schubert and Oud, 1997). Nuclear material in large metazoan cells was observed by light microscopy to be organized into large distinct physically separated structures in the nucleus long before the function of DNA was understood (Boveri, 1909; reviewed in Cremer and Cremer, 2010). These physically separate structures were later shown to be composed of single chromosomes by *in situ* hybridization (Manuelidis, 1985; Schardin et al., 1985). These observations have since been comprehensively confirmed by orthogonal sequencing based techniques that do not involve denaturation of the DNA (Lieberman-Aiden et al., 2009). These physically separated regions of the nucleus occupied by a single chromosome are known as chromosome territories and have been observed in eukaryotes ranging from yeast to plant cells (Cremer and Cremer, 2010).

Although chromosome territories can be quite easily detected using both imaging-based techniques and sequencing based techniques, the factors that regulate the organization of chromosome territories are poorly understood. In *Drosophila* embryos, the SMC family complex condensin II is necessary to maintain chromosome territories (Bauer et al., 2012; Li et al., 2015; Rosin et al., 2018), however, it is unclear if condensin II plays a similar role in other organisms. This role of condensin II in suppressing *trans* interactions may also play a role in suppressing transvection (Hartl et al., 2008) and translocation (Rosin et al., 2019). Such a role may also maintain genetic diversity by reducing recombination among alleles on different chromosomes.

It is also unclear if this role of condensin II is related to its mitotic role (Ono et al., 2003, 2013). During mitosis in many eukaryotes, all chromosomes are compacted into rod-like structures which isolate chromosomes from each other (Flemming, 1882). Since chromosome movements in interphase nuclei are restricted by the size of each chromosomal DNA molecule (Marshall et al., 1997), chromosome territories in interphase could be the result of a short time

spent in interphase between mitoses (Rosa and Everaers, 2008). Such a kinetic mechanism would suggest that solely mitotic role for condensin II could still explain difference in interphase chromosome territories. If chromosome territories are a kinetic phenomenon, then one would expect terminally differentiated cells to slowly lose chromosome territories. Although a thorough analysis of this has not been reported, terminally differentiated cells appear to show weaker chromosome territories (Branco et al., 2008; Falk et al., 2019).

Chromosome compartments

The eukaryotic genome has been long divided into euchromatin and heterochromatin based on their relative staining with DNA staining dyes (Passarge, 1979). Subsequent work has gone on to show that heterochromatin regions are gene poor and transcriptionally silent, whereas euchromatin regions are gene rich and transcriptionally active (Bickmore and Van Steensel, 2013). Heterochromatin and euchromatin regions were also shown to be spatially segregated (Bickmore and Van Steensel, 2013).

Interrogation of the whole genome structure using the chromosome conformation capture technique Hi-C also showed that the genome can be divided into two different compartments A and B, where interactions between loci show higher propensity to interact with other loci in their own compartments and avoid those in the other compartment (Lieberman-Aiden et al., 2009). These A and B compartments also overlap quite well with known euchromatin and heterochromatin domains respectively, suggesting that the spatial segregation is a genome wide feature. These observations about interaction likelihood were also confirmed using high-resolution 3D-fluoresence *in situ* hybridization imaging (Bintu et al., 2018; Boettiger et al., 2016). A and B compartments can be further subdivided using higher

resolution Hi-C data, suggesting additional factors can change the interaction strength (Rao et al., 2014).

Depletion of the insulator protein CTCF has no effect on chromosome compartments (Nora et al., 2017) and depletion of the SMC family complex cohesin results in a slight increase in compartmentalization (Rao et al., 2017; Schwarzer et al., 2017). Condensin II removal also has a minimal effect on compartmentalization (Rowley et al., 2019). However, increased cohesin residence times by depleting WAPL or PDS5A/B complex results in a loss of compartmentalization (Wutz et al., 2017). Since these chromosomes form 'vermicelli' which resemble mitotic chromosomes, this is consistent with the loss of compartmentalization in mitotic chromosomes (Naumova et al., 2013; Tedeschi et al., 2013). This suggests that long chromosomal loops can prevent compartmentalization, but the usual shorter cohesin loops in interphase do not play a role in this process.

Transcriptional inhibition appears to have some effect on compartmentalization (Amat et al., 2019; Rowley et al., 2019) and chromosome hyperacetylation results in the generation of a new chromosome compartment (Rosencrance et al., 2020). Compartmentalization in archaeal chromosomes is also independent of condensin like proteins and is abolished by transcriptional inhibition (Takemata et al., 2019). These data suggest that chromosome compartmentalization may be a chromatin intrinsic feature that is determined by the interaction affinities of nucleosomes. Recent work using Hi-C performed on restriction enzyme digested interphase nuclei showed that compartmentalization is preserved on intermediate size fragments but not on smaller fragments (Belaghzal et al., 2021). The authors suggest that this supports a micro phase separation theory of chromosome compartmentalization which posits that chromosomal loci that belong to the same compartment form small dynamic phase separated domains (Hildebrand and Dekker, 2020). Although phase separation has been observed for heterochromatin domains *in vivo* (Erdel et al., 2020; Strom et al., 2017), the

mechanisms of phase separation in chromatin containing a variety of distinct epigenetic states are unclear.

As the mechanisms of compartmentalization remain a mystery, the regulation of chromosome compartments and their significance also remains to be understood. Chromosome compartments are dissolved in mitosis and complete reestablishment is only completed after several hours in G1 phase of the next cell cycle (Abramo et al., 2019). This is consistent with the role of transcription in compartmentalization. It is also unclear if factors that enhance phase separation of oligonucleosomes *in vitro*, such as linker length and linker histone H1, also drive compartmentalization *in vivo* (Gibson et al., 2019). Interestingly, histone acetylation drives phase separation *in vitro* (Gibson et al., 2019) and chromosome compartment formation *in vivo* (Rosencrance et al., 2020).

Loops and TADs

Mesoscale compaction by nucleosome fibers regulates DNA compaction in eukaryotes up to a few kilobases. Several processes in the DNA such as transcriptional regulation require persistent DNA interactions across several megabases of DNA (Furlong and Levine, 2018). Such long-range interactions are enhanced by DNA loops actively formed by members of the structural maintenance of chromosomes (SMC) family of protein complexes. SMC-ScpAB complexes area loaded at the ParS site near the replication origin in the *B. subtilis* genome and zip up the chromosome progressively in an ATP dependent manner (Wang et al., 2015, 2017, 2018).

In eukaryotic cells, low resolution Hi-C maps, showed very few stable loops (Duan et al., 2010; Lieberman-Aiden et al., 2009; Mizuguchi et al., 2014). However, higher resolution Hi-C or micro-C data confirmed the presence of loops in budding yeast and mammalian cells

(Hsieh et al., 2015, 2020; Krietenstein et al., 2020; Rao et al., 2014). Since the increase in resolution results in an increased signal-to-noise ratio, the appearance of the loops only in high resolution data suggests that these loops are not particularly stable. Interestingly, fission yeast do not show loops in interphase or mitosis even at the highest resolution (Hsieh et al., 2016; Kim et al., 2016). Almost all of the loops identified using high resolution Hi-C in human and mouse cells were cohesin and CTCF dependent (Nora et al., 2017; Rao et al., 2014, 2017). Loss of cohesin resulted in the enhancement of a few loops at loci enriched in super-enhancers. These loops were also much larger compared to cohesin mediated loops (Rao et al., 2017). However, further increasing the signal-to-noise ratio by using micro-C resulted in the detection of substantially more loops in mammalian cells (Hsieh et al., 2020; Krietenstein et al., 2020). Although a large fraction of these loops are still associated strongly with CTCF and cohesin ChIP-seq peaks, many enhancer-promoter loops were identified that were not previously observed. Although these loops are enriched at highly transcribed genes, the role of cohesin in mediated these loop still needs to be resolved (Bonev et al., 2017; Hsieh et al., 2020).

Hi-C data also showed that loci in the A and B compartments were further sub-divided into smaller units of self-interacting domains (Nora et al., 2012; Phillips-Cremins et al., 2013; Sexton et al., 2012). These loci were termed topologically associated domains (TAD) (Dekker and Heard, 2015). These domains encompass genomic loci, around 800 kb in mammalian and 60 kb in *Drosophila* cells, which interact at higher frequency with each other than loci outside the domain. The existence of such domains has also been confirmed using high resolution microscopy in many different systems (Bintu et al., 2018; Mateo et al., 2019; Szabo et al., 2018, 2020). Similar domains were later also found in fission yeast (Mizuguchi et al., 2014). Budding yeast containing much smaller domains (called self-interacting domains) encompassing only one or two genes were found later using a higher resolution conformation mapping technique

micro-C (Hsieh et al., 2015). Similar domains were also found in *C. crescentus* bacteria (Le et al., 2013).

Early studies on mammalian TADs showed that TAD boundaries were associated with binding sites of the insulator CTCF and cohesin and cohesin was required to form these domains (Dixon et al., 2012; Phillips-Cremins et al., 2013; Sofueva et al., 2013). *Drosophila* TADs were also flanked by a variety of insulators including CTCF and su(Hw) (Sexton et al., 2012). Consistent with the role of cohesin in TAD formation, TADs are dissolved in mitosis and are reformed in telophase (Abramo et al., 2019; Naumova et al., 2013). In support of the polymer modeling showing the requirement of continuous loop extrusion, dynamic cohesin binding due to WAPL and PDS5A/5B was also necessary to maintain TAD structure (Rao et al., 2017; Schwarzer et al., 2017). Interestingly, although CTCF is required for TAD formation, CTCF mediated stabilization of cohesin appears to be dispensable for TADs (Li et al., 2020). TADs appear to be weak or absent in oocyte and early embryonic mouse chromosomes and are established after genome activation (Du et al., 2017; Ke et al., 2017). *Drosophila* embryos show similar TAD establishment kinetics and in these embryos, replication but not transcription was required for TAD formation (Hug et al., 2017). TAD like structures in yeast and bacteria appear to require transcription for their formation, suggesting a possible role of supercoiling in generating interaction domains in these organisms (Benedetti et al., 2014; Hsieh et al., 2015; Le et al., 2013).

Early models of metazoan TADs envisioned a globular unstructured region of the genome that was isolated from the rest of the genome by a stable cohesin loop (Dixon et al., 2012; Mizuguchi et al., 2014). Since no stable loop was observed at the boundaries of many TADs (Dixon et al., 2012; Rao et al., 2014), such a structure does not appear to be commonly found. Further, polymer modelling shows that a single cohesin loop does not lead to the isolation of a genomic region from neighboring loci (Fudenberg et al., 2016). Such modelling

also shows that TAD formation requires continuous loop extrusion on a region bounded by insulator binding sites (Sanborn et al., 2015). This model of TAD organization is also supported by the large variation in genomic structure among single cells by high throughput imaging and single cell Hi-C (Finn et al., 2019; Nagano et al., 2013; Stevens et al., 2017).

Since TADs by definition are characterized by preferential interactions, they were proposed as a mechanism to control gene expression through regulating enhancer promoter loops (Dekker and Heard, 2015). The changes in TAD structure during development provided more evidence of a possible role for TADs in gene regulation (Bonev et al., 2017; Du et al., 2017; Ke et al., 2017). However, this TAD establishment was independent of transcription (Du et al., 2017; Hug et al., 2017). Moreover, complete loss of TADs by cohesin dysregulation or CTCF depletion did not show any large gene expression changes (Nora et al., 2017; Rao et al., 2017; Vian et al., 2018). However, TADs do appear to play a role in some developmental reprogramming steps and the functional roles of TADs in gene regulation is yet to be determined (reviewed in Cavalheiro et al., 2021). TADs were also identified as a means to control replication timing in cells (Pope et al., 2014).

Local compaction-mechanisms and regulation

Determinants of local compaction

The basic unit of chromatin fiber is the nucleosome core particle (Luger et al., 1997). The canonical nucleosome consists of 2 copies each of the core histones H2A, H2B, H3 and H4 wrapped around 147 bp of DNA. Nucleosomal DNA ‘breathes’ spontaneously (Li et al., 2005) and this dynamics can be regulated. Both DNA and protein components of the nucleosome particle affect nucleosome flexibility. As DNA sequences are strong determinants of nucleosome stability (Lowary and Widom, 1998), nucleosome positioning appears to exert

some evolutionary pressure on DNA sequences (Basu et al., 2021; Jiang and Pugh, 2009). Cells express a number of histone variants that serve unique roles (Kurumizaka et al., 2020). Some histone variants, such as the centromeric H3 variant CENP-A form more flexible nucleosomes (Roulland et al., 2016). Others such as the H2A.Bbd variant form nucleosome particles that wrap only 118 bp of DNA (Bao et al., 2004). Although these nucleosome variants do not occupy a large fraction of the genomic DNA, they are enriched in some regions or in response to stresses and their unique properties enable them to regulate local compaction to serve their role (Luger et al., 2012).

A linear array of nucleosomes can be packed in order to generate a higher order structure. The most commonly observed such structure *in vitro* is the '30 nm fiber' which is so named since the diameter of the fiber is around 30 nm (Tremethick, 2007). The '30 nm fiber' structure *in vitro* involves interactions between the N-terminal tail of H4 of one nucleosome and the acidic patch of H2A belonging to the N+2 nucleosome (i.e two nucleosomes away) (Dorigo et al., 2004; Zhou et al., 2007). These simple interactions determine the compaction of the chromatin fiber in many different contexts. Point mutants in the acidic patch, such as those in H2A.Bbd or H2A.Z, can both antagonize or stabilize interactions with the H4 tail, and thus can control fiber compaction (Matsubara et al., 2007; Zhou et al., 2007). Reciprocally, acetylation of the H4 tail also leads to a large reduction in acidic patch interactions and decreased compaction (Allahverdi et al., 2011; Shogren-Knaak et al., 2006).

Several other factors can also regulate the formation of the '30 nm fiber' or similar compaction *in vitro.* Salt concentration and linker histones were some of the earliest and most well studied factors that affect the 'tetranucleosome' structure that underpins the 30 nm fiber (Li et al., 2016; Thoma et al., 1979a). Both high salt and the linker histone constrain the DNA entry and exit angles of the nucleosome. This suggests that other 'crosslinkers' that can stabilize inter-nucleosome interactions may also be able to stabilize the '30 nm fiber' structure.

HP1 and PRC2, two factors associated with heterochromatin have been shown to stabilize inter-nucleosome interactions (Machida et al., 2018; Poepsel et al., 2018).

Two basic models for the ’30 nm’ fiber were postulated, the one-start solenoid model and the two-start zig-zag model (Tremethick, 2007). Molecular simulations of these models have been able to predict the effect of varying the linker length between nucleosomes, adding or removing linker histone and varying the salt concentration (Collepardo-Guevara and Schlick, 2014; Perišić et al., 2010). Comparing these models to the inter-nucleosome interactions observed *in vitro* on nucleosome arrays shows that the fiber adopts a ‘polymorphic’ two-start structure, which is a modification of the two-start zig-zag model with some linker DNA characteristics of the one-start model.

Local compaction in cells

The ’30 nm fiber’ was proposed to be the building block of the mitotic chromosome structure as a part of the hierarchical compaction model (Finch and Klug, 1976). The 30 nm structure was observed in some nuclear preparations, such as those that involved permeabilizing the cells (Bednar et al., 1998; Belmont and Bruce, 1994; Kireeva et al., 2004; Rydberg et al., 1998). However, more careful analyses have questioned the existence of such a structure (Eltsov et al., 2008; Nishino et al., 2012). Orthogonal imaging approaches performed in recent years observe small stretches of folded fiber resembling tetranucleosome structures, though these stretches do not repeat uniformly (Cai et al., 2018b, 2018a; Ou et al., 2017). The use of modern sequencing based approaches has now enabled the interrogation of chromatin structure at unique genomic loci (Hsieh et al., 2015, 2020; Krietenstein et al., 2020; Risca et al., 2016). These analyses report the interaction profile between nucleosomes. By comparing the interaction data to molecular models, it is possible to ascertain the probably local chromatin

structure. These studies, confirming observations from the electron microscopy and Cryo-EM studies, show that there are small stretches of tetranucleosome like motifs in the chromatin.

Condensation and phase separation

Although no ordered ’30 nm fiber’ like structures are abundant in intact cells, there are however many compact regions of the genome. These regions show a large number of inter-nucleosome interactions but lack an ordered structure (Krietenstein et al., 2020; Risca et al., 2016). Reconciling these two observations, recent studies have shown that, instead of a static compact structure, heterohromatic regions form liquid like ‘condensates’ that are highly dynamic (Larson et al., 2017; Strom et al., 2017). In these condensates, the inter-nucleosome interactions appear to be driven by HP1 mediated bridging of nucleosomes (Machida et al., 2018; Sanulli et al., 2019). These liquid-like condensates can achieve a high concentration of nucleosomes, maintain a dynamic structure and regulate access to permitted factors (Mir et al., 2019). Nucleosome arrays appear to be able to phase separate *in vitro* quite readily and several factors that affect compaction such as linker length, linker histones and H4-acidic patch interactions affect this phase separation (Gibson et al., 2019). Although several other chromatin components cluster (Boehning et al., 2018; Hansen et al., 2019), it is unclear if other chromatin condensates are ubiquitous (Mir et al., 2019).

Linker histones

Basic structure and binding

Linker histones are highly abundant DNA binding proteins so named because they bind to the 'linker' DNA between the nucleosomes (Simpson, 1978; Zhou et al., 2015). Linker histones have a tripartite structure where a globular domain is flanked by a short N-terminal tail and a long highly charged C-tail (**Figure 1-3A**)(Allan et al., 1980). The globular domain, which contains a winged helix DNA binding domain, and the charged C-terminal tail are both essential for linker histone binding in cells, although the globular domain is sufficient for nucleosome binding *in vitro* (Allan et al., 1980; Hendzel et al., 2004; Misteli et al., 2000; Ramakrishnan et al., 1993). The C-terminal tail of the linker histone is unstructured in solution and is partially ordered upon binding to the nucleosome (Fang et al., 2012). Nucleosome bound linker histones have been observed in two different binding modes: *on dyad* and *off dyad* (Bednar et al., 2017; Song et al., 2014; Zhou et al., 2015, 2016, 2021). Intact nucleosomes isolated from *Xenopus* egg extracts show an *on dyad* binding mode (**Figure 1-3B**) (Arimura et al., 2020).

Linker histone variants

Linker histones, unlike core histones, have undergone more rapid evolution. Thus, humans and mice express 11 linker histone variants (Izzo et al., 2008). These linker histone variants can be broadly split into two types, *replication-dependent* and *replication-independent* depending on whether they are expressed during replication or throughout the cell cycle respectively. In humans and mice, linker histone variants H1.1 to H1.5 and the testes specific H1t are *replication-dependent* whereas H1.0 (H1F0), H1Foo (H1.8), H1x and H1t2 are *replication-independent*. The globular domain of all the linker histone variants is derived from the H5

linker histone domain and thus share homology. The N and C-terminal tails are highly divergent between the paralogs. The orthologs of each linker histone also share more homology than the paralogs in the same species. Only five variants have been found in *X. laevis*; Budding , fission yeasts and *Drosophila* express only one variant (Izzo et al., 2008).

All linker histone variants are not ubiquitously expressed in an organism. Some of the variants such as H1Foo (also known as H1.8, H1M) are expressed only in oocytes and early embryonic cells. H1t and H1t2 are similarly only expressed in the male germline. H1.1 to H1.5 are more ubiquitously expressed although they do show some differences in their expression patterns as well (Izzo et al., 2017). Oocyte linker histone variants are essential for oocyte maturation (Furuya et al., 2007; Yun et al., 2014). The oocyte linker histones are replaced by the replication-dependent variants early on in embryonic development to enable more control over gene expression (Hayakawa et al., 2012; Izzo et al., 2017; Saeki et al., 2005). These are then largely replaced by H1.0 (H1F0) which is expressed in terminally differentiated cells and is required to silence the pluripotent genes in these cells and prevent de-differentiation (Terme et al., 2011). Linker histone stoichiometry (i.e the number of linker histones per nucleosome) regulates the nucleosome repeat length in a given cell and both these vary quite widely among cell types (Woodcock et al., 2006).

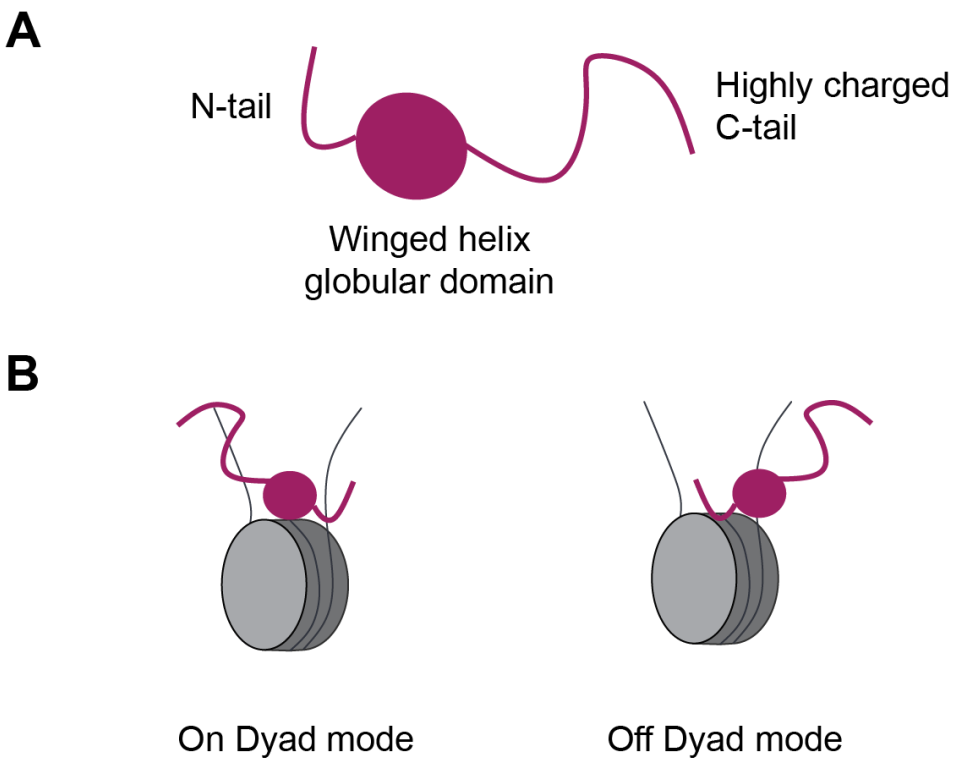

Figure 1-3 Linker histone structure and binding mode

A) Domain structure of linker histones. Linker histones have a globular domain containing a winged-helix DNA binding domain flanked by a short unstructured N-terminal tail and a long highly charged C-terminal tail that is essential for DNA binding *in vivo*.

B) The two reported binding modes of linker histone to nucleosomes *in vitro.*

Linker histone functions

Linker histones compact oligonucleosomes *in vitro* through restricting the positioning of DNA at the entry and exit sites of the DNA (Bednar et al., 1995, 2017; White et al., 2016). This leads to a stabilization of tetranucleosome units and 30 nm fiber like structures (Bednar et al., 1998; Finch and Klug, 1976; Li et al., 2016; Song et al., 2014; Thoma et al., 1979). Linker histones inhibit histone acetylation and repress transcription on chromatin templates *in vitro* (Herrera et al., 2002; Shimada et al., 2019; Zhang et al., 2015) and are enriched at heterochromatin loci in cells (Izzo et al., 2013; Th'ng et al., 2005). Depleting the single linker histone in *Drosophila* leads to loss of silencing at heterochromatic repeats (Iwasaki et al., 2016; Lu et al., 2009, 2013). Putting these data together, it is tempting to conclude that linker histone mediated compaction of chromatin represses gene expression and supports heterochromatin formation *in vivo*. However, linker histones appear to silence repetitive elements by direct recruitment of other silencing factors such as histone methyltransferases and HP1 (Healton et al., 2020; Lu et al., 2013).

Linker histones have also been implicated in many other roles, although it is unclear how many of these roles are directly or indirectly linked to their gene regulation impacts. Linker histones affect replicating timing (Andreyeva et al., 2017; Thiriet and Hayes, 2009). H1.2/H1.4 eviction at sister chromatid interfaces by mitotic phosphorylation has been shown to be necessary for proper resolution of sister chromatids (Krishnan et al., 2017). Citrullination of H1 leading to its eviction is essential for mouse development (Christophorou et al., 2014) and H1.2 serves as an apoptotic signal (Konishi et al., 2003). Depletion of linker histone in budding yeast leads to defective homologous recombination (Downs et al., 2003). Since linker histones are one of the most abundant chromatin components, they have been adapted for use in regulating many pathways, and several of these processes involve essential posttranslational modifications (Fyodorov et al., 2018; Izzo and Schneider, 2016).

Mitotic chromosomes-Local and global compaction

Global compaction in mitosis

As discussed earlier, the phases of global mitotic compaction were chromosome territories, chromosome compartments, TADs and loops. Chromosome compartments and TADs in vertebrate cells are dissolved in mitosis (Du et al., 2017; Gibcus et al., 2018; Naumova et al., 2013). Since TADs are established by cohesin and cohesin is largely removed from chromosome arms by the prophase pathway in these cells, this is as expected (Giménez-Abián et al., 2004; Shintomi and Hirano, 2009). Since the mechanisms of establishment of chromosome compartments are not clear, it is not obvious that they should be regulated in mitosis. However, since chromosome compartments are coupled to transcription, the shutdown of transcription in mitosis may be responsible for the loss of compartmentalization (Amat et al., 2019; Rowley et al., 2019; Takemata et al., 2019). Moreover, the loss of compartments due to formation of longer cohesin loops upon WAPL and PDS5A/B depletion also suggests that the long condensin loops in mitosis may also serve a similar purpose (Wutz et al., 2017).

Chromosome territories in mitosis are highly defined as the chromosomes can be separated from each other visually in many cases. This follows from the need for each chromosome to independently align at the metaphase plate and satisfy the spindle checkpoint. Theoretical analysis of interchromosomal interactions at different loop sizes also suggests that the loop sizes of mitotic chromosomes were optimized to minimize overlap of loops and thus spurious interchromosomal links (Brahmachari and Marko, 2019). However, unresolved inter-chromosomal links in mitosis have been noted in some cases (Potapova et al., 2019; Sun et al., 2018). The prevalence and significance of these links remains unclear.

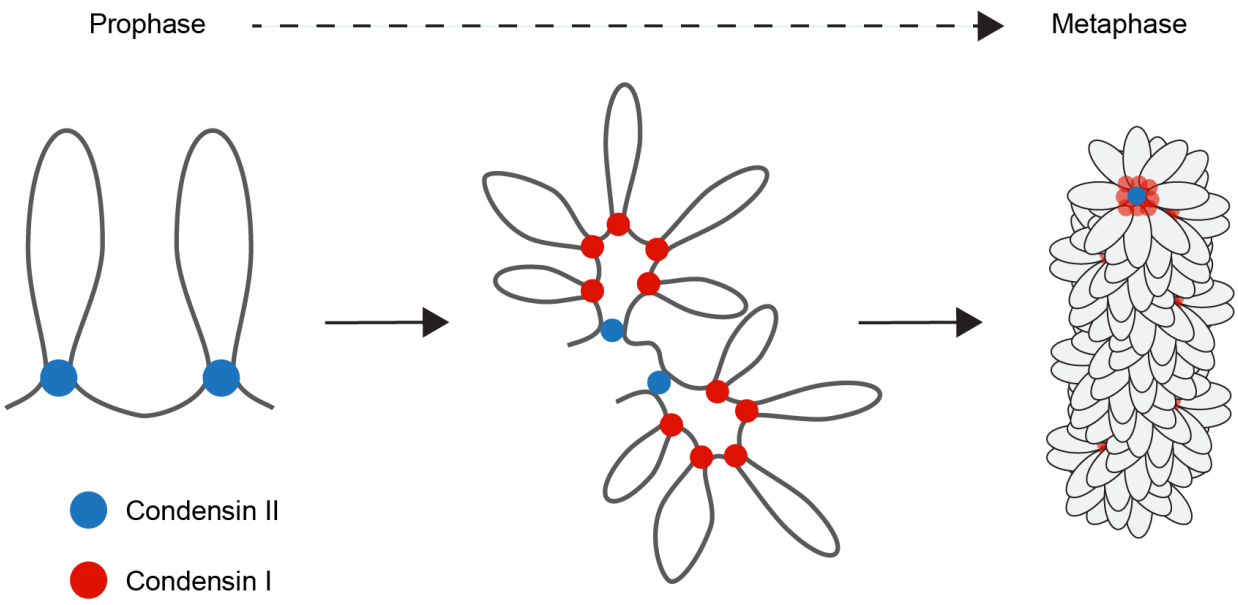

Figure 1-4 Condensin loop array maturation in vertebrates

Large condensin II loops formed in prophase are split by condensin I in late prophase and mature to form the loop arrays of a mitotic chromatid. The cartoon is based on the data from Gibcus et al., (2018).

Budding yeast

Budding yeast mitotic compaction is unlike those in metazoans and fission yeast. Mitotic chromosomes do not have the characteristic rod-like structure apparent in many other species (Guacci et al., 1994). Mitotic compaction in budding yeast requires both cohesin and condensin. Unlike metazoans and fission yeast however, cohesin loops established in S phase organize the chromosomes until anaphase begins, whereas condensin only plays a role in the compaction of rDNA arrays (Costantino et al., 2020; Guacci et al., 1997; Lavoie et al., 2000; Schalbetter et al., 2017). In anaphase condensin that is accumulated at the centromere is phosphorylated by Cdc5 (Polo kinase) and redistributed to the chromosome arms, where it compacts the chromosome arms and resolves sister chromatid intertwines (Baxter et al., 2011; Leonard et al., 2015; St-Pierre et al., 2009). Cohesin degradation in anaphase is also essential for the resolution process (Farcas et al., 2011).

Loop arrays in vertebrate cells and fission yeast

Proteomic studies on the purified 'chromosome scaffold' identified condensins and DNA topoisomerase II as the major and essential components to organize mitotic chromosomes (Adolphs et al., 1977; Hirano and Mitchison, 1994; Uemura et al., 1987). Condensins were then proposed to organize the loops identified by electron microscopy (Nasmyth, 2001; Paulson and Laemmli, 1977). Supporting this proposal, more recent observations, using Hi-C data from HeLa cells and chicken DT40 cells, show that the mitotic chromosome is composed of two sets of nested loops formed by condensin I and condensin II (Gibcus et al., 2018; Naumova et al., 2013) (**Figure 1-4**). Condensin II binds earlier to the chromosomes and thus forms the stable inner loops, which are then split into smaller condensin I mediated loops. This nested structure leads to a layered organization where condensin II organizes layers of condensin I loops (Gibcus et al., 2018). Condensin II loops also appear to adopt a helical staircase like structure,

consistent with previous observations on condensin II depleted chromosomes (Green et al., 2012; Hirota et al., 2004; Ono et al., 2003). The estimated size of condensin I mediated loops in HeLa and DT40 cells is ~100kb which is remarkably close to the observations made by electron microscopy on histone depleted chromosomes (Paulson and Laemmli, 1977). The localization of condensins by super-resolution microscopy in HeLa cells also supports this model (Walther et al., 2018). Fission yeast express a single condensin, which is loaded onto the mitotic chromosomes by Cdk1 phosphorylation (Aono et al., 2002; Sutani et al., 1999). However, the Hi-C maps show similar layered organization of the mitotic chromosome, although the loops are much smaller, presumably to account for the smaller chromosomes (Kakui et al., 2017).

Mechanical properties of mitotic chromosomes

The mechanistic basis for the second core function of mitotic compaction, mechanical rigidity, is still not clear. Restriction enzyme digestion experiments on purified mitotic chromosomes show that the mechanical properties of the chromosome are dependent on a continuous DNA polymer and that no independent protein scaffold seems to exist (Marko, 2008; Poirier and Marko, 2002). Immunofluorescence studies on stretched chromosomes and super-resolution imaging of native chromosomes also confirms that the chromosome 'axis' is discontinuous (Sun et al., 2018; Walther et al., 2018). However, condensin I and condensin II are essential to maintain lateral and axial rigidities respectively (Gerlich et al., 2006; Sun et al., 2018). This is consistent with the reported roles for condensin I and condensin II in regulating lateral and axial compaction respectively (Elbatsh et al., 2019; Green et al., 2012; Hirota et al., 2004; Ono et al., 2004; Samejima et al., 2012). Condensin I binding is also very dynamic (Gerlich et al., 2006). It is unclear if an array of loops without any stable interactions between the loop anchors can drive mechanical rigidity and the emergence of mechanical properties from loop arrays still requires further investigation.

Sister chromatid resolution in vertebrates

After replication, the sister chromatids are linked together by both cohesins and by topological catenations (Losada et al., 2002; Sundin and Varshavsky, 1981). As cohesin is dispensable for mitotic compaction, it is actively removed from mitotic chromatin by WAPL and Plk1-mediated phosphorylation to enable quick decoupling of sister chromatids at the beginning of anaphase (Giménez-Abián et al., 2004; Shintomi and Hirano, 2009). Depletion of WAPL leads to severe resolution defects as the stable cohesins prevent condensin mediated resolution (Tedeschi et al., 2013). It is not clear if the interactions between stable cohesin loops and mitotic condensin loops similar to those in telophase play a role in generating this phenotype (Abramo et al., 2019). Sister chromatids are linked by centromeric cohesin ,which is protected by Shugoshin, and the small amount of 'cohesive cohesin' on chromosome arms is protected by Sororin (Hara et al., 2014; McGuinness et al., 2005; Mitter et al., 2020). The significance of this small amount of arm cohesin is still unclear though it may play a role in preventing cohesion fatigue (Daum et al., 2011). Separase mediated cohesin removal in anaphase is essential for chromosome segregation (Hara et al., 2014; McGuinness et al., 2005; Waizenegger et al., 2000).

The resolution of topological links between sister chromatids is performed by topo II in prophase. This process requires Cdk1 activated condensin II (Abe et al., 2011; Bakhrebah et al., 2015; Nagasaka et al., 2016). However, condensin I activity is also required to maintain resolved sister chromatids (Houlard et al., 2015; Piskadlo et al., 2017a). The role of condensins in resolving sister chromatids can be explained by its loop extrusion activity (Goloborodko et al., 2016b; Orlandini et al., 2019). However, condensins can also drive decatenation through supercoiling, so it is not clear which condensin activity is involved in this process (Baxter et al., 2011; Bazett-Jones et al., 2002).

Chromosome shape regulation

Loop extrusion simulations can recapitulate condensin mediated chromatid formation (Alipour and Marko, 2012; Banigan et al., 2020; Goloborodko et al., 2016b). These simulations can also then predict the factors that would regulate the chromosome shape (**Figure 1-5A**). From these simulations, we can simplify condensin regulation to these independent parameters: i) Condensin ON rate- The rate at which cytoplasmic condensin loads onto the DNA. ii) Loop extrusion rate- The amount of DNA extruded per unit time, iii) Condensin OFF rate- The half-life of a condensin molecule on chromatin.

Condensin is a non-specific DNA binding protein but its cellular role appears to involve topological entrapment of the DNA molecule in the SMC-kleisin ring (Cuylen-Haering et al., 2011). This process, which stabilizes the condensin-DNA complex, requires ATP and the SMC-kleisin ring and one of the HEAT repeat subunits (Eeftens et al., 2017; Kschonsak et al., 2017). However, the first step in this process involves non-specific charge based condensin binding to DNA. Although the complex substrate preferences for eukaryotic condensins are not clear, condensins prefer to bind non-nucleosomal DNA (Kong et al., 2020; Shintomi et al., 2017; Zierhut et al., 2014). This indicates that the amount of non-nucleosomal DNA in a cell strongly determines condensin loading. As linker DNA is also a preferred substrate (Kong et al., 2020), the nucleosome repeat length and the linker histone stoichiometry, both of which are correlated (Woodcock et al., 2006), strongly determine condensin loading. Since nucleosomal core particles occupy a large majority of the genomic DNA (Lee et al., 2007), small changes in the remaining DNA will affect condensin loading. In support of this idea, active nucleosome eviction in mitosis by Gcn5 histone acetyltransferase and the RSC complex has been shown to enable proper condensin loading (Toselli-Mollereau et al., 2016a). The topological entrapment of DNA by condensin also requires dynamic structural transformations

in condensin, some of which are regulated by phosphorylation in mitosis (Kschonsak et al., 2017).

Other similar regulation may also be required to enable effective condensin loading onto mitosis. Cofactors, such as Scc2-Scc4 complex for cohesin (Ciosk et al., 2000), can also strongly influence ON rates for molecules. No such obligate cofactors have been identified for condensins but PP2A and Rb have been shown to be required for recruitment of condensin II to mitotic chromatin in some systems (Longworth et al., 2008; Takemoto et al., 2009). No such factors have been identified for condensin I, although depletion of KIF4A leads to defects in condensin I loading on chromatin in some cases (Samejima et al., 2012; Takahashi et al., 2016; Takata et al., 2018). Condensin binding to chromatin in mitosis is also strongly enhanced by phosphorylation, although it is unclear if this is due to changes in ON or OFF rates (Kschonsak and Haering, 2015; Thadani et al., 2018). Given constant loop extrusion rate and OFF rates, the net effect of a higher ON rate is increased condensin loading and subsequently to reduce loop size, increase chromosome length and enable faster resolution (**Figure 1-5B**).

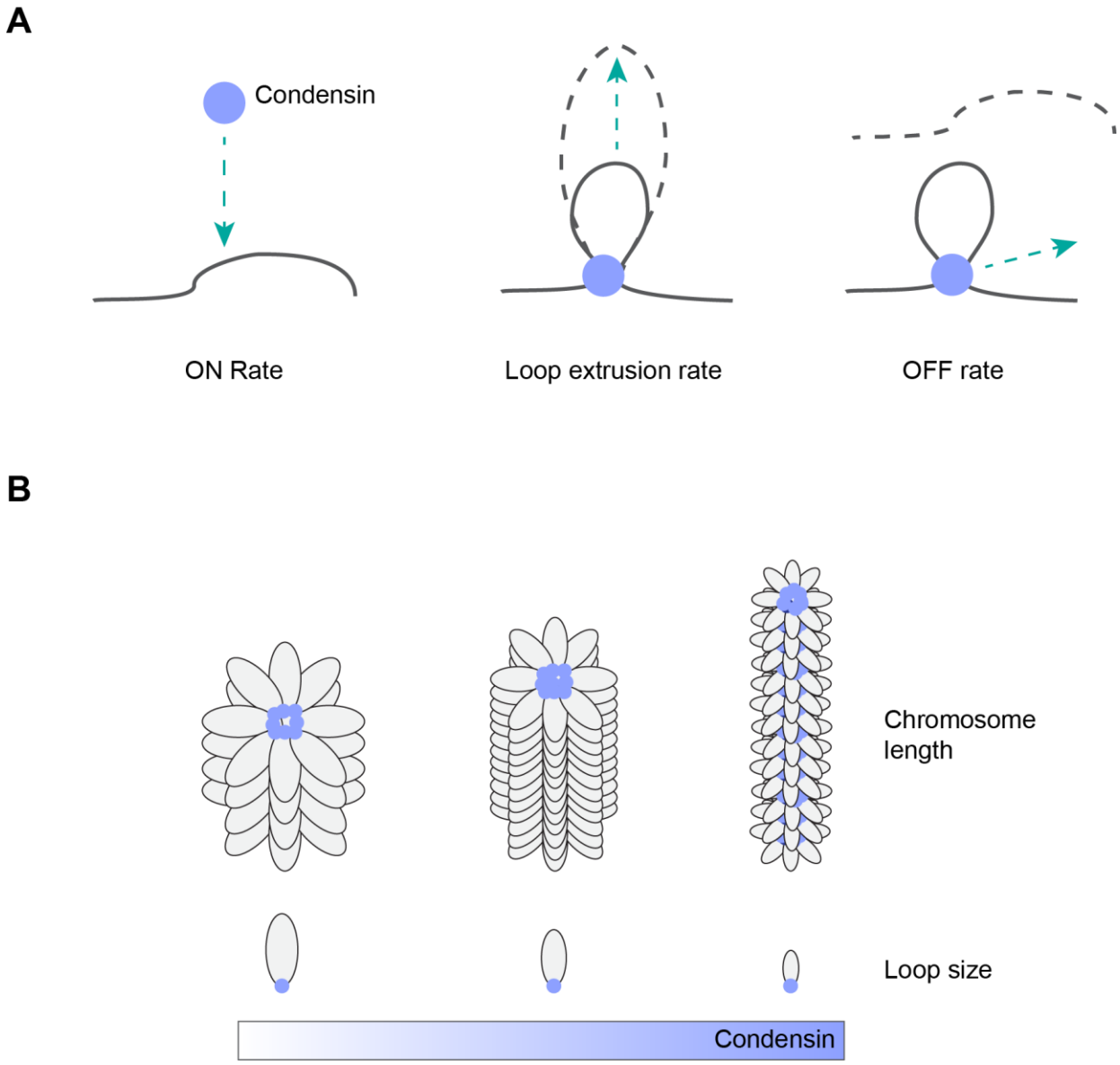

Figure 1-5 Condensin factors that influence chromosome compaction

A) The three independent parameters that influence condensin mediated chromosome length and resolution

B) Model figure showing the change in chromosome structure based on a change in loop sizes due to increased condensin loading.

Although loop extrusion has been demonstrated recently by condensins from different organisms, much of the biochemistry of the process remains a mystery (Cutts and Vannini, 2020; Datta et al., 2020; Ganji et al., 2018; Golfier et al., 2020; Kong et al., 2020). Loop extrusion rates were shown to be effected by salt, ATP concentration and by tension in the DNA strand (Ganji et al., 2018; Kim et al., 2020). However, since these experiments were conducted on either DNA or substrates with 1-2 nucleosomes, loop extrusion rates on cellular chromatin substrates, whose compaction is also salt sensitive, need investigation. Further, if loop extrusion through nucleosomes requires local hopping (Marko et al., 2019), this may suggest that availability of accessible DNA substrates (discussed in previous paragraph) may also affect extrusion rates.

The half-life of DNA binding proteins is generally a protein intrinsic factor. However, active removal by other proteins can influence the half-life. WAPL and PDS5A-5B complexes strongly reduce the half-life of cohesin complexes on DNA, ensuring interphase cohesin loops remain small (Gandhi et al., 2006; Tedeschi et al., 2013; Wutz et al., 2017). No such factors have been identified for condensins, although human microencephaly protein MCPH1 appears to perform a complex regulation of condensin II that may involve active eviction (Yamashita et al., 2011). The phosphorylation of condensins in mitosis may also influence the OFF rates, but no direct measurements of these have been reported (Kschonsak and Haering, 2015).

Non condensin factors

Although recent studies have clarified the role of condensins on mitotic chromosomes, the roles of other structural factors such as KIF4A, topo II and Ki-67 are unclear. Mitotic topoisomerase activity is performed by the topo II isoform TOP2A and cannot be substituted by TOP2B (Christensen et al., 2002; Farr et al., 2014; Nielsen et al., 2020). TOP2A activity is essential for mitotic compaction and also for maintaining the compacted metaphase structure (Adachi et

al., 1991; Nielsen et al., 2020; Piskadlo et al., 2017a). TOP2A depletion also results in longer chromosomes, although it is unclear if this is due to incomplete decatenation or a structural role for TOP2A (Nielsen et al., 2020; Samejima et al., 2012). Interestingly, mitotic chromosomes also appear to contain a salt stable population of TOP2A (Cuvier and Hirano, 2003; Laemmli et al., 1978). However, simulation studies show that chromosome compaction by condensins can proceed with only an enzymatic role for topo II, thus the significance of any non-enzymatic role for TOP2A is unclear (Goloborodko et al., 2016b).

TOP2A activity is enhanced in mitosis (Hirano and Mitchison, 1991), although it is unclear which kinase is responsible for this mitotic activation. Topo II activity is also directed by condensins (Charbin et al., 2014; Cuvier and Hirano, 2003; Dyson et al., 2020; Piskadlo et al., 2017a), but condensins can also increase the catalytic activity of TOP2A in some cases (Baxter et al., 2011; Orlandini et al., 2019). TOP2A activity can also be regulated by its recruitment to chromatin, however the substrate preferences of TOP2A have still not been elucidated. The existence of a small 'chromatin tether' domain at the C-terminus of TOP2A that recruits TOP2A to methylated histones on chromatin raises an interesting possibility, but the significance of this weak binding is still unclear (Lane et al., 2013).

Local compaction in mitosis

Two models of the mitotic chromosome structure were postulated to explain mitotic compaction, the hierarchical model and the loop array model (Swedlow and Hirano, 2003). The hierarchical model postulated that the mitotic chromosome was organized as a coiled superhelix of the 30 nm fiber (Finch and Klug, 1976). The loop array model posited that the mitotic chromosome is organized as a series of loops organized around a central protein scaffold (Paulson and Laemmli, 1977). Since condensins are essential for mitotic chromatid

formation in many species (Hirano and Mitchison, 1994; Hirota et al., 2004; Ono et al., 2004) and nucleosomes are dispensable (Shintomi et al., 2017), mitotic chromosomes appear to be organized by condensins as an array of loops. The lack of evidence for a 30 nm fiber *in vivo* also supports this observation (Eltsov et al., 2008; Hsieh et al., 2020; Krietenstein et al., 2020; Ou et al., 2017; Risca et al., 2016).

Although condensins appear to be essential for the rod-like mitotic chromosome compaction, a large reduction in the chromatin volume that also occurs during mitosis appears to be independent of condensins (Mora-Bermúdez et al., 2007; Nagasaka et al., 2016; Samejima et al., 2018). This indicates that the nucleosome fiber compaction increases drastically upon mitotic entry. Since the chromatin fiber occupies only a small fraction of the nuclear volume in interphase, this suggests that the large apparent reduction in DNA volume is at least partially a result of microscopy resolution (Ricci et al., 2015a). However, direct analysis of the chromatin fiber structure in mitosis shows substantially increased interactions with nucleosomes that are farther away (Grigoryev et al., 2016). This suggests increased higher order structures in mitotic chromatin. Similarly, local nucleosome concentration by the electron microscopy technique ChromEMT shows that mitotic nucleosome density is higher than the median nucleosome density in interphase chromatin, but lower than the nucleosome density at some condensed regions in interphase (Ou et al., 2017).

Mechanisms driving local compaction in mitosis

Although nucleosome composition itself does not change significantly during mitosis, the loss of chromatin remodelers and transcription factors in mitosis leads to changes in nucleosome positioning and stability (Gutierrez et al., 2019; Jenness et al., 2018). There are also many conserved mitosis specific posttranslational modifications such as histone H3 phosphorylation at serine 10 and serine 28 and threonine 3 (Crosio et al., 2002; Dai et al., 2005; Hsu et al.,

2000). However, H3 phosphorylation at serine-10 does not change directly affect nucleosome fiber compaction *in vitro* (Fry et al., 2004) and replacing H3 with unphosphorylatable H3S10A mutants does not affect mitotic compaction.

Histone H4 tail acetylation abrogates acidic patch interactions and nucleosome fiber compaction (Allahverdi et al., 2011; Shogren-Knaak et al., 2006). Interestingly, histone acetylation and H2A-H4 interactions were both decreased in budding yeast metaphase by H3S10p mediated recruitment of histone deacetylase Hst2 (Wilkins et al., 2014). This appears to be a promising possibility for a mitotic chromatin compaction mechanism. However, hyper-acetylation of histones in mitosis by inhibiting histone deacetylases (HDACs) does not seem to affect chromatin compaction in human cells (Kruhlak et al., 2001). Further, DNA volume is lowest during anaphase (Nagasaka et al., 2016). This does not appear to coincide with the proposed mechanism of H3S10p recruiting Hst2 deacetylase to chromatin since phosphatase PP1 dephosphorylates H3 strongly in anaphase (Vagnarelli et al., 2006; Wilkins et al., 2014). This increased anaphase compaction also strongly corresponds to a second phase of condensin I recruitment to vertebrate cells and condensin relocalization to chromosome arms in budding yeast (Leonard et al., 2015; Walther et al., 2018). This suggests that the overall DNA compaction may also be directly related to condensin activity.

Although histone modifications do not appear to directly regulate any large-scale compaction in mitosis, it may be possible that these modifications, either directly or through chromatin fiber changes, change the recruitment or activity of condensins or other global compaction regulators. The mitotic kinases Aurora B and Plk1 have been shown to regulate condensin loading or activity in a number of contexts (Abe et al., 2011; Giet and Glover, 2001; Lipp et al., 2007; St-Pierre et al., 2009). However, these kinases also phosphorylate condensins directly and blocking aurora B phosphorylation in *Xenopus* egg extracts does not affect condensin loading or activity while it completely eliminates histone H3 phosphorylation at

both Serine-10, 28 directly and threonine-3 indirectly (MacCallum et al., 2002; Murnion et al., 2001). Thus, any possible regulation of the activity of condensins or topoisomerase II would have to be indirectly through changing chromatin fiber properties. The binding preferences and the enzymatic activities of condensins and topo II on chromatin have not been characterized in much detail and remain an open area of inquiry (Kschonsak and Haering, 2015).

Linker histone modifications have also been implicated in mitotic chromosome regulation, owing to their ubiquity and strong regulation in mitosis (Roth and Allis, 1992). Due to the large number of variants expressed in cells and their role in gene regulation, it has been difficult to study the role of linker histones in mitosis (Hergeth and Schneider, 2015). Using *Xenopus* egg extracts which contain a single H1 variant and no transcription, it was shown that H1 is not essential for chromosome compaction in mitosis (Ohsumi et al., 1993). However, these chromosomes are substantially elongated and mechanically fragile (Maresca et al., 2005; Ohsumi et al., 1993), suggesting that H1 does play a role in maintaining normal mitotic chromosome structure. The role of linker histone phosphorylation still remains a mystery. The C-terminal tail phosphorylation in different species has been shown to have different effects on linker histone stability in mitosis (Dou et al., 2002; Freedman and Heald, 2010). Variant specific linker histone phosphorylation of H1.2/H1.4 at the N-terminus has been shown to locally evict them and enable sister chromatid resolution (Krishnan et al., 2017). Although no global mechanism is evident, linker histone eviction does seem to affect chromosome compaction processes in mitosis. Since linker histone stoichiometry varies quite widely, it is important to understand how linker histones regulate mitotic compaction.

Xenopus egg extract system

X. laevis egg extracts are a cell-free system that has been used to study many ubiquitous cellular processes (Gillespie et al., 2012; Hoogenboom et al., 2017). Frog egg extracts are prepared by crushing unfertilized frog eggs, that are arrested in meiotic metaphase II, by centrifugation (Lohka and Masui, 1984). This separates the cytoplasm of the frog eggs from the other components into a separate layer that is referred to as cytostatic factor arrested (CSF) egg extracts (**Figure 1-6A**). These cytoplasmic extracts are largely DNA-free. However, these extracts can assemble nucleosomes on exogenously provided DNA (Laskey et al., 1977). Upon release of the mitotic arrest by the addition of calcium, egg extracts can assemble a nuclear envelope around DNA substrates and replicate the DNA (Blow and Laskey, 1986)(**Figure 1-6B**). It can also assemble spindles around sperm DNA or other DNA substrates (Heald et al., 1996; Sawin and Mitchison, 1991).

Frog egg extracts are an ideal system for studying the role of linker histones for two reasons. As frog egg extracts are made from embryonic cells, extracts are transcriptionally silenced (Amodeo et al., 2015; Newport and Kirschner, 1982). As one of the major roles of linker histones is in regulating transcription in interphase, depleting linker histones leads to changes in transcriptional programs in cells (Izzo et al., 2008). As extracts are transcriptionally silenced, this issue can be bypassed.

Frog egg extracts also contain a single dominant version of the linker histone H1.8 (also known as B4, H1foo, H1oo or H1M) (Dworkin-Rastl et al., 1994; Wühr et al., 2014) which is not required for replication (Dasso et al., 1994) or cell cycle specific changes in extract (Ohsumi et al., 1993). This enables the easy depletion of a single variant without affecting basic extract functions, enabling the investigation of direct linker histone functions.

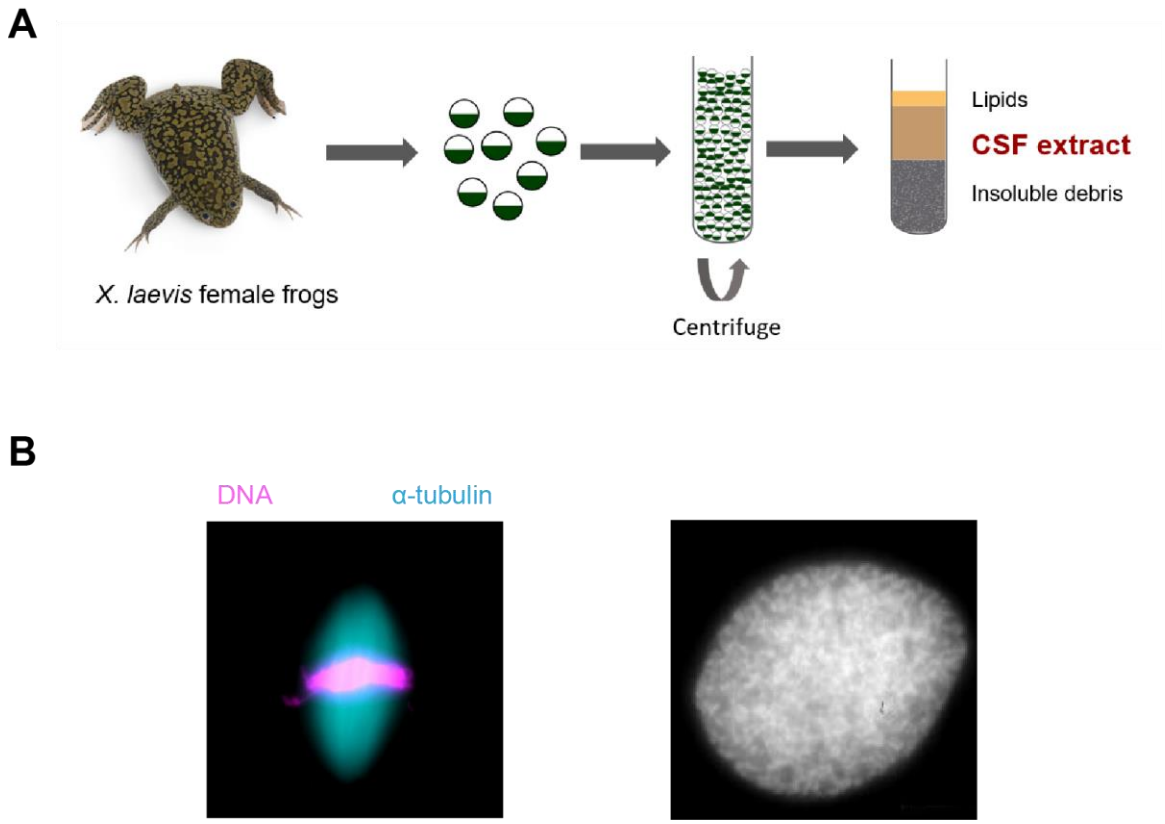

Figure 1-6 Xenopus egg extract system is capable of cellular functions

A) Protocol to prepare frog egg extracts. Female *X. laevis* frogs are injected with human chorionic gonadotropin to induce maturation and laying of mature eggs. These eggs are treated to remove the gelatinous coat and enable lysis of the eggs by centrifugation. This separates the eggs into several layers where a majority of the lipids and the cell walls of the eggs are separated from the cytoplasmic extract.

B) Egg extracts can generate spindles around sperm DNA in mitosis (left) and also nuclear envelope in interphase (right).

Open questions and Significance

Linker histone mediated mitotic compaction

Linker histones were once proposed to be the sole driver of mitotic chromosome compaction (Roth and Allis, 1992) as they are one of the primary regulators of inter-nucleosome contacts that regulate higher order fiber structures (Song et al., 2014; Thoma et al., 1979a). Although evidence later showed that mitotic compaction was regulated by condensins (Hirano and Mitchison, 1994) and that linker histones were not essential for this process (Ohsumi et al., 1993), linker histone depletion did result in severe misregulation of the mitotic chromosomes in *Xenopus* egg extracts (Maresca et al., 2005). Linker histones are a highly abundant chromatin component in most eukaryotic cells (Izzo et al., 2008), but the mechanism by which linker histone regulates mitotic chromosome compaction remains unclear. The *Xenopus* egg extract, where transcription is largely silenced (Newport and Kirschner, 1982), is an ideal system to ask this question since the effect of depleting a single dominant linker histone variant on mitotic chromosome organization can be addressed without perturbing the transcriptional landscape.

Regulation of condensins by local chromatin compaction

Condensin mediated loops have been shown to organize organisms ranging from bacteria to human cells (Kakui et al., 2017; Naumova et al., 2013; Wang et al., 2015). Condensin function and its regulation have been investigated by depletions or blocking phosphorylation (Bakhrebah et al., 2015; Hirota et al., 2004; Lipp et al., 2007; Ono et al., 2003; Shintomi and Hirano, 2011), and its biochemical function to DNA (Ganji et al., 2018; Kimura et al., 1999; Kong et al., 2020). However, eukaryotic condensins act on complex highly compact chromatin substrates (Grigoryev et al., 2016; Ou et al., 2017). The binding characteristics and enzymatic activity of condensin on chromatin substrates was completely unknown and still remains

largely a mystery. The accessibility of chromosome conformation assays and the well-developed biochemistry of the *Xenopus* extract system allowed me to address these questions.

Chapter 2- Controlling mitotic chromosome size through linker histone H1.8

H1.8 suppresses condensin loading on chromatin

H1.8 depletion leads to increased loading of condensins on chromatin

As noted in the previous section, condensin I enrichment on chromatin determines chromosome length in *Xenopus* egg extracts (Shintomi and Hirano, 2011). Since H1.8 depletion leads to thinner and elongated chromosomes (Maresca et al., 2005), I asked if H1.8 depletion affects the enrichment of condensins on chromatin. Previous reports, albeit done without rigorous quantitative analysis, suggest that H1.8 depletion does not have a large effect on the chromatin enrichment of major chromatin proteins (Maresca et al., 2005). Since chromosome length is regulated by condensin I enrichment on chromosomes (Shintomi and Hirano, 2011), I quantified the change in chromosome enrichment of condensin I upon depleting H1.8. *Xenopus* egg extracts arrested at meiotic metaphase II with cytostatic factor (CSF extracts) were first incubated with protein-A-beads coupled with control rabbit IgG and antibodies against H1.8 for mock deletion (ΔIgG) and H.8 depletion (ΔH1.8), respectively. These depleted extracts containing sperm nuclei were treated with calcium to release into interphase, during which chromosomes were replicated. After 90 min of incubation, which completes DNA replication, corresponding fresh CSF depleted extracts were added to generate replicated metaphase chromosomes. Since chromosome-spindle interaction could affect chromosome shape by microtubule dependent force, nocodazole was added to inhibit spindle formation (**Figure 2-1 A, B**). These chromosomes were fixed and the levels of condensin I were assessed by immunofluorescence microscopy using an antibody to the CAP-G subunit of condensin I. Depletion of H1.8 (ΔH1) resulted in a ~2.5 fold increase in CAP-G signal, which was normalized by DNA staining with Hoechst 33342, whereas the addition of recombinant H1.8 (rH1.8) rescued this depletion phenotype (**Figure 2-1 C, D**). To validate the effect of the signal

normalization with Hoechst 33342, whose DNA binding may potentially be affected by changes in chromatin organization in ΔH1 extracts, I used fluorescent dUTPs that are incorporated into chromosomes during replication (**Figure 2-1 E**). H1.8 depletion did not affect dUTP incorporation (**Figure 2-1 F**), consistent with a previous observation that H1.8 is not required for DNA replication (Dasso et al., 1994). Normalization using this fluorescent dUTP signal showed a similar increase in CAP-G signal in ΔH1.8 extracts (**Figure 2-1 G**), suggesting that the increase in CAP-G signal upon H1.8 depletion was not due to differential staining of ΔH1 chromosomes by Hoechst 33342.

To measure the chromatin levels of condensin II, I stained the chromosomes using antibodies against the CAP-G2 subunit of condensin II (**Figure 2-1 H**). This showed a ~ 2.5 fold increase in CAP-G2 on ΔH1 chromosomes as well. This suggests that H1.8 depletion results in increased levels of both condensin I and condensin II on the chromatin. To verify if loss of H1.8 results in a global increase in chromatin proteins, I measured the levels of several known chromatin proteins upon H1.8 depletion. Proteins that have been shown to prefer to bind nucleosomes (RCC1 and Dasra A) and proteins that prefer to bind DNA (Dppa2 and Xkid) (Zierhut et al., 2014) both did not show similar increases upon H1.8 depletion (**Figure 2-2, A-1, Table A-1**). This also informed me that there was no systematic change in immunofluorescence signal due to a change in chromatin structure or chromosome morphology upon H1.8 depletion.

I also attempted to confirm enrichment of both condensins by an orthogonal biochemical approach. To do this, I purified mitotic chromosomes through a sucrose cushion (**Figure 2-3A**). Confirming the immunofluorescence observations, both western blotting and mass spectrometry showed a similar 2-2.5 fold increase in CAP-G (condensin I) and CAP-G2 (condensin II) (**Figure 2-3 B, C, A-1, Table A-1**).

Figure 2-1 H1.8 depletion leads to accumulation of condensins on mitotic chromatin

A) Experimental scheme to generate replicated chromosomes in *Xenopus* egg extracts. B) Western blots of total extracts showing depletion of H1.8 from *Xenopus* egg extracts and rescue with recombinant H1.8 (rH1.8). C) Representative images of DNA (Hoechst 33342), CAP-G (condensin I) immunofluorescence on chromosomes in metaphase extracts treated with nocodazole in the indicated conditions. Bar, 10 μm. D) Quantification of CAP-G (condensin I) immunofluorescence signals normalized to the DNA (Hoechst) signal for the indicated conditions. Each grey or magenta dot represents the average signal intensity of a single chromosome cluster (from one nucleus). Each black dot represents the median signal intensity from a single experiment. Bars represent mean and range of the medians of two independent experiments. For each experiment, >20 chromosome clusters were counted. E) Experimental scheme to incorporate Cy3-labelled nucleotides to use normalization of immunofluorescence signals on chromosomes. F) Quantification of Cy3-dUTP signals normalized to Hoechst 33342 signals, showing uniform normalization across two coverslips used for quantification of condensin I and TOP2A. The result also indicates no detectable defect in DNA replication in ΔH1 extracts. G) CAP-G (condensin I) and TOP2A immunofluorescence signal levels on chromosomes normalized with Hoechst and incorporated Cy3-dUTP. H) Representative images of CAP-G2 (condensin II) immunofluorescence on chromosomes in metaphase extracts with nocodazole in the indicated conditions. Bar, 10 μm. I) Quantification of the CAP-G2 (condensin II) normalized to the DNA (Hoechst) signal for the indicated conditions. Each grey or purple dot represents the average signal intensity of a single chromosome cluster (from one nucleus). Each black dot represents the median signal intensity from a single experiment. Bars represent mean and range of the median of two independent experiments. For each experiment, signals on >20 chromosome clusters were counted.

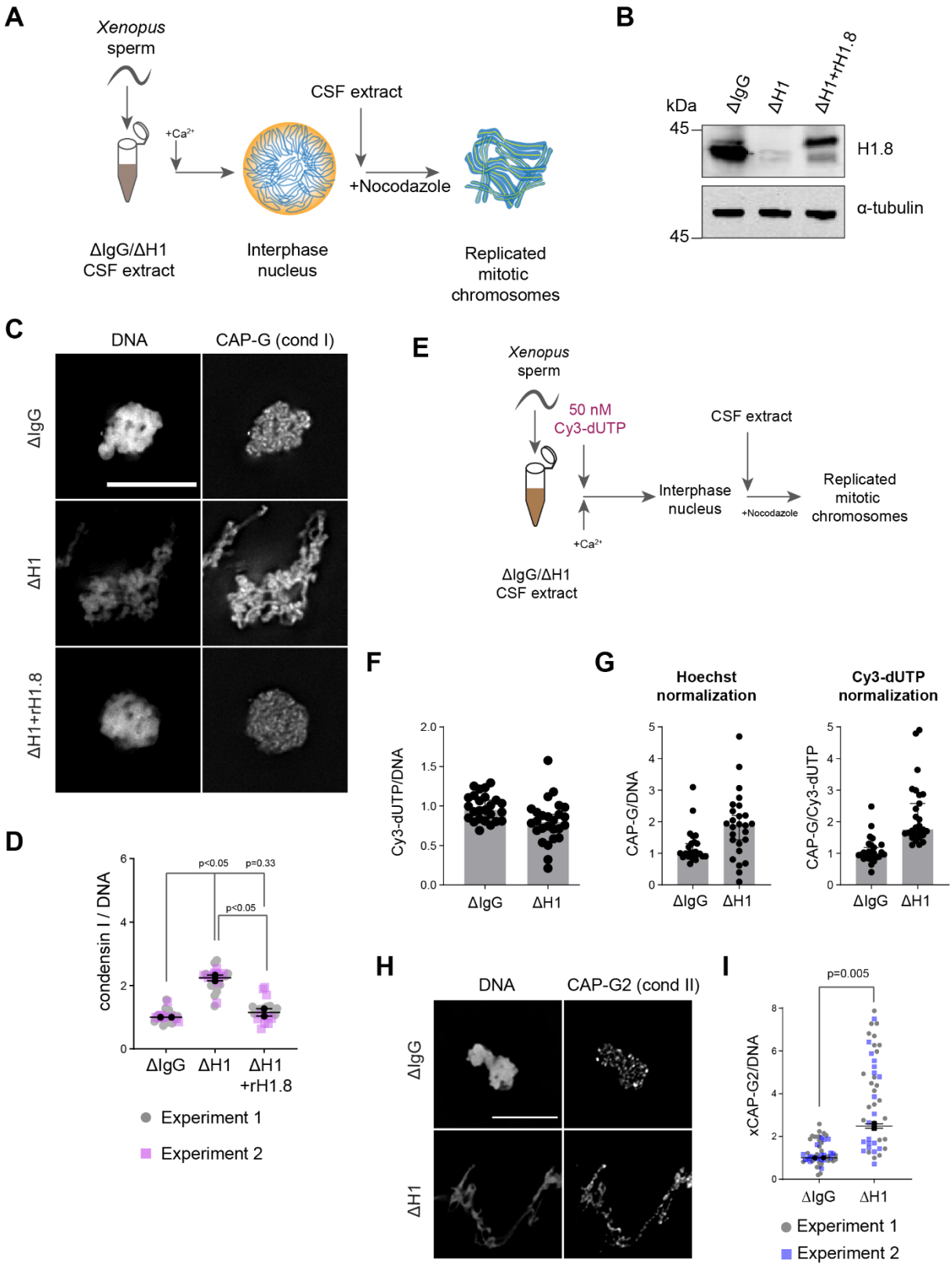
A
Xenopus sperm
+Ca2+
CSF extract
+Nocodazole
ΔIgG/ΔH1 CSF extract
Interphase nucleus
Replicated mitotic chromosomes
B
kDa
ΔIgG
ΔH1
ΔH1+rH1.8
45
H1.8
α-tubulin
45
C
DNA
CAP-G (cond I)
ΔIgG
ΔH1
ΔH1+rH1.8
D
condensin I / DNA
p<0.05
p=0.33
p<0.05
ΔIgG
ΔH1
ΔH1 +rH1.8
Experiment 1
Experiment 2
E
Xenopus sperm
50 nM Cy3-dUTP
CSF extract
Interphase nucleus
+Nocodazole
Replicated mitotic chromosomes
+Ca2+
ΔIgG/ΔH1 CSF extract
F
Cy3-dUTP/DNA
ΔIgG
ΔH1
G
Hoechst normalization
Cy3-dUTP normalization
CAP-G/DNA
CAP-G/Cy3-dUTP
ΔIgG
ΔH1
H
DNA
CAP-G2 (cond II)
ΔIgG
ΔH1
I
p=0.005
xCAP-G2/DNA
ΔIgG
ΔH1
Experiment 1
Experiment 2

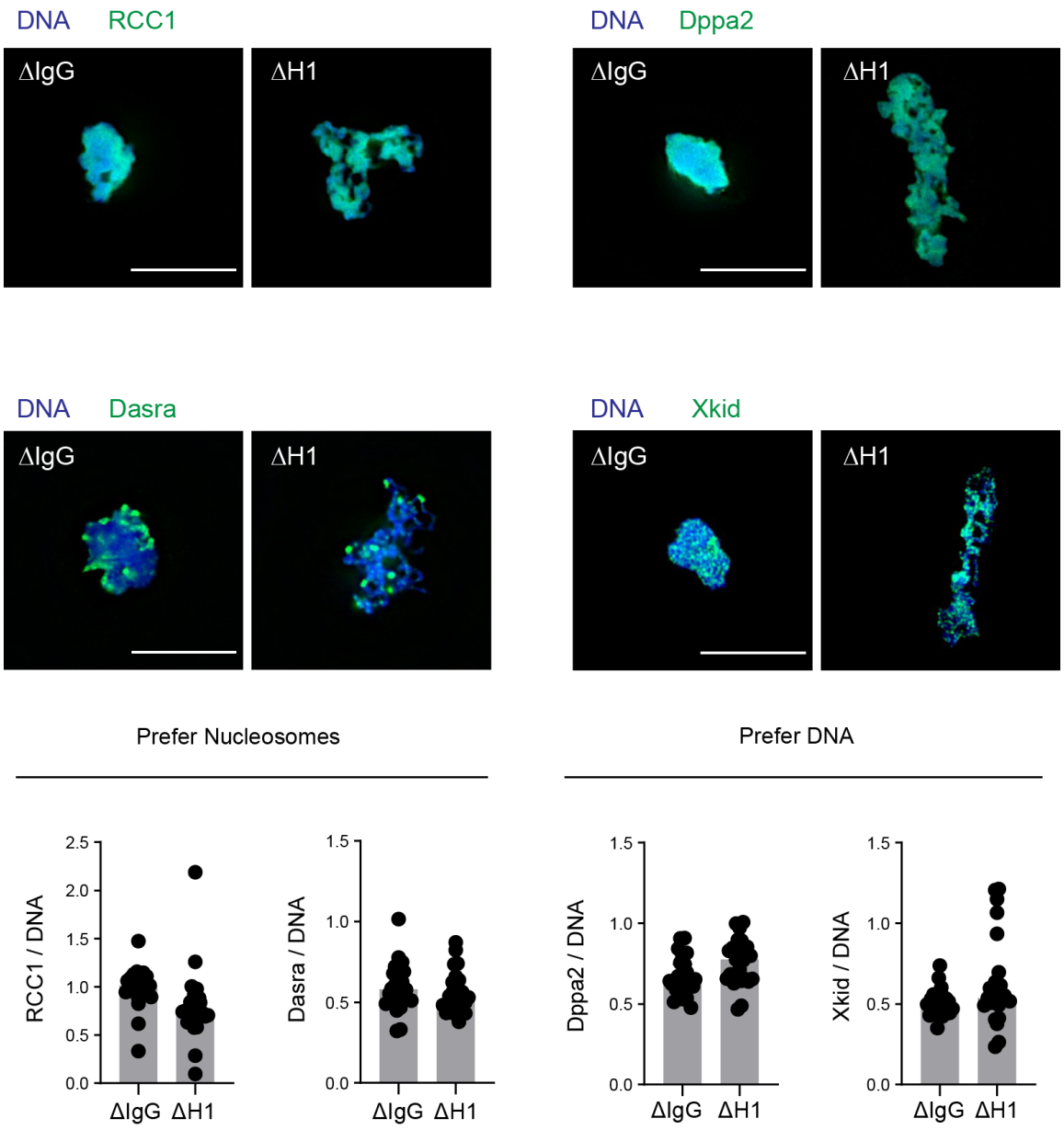

Figure 2-2 H1 depletion doesn't lead to non-specific accumulation of chromosomal proteins

Representative images of immunofluorescence staining of candidate proteins (top). Scale bar 10 µm. Quantification of scaled intensities (bottom). Each dot represents the average intensity of the indicated antibody normalized to the DNA (Cy3-dUTP) for a single nucleus. The data plotted is median and 95 % C.I.

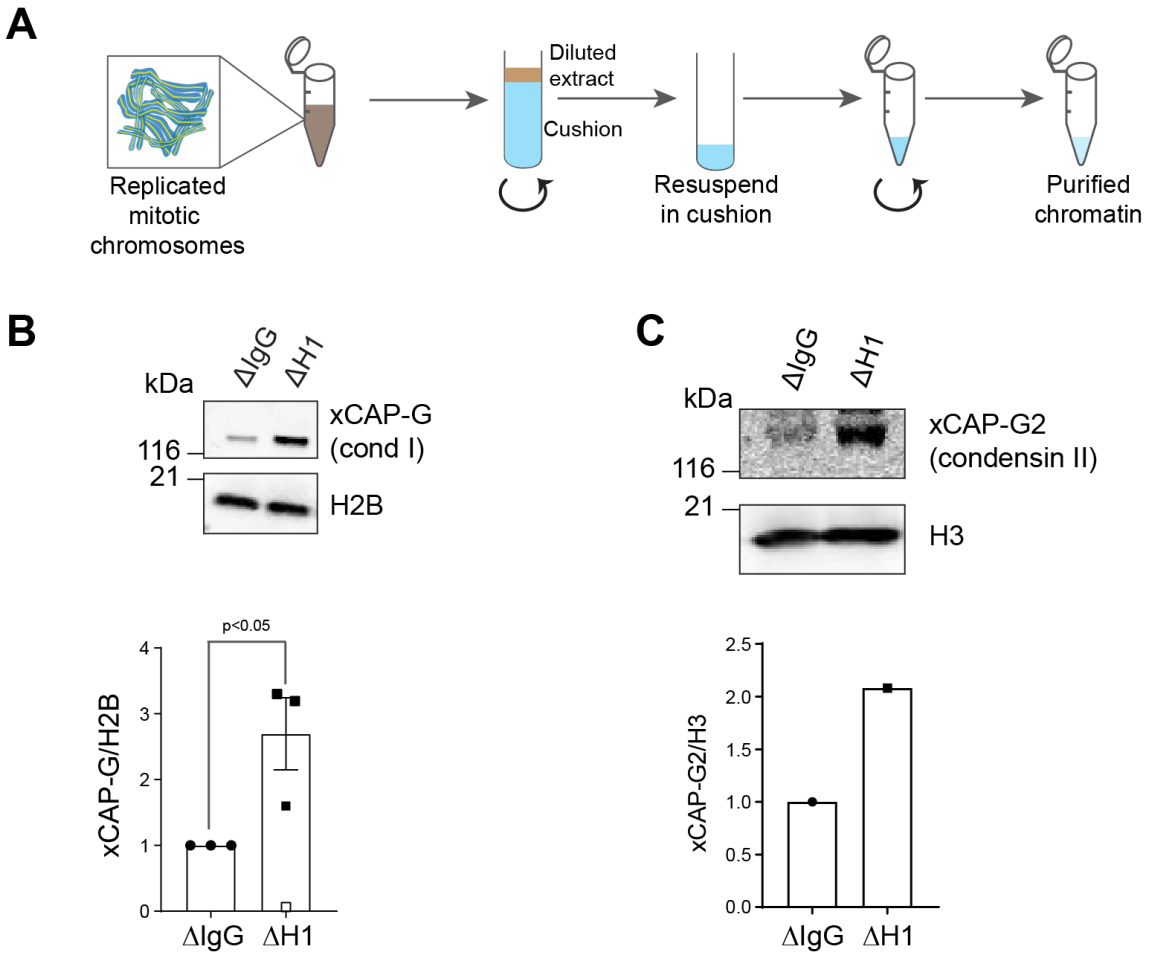

Figure 2-3 Condensins accumulate on chromosomes purified from H1.8 depleted extracts

A) Schematic for purification of mitotic chromosomes from extract by layering extract over a sucrose cushion. The pellet is resuspended in the remaining cushion, transferred to a new tube and centrifuged again to obtain purified chromatin. B) Western blots of mitotic chromatin purified from mock (ΔIgG) and H1.8-depleted (ΔH1) extracts (top) and quantification of band intensities normalized to H2B or H3 (below). Mean and SEM from 3 experiments. C) same as B) for CAP-G2 (condensin II).

Condensin I and Condensin II loading on chromatin are independent of each other

Since H1.8 depletion results in an increase in both condensins, I wanted to verify if both condensins were independently regulated by H1.8. To do this, I performed co-depletions of H1.8 and condensin I (ΔH1ΔCAP-G) or condensin II (ΔH1ΔCAP-D3) (**Figure 2-4A**). CAP-G levels in both condensin II depletion (ΔCAP-D3) and H1.8, condensin II co-depletion (ΔH1ΔCAP-D3) are indistinguishable from those in control (ΔIgG) and H1.8 depletion (ΔH1) respectively (**Figure 2-4 B, C**). This suggests that condensin I levels are independent of condensin II. Similarly, CAP-G2 levels are also largely independent of condensin I levels. Condensin I depletion seems to result in small increases in CAP-G2 levels in both control and H1.8 depleted backgrounds, suggesting that the more abundant condensin I may compete with condensin II for loading onto chromatin as well. This is also consistent with the observations that the ratio of condensin I to condensin II but not their absolute levels in extract regulates the chromosome length (Shintomi and Hirano, 2011). However, this data confirms that condensin I and condensin II can be loaded on chromatin independently and that H1.8 depletion independently leads to increased levels of both condensins.

Figure 2-4 Condensin I and II levels on chromatin are independent of each other.

A) Western blots of extract samples showing depletion of CAP-G (condensin I), CAP-D3 (condensin II) and H1.8. B) Representative images of chromosomes in the indicated conditions showing the increase in accumulation of CAP-G by immunofluorescence. C) Quantification of CAP-G (condensin I) immunofluorescence normalized to the DNA signal for the indicated conditions. Each grey or orange dot represents the average signal intensity of a single chromosome cluster (from one nucleus). Each black dot represents the median signal intensity from a single experiment. Bars represent mean and range of the medians of two independent experiments. >20 nuclei were quantified for each condition in every experiment. D) Quantification of CAP-G2 (condensin II) immunofluorescence intensity, normalized to the DNA signal for the indicated conditions. Each grey or magenta dot represents the average signal intensity of a single chromosome cluster (from one nucleus). Each black dot represents the median signal intensity from a single experiment. Bars represent mean and range of the medians of two independent experiments. >20 nuclei were quantified for each condition in every experiment.

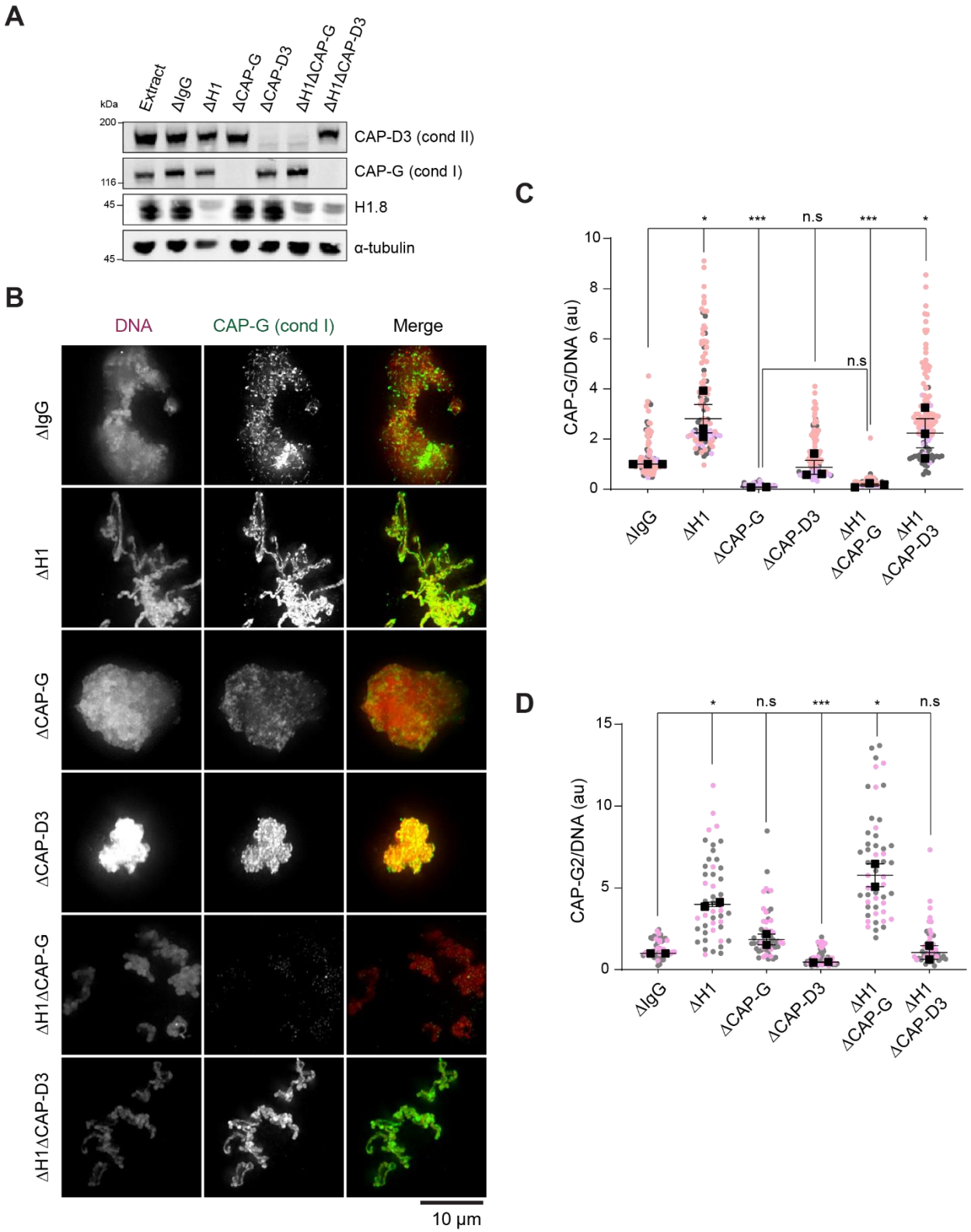
A
Extract
ΔIgG
ΔH1
ΔCAP-G
ΔCAP-D3
ΔH1ΔCAP-G
ΔH1ΔCAP-D3
kDa
200
116
45
45
CAP-D3 (cond II)
CAP-G (cond I)
H1.8
α-tubulin
B
DNA
CAP-G (cond I)
Merge
ΔIgG
ΔH1
ΔCAP-G
ΔCAP-D3
ΔH1ΔCAP-G
ΔH1ΔCAP-D3
10 µm
C
CAP-G/DNA (au)
0
2
4
6
8
10
*
***
n.s
n.s
***
*
ΔIgG
ΔH1
ΔCAP-G
ΔCAP-D3
ΔH1 ΔCAP-G
ΔH1 ΔCAP-D3
D
CAP-G2/DNA (au)
0
5
10
15
*
n.s
***
*
n.s
ΔIgG
ΔH1
ΔCAP-G
ΔCAP-D3
ΔH1 ΔCAP-G
ΔH1 ΔCAP-D3

Condensin I binding to nucleosome arrays is sensitive to magnesium concentration

As H1.8 depletion from *Xenopus* extracts leads to increased loading of condensins on mitotic chromatin, I then asked how H1.8 restricts the binding of condensins on chromatin. Loss of H1.8 does not lead to a change in nucleosome spacing in *Xenopus* extracts (Ohsumi et al., 1993). This suggests that the loss of H1.8 exposes more accessible linker DNA between nucleosomes. Since condensins prefer to bind nucleosome free DNA (Kong et al., 2020; Shintomi et al., 2017; Toselli-Mollereau et al., 2016a; Zierhut et al., 2014), the increased binding of condensins upon H1.8 depletion could be due to the increase in available free DNA.

To test this hypothesis, I biochemically reconstituted chromatin and purified condensins and asked if the effect of H1.8 can be recapitulated *in vitro*. Vertebrate condensins share significant homology (Nasmyth and Haering, 2005) and human condensins isolated from HeLa cells can rescue chromatid formation in condensin depleted *Xenopus* egg extracts (Kimura et al., 2001), so we performed the following experiments with purified human condensins. This work was done with the help of Dr. Erin Cutts in the Vannini lab (Institute of Cancer Research, London), who purified recombinant human condensins from insect cell cultures (Kong et al., 2020) and provided them to me. I reconstituted nucleosome arrays using purified *X. laevis* histones deposited onto a biotinylated 19-mer array of the Widom 601 positioning sequence using salt dialysis (Lowary and Widom, 1997; Zierhut et al., 2014). These reconstituted biotinylated nucleosome arrays were coupled to Streptavidin DynaBeads, washed, and incubated with the purified condensin (**Figure 2-5 A**). After 30 min of binding at room temperature, samples were collected for total binding reaction (Input) and the washed beads (Beads).

Although it has been shown condensins poorly bind to mononucleosomes with short linker DNA *in vitro* (Kong et al., 2020), the binding properties of condensins to arrays of

nucleosomes were still unknown. Using this assay, I wanted to first establish optimal binding conditions to assess the binding affinity differences. Condensins are ATPases that exhibit several ATP dependent changes in structure (Cutts and Vannini, 2020; Datta et al., 2020). So, I asked whether the addition of ATP changes the binding affinity of condensin I to nucleosome arrays. In the presence of 2.5 mM $MgCl_2$, the addition of 5 mM ATP significantly increased the binding affinity of condensins (**Figure 2-5 B**). However, this ATP dependent enhancement of binding affinity only occurred when ATP concentration was higher than the $MgCl_2$ concentration (**Figure 2-5 C**). The addition of 1 mM ATP only increased the binding in the presence of 1 mM $MgCl_2$, but not 2.5 mM $MgCl_2$. Importantly, this observation was also repeated for the Q-loop mutant of condensin I that cannot bind ATP (Hopfner et al., 2000; Kong et al., 2020; Löwe et al., 2001). This suggested to me that the changes in binding affinity of condensin I due to the addition of ATP were due to its magnesium chelation. Free magnesium ions induce chromatin compaction (Eltsov et al., 2008; Finch and Klug, 1976) and this change in the structure of nucleosome arrays may also affect the binding of condensin I. To verify this possibility, I asked whether EDTA chelation of magnesium recapitulates the ATP dependent enhancement of condensin I binding. This is indeed what I observed for the Q-loop mutant of condensin I (**Figure 2-5 D**), supporting my observation that condensin I binding to nucleosome arrays is sensitive to magnesium concentration.

There are two simple mechanisms to explain this magnesium sensitivity of condensin binding. The first is a simple salt sensitive binding of DNA binding proteins such as condensin I. The second is that higher order chromatin structure changes caused by magnesium addition affect condensin binding (Eltsov et al., 2008). To investigate which of these two possible mechanisms might be involved in the ATP sensitivity of condensin binding, I asked if condensin binding to mononucleosomes shows similar binding sensitivity to magnesium concentration. Since mononucleosomes do not have a higher order structure (by definition) or

aggregate at low magnesium concentrations (White et al., 2016), the change in magnesium concentration can only affect condensin binding through simple salt competition. Interestingly however, addition of ATP did not increase the binding affinity of wildtype condensin I to mononucleosomes (**Figure 2-5E, F**). This indicates that the increased condensin binding to nucleosome arrays at low magnesium concentrations is likely due to changes in higher order chromatin structure at low magnesium concentrations.

Figure 2-5 Condensin I binding is sensitive to magnesium concentration

A) Experimental scheme for pulldowns of condensin I using chromatin array beads. B) Purified recombinant human condensin I was incubated with nucleosome array beads in buffer containing 2.5 mM $MgCl_2$ with and without 5 mM ATP. Coomassie staining of input and bead fractions are shown. C) Purified human condensin I or condensin I Q loop mutant was incubated with nucleosome array beads in buffer containing 1 or 2.5 mM $MgCl_2$ with and without 1 mM ATP. Coomassie staining of input and bead fractions are shown. D) Purified human condensin I Q loop mutant was incubated with nucleosome array beads in buffer containing 2.5 mM $MgCl_2$ with the addition of 5 mM ATP or 5 mM EDTA. Coomassie staining of input and bead fractions are shown. E) Alexa647-labelled 196 bp mononucleosomes were incubated with indicated concentrations of condensin I in buffer containing 2.5 mM $MgCl_2$ and with or without 5 mM ATP and electrophoresed on a 5 % native PAGE. Alexa647-labeled DNAs are shown. Bands at the well represent the nucleosome-condensin complex. Absence of signals at the well in the absence of Condensin I indicates that mononucleosomes did not form large aggregates. F) Condensin I binding curves with mononucleosomes with and without ATP, showing no increase in binding affinity due to ATP addition.

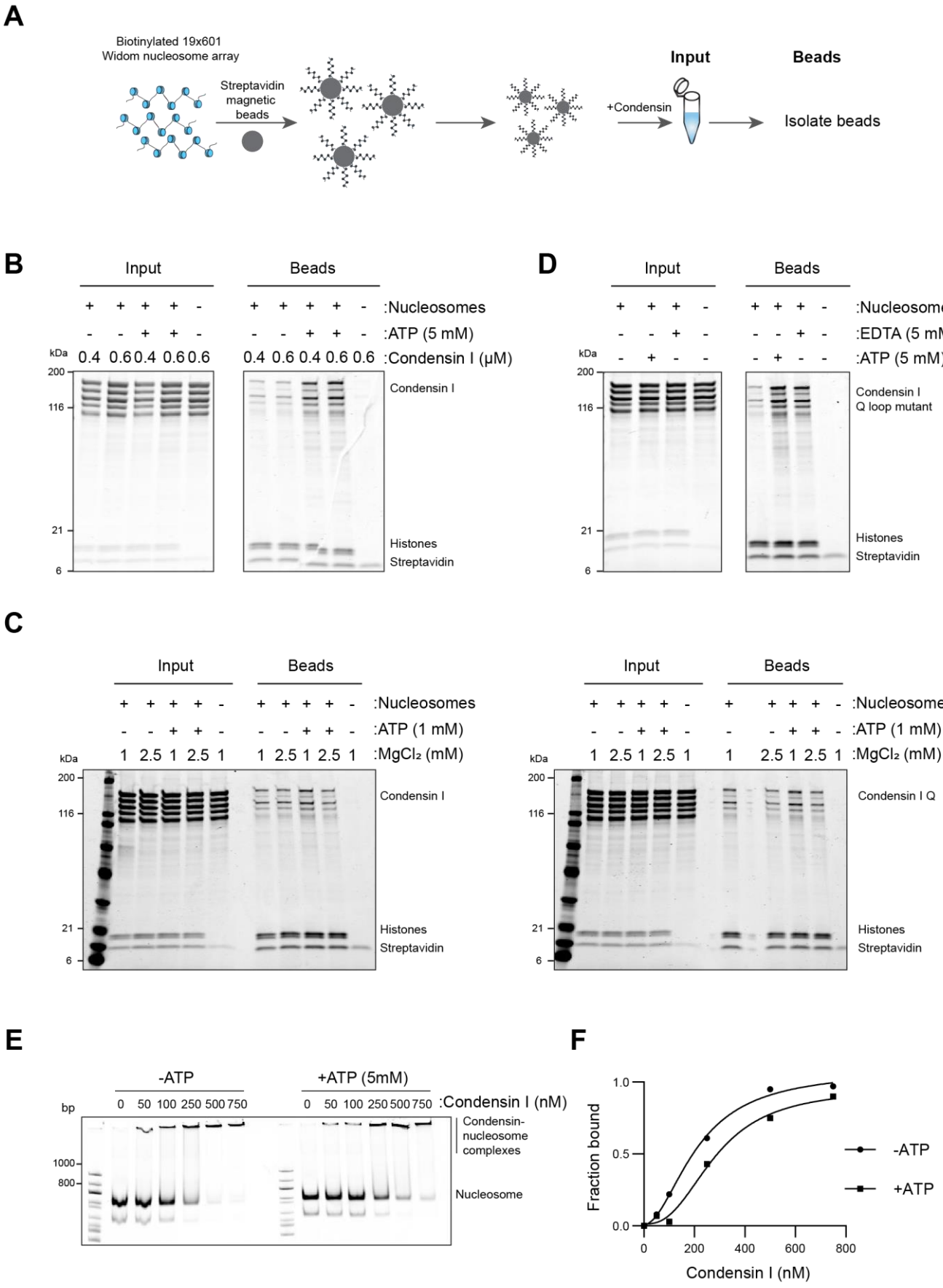
A
Biotinylated 19x601
Widom nucleosome array
Streptavidin
magnetic
beads
Input
Beads
+Condensin
Isolate beads
B
Input
Beads
:Nucleosomes
:ATP (5 mM)
kDa
0.4 0.6 0.4 0.6 0.6
:Condensin I (μM)
200
116
21
6
Condensin I
Histones
Streptavidin
D
Input
Beads
:Nucleosomes
:EDTA (5 mM)
:ATP (5 mM)
Condensin I
Q loop mutant
Histones
Streptavidin
C
Input
Beads
:Nucleosomes
:ATP (1 mM)
1 2.5 1 2.5 1
:MgCl₂ (mM)
Condensin I
Histones
Streptavidin
Condensin I Q
E
-ATP
+ATP (5mM)
bp
0 50 100 250 500 750
:Condensin I (nM)
1000
800
Condensin-
nucleosome
complexes
Nucleosome
F
Fraction bound
1.0
0.5
0.0
0 200 400 600 800
Condensin I (nM)
-ATP
+ATP

H1.8 inhibits binding of condensins to nucleosome *in vitro*

Having established optimal binding conditions for condensin binding *in vitro,* I asked if H1.8 blocks the binding of condensins to the nucleosome arrays. To do this, I split the nucleosome array bound beads and loaded recombinant H1.8 onto one-half of the beads (**Figure 2-6 A, B**). I then added recombinant condensins to these beads and asked whether H1.8 affects condensin binding at different salt concentrations. All these experiments were done in the presence of 2.5 mM $MgCl_2$ and 5 mM ATP. Condensin I exhibited salt sensitive binding to nucleosome arrays, consistent with the known non-specific electrostatic binding of condensins (**Figure 2-6 C, D**) (Eeftens et al., 2017). The presence of H1.8 on the nucleosome arrays resulted in a ~ 4-5 fold reduction in condensin binding to nucleosome arrays at all the assayed salt concentrations. The Q-loop mutant of condensin I showed similar binding at all assay conditions. These data are consistent with condensin I binding to these nucleosome arrays being dependent on charge-based interactions and the idea that H1.8 inhibits this binding. Condensin II showed stronger binding and reduced sensitivity to salt concentration, consistent with its increased affinity to DNA (Kong et al., 2020). However, similar to condensin I, condensin II showed a ~ 2 fold lower affinity to H1.8 loaded nucleosome arrays (**Figure 2-7**). The Q-loop mutant of condensin II behaved indistinguishably from the wildtype condensin II in these binding assays.

Since condensins show preference for binding to naked DNA over nucleosomal DNA (Kong et al., 2020; Toselli-Mollereau et al., 2016a; Zierhut et al., 2014), the increased condensin binding to H1.8 free nucleosome arrays could be the result of accessible linker DNA on these nucleosome arrays. However, linker histones also lead to the formation of higher order chromatin fiber structures (Song et al., 2014; Thoma et al., 1979a). This more compact chromatin fiber in the presence of H1.8 could also result in decreased condensin binding. To distinguish between these two hypotheses, I asked whether condensin binding to mononucleosomes is also inhibited by H1.8. Since mononucleosomes have no higher order

structures, a change in condensin binding to mononucleosomes would suggest that H1.8 directly blocks access of condensins to linker DNA. To assay condensin binding to mononucleosomes, I performed electrophoretic mobility shift assays (EMSA) with mononucleosomes made on Alexa647 labelled DNA. In these assays, condensin-nucleosome/chromatosome complexes show significant reduction in gel mobility compared to the nucleosome/chromatosome bands. Consistent with the linker DNA competition hypothesis, H1.8 inhibited condensin I binding to mononucleosomes (**Figure 2-8 A**). Quantifying the binding affinity, I observed a ~ 5 fold reduction in binding affinity upon addition of H1.8. This is consistent with the 4-5 fold reduction of condensin I binding to nucleosome arrays loaded with H1.8.

Figure 2-6 H1.8 inhibits condensin I binding to nucleosome arrays *in vitro*

A) Experimental scheme for testing the effect of recombinant H1.8 (rH1.8) on binding of purified condensin I to arrays of nucleosomes assembled on the Widom 601 nucleosome positioning sequence. B) Native PAGE gel analysis of nucleosome array beads loaded with or without H1.8 after digestion of the array with *Ava*I, which released monomers of nucleosome positioning sequence. A complete shift of monomer bands by H1.8 addition indicates the saturated occupancy of nucleosome and H1.8. C) Coomassie staining of SDS-PAGE gels, showing input (top) and nucleosome-array bound fraction (middle) of condensin I, rH1.8 and core histones. The right most lanes represent the streptavidin beads only negative control. Buffer contains 2.5 mM $MgCl_2$, 5 mM ATP and indicated concentrations of NaCl. D) The band intensities of condensin I subunits were normalized to the histone bands and the binding at 50 mM NaCl for nucleosome arrays without H1.8. Mean and S.E.M of three independent experiments are shown (bottom).

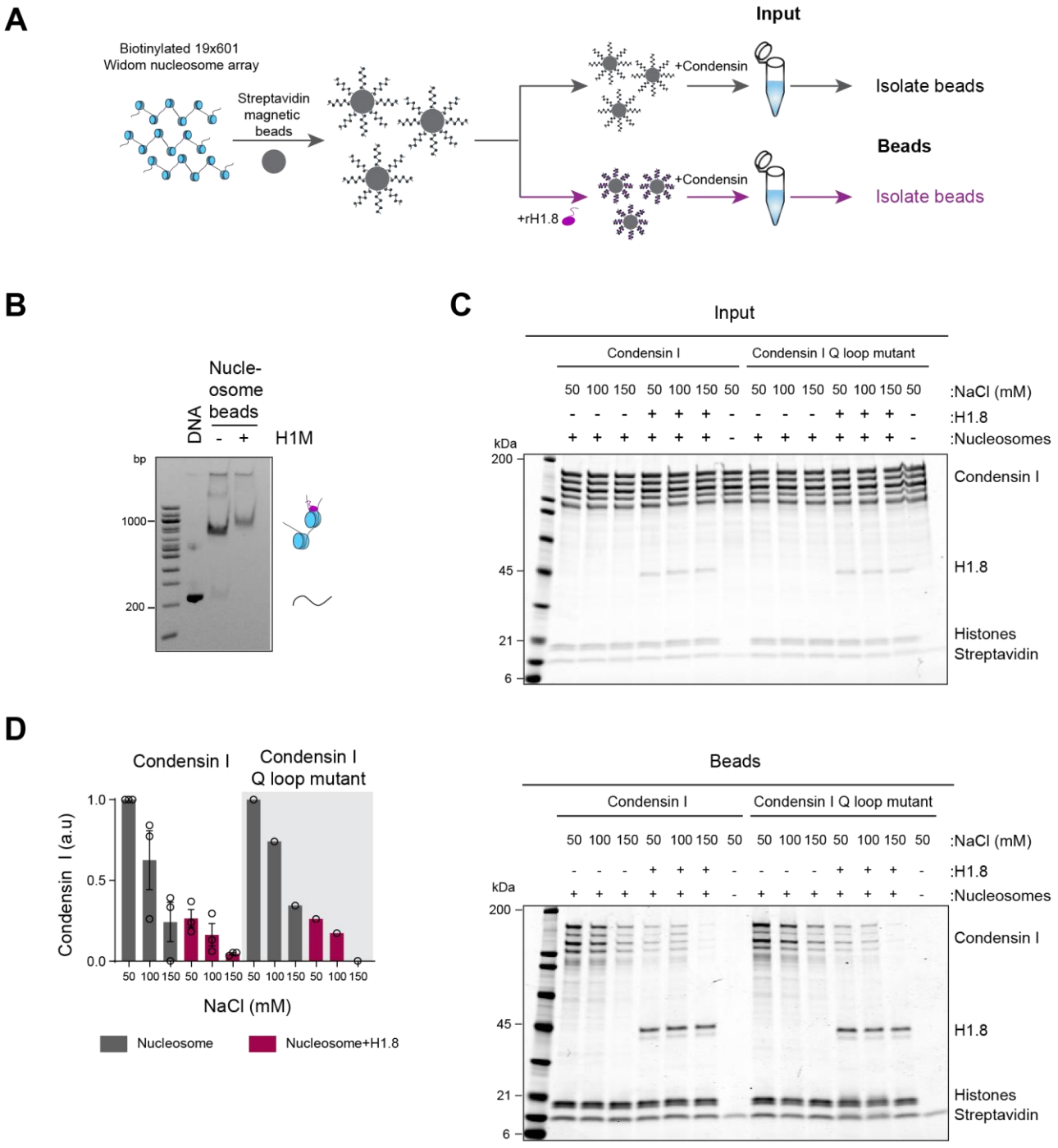
A
Biotinylated 19x601
Widom nucleosome array
Streptavidin
magnetic
beads
Input
+Condensin
Isolate beads
Beads
+Condensin
+rH1.8
Isolate beads
B
Nucle-
osome
beads
DNA
- +
H1M
bp
1000
200
C
Input
Condensin I
Condensin I Q loop mutant
50 100 150 50 100 150 50 50 100 150 50 100 150 50
:NaCl (mM)
:H1.8
:Nucleosomes
kDa
200
45
21
6
Condensin I
H1.8
Histones
Streptavidin
D
Condensin I
Condensin I
Q loop mutant
Condensin I (a.u)
1.0
0.5
0.0
50 100 150 50 100 150 50 100 150 50 100 150
NaCl (mM)
Nucleosome
Nucleosome+H1.8
Beads
Condensin I
Condensin I Q loop mutant
50 100 150 50 100 150 50 50 100 150 50 100 150 50
:NaCl (mM)
:H1.8
:Nucleosomes
kDa
200
45
21
6
Condensin I
H1.8
Histones
Streptavidin

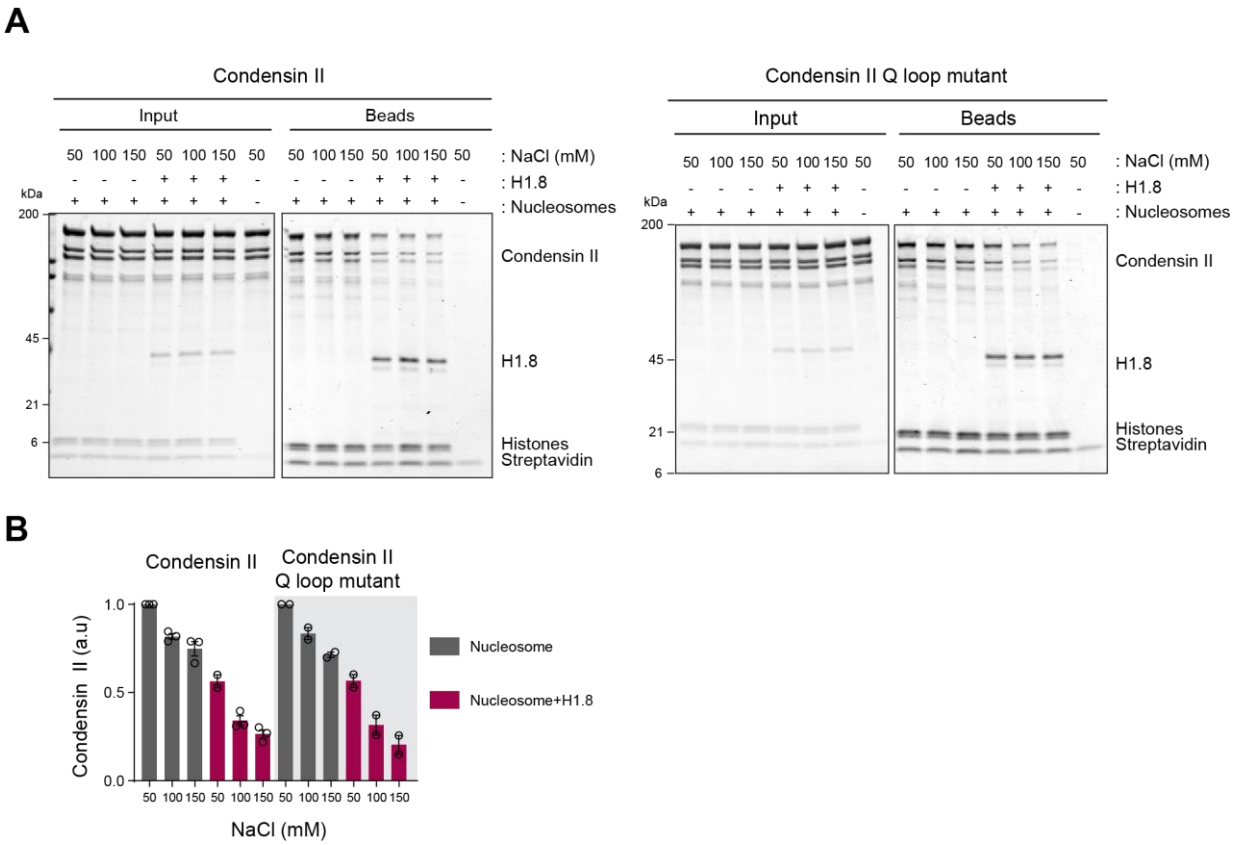

Figure 2-7 H1.8 inhibits condensin II binding to nucleosome arrays *in vitro*

A) Coomassie staining of SDS-PAGE gels, showing input and nucleosome-array bound fraction (Beads) of condensin II (left) and condensin II q-loop mutant (right), rH1.8 and core histones. The right most lanes represent the streptavidin beads only negative control. Buffer contains 2.5 mM $MgCl_2$, 5 mM ATP and indicated concentrations of NaCl. B) The band intensities of condensin II subunits were normalized to the histone bands and the binding at 50 mM NaCl for nucleosome arrays without H1.8. Mean and S.E.M of three independent experiments are shown (bottom).

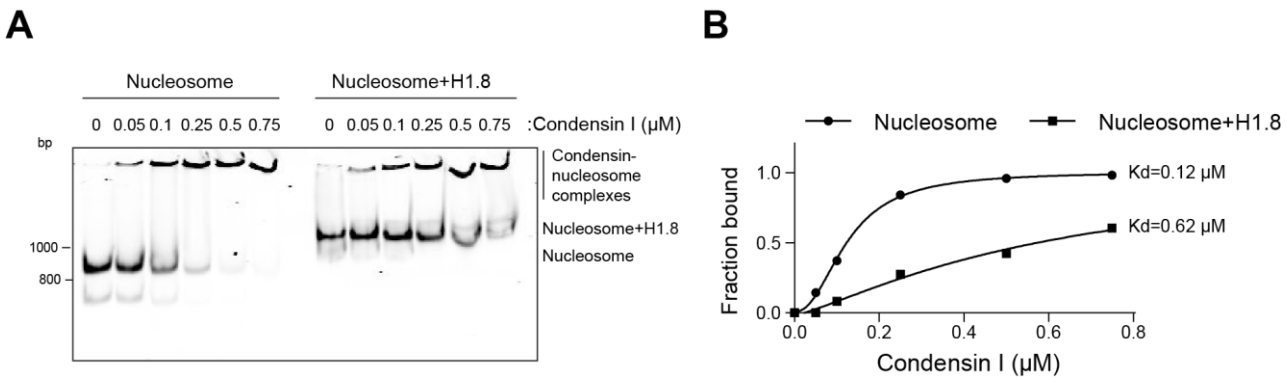

Figure 2-8 H1.8 inhibits condensin I binding to mononucleosomes

A) Alexa647-labelled 196 bp mononucleosomes with or without H1.8 were incubated with indicated concentrations of condensin I and electrophoresed on a 5 % native PAGE. Alexa647-labeled DNAs are shown. Bands at the well represent the nucleosome-condensin complex. Absence of signals at the well in the absence of Condensin I indicates that mononucleosomes do not form large aggregates in the presence or absence of rH1.8 under the experimental condition. B) Condensin I binding curves with mononucleosomes with and without H1.8, showing the large increase in binding constant in the presence of H1.8.

Condensin accumulation on chromatin can be titrated using H1 stoichiometry

Linker histone stoichiometry varies widely among different cell types and H1 variants (Woodcock et al., 2006). Since the data in the previous section shows that H1 and condensin directly compete for binding to linker DNA, it suggests that the amount of condensin on chromatin can be controlled by changing the stoichiometry of linker histone. To verify if changing linker histone stoichiometry in experimentally observed ranges would result in titrating condensin levels, I generated a simple competition model for condensin binding to chromatin (**Figure 2-9A**). In this model, condensin can bind to nucleosomes with and without H1 with differing binding strengths. Since condensin I is unable to displace H1.8 from the nucleosomes, even at a much higher condensin I/H1.8 ratio than in *Xenopus* extracts (**Figure 2-8A**), this suggests that linker histone binding can be treated to be independent of condensins. The affinity of other linker histones to nucleosomes (~0.1 nM) is also much higher than those of condensin I (~600-700 nM), suggesting that this assumption may be safely applied for analysis in other systems as well (Kong et al., 2020; White et al., 2016). To model this assumption, I assume that the exchange rates of condensin are much slower than that of H1.8 (K_{on}^{H1}, K_{off}^{H1} >> K_{on}, K_{off} , K_{on}^{*}, K_{off}^{*}). Under these conditions, using the quasi-steady state assumption (Segel and Slemrod, 1989), we can estimate the condensin enrichment in the absence of H1 as a function of two parameters 1) S, the stoichiometry of H1 on chromatin, i.e the number of H1 per nucleosome and 2) E, the fold increase in condensin binding affinity to nucleosomes lacking H1 (**Figure 2-9B**). The experimentally observed enrichment of ~ 2 fold in the absence of H1.8 in egg extracts was recaptured at a stoichiometry of 0.6 at E=5, which is the *in vitro* enhancement in condensin binding without H1.8. The H1.8 stoichiometry on nucleosome arrays in *Xenopus* egg extracts is around 0.5 (Jenness et al., 2018), which yields a similar predicted enrichment of around 1.7-fold. Moreover, this model indicates that removing

half the linker histones, *e.g* by phosphorylation, at experimentally observed stoichiometries would result in a ~2-fold increase in condensin enrichment.

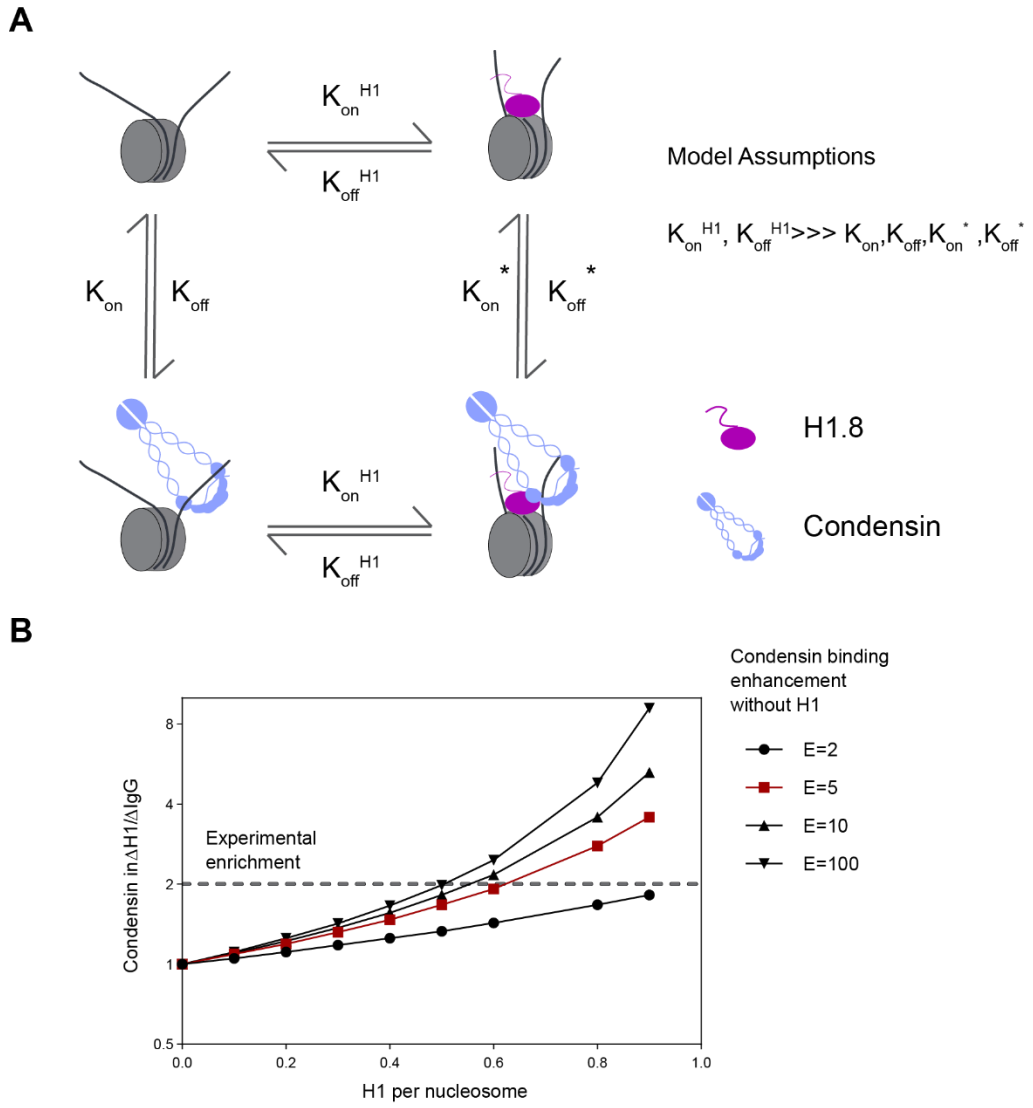

Figure 2-9 H1 stoichiometry and linker DNA competition determine condensin accumulation on chromatin

A) Simple equilibrium binding scheme for competition between H1.8 and condensin to bind linker DNA (left). The assumptions for the model, for H1 binding independent of condensin are shown (right). B) Increased condensin accumulation in the absence of H1 plotted against the two parameters, H1 stoichiometry (x-axis) and ratio of condensin binding strength without H1 to binding strength with H1.8. E=5, shaded in red represents the observed *in vitro* condensin binding enrichment to chromatin without H1.8.

H1.8 regulates chromosome length solely through condensin I accumulation on chromatin

H1.8 depletion results in chromosome elongation (Maresca et al., 2005) and condensin I controls chromosome length in *Xenopus* egg extracts (Shintomi and Hirano, 2011). I showed in the previous section that H1.8 suppresses the loading of both condensins on mitotic chromatin. To verify if the increased condensins result in chromosome elongation in ΔH1 extracts, I performed co-depletions of H1.8 and CAP-G (condensin I) or CAP-D3 (condensin II) and asked if this can rescue the chromosome elongation observed in H1.8 depleted extracts. The mitotic nuclei arrested in nocodazole (**Figure 2-1C**) are clusters of many chromosomes, and it is quite difficult to measure chromosome length in those clusters. To enable measurement of individual chromosome length, I dispersed the chromosomes by diluting metaphase extracts in buffer before fixing them with formaldehyde (Funabiki and Murray, 2000)(**Figure 2-10A**). This resulted in the formation of individual chromosomes, where I measured the chromosome length manually by tracing the chromosome contour (**Figure 2-10B**).

Chromosome length of individual chromosomes in mock (ΔIgG) extracts showed a modest variance since a mixture of all 18 chromosomes are being measured and plotted (**Figure 2-10C, D**). H1.8 depletion led to a ~50 % increase in chromosome length. This is consistent with previous reports (Maresca et al., 2005). Condensin I co-depletion (ΔH1ΔCAP-G) rescued this chromosome elongation. In fact, the chromosome length in these extracts was lower than those of control extracts. This phenotype is consistent with extracts containing substantially reduced condensin I (Shintomi and Hirano, 2011). Condensin II co-depletion (ΔH1ΔCAP-D3) did not change the chromosome length from those seen in ΔH1 extracts. This is also consistent with the lack of any effect of condensin II depletion (ΔCAP-D3) on chromosome length (**Figure 2-10E**).

These above experiments still do not completely establish whether H1.8 regulates chromosome length through condensin I. To test whether H1.8 regulates chromosome length independently of condensin I, I assembled mitotic chromosomes in the extracts containing varying concentrations of condensin I in the presence or absence of linker histone H1.8. If H1.8 controls chromosome length entirely through regulating the chromatin-binding of condensin I, chromosomes containing the same amount of condensin I should show the same chromosome lengths regardless of the H1.8 levels. Since condensin I loading is suppressed by H1.8, to load condensin I to chromosomes in ΔH1.8 extracts at the levels seen in control (ΔIgG) extracts, I assembled chromosomes in extracts where condensin I was partially depleted (**Figure 2-11A**). When mitotic chromosomes were assembled in ΔH1.8 extracts that contain 40 % (of ΔIgG) condensin I (CAP-G), condensin I level on these chromosomes was equivalent to those on chromosomes in control (ΔIgG) extracts (**Figure 2-11B**). Consistent with the hypothesis that H1.8 does not contribute to chromosome length regulation independently of condensin I, chromosome lengths are essentially identical between these two conditions (ΔH1 40 % CAP-G and ΔIgG) (**Figure 2-11C**). These chromosomes were substantially longer than the chromosomes in the ΔH1ΔCAP-G extracts that have significantly less condensin I on chromatin (**Figure 2-11B**). Similarly, partial reduction of condensin I in the presence of H1.8 (ΔIgG, 50% CAP-G) led to a small reduction in condensin I levels and chromosome length, and a partial reduction of condensin I in ΔH1 background (ΔH1, 70% CAP-G) led to no change in both condensin I on the chromatin compared to ΔH1 extracts and no change in the chromosome length. These results show that condensin I levels on chromatin alone control the chromosome lengths in *Xenopus* egg extracts. These results also clearly demonstrate that H1.8 controls mitotic chromosome lengths primarily through limiting the chromosome binding of condensin I.

Figure 2-10 Condensin I co-depletion rescues chromosome length elongation upon H1.8 depletion

A) Schematic of extract dilution to disperse individualized chromosomes. B) Schematic of chromosome tracing done to measure chromosome contour length. C) Representative images of mitotic chromosomes after dilution of indicated extracts. Bar, 10 μm. D) Quantification of the chromosome length. Data distribution of the length of individual chromosomes from three independent experiments (green, purple, grey) is shown. Each black dot represents the median length of chromosomes from a single experiment. Bar represents mean and S.E.M of three independent experiments. The length of >50 chromosomes were measured in each condition for every experiment. E) Chromosome length measurements from the indicated extracts. Each dot represents the length of a single chromosome. Bar represents median and error bars are 95 % confidence intervals.

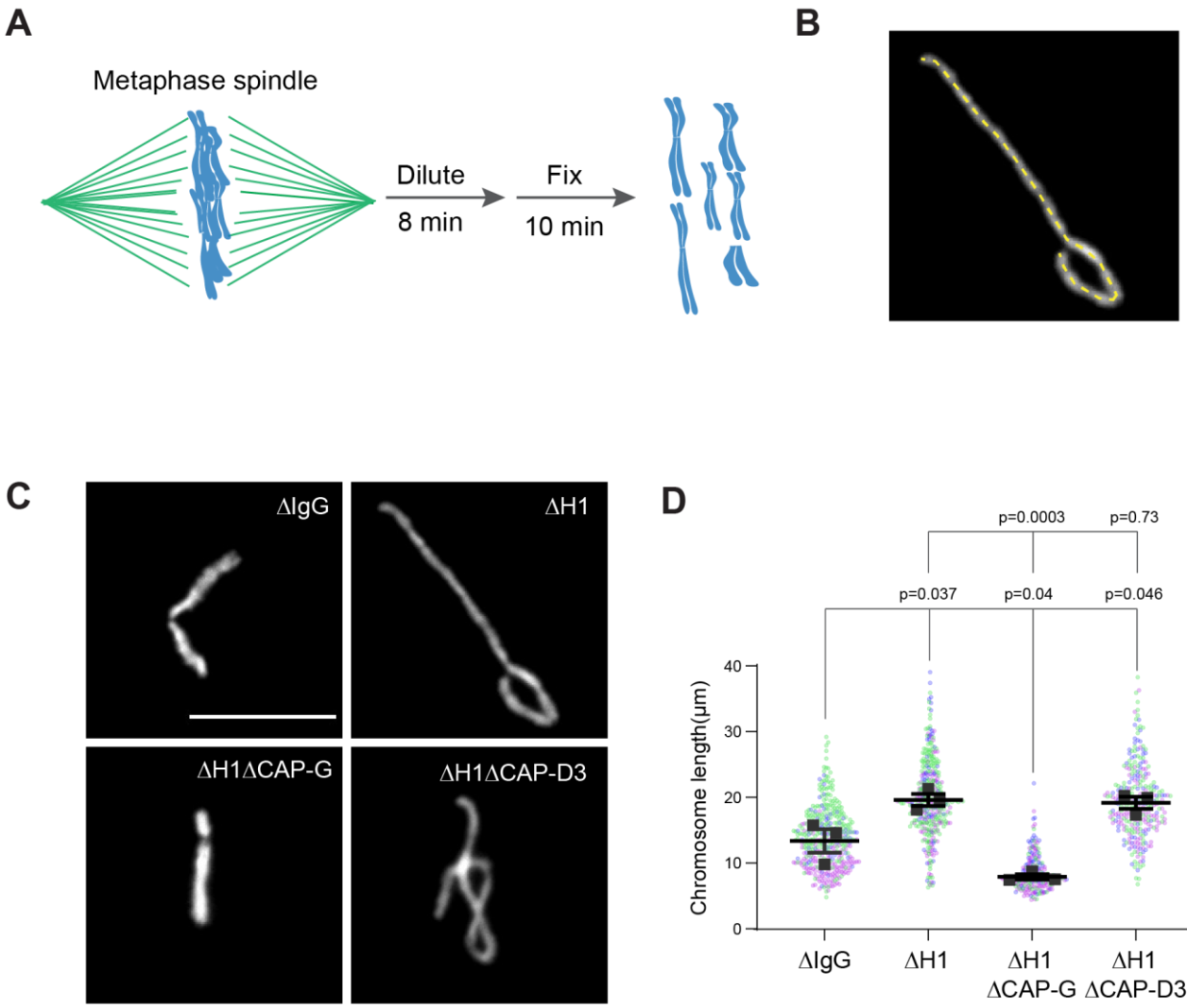
A
Metaphase spindle
Dilute
8 min
Fix
10 min
B
C
ΔIgG
ΔH1
ΔH1ΔCAP-G
ΔH1ΔCAP-D3
D
p=0.0003
p=0.73
p=0.037
p=0.04
p=0.046
Chromosome length(μm)
40
30
20
10
0
ΔIgG
ΔH1
ΔH1 ΔCAP-G
ΔH1 ΔCAP-D3
E
p=0.83
Chromosome length(μm)
30
20
10
0
ΔIgG
ΔCAP-D3

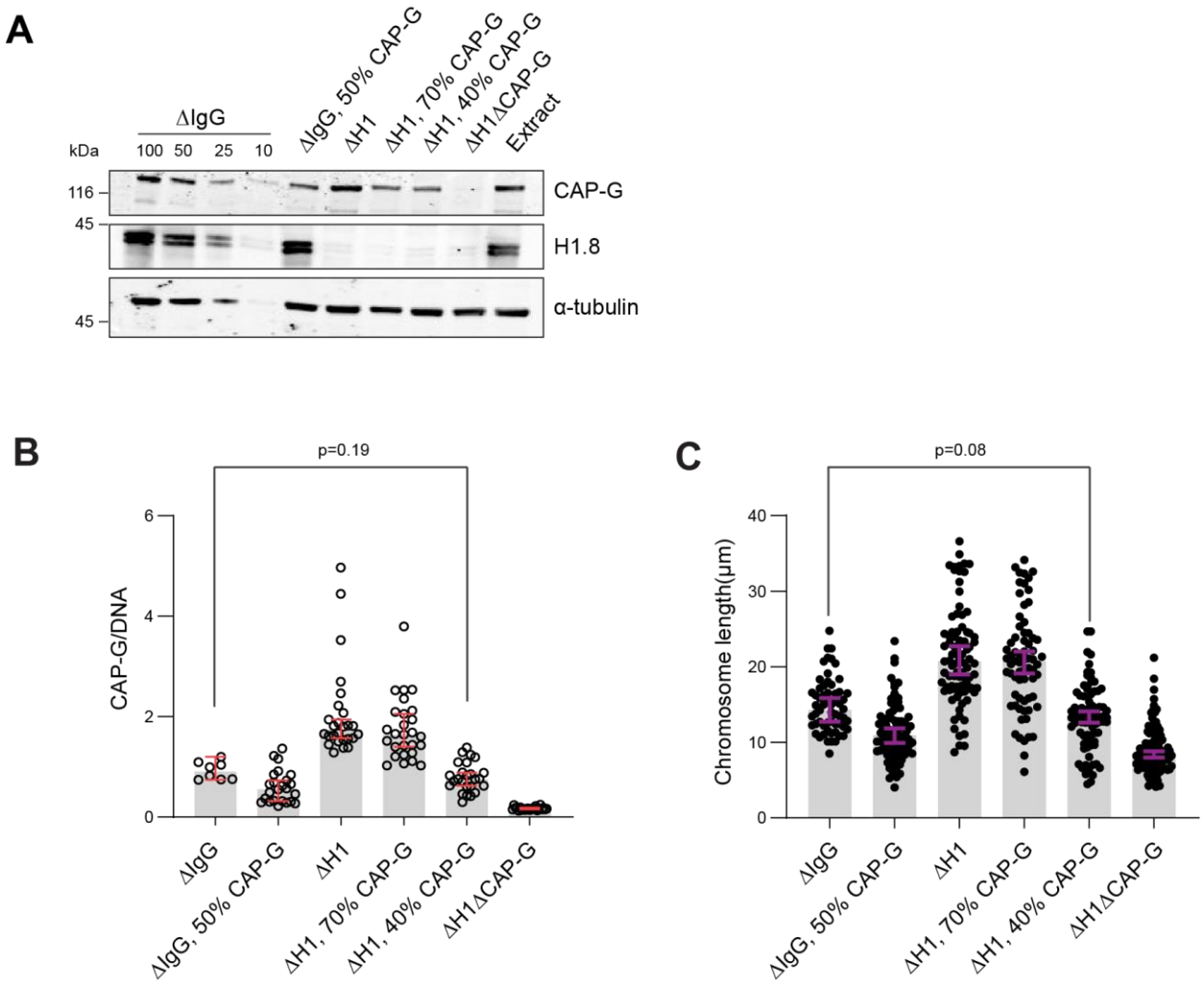

Figure 2-11 Condensin I levels on chromatin determine chromosome length

A) Total extract blots showing the condensin I levels in the indicated conditions. B) Quantification of condensin I (CAP-G) immunofluorescence levels on chromosomes normalized to DNA in indicated extracts. Each dot represents the average signal intensity of a single chromosome cluster (from one nucleus). Data plotted is median and 95 % C.I. >15 nuclei were quantified for each condition plotted. C) Chromosome length measurements from the indicated extracts. Each dot represents the length of a single chromosome. Bar represents median and error bars are 95 % confidence intervals. > 80 chromosomes were counted in each condition.

H1.8 suppresses long range chromosomal contacts

This work was performed with the help of Bastiaan Dekker in the Dekker lab at U. Mass Medical School.

Condensins organize mitotic chromosomes into loops (Gibcus et al., 2018; Naumova et al., 2013) and the number of condensins on mitotic chromatin controls chromosome length through changing the loop size (Goloborodko et al., 2016b). Since H1.8 seems to control chromosome length through changing condensin I loading on mitotic chromosomes, I wondered if H1.8 also changes the mitotic loop size on these chromosomes. Condensin I driven mitotic loops have not been visualized directly due to the compact organization of the mitotic chromosomes, however, the loop sizes have been inferred through their effect on the polymer structure of the chromosomal DNA (Naumova et al., 2013). To obtain more detailed information on the loop sizes and the effect of H1.8 on the higher order organization of the mitotic chromosome, I performed Hi-C on *Xenopus* extract chromosomes.

Hi-C is a member of the chromosomal conformation capture techniques which provide information about the proximity of chromosomal loci by detecting loci that are crosslinked through chromosomal contacts (Belton et al., 2012; Lieberman-Aiden et al., 2009). Using this proximity data, we can infer the underlying polymeric structure of the chromosomes in a variety of contexts (Fudenberg and Mirny, 2012; Gibcus et al., 2018; Naumova et al., 2013). To perform Hi-C, I generated replicated metaphase chromosomes in nocodazole treated extracts depleted of the indicated proteins. These chromosomes were then fixed in buffer containing 1% formaldehyde, collected by centrifugation, and processed for Hi-C library preparation and sequencing (**Figure 2-12A**). The Hi-C library preparation and sequencing were performed by Bastiaan Dekker and the analysis was done with the help of Bastiaan Dekker and Job Dekker.

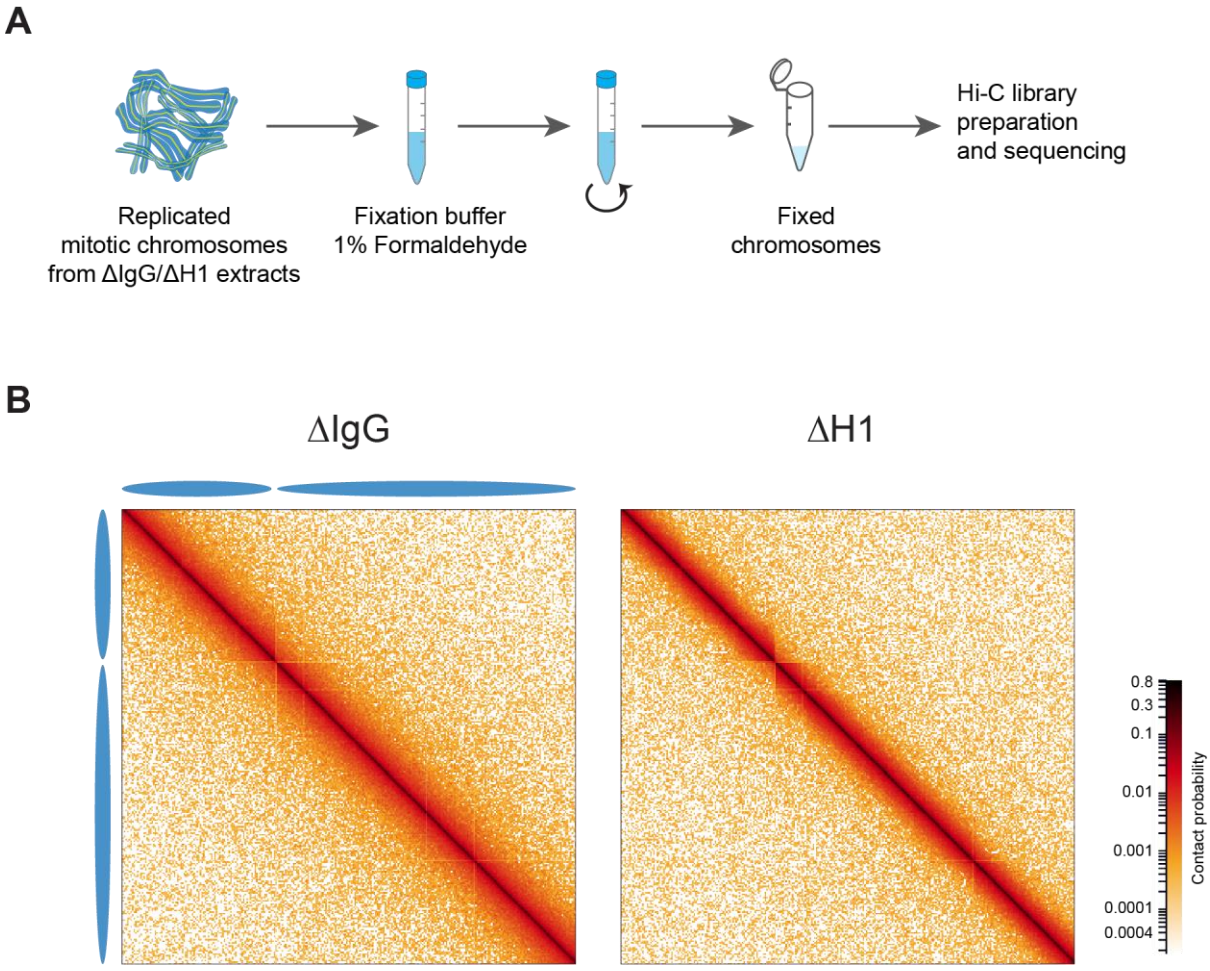

Figure 2-12 Hi-C on mitotic chromosomes prepared from *Xenopus* egg extracts

A) Schematic for performing Hi-C on replicated mitotic chromosomes from mock (ΔIgG) and H1.8 depleted (ΔH1) extracts. B) Hi-C maps showing pairwise interactions along representative mitotic chromosome 3S.

The chromosomal loci proximity data were normalized to the input and represented as a contact probability, which informs us of the likelihood of any given pair of loci being close enough in the mitotic chromosome to be crosslinked and ligated into the same species. The Hi-C contact probability was reported then as a Hi-C contact probability map (**Figure 2-12B**), where the axes of the square are the genomic loci of a single chromosome. Since there is no directionality to the interactions between the loci, the Hi-C maps are symmetrical across the main diagonal. As loci separated in the linear genome by a larger distance are generally less likely to interact in the actual nucleus (Finn et al., 2019; Fudenberg and Imakaev, 2017), the general feature of these maps is higher interactions at the main diagonal and decaying interactions further away from the diagonal. Interphase chromosomes are separated into active and passive compartments (Rao et al., 2014) which is indicated by a characteristic checkerboard pattern in Hi-C maps. Mitotic chromosomes are characterized by a loss of all compartmentalization (Naumova et al., 2013). Consistent with this, both control (ΔIgG) and H1.8 depleted (ΔH1) chromosomes showed no characteristic checkerboard pattern (**Figure 2-12B**).

The ΔH1 Hi-C map showed a narrower diagonal compared to the control (ΔIgG) chromosomes. This suggests that the long-distance interactions are reduced in these chromosomes. To quantify these differences, I plotted the average contact probability between any two loci as a function of the genomic distance between the two loci, P(s). Using this, I confirmed the observation that H1.8 depletion resulted in decreased interactions at longer genomic distances (**Figure 2-13A**). The contact probability decay curves were also consistent among two biological replicates. The Hi-C maps and the subsequent contact probability curves were also consistent among all the chromosomes (**Figure 2-13B, C**).

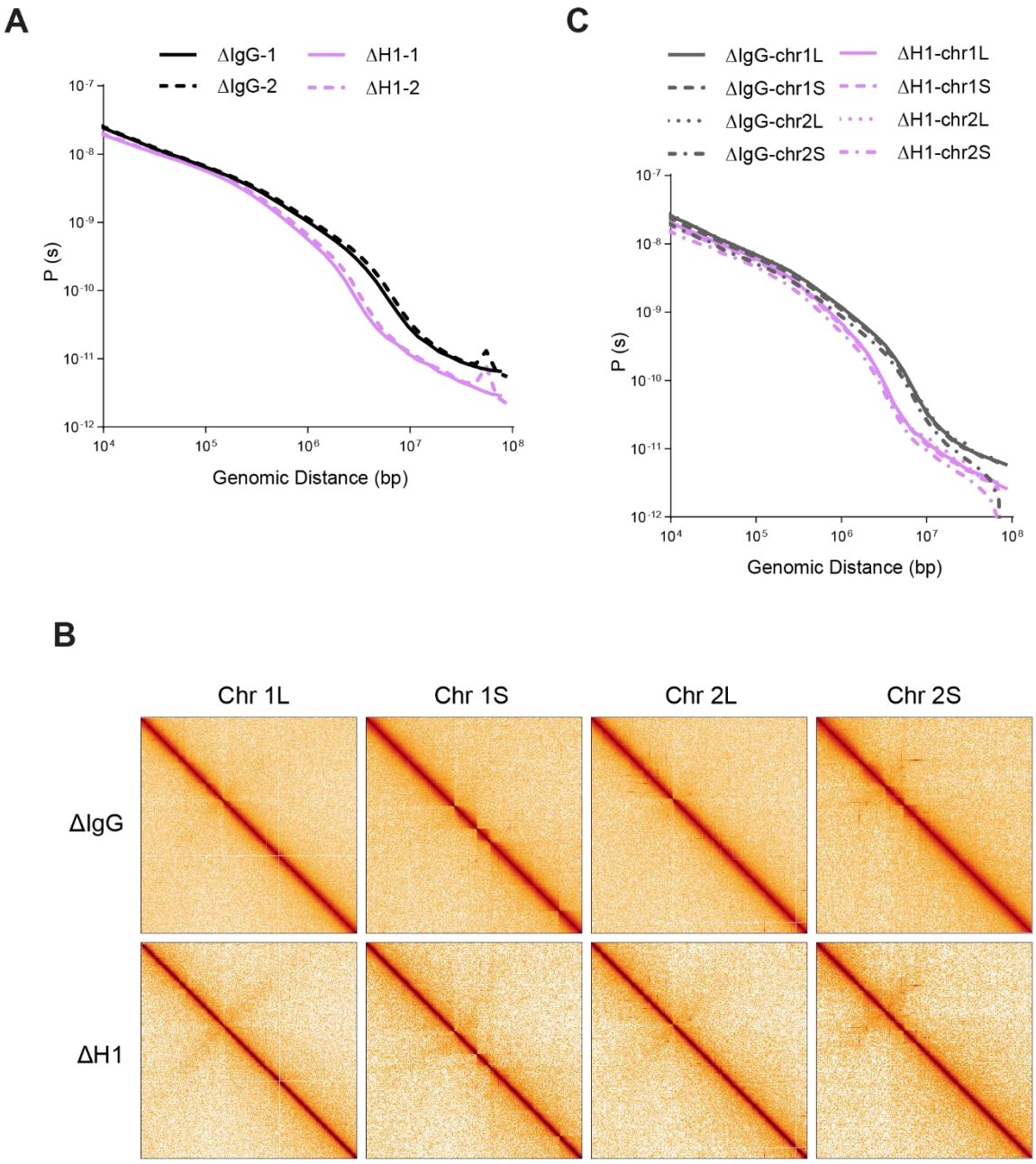

Figure 2-13 H1.8 depletion reproducibly reduces long range contacts in all chromosomes

A) Contact probability curves from mock (ΔIgG) and H1.8 depleted (ΔH1) extracts from two independent experiments. B) Hi-C maps in the indicated conditions for four different chromosomes. C) Contact probability curves from the Hi-C maps in B) showing the consistent changes in long range contacts.

H1.8 suppresses layer size through condensin I

I then asked if these changes in chromosome structure are mediated by condensin I or condensin II. To do this, first I performed Hi-C on samples depleted of either CAP-G (condensin I) or CAP-D3 (condensin II). The Hi-C maps for these conditions show that condensin I depletion (ΔCAP-G) resulted in a dramatic expansion of the diagonal, indicating increased interactions at longer distances (**Figure 2-14A**). Condensin II depletion (ΔCAP-D3) did not have a significant impact on the interaction maps.

The mitotic chromosome is composed as an array of condensin driven loops (Earnshaw and Laemmli, 1983; Naumova et al., 2013) that is arranged in layers (Gibcus et al., 2018). Uniform polymeric structures result in a linear slope in the log-log contact probability map. So, the mitotic chromosome is composed of three distinct linear regimes (**Figure 2-14B**). The first linear regime, which contains contacts among loci that are present within a single condensin I driven loop, extends up to ~ 100 kb and is called the intra-loop regime. The second inter-loop regime, which describes contacts among multiple loops in a single layer, is characterized by a slight increase in the slope of the P(s) curve. This is due to the fact that interactions among loci that are separated by more than one loop size are comparatively rarer. The third regime, which characterizes inter-layer interactions, is accompanied by the steep increase in the slope of the P(s) curve. This results from the increased separation provided by the hierarchical loop array structure of a mitotic chromosome. Condensin I depletion (ΔCAP-G) resulted in an overall flattening of the P(s) curve, consistent with the role of condensin I in organization of the loop array. Condensin II depletion (ΔCAP-D3) had no effect on the shape of the P(s) curve. This is as predicted from the reduced role of condensin II in *Xenopus* egg extracts in chromosome length regulation (**Figure 2-10E**)(Shintomi and Hirano, 2011).

To quantify the changes in the loop organization in these chromosomes, I plotted the derivative curve which is the slope of the P(s) curve. As the slope of the P(s) curve drops sharply in the inter-layer regime, this results in a sharp drop in the derivative plot. This reduction in slope occurs at the genomic distance indicated by the amount of DNA in each layer of DNA loops (**Figure 2-14C**). Using this, I estimated the amount of DNA in each layer as the layer size in each condition (**Figure 2-14D**). The layer size drastically increased upon condensin I depletion (ΔCAP-G) and was unaffected by condensin II depletion (ΔCAP-D3). H1.8 depletion (ΔH1) resulted in a 1.5-fold smaller layer size. This is consistent with the 1.5-fold increase in chromosome length in control extracts as compared to ΔH1 extracts.

Next, I asked whether co-depletion of condensin I or condensin II can rescue the ΔH1 chromosome phenotypes. I prepared mitotic chromosome samples from H1, condensin I (ΔH1ΔCAP-G) and H1.8, condensin II (ΔH1ΔCAP-D3) co-depleted extracts and Bastiaan Dekker prepared the Hi-C libraries and sequenced them. The Hi-C maps show that condensin I co-depletion (ΔH1ΔCAP-G) rescued long range interactions (**Figure 2-15A**), whereas condensin II co-depletion (ΔH1ΔCAP-D3) did not seem to change the interaction map. This is quantitatively seen in the P(s) curves (**Figure 2-15B**), where the ΔH1ΔCAP-G samples showed increased long-range interactions, whereas ΔH1ΔCAP-D3 curve overlaps almost completely with the ΔH1 sample curve. I then went on to ask if the layer sizes in these samples correspond to the observed chromosome lengths (**Figure 2-10D**). The derivative plots for these samples are shown in **Figure 2-15C** and the estimated layer sizes show the predicted rescue of layer size in ΔH1ΔCAP-G samples and the lack of any change in the ΔH1ΔCAP-D3 samples (**Figure 2-15D**). This is once again consistent with the observed chromosome length phenotypes where only condensin I co-depletion (ΔH1ΔCAP-G) rescued the chromosome length. The increased layer size beyond the control in these extracts is also consistent with the shorter stubbier chromosomes in this condition as well.

Figure 2-14 Condensin I controls long range contacts and the layer size

A) Hi-C maps of representative mitotic chromosome 3S in the indicated condition. B) Genome wide average contact probability curves in the indicated conditions. C) Derivative plots of the genome average contact probabilities in B) showing the measurement of layer sizes from the location of the derivative minima. D) Layer size estimates from two independent experiments showing the large increase in layer size upon condensin I depletion.

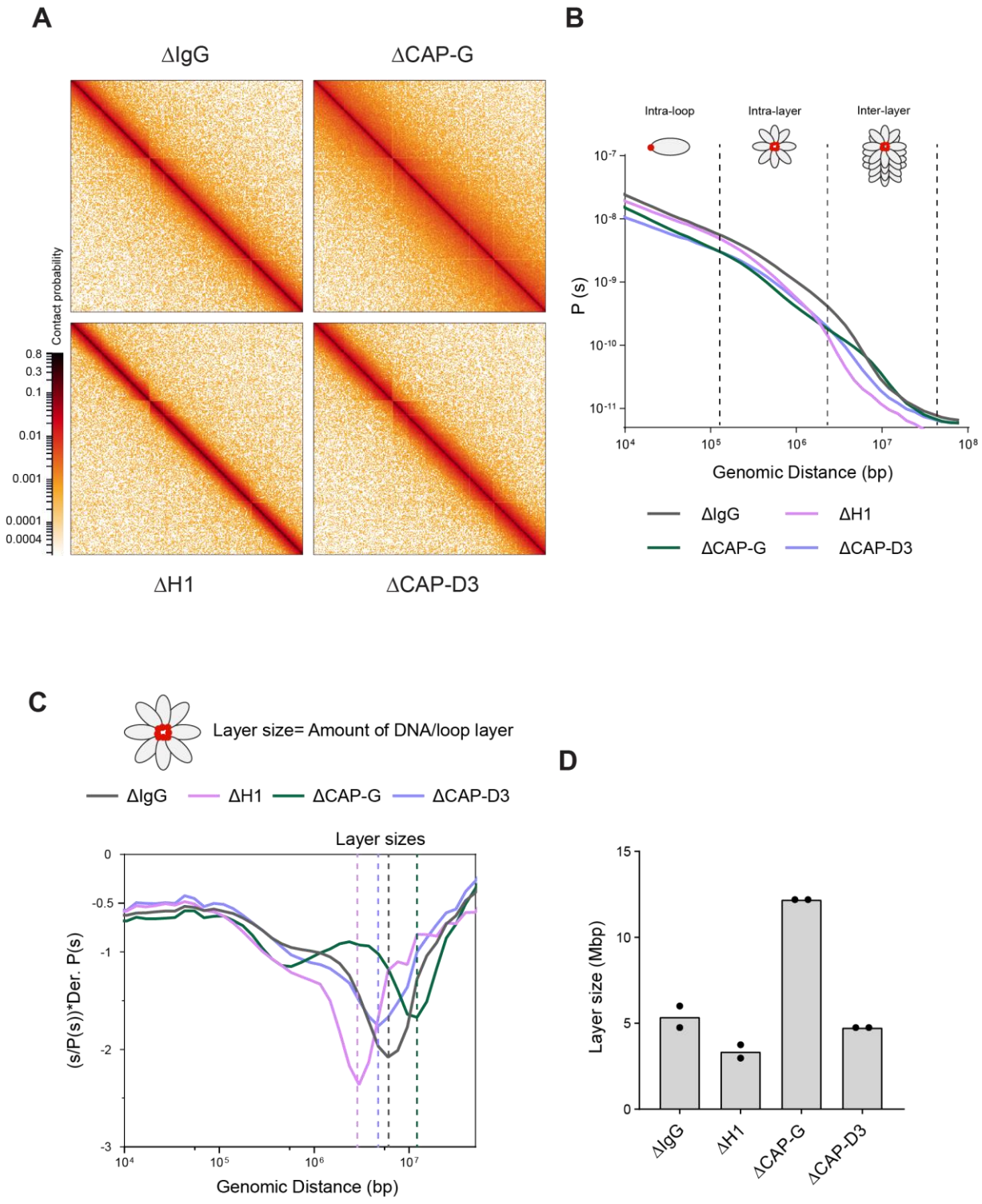
A
ΔIgG
ΔCAP-G
ΔH1
ΔCAP-D3
Contact probability
0.8
0.3
0.1
0.01
0.001
0.0001
0.0004
B
Intra-loop
Intra-layer
Inter-layer
P (s)
Genomic Distance (bp)
ΔIgG
ΔH1
ΔCAP-G
ΔCAP-D3
C
Layer size= Amount of DNA/loop layer
ΔIgG
ΔH1
ΔCAP-G
ΔCAP-D3
Layer sizes
(s/P(s))*Der. P(s)
Genomic Distance (bp)
D
Layer size (Mbp)
ΔIgG
ΔH1
ΔCAP-G
ΔCAP-D3

Figure 2-15 Condensin I co-depletion rescues layer size upon H1.8 depletion

A) Hi-C maps of representative mitotic chromosome 3S in the indicated condition. B) Genome wide average contact probability curves in the indicated conditions. C) Derivative plots of the genome average contact probabilities in B) showing the measurement of layer sizes from the location of the derivative minima. D) Layer size estimates from two independent experiments showing the large increase in layer size upon condensin I depletion.

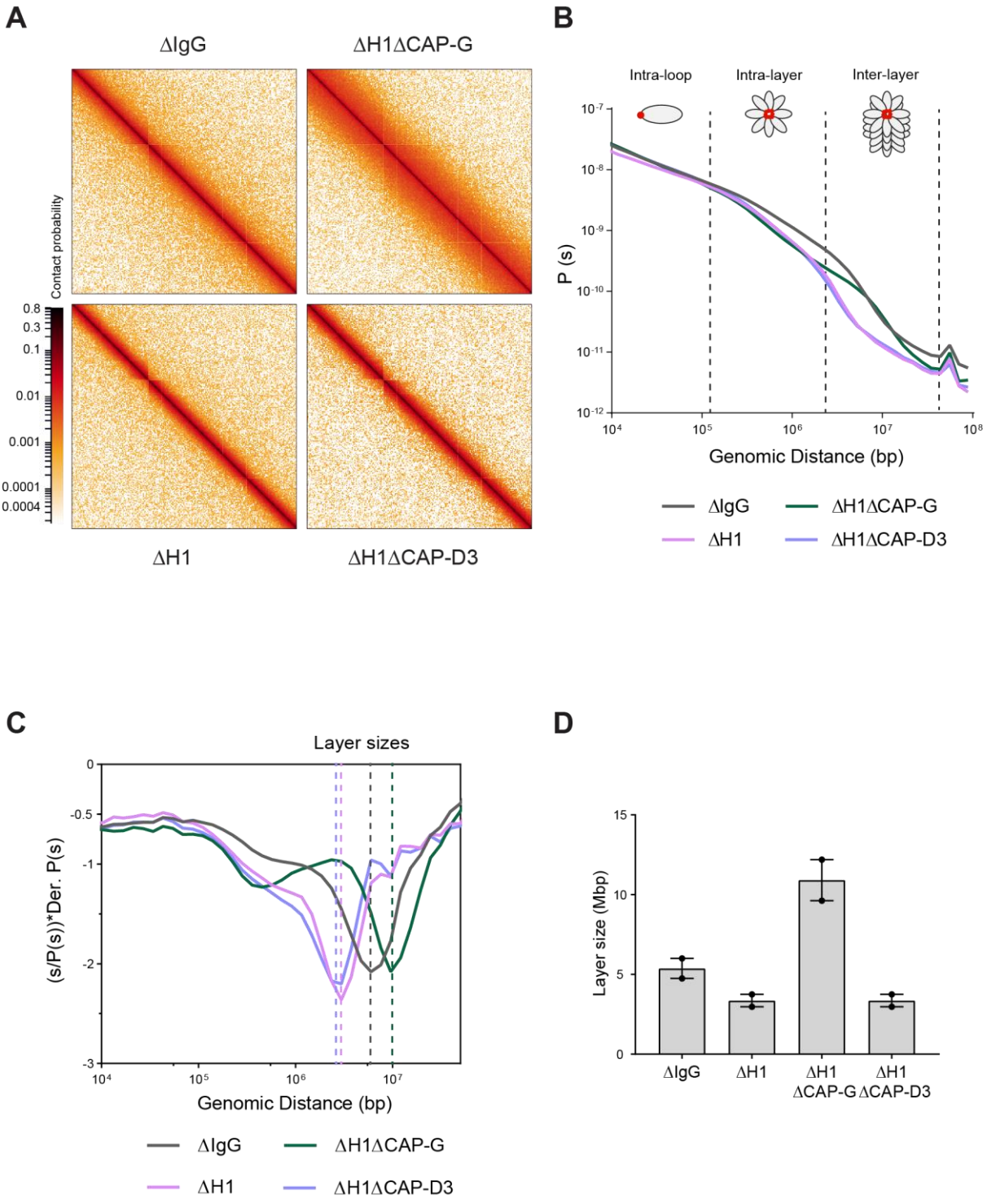
A
ΔIgG
ΔH1ΔCAP-G
Contact probability
0.8
0.3
0.1
0.01
0.001
0.0001
0.0004
ΔH1
ΔH1ΔCAP-D3
B
Intra-loop
Intra-layer
Inter-layer
P (s)
Genomic Distance (bp)
ΔIgG
ΔH1ΔCAP-G
ΔH1
ΔH1ΔCAP-D3
C
Layer sizes
(s/P(s))*Der. P(s)
Genomic Distance (bp)
ΔIgG
ΔH1ΔCAP-G
ΔH1
ΔH1ΔCAP-D3
D
Layer size (Mbp)
ΔIgG
ΔH1
ΔH1 ΔCAP-G
ΔH1 ΔCAP-D3

Condensin I enrichment on chromatin controls loop size

The Hi-C data discussed in the previous section adds to the observations from the chromosome morphology measurements in showing the dominant role of condensin I in maintaining mitotic chromosome morphology in *Xenopus* egg extracts. Since condensin I regulates chromosome morphology through its loop extrusion activity, increased condensin I loading in ΔH1 extracts is predicted to result in smaller average loop sizes (Goloborodko et al., 2016b). This is thought to occur due to the condensin molecules encountering another condensin molecule earlier during loop extrusion. Although recent reports indicate yeast and bacterial condensin molecules appear to be able to pass each other during extrusion (Brandão et al., 2020; Kim et al., 2020), increased condensin loading still appears to reduce loop size experimentally (Fitz-James et al., 2020). So, I asked if the loop size is indeed reduced in ΔH1 extracts.

Average mitotic loop size can be estimated from the location of the peak in the derivative plots (Gassler et al., 2017; Patel et al., 2019). I therefore looked for a peak in the 10 kb-1 Mb range of the derivative plots. The peak in ΔH1 extract samples was shifted to the left as compared to the peak in the control (ΔIgG) extract samples (**Figure 2-16A**). Since the peak is relatively flat, this made it difficult to get an accurate estimate of the loop size. However, the data showed a consistent shift towards a smaller peak size in both biological replicates for the ΔH1 samples. This suggests that the condensin-driven loops are indeed smaller upon H1.8 depletion, as I expected from the increased condensin loading.

I then also repeated this analysis in Hi-C data generated from dispersed chromosome samples. To generate these samples, the extracts containing the mitotic chromosomes (not treated with nocodazole) were diluted in chromosome dilution buffer to disperse the chromosomes before fixing them (**Figure 2-16B**). The chromosomes were then collected and processed for Hi-C library preparation and sequencing. The derivative plots from these samples

were largely similar to those from the undispersed nocodazole treated nuclei (**Figure 2-16C**). However, these chromosomes showed a more distinct peak in the expected range enabling a more accurate loop size estimate. These derivative plots show that an average loop size of ~140 kb in control (ΔIgG) chromosomes was reduced to ~110 kb in ΔH1 chromosomes, supporting the reduced loop size observation from the undispersed samples.

I then asked if increased condensin loading by other mechanisms also leads to reduced loop sizes. As discussed previously, nucleosomes inhibit condensin loading (Shintomi et al., 2017; Toselli-Mollereau et al., 2016a; Zierhut et al., 2014). To ask if loss of nucleosomes reduces loop size, I depleted H3-H4 tetramers from *Xenopus* extracts using an antibody to the acetylated lysine-12 of histone H4 (H4K12ac) (Zierhut et al., 2014) (**Figure 2-17A**). Since *X. laevis* sperm is preloaded with paternal H4-H4 tetramers, this depletion leads to at most ~50% decrease in total H3-H4 from the mitotic chromosomes. Since histones occupy such a large fraction of the chromosomal DNA, this led to substantially increased condensin I enrichment even compared to H1.8 depletion (**Figure 2-17B**). I then asked if the loop size is indeed reduced upon H3-H4 depletion. Consistent with this expectation, the peak showed a large leftward shift upon H3-H4 depletion (**Figure 2-17C**). The loop size in these samples is reduced to ~ 12 kb. This marked reduction in loop size even compared to ΔH1 chromosomes is also consistent with the large increase in condensin loading beyond that observed in ΔH1 chromosomes. This suggests that both core histones and the linker histone H1.8 regulate mitotic chromosome shape by regulating condensin I loading.

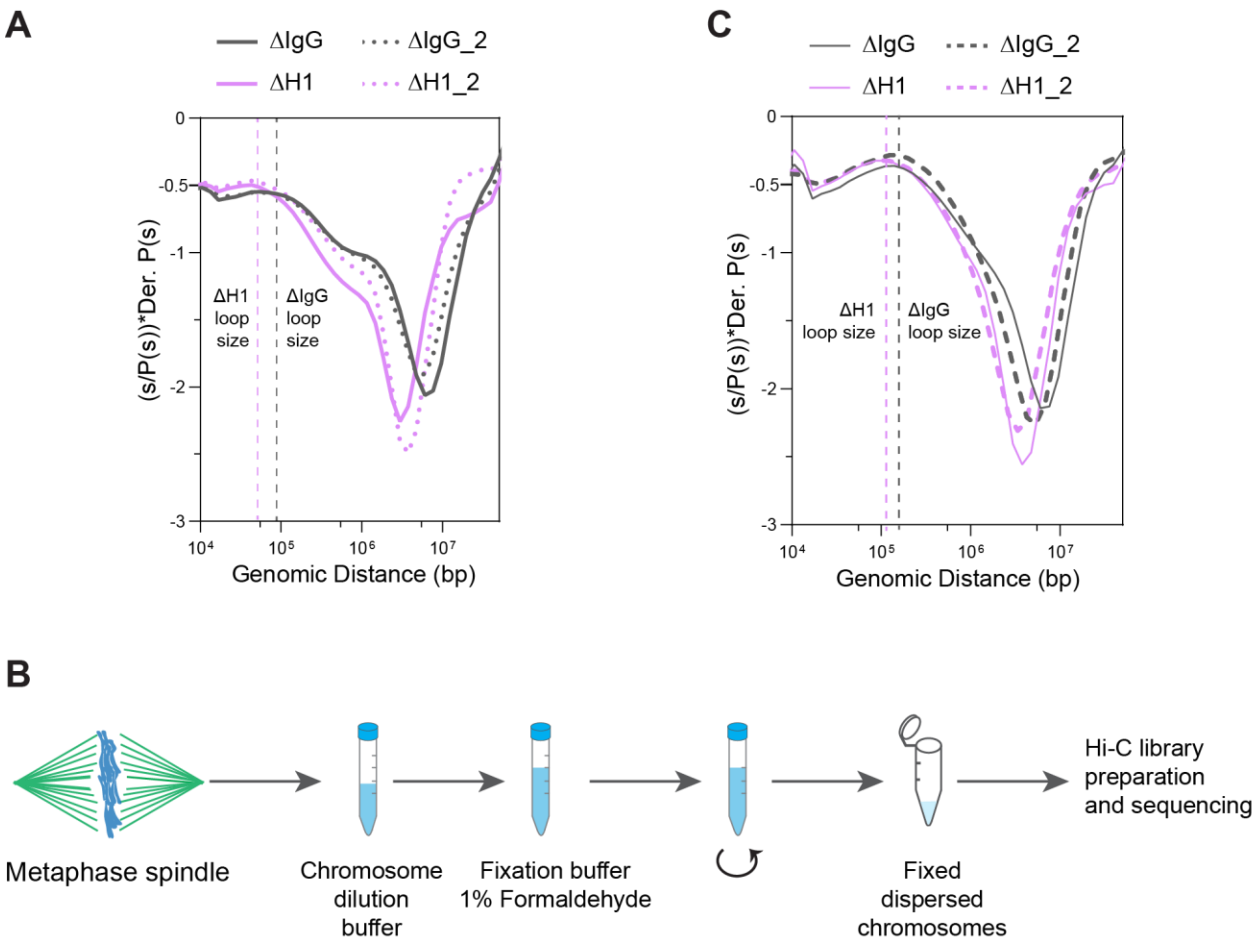

Figure 2-16 H1.8 depletion reduces the average loop size in mitotic chromosomes

A) Derivative plots in the mock (ΔIgG) and H1.8 depleted (ΔH1) chromosomes from two independent experiments showing the reproducible leftward shift in peak location. B) Protocol to perform Hi-C on dispersed chromosomes. C) Derivative plots from genome wide average contact probability in dispersed chromosomes showing the leftward shift of a distinct peak upon H1.8 depletion.

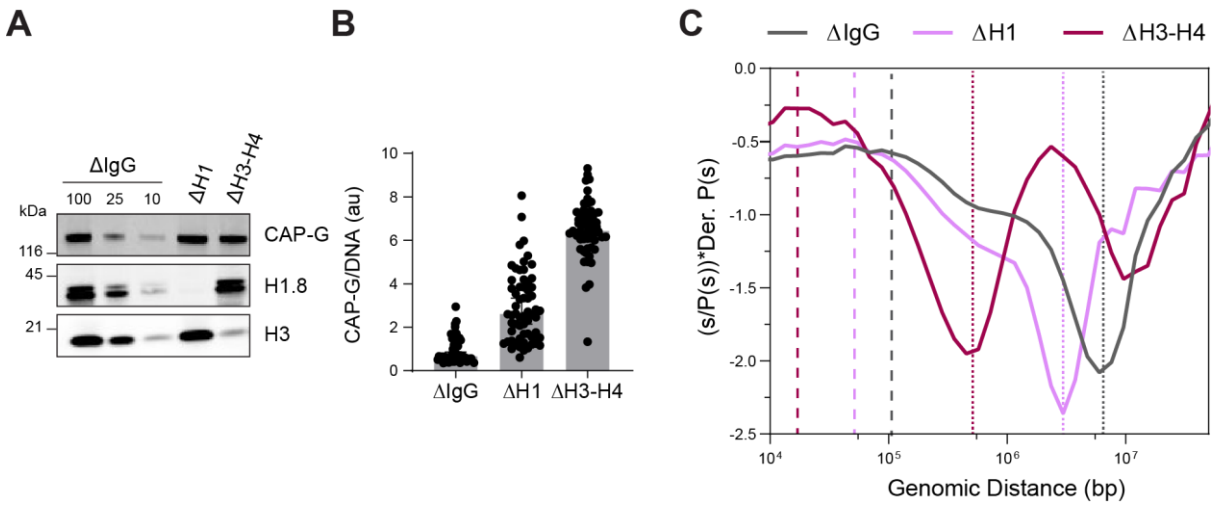

Figure 2-17 H3-H4 depletion further reduces loop size

A) Western blotting showing the depletion of H3-H4 in extract using the H4K12ac antibody (Zierhut et al., 2014). B) Quantification of condensin I (CAP-G) immunofluorescence levels on chromosomes normalized to DNA in ΔH1 and ΔH3-H4 extracts. Each dot represents the average signal intensity of a single chromosome cluster (from one nucleus). Data plotted is median and 95 % C.I. >40 nuclei were quantified for each condition plotted. C) Hi-C probability decay derivative plots estimating the loop sizes in ΔH1 and ΔH3-H4 extracts. The dashed lines indicate the loop sizes in the corresponding conditions. The dotted lines indicate the layer sizes.

Condensin II activity is suppressed in the presence of condensin I

Chromosome length measurements (Shintomi and Hirano, 2011, **Figure 2-10, 2-11**) suggest that condensin II plays a minor role in the presence of condensin I. Condensin II plays a significant role in DT40 cells, where it forms the outer loops of the nested loops that organize the mitotic chromosome (Gibcus et al., 2018; Green et al., 2012). Condensin II also generates the helical chromosome axis around which the condensin I loops are organized. This helical organization, detected as a second diagonal in Hi-C maps, results in a second peak in the derivative plots around the layer size (Gibcus et al., 2018). In mock depleted extracts (ΔIgG), this peak appears to have flattened into a shoulder (**Figure 2-18A**). This is consistent with the reduced role of condensin II in this background. Condensin I depletion (ΔCAP-G) surprisingly generates a second peak, suggesting a stronger helical organization but condensin II co-depletion (ΔCAP-GΔCAP-D3) has only a small effect on this peak. However, this may be due to incomplete condensin II depletion using the CAP-D3 antibody (**Figure 3-3A**).

Loss of H1.8 mediated suppression of condensin II did not result in a second diagonal (**Figure 2-18B**) suggesting that the increased condensin I in this condition still outcompetes condensin II. But the second peak reappears upon condensin I co-depletion (ΔH1ΔCAP-G) and the peak is suppressed by condensin II co-depletion (ΔH1ΔCAP-GΔCAP-D3). Taken together, this suggests that condensin II activity is indeed suppressed by both H1.8 and condensin I individually and that in wildtype conditions for both H1.8 and condensin I, condensin II plays a minimal role.

Both condensins promote rod-like structure of mitotic chromosome

Mitotic chromosomes, unlike interphase chromosomes, are arranged into a rod like structure. This serves two purposes, maintaining mechanical rigidity to survive spindle forces and to enable resolution of sister chromatids (Gerlich et al., 2006; Nagasaka et al., 2016). Rod like chromosomes are characterized by the formation of layered loop organization that matures during prometaphase (Gibcus et al., 2018; Naumova et al., 2013). This layered organization prevents inter-layer contacts and more rod like chromosomes are characterized by lower inter-layer contacts and more globular, interphase like, chromosomes have higher inter-layer contacts (**Figure 2-19A**). To quantify how layered the chromosomes are, I created a metric called the inter-layer insulation score. To do this, I used the contact probability derivatives. The local derivative value is representative of the underlying polymeric structure. Lower derivative values are indicative of a more ordered structure that prevents long range interactions. Thus, I defined the inter-layer insulation score as the difference between the lowest inter-layer contact probability derivative (representing the steepest drop off in intra-layer contacts) and the average intra-layer contact probability derivative at the range of 10 – 100 kb (representing chromatin intrinsic probability decay) (**Figure 2-19B**).

Consistent with its effect on the layer size, condensin I depletion (ΔCAP-G) reduced the insulation score (**Figure 2-19C**). However, unlike the layer size, condensin II co-depletion (ΔCAP-GΔCAP-D3) had a small effect on the insulation score. This suggests that although condensin I mainly organizes the rod-like chromosomes, condensin II also plays a smaller role in this process. As expected from increased loading of both condensins upon H1.8 depletion, ΔH1 chromosomes had a higher insulation score. Both condensin I co-depletion (ΔH1ΔCAP-G) and condensin II co-depletion (ΔH1ΔCAP-D3) partially reduced the rigidity. In contrast to the chromosome length rescues, the ΔH1ΔCAP-G chromosomes were still more rigid that control (ΔIgG) chromosomes. Condensin II appears to plays a large role in this rigidity as

condensin II co-depletion (ΔH1ΔCAP-GΔCAP-D3) significantly reduced the insulation score. The difference in the insulation score between chromosomes from ΔCAP-GΔCAP-D3 and ΔH1ΔCAP-GΔCAP-D3 chromosomes suggests a possible condensin independent method of rigidity upon H1.8 depletion. However, since depletion of neither condensin I nor II is complete, it is difficult to eliminate the role of the remaining condensins in this process.

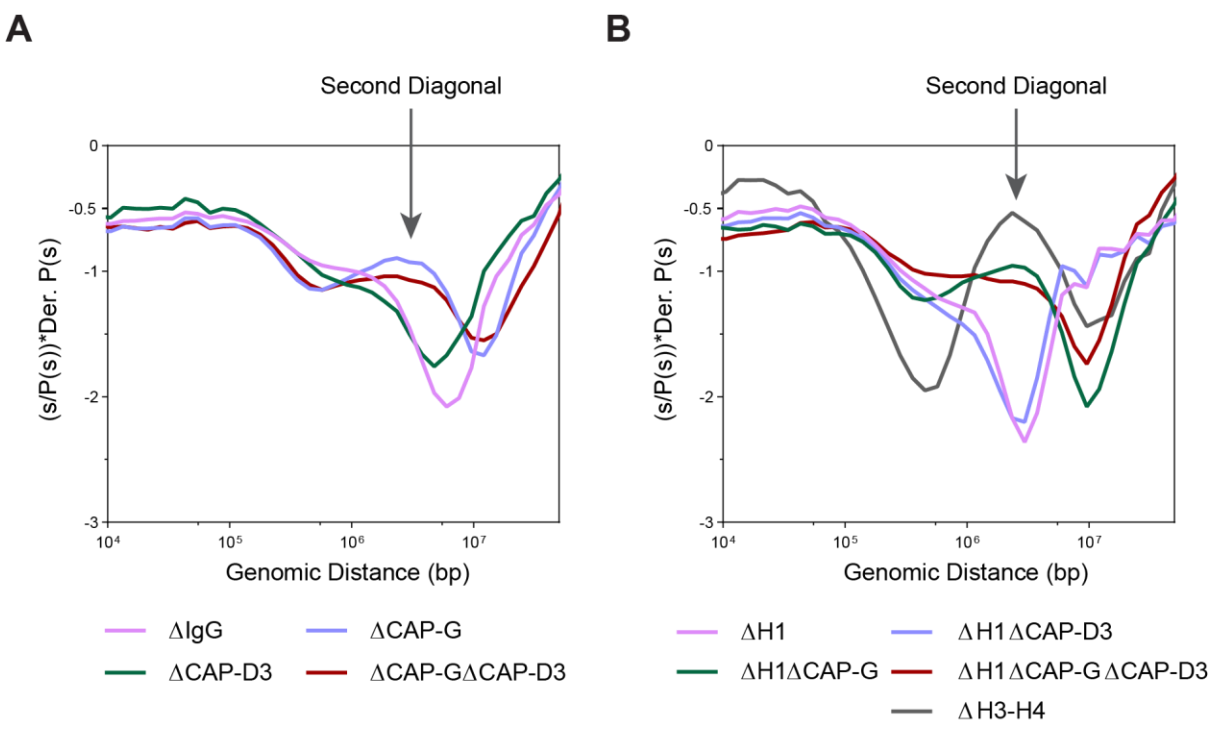

Figure 2-18 H1.8 suppresses helical organization through suppressing condensin II activity

A) and B) Derivative plots upon depleting condensins in control (ΔIgG-A) and H1.8 depletion (ΔH1-B) backgrounds. The height of the second diagonal represents the strength of the helicity of the condensin I loop anchors. H1.8 and condensin I both suppress condensin II which is responsible for the helical organization.

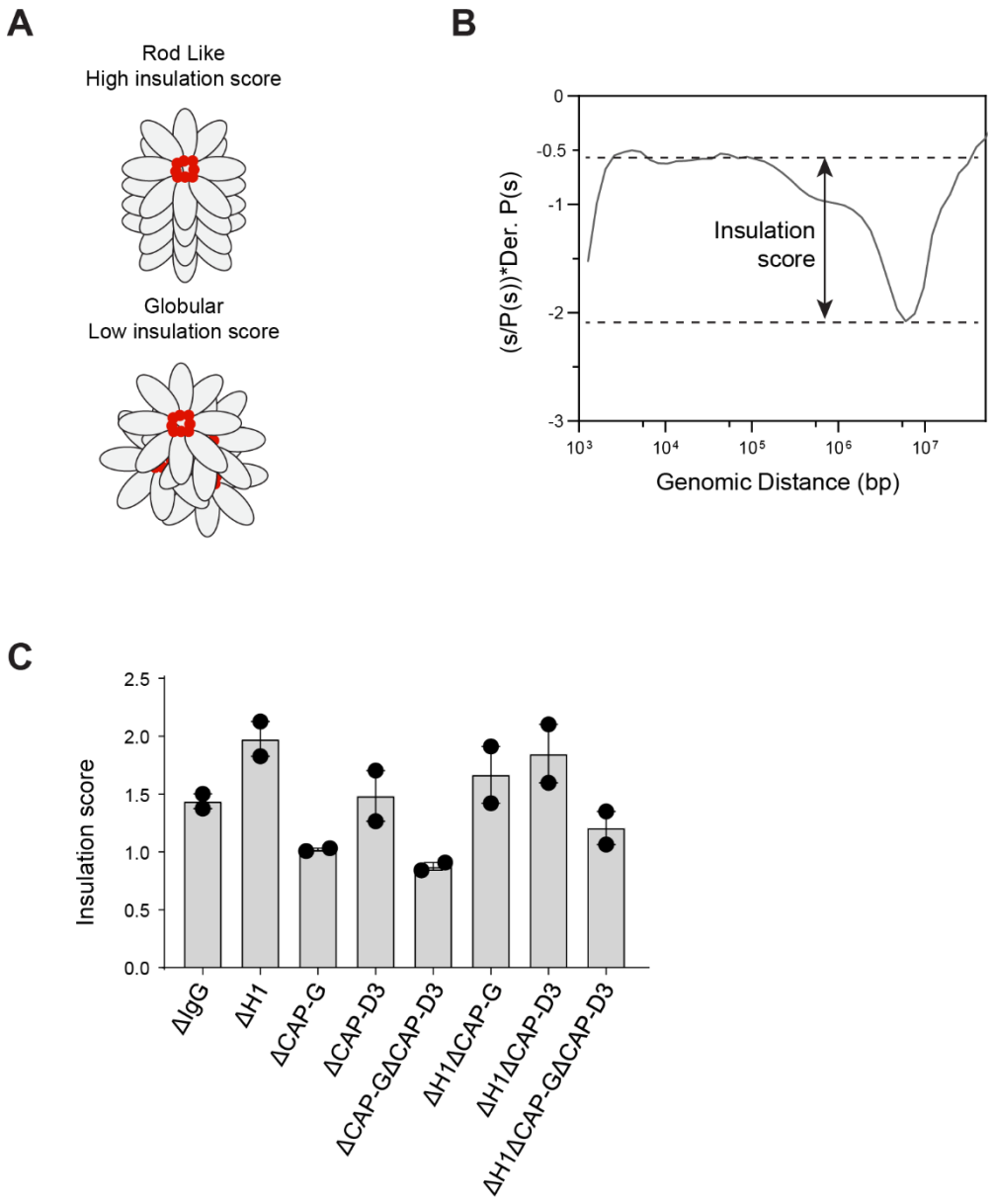

Figure 2-19 H1.8 regulates chromosomes rigidity through condensins

A) Schematic showing rigid chromosomes prevent inter-layer contacts. B) Schematic to show calculation of the insulation score from derivative plots. C) Insulation scores in the indicated conditions. Each dot represents the insulation score from each independent biological replicate.

Discussion and Perspective

Regulating condensin enrichment on chromatin

Mitotic chromosomes are organized into DNA loops by condensins (Earnshaw and Laemmli, 1983; Gibcus et al., 2018). Condensins prefer to bind naked DNA over nucleosomal DNA (Kong et al., 2020; Zierhut et al., 2014). Since the eukaryotic genome is wrapped up in histones, condensins show preferential accumulation at nucleosome free regions (Sutani et al., 2015; Toselli-Mollereau et al., 2016a). This suggests a possible mechanism for regulating condensin accumulation on the chromatin by modulating the nucleosome free regions on the mitotic chromosome. Outside of nucleosome free regions at promoters and other transcription factor bound sites used perhaps for bookmarking (Teves et al., 2016), a large amount of linker DNA is available for binding between nucleosomes. Linker histones are an abundant class of chromatin binding proteins that prefer to bind nucleosomes at or near the nucleosome dyad (Bednar et al., 2017; Zierhut et al., 2014). Linker histones are also a much more dynamic chromatin binding protein than core histones (Hergeth and Schneider, 2015; Kimura and Cook, 2001; Misteli et al., 2000). If linker histones can compete with condensins for binding to the linker DNA, this represents a more readily accessible form of regulating DNA binding sites for proteins that prefer to bind naked DNA.

Since condensin I enrichment on chromatin leads to longer chromosomes (Shintomi and Hirano, 2011), I asked whether H1.8 mediated blocking of condensin I is responsible for the reported chromosome elongation in this condition (Maresca et al., 2005). Previous reports didn't indicate any change in major chromatin binding proteins in the absence of H1.8 (Maresca et al., 2005). However, these studies did not quantify these changes carefully. Since condensin stoichiometrically forms mitotic loops (Ganji et al., 2018; Golfier et al., 2020), this suggests that a ~50% increase in condensin binding has a large change in the chromosome length

(Goloborodko et al., 2016b). I addressed this concern by careful quantitative immunofluorescence microscopy (**Figure 2-1**) and showed that both condensin I and condensin II shows at least a ~2-fold increase in binding upon H1.8 depletion. I then enquired whether this observed increase in condensins is shared with other chromatin binding proteins. Proteins that bind chromatin can be split into two broad categories, ones that prefer to bind nucleosomal DNA, and ones that prefer to bind naked DNA (Zierhut et al., 2014). Choosing two representative members of these classes, I showed that these proteins do not show a similar increase in chromatin affinity in the absence of H1.8 (**Figure 2-2**). However, unlike nucleosome binding proteins, DNA-binding proteins do show some increase in binding mitotic chromatin upon depletion of H1.8. Condensins are among the most abundant proteins on mitotic chromosomes (Hirano and Mitchison, 1994), so this suggests that the larger increase in binding of condensins over these proteins may be a result of the different abundance and binding strength among these proteins. Condensins also show additional more stable modes of binding DNA after binding ATP (Cutts and Vannini, 2020; Datta et al., 2020). These additional binding modes may lead to stronger apparent binding affinity for condensins over other non-specific DNA binding proteins. The immunofluorescence data of these other proteins also confirms that there is no systematic error in the measurement due to antibody accessibility or change in chromosome structure in the absence of H1.8. I also verified this increase in binding of condensins orthogonally by purifying mitotic chromosomes and performing quantitative western blots (**Figure 2-3**).

Condensin II depletion does not affect the condensin I on chromatin (**Figure 2-4**), confirming previous observations (Ono et al., 2003; Shintomi and Hirano, 2011). However, depleting condensin I results in a small increase in condensin II on chromatin both in ΔIgG and ΔH1 backgrounds. This suggests that the condensin II competes with condensin I for chromatin

binding sites. Since condensin I is much more abundant than condensin II (Shintomi and Hirano, 2011), condensin II depletion doesn't seem to affect condensin I loading on chromatin.

Although the immunofluorescence and biochemistry data showed the expected changes in condensins upon H1.8 depletion, the existence and significance of any direct competition between linker histone and condensins was still in question. I addressed this problem by performing *in vitro* reconstitutions using purified human condensins (purified by Dr. Erin Cutts, ICR London). The binding properties of human condensins to nucleosomal DNA in various conditions has still not been studied in much detail previously. Previous reports have confirmed the preference affinity for naked DNA over nucleosomal DNA (Kong et al., 2020) at the mononucleosomal level, however the role of higher order structures that nucleosome arrays can exhibit was still unknown.

Nucleosome arrays show both ordered and disordered compaction upon addition of magnesium ions (Eltsov et al., 2008; Finch and Klug, 1976). The significance of the more compact '30 nm fiber' like structures *in vivo* is still unclear (Maeshima et al., 2010), however at least small stretches of more compact chromatin fiber structures seem to exist *in vivo* (Hsieh et al., 2020; Risca et al., 2016). My observations using reconstituted nucleosome arrays show that condensin binding to nucleosome arrays, but not mononucleosomes, is highly sensitive to magnesium concentration (**Figure 2-5**). This suggests that regions of the genome that contain more of these compacted nucleosome fiber structures such as heterochromatin (Hsieh et al., 2020; Risca et al., 2016) may impact the recruitment of condensins. This data also suggests that the removal of HP1 from mitotic chromatin due to aurora B phosphorylation (Fischle et al., 2005; Mateescu et al., 2004) may play a role in allowing condensin binding to heterochromatic regions. However this contrasts with previous reports of higher available magnesium concentration helping compaction in mitotic cells (Maeshima et al., 2018). Other members of the SMC family such as cohesin may also show similar preference for less compact

regions of the genome in the absence of recruitment by additional mechanisms. My observations also indicate that no ATP dependent mode of binding can be observed *in vitro* on these short nucleosome arrays. This data however does not preclude the possibility of such a mechanism existing on longer chromatin substrates.

In the presence of mostly chelated magnesium, I show that both condensin I and condensin II binding to chromatin is inhibited by the presence of linker histone H1.8 (**Figure 2-6, 2-7**). I also verified that this H1.8 mediated inhibition of condensin binding is not the result of a change in chromatin structure (Song et al., 2014), but is likely due to direct competition for the linker DNA by linker histone binding (**Figure 2-8**). Combining these observations with the condensin binding data from *Xenopus* egg extract mitotic chromosomes, I suggest that the linker DNA is a major target for condensin recruitment to mitotic chromatin and that the linker histone is a competitor for the same substrate. A basic competition model for condensin binding (**Figure 2-9**) demonstrates the rheostat like mechanism for condensin enrichment on DNA by controlling the stoichiometry of H1 on chromatin. This mechanism is quite universal and suggests that other linker histone isoforms can compete with other DNA binding proteins on interphase chromatin. Although this data confirms the mechanism for increased recruitment of condensins in the presence of H1.8, the effect of H1.8 on the loop extrusion activity on chromatin is still unclear.

Chromosome length

Most of the eukaryotic genomic DNA is wrapped in nucleosomes and a large fraction of the rest is linker DNA (Chereji et al., 2019; Lee et al., 2007). Both nucleosome spacing and linker histone occupancy play a major role in controlling the chromatin fiber structure (Collepardo-Guevara and Schlick, 2014; Grigoryev et al., 2016; Routh et al., 2008). My data shows that

both nucleosome fiber compaction (**Figure 2-5**) and linker histone (**Figure 2-6, 2-7, 2-8**) control condensin binding to nucleosome arrays. Since condensin binding controls chromosome shape, this suggests a new mechanism to control mitotic chromosome structure by changing either nucleosome spacing or by changing linker histone occupancy. Nucleosome repeat lengths and linker histone stoichiometry vary quite widely among different cell types (Woodcock et al., 2006). Cell sizes also vary quite widely among different cell types (Ginzberg et al., 2015a). This would imply that chromosome sizes in these cells also need to be regulated widely between these different cell types. Changing the nucleosome repeat lengths or linker histone occupancy to control condensin loading on mitotic chromatin is a simple way to control the chromosome sizes in different cell types.

Linker histones are a very dynamic component of chromatin (Misteli et al., 2000). Linker histone occupancy varies widely (Woodcock et al., 2006), and can be controlled by both the linker histone variant and their posttranslational modifications (Christophorou et al., 2014; Hergeth and Schneider, 2015; Th'ng et al., 2005). Linker histone variant expression is also changed during development (Dworkin-Rastl et al., 1994) and some variants appear to be specialized for early development (Freedman and Heald, 2010; Hayakawa et al., 2012; Pérez-Montero et al., 2013) where mitotic chromosome size changes rapidly (Kieserman and Heald, 2011; Ladouceur et al., 2015). The changes in linker histone variants and occupancy at these stages presents a very interesting candidate as a possible mechanism for these chromosome size changes.

Mitotic chromosomes in *Xenopus* egg extract

Mitotic chromosomes are organized in layers of loops which maintain the rigid rod-like structure of the mitotic chromosome. Condensin II, but not condensin I appears to control this

organization in chicken DT40 cells (Gibcus et al., 2018). Comparing the results of condensin I (ΔCAP-G) and condensin II (ΔCAP-D3) depletions to these previously reported data from chicken DT40 cells (Gibcus et al., 2018), we can confirm that condensin I and not condensin II is the important factor regulating the layer size in *Xenopus* egg extracts (**Figure 2-14, 2-15**). This observation of reduced role for condensin II is further supported by its role in regulating chromosome length (**Figure 2-10**) and reduced helical organization by condensin II in the presence of condensin I and H1.8 (**Figure 2-18**). Since these observations were made in egg extract chromosomes which are representative of early embryonic stage chromosomes, it is unclear if this change in the roles of condensins is a general feature of *X. laevis* condensins or specific to egg extract chromosomes.

Condensin I is an ATP-dependent enzyme that has been proposed to generate the mitotic loops by its loop extrusion activity (Ganji et al., 2018; Kong et al., 2020). Since Hi-C is a technique that queries the steady state ensemble of loops in mitotic chromosomes, we cannot comment on the process by which these loops were generated. However, the loop size can be inferred from the contact probability curves generated by Hi-C (Gassler et al., 2017). This investigation of loop sizes confirmed predictions from *in silico* simulations that increased condensin loading lead to smaller loop sizes (Goloborodko et al., 2016a, 2016b) (**Figure 2-16, 2-17**). These predictions from polymer simulations relied on two assumptions, 1) Condensins perform two-sided loop extrusion and 2) Condensins stop extruding loops when they encounter each other. Recent experimental observations of condensin I loop extrusion on naked DNA substrates have shown that both of these assumptions are incorrect (Golfier et al., 2020; Kim et al., 2020; Kong et al., 2020). However, more complicated models of loop extrusion involving condensin dimers can generate effective two-sided loop extrusion (Banigan et al., 2020). These models also predict that condensin enrichment can control loop sizes.

Several details about condensin I driven loop extrusion on complicated chromatin substrates are still unclear. Condensin I has a very slow ATP hydrolysis rate *in vitro* and the estimated step size for loop extrusion is around 50 nm per ATP (Ganji et al., 2018). This is much higher than conventional DNA bound motor proteins and suggests an unconventional mechanism. Continuous loop extrusion through nucleosomes would not appear to be possible by the proposed mechanisms (Datta et al., 2020) since the DNA wrapped around the nucleosome presents a barrier for condensin binding during the intermediate steps of loop extrusion. If loop extrusion through nucleosomes proceeds through at least partial diffusive search mechanisms, this suggests that the additional linker DNA sites opened up in the absence of linker histones can also speed up loop extrusion. This suggests that H1.8 depletion can lead to smaller loops through both increased condensin loading and also faster loop extrusion by individual condensin molecules. By performing Hi-C on samples during the maturation of condensin loops in ΔH1 extracts, it may be possible to investigate whether loop extrusion is also faster in these extracts.

Condensin II plays a significant role in the maintenance of mitotic chromosome structure in HeLa cells and chicken DT40 cells through the establishment of the outer set of mitotic loops (Gibcus et al., 2018). This role of condensin II in prophase is also accompanied by its role in directing sister chromatid resolution (Nagasaka et al., 2016). In *Xenopus* egg extracts, the role of condensin II in organizing the helical loop organization appears to be suppressed by both H1.8 and condensin I (**Figure 2-18**) and condensin II appears to have a reduced role in maintaining chromosome length in the presence of normal levels of condensin I (Shintomi and Hirano, 2011, **Figure 2-10**). This raises the question of how topological resolution is driven in *Xenopus* egg extract chromosomes and how H1.8 affects this process.

Chapter 3- Mitotic chromosome individualization regulation by H1.8, condensins and DNA topoisomerase II

H1.8 suppresses condensin driven individualization

Condensin driven mitotic compaction is required to both maintain the shape and to complete sister-chromatid resolution (Nagasaka et al., 2016; Piskadlo et al., 2017b). *In silico* simulations of mitotic compaction also suggest that loop extrusion activity is required to drive decatenation (Goloborodko et al., 2016b). Although the nature of inter-chromatid contacts and their resolution has been the subject of many investigations, inter-chromosomal contacts are not well understood. Some studies have reported direct observations of inter-chromosomal contacts (Potapova et al., 2019; Sun et al., 2018) and the loss of Ki-67 on the surface of chromosomes results in the clustering of chromosomes (Cuylen et al., 2016). However, more recent studies on the topological status of HeLa nuclei suggest that inter-chromosomal contacts do not result in any substantial entanglement (Goundaroulis et al., 2020; Tavares-Cadete et al., 2020). Thus, the nature of inter-chromosomal contacts and their prominence is still unclear.

Condensins are essential for chromatid formation in *Xenopus* egg extracts (Cuvier and Hirano, 2003; Hirano and Mitchison, 1994). Condensin I depletion alone leads to chromatid formation, but chromosome individualization is unclear from reported data (Shintomi and Hirano, 2011). To verify if condensin I depletion does result in faulty individualization, I performed a chromosome individualization assay. To do this, I dispersed the chromosomes by diluting the extract in buffer before fixation (**Figure 3-1A**). This results in the formation of single chromosomes in control (ΔIgG) extracts (**Figure 3-1C**). However, depletion of condensin I (ΔxCAP-G) (**Figure 3-1B**) resulted in the formation of chromosome clusters (**Figure 3-1C**). Addition of recombinant human condensin I (provided by Dr. Erin E. Cutts) but not its Q-loop mutant results in single chromosomes again (**Figure 3-1B, C**). This suggests

that inter-chromosomal contacts do indeed exist in *Xenopus* egg extract chromosomes and that condensin activity may be needed to resolve these linkages.

To quantify the chromosome individualization, I stained the chromosomal masses from the individualization assay with CENP-A antibody and counted the number of CENP-A foci per chromosomal mass (**Figure 3-2A**). At this resolution, each CENP-A doublet of sister-chromatids is counted as one focus. In mock depleted extracts (ΔIgG), almost all the chromosomal masses were single chromosomes (**Figure 3-2B**). Condensin I depletion (ΔCAP-G) resulted in many chromosome clusters and the histogram showed a wide variety of cluster sizes in this condition.

Using this assay, I decided to ask if the H1.8 mediated suppression of condensins also suppresses chromosome individualization. Both control (ΔIgG) extracts, H1.8 depletion alone (ΔH1) (**Figure 3-3A**) resulted in largely single chromosomes (**Figure 3-3B, C**). I counted all chromosome clusters containing <4 CENP-A foci as single chromosomes, as some chromosomes come together on the coverslip stochastically (**Figure 3-3D**). The relative individualization metric did not change when only masses with <2 CENP-A were counted (**Figure 3-3E**). Condensin I depletion (ΔCAP-G) showed a large reduction in clusters with <4 CENP-A foci. Surprisingly, H1.8, condensin I co-depletion (ΔH1ΔCAP-G) largely rescued individualization and most chromosomes were individualized. Condensin I depletion using a CAP-G antibody depletes >90% of the CAP-G subunit, however ~20% of the CAP-D2 subunit remained in extract (**Figure 3-3A**). This raised the possibility that increased loading of remaining condensin I partial complex upon H1.8 depletion may rescue the condensin I activity on chromatin. The other possibility is that the increased condensin II loading (**Figure 2-4**) in ΔH1ΔCAP-G extracts is responsible for this individualization. Consistent with previous reports (Shintomi and Hirano, 2011), condensin II depletion alone (ΔCAP-D3) or H1.8, condensin II co-depletion (ΔH1ΔCAP-D3) did not inhibit chromosome individualization (**Figure 3-3B-D**).

Along with the defective individualization in ΔCAP-G extracts, this suggests that condensin II may be dispensable for individualization. However, as noted previously, H1.8 depletion resulted in increased condensin II on mitotic chromosomes (**Figure 2-1, 2-3**) and this was independent of condensin I (**Figure 2-4**). It is thus possible that this increased condensin II upon H1.8 depletion may be capable of rescuing individualization. Consistent with this, co-depletion of H1.8 along with both condensins (ΔH1ΔCAP-GΔCAP-D3) resulted in accumulation of unindividualized chromosomes (**Figure 4-3 B-D**). This shows that condensin II is indeed responsible for the chromosome individualization in ΔH1ΔCAP-G extracts.

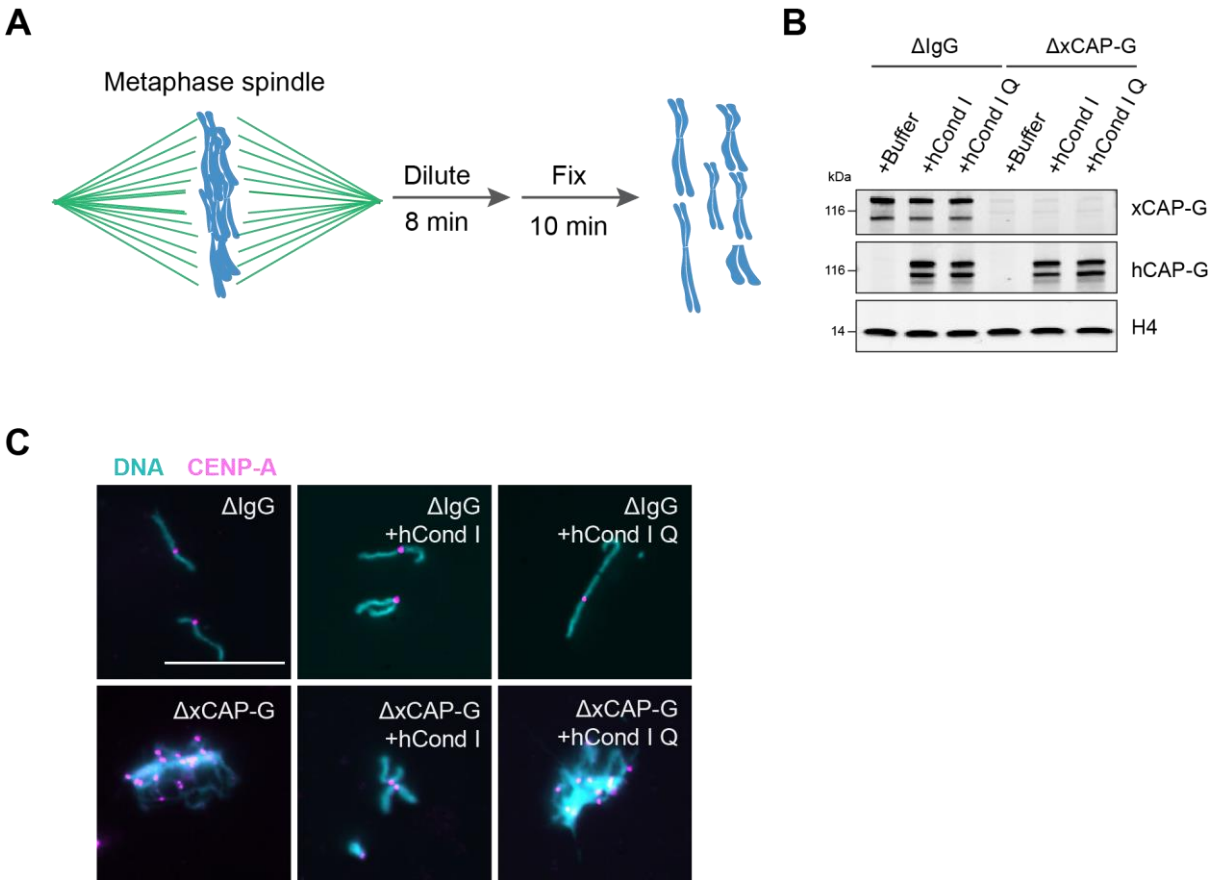

Figure 3-1 Condensin I activity is required for chromosome individualization

A) Schematic of chromosome dispersal assay to measure chromosome individualization. B) Western blots of condensin I depletion and rescue with human condensin I and the Q-loop mutant of condensin I. C) Representative Hoechst (DNA) and CENP-A immunofluorescence images of chromosomes in indicated metaphase egg extracts after dilution, which disperses individualized chromosomes. Extracts depleted of condensin I (ΔCAP-G) were complemented with recombinant human condensin I and condensin I Q loop mutant protein complexes.

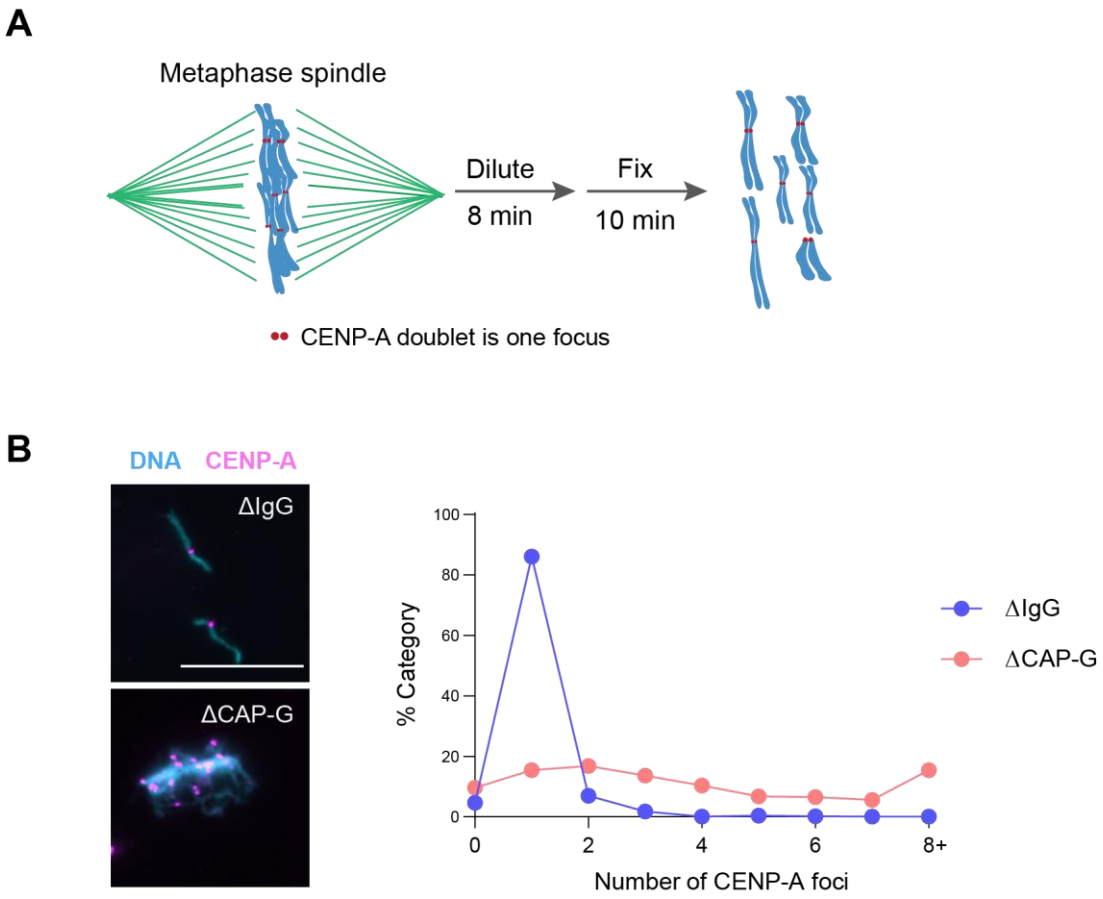

Figure 3-2 Schematic to quantify the chromosome individualization

A) Scheme to show the CENP-A counting as an assay for chromosome individualization. B) Representative images of the chromosome clusters obtained in the chromosome individualization assay in control and ΔCAP-G depleted extracts (left) and a histogram of the number of CENP-A foci in each chromosome cluster in the indicated condition.

Figure 3-3 H1.8 suppresses condensins to regulate chromosome individualization

A) Western blots of total extracts showing depletion of condensin I and condensin II subunits * represents non-specific band B) Representative images of chromosomes after extract dilution, which disperses individualized chromosomes. DNA and centromere-associated CENP-A immunofluorescence are shown. Bar, 20 μm. C) Percentage of chromosome masses that contain the indicated number of CENP-A foci in each condition. All masses with more than 8 CENP-A foci were added to the 8+ category. D) Percent of chromosome masses that are individualized chromosomes (0-3 CENP-A foci) in the indicated conditions. A large majority of DNA masses with no CENP-A foci are derived from ΔCAP-D3 extracts, where CENP-A loading is compromised (Bernad et al., 2011). E) Percent of chromosome masses that have <2 CENP-A foci from the same data as D) showing that the relative 'individualization' remains similar regardless of the number of CENP-A foci used as a cutoff.

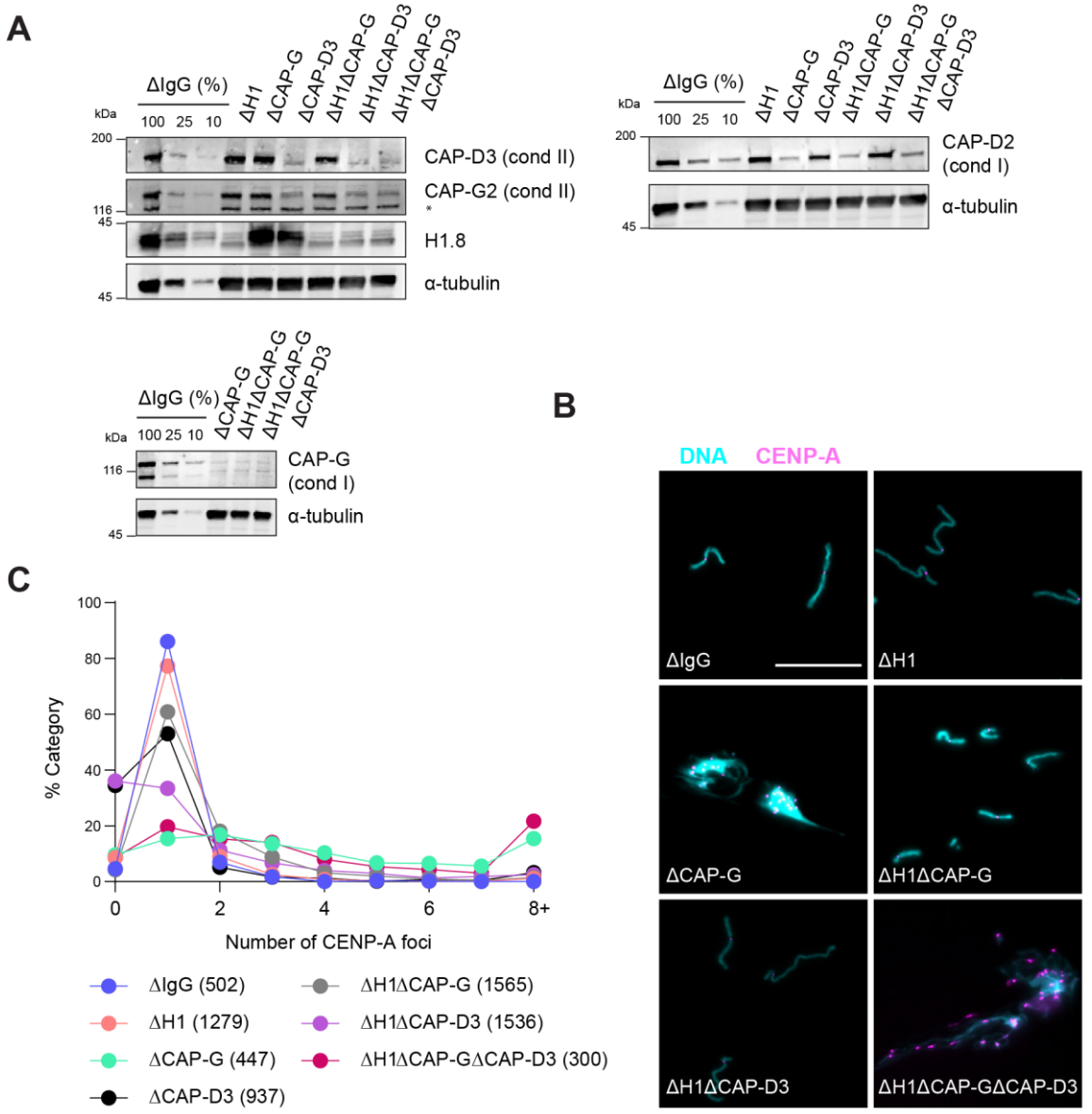
A
ΔIgG (%)
100 25 10
ΔH1
ΔCAP-G
ΔCAP-D3
ΔH1ΔCAP-G
ΔH1ΔCAP-D3
ΔH1ΔCAP-G ΔCAP-D3
kDa
200
116
45
CAP-D3 (cond II)
CAP-G2 (cond II)
*
H1.8
α-tubulin
CAP-D2 (cond I)
CAP-G (cond I)
B
DNA
CENP-A
ΔIgG
ΔH1
ΔCAP-G
ΔH1ΔCAP-G
ΔH1ΔCAP-D3
ΔH1ΔCAP-GΔCAP-D3
C
% Category
Number of CENP-A foci
ΔIgG (502)
ΔH1 (1279)
ΔCAP-G (447)
ΔCAP-D3 (937)
ΔH1ΔCAP-G (1565)
ΔH1ΔCAP-D3 (1536)
ΔH1ΔCAP-GΔCAP-D3 (300)
D
% Individualized chromosomes
p=0.74 p=0.04 p=0.31 p=0.57 p=0.25 p<0.04
E
% Single chromosomes

Topo II activity is needed to resolve interchromosomal catenations

Condensins and topo II act in concert to generate mitotic chromosomes from decondensed interphase nuclei (Cuvier and Hirano, 2003). Both experimental observations and *in silico* experiments also suggest that condensin is required to complete decatenation of sister-chromatids (Dyson et al., 2020; Goloborodko et al., 2016b; Nagasaka et al., 2016). Condensin is also required to keep decatenating sister chromatids in metaphase (Piskadlo et al., 2017b). Although it has been suggested that condensin-mediated chromosome compaction promotes chromosome individualization (Brahmachari and Marko, 2019; Sun et al., 2018), it remains to be established if different linear chromosomes (non-sisters) are catenated with each other even after completion of mitotic compaction, since Ki-67 on chromosome surface may act as a barrier to prevent interchromosomal DNA interaction during mitosis (Cuylen et al., 2016). To investigate if substantial interchromosomal entanglements exist in metaphase *Xenopus* egg extracts, I asked if topo II inhibitor ICRF-193 blocks chromosome individualization after mitotic chromosome compaction (**Figure 3-4A**). While chromosomes clustered on the metaphase spindle in DMSO-treated control extracts were effectively dispersed into individualized chromosomes after diluting extracts, most chromosomes remained clustered when ICRF-193 was added at the beginning of mitotic induction and incubated for 50 min (**Figure 3-4B, C, ICRF-50 min**). Even when ICRF-193 was added to metaphase egg extracts after completion of metaphase spindle formation but 2 min before extract dilution (**Figure 3-4A**, bottom), efficiency of chromosome individualization decreased (**Figure 3-4B, C**, ICRF-2 min). These results suggest that substantial interchromosomal topological catenations remain unresolved in metaphase.

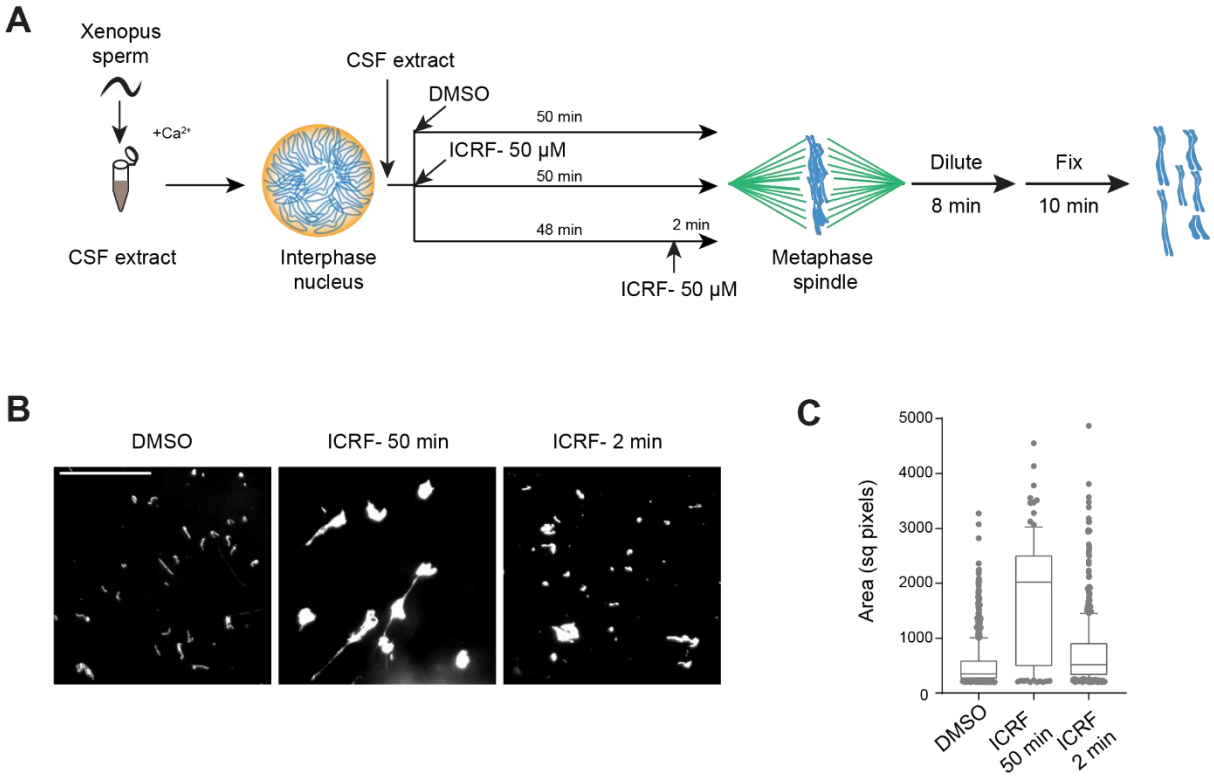

Figure 3-4 ICRF-193 addition inhibits chromosome individualization

A) Schematic of ICRF-193 addition to check for requirement of topo II activity in individualizing chromosomes. Topo II inhibitor ICRF-193 (50 µM) was added to interphase egg extracts after replication was completed, either together with fresh CSF extracts and incubated for 50 min (ICRF-50 min), or 48 min after adding the fresh CSF extracts, followed by 2 min incubation with ICRF-193 (ICRF-2 min). B) Metaphase extracts processed as in A) were diluted in buffer to disperse individualized chromosomes. Representative Hoechst images of chromosomes are shown. Bar, 20 µm. C) Quantification of the Hoechst-stained area of chromosomes in B). Each dot represents the area of a single chromosome or a chromosome cluster. Large values indicate clusters of more chromosomes. The box shows the 10^{th}-90^{th} percentile limits of the sample values. >100 chromosomes or chromosome clusters were counted for each condition.

H1.8 suppresses topo II loading on chromatin

H1.8 suppresses topo II loading on mitotic chromatin

I showed that H1.8 suppresses chromosome individualization (**Figure 3-3**) and that topoisomerase activity is needed to continuously resolve interchromosomal linkages (**Figure 3-4**). I then asked if H1.8 suppresses chromosome individualization by suppressing topo II. Topo II is a DNA binding protein (Berger et al., 1996) but it's preference for nucleosome free DNA over nucleosomal DNA is still unclear (Zierhut et al., 2014). To clarify whether H1.8 modulates topo II binding in mitosis, I performed immunofluorescence on TOP2A, the only isoform of topo II in extracts, on nocodazole treated metaphase chromosomes in ΔH1 extracts (**Figure 3-5A**). TOP2A was enriched in H1.8 depleted extracts and this enrichment was rescued by the addition of recombinant H1.8 (**Figure 3-5A, B**). This enrichment was also confirmed by quantitative western blots on purified metaphase chromosomes (**Figure 3-5C**) and mass spectrometry (**Figure A-1, Table A-1**). This suggests that similar to condensins, H1.8 suppresses topo II binding to chromatin. To verify if this TOP2A enrichment on ΔH1 chromatin is direct, I attempted to measure TOP2A binding to chromatin *in vitro*. To do this, I reconstituted nucleosome arrays using salt dialysis and using *X. laevis* TOP2A purified from yeast, I asked whether TOP2A binding is affected by the presence of H1.8 (**Figure 2-6A**). At lower salt concentrations (40, 80 mM NaCl), H1.8 did not affect TOP2A binding. However, at 120 mM NaCl, which represents a more physiological cation concentration, H1.8 significantly suppressed TOP2A binding (**Figure 3-5D**). This indicates that H1.8 can directly inhibit binding of TOP2A to chromatin even in the absence of condensins.

Figure 3-5 H1.8 inhibits topo II loading onto chromatin

A) Representative images of DNA (Hoechst 33342) and TOP2A immunofluorescence on chromosomes in metaphase extracts treated with nocodazole in the indicated conditions. Chromosomes in each nucleus remain clustered in the presence of nocodazole. Bar, 10 μm. B) Quantification of TOP2A immunofluorescence signals normalized to the DNA (Hoechst) signal for the indicated conditions. Each grey or magenta dot represents the average signal intensity of a single chromosome cluster (from one nucleus). Each black dot represents the median signal intensity from a single experiment. Bars represent mean and range of the medians of two independent experiments. For each experiment, signals on >20 chromosome clusters were counted. C) Western blots of mitotic chromatin purified from mock (ΔIgG) and H1.8-depleted (ΔH1) extracts (top) and quantification of band intensities normalized to H3. Mean and range from 2 experiments. D) Coomassie staining of SDS-PAGE gels, showing input (left) and nucleosome-array bound fraction (middle) of TOP2A, rH1.8 and core histones. The right most lanes represent the streptavidin beads only negative control. Buffer contains 1 mM $MgCl_2$ and indicated concentrations of NaCl. The band intensities of TOP2A were normalized to the core histone bands and the binding at 40 mM NaCl for nucleosome arrays without H1.8. Mean and range of two independent experiments are shown (right).

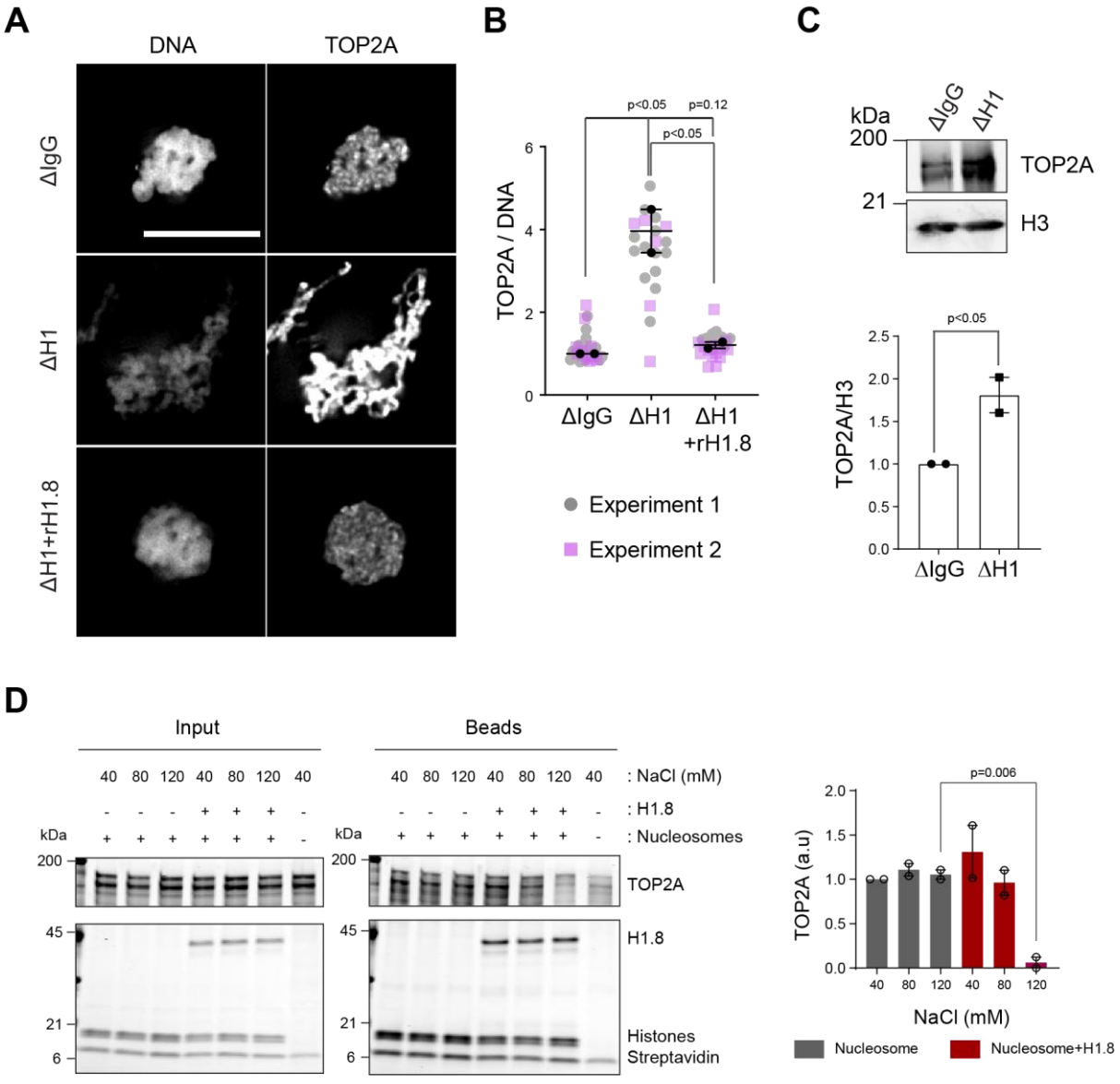
A
DNA
TOP2A
ΔIgG
ΔH1
ΔH1+rH1.8
B
p<0.05
p=0.12
p<0.05
TOP2A / DNA
ΔIgG
ΔH1
ΔH1 +rH1.8
Experiment 1
Experiment 2
C
kDa
ΔIgG
ΔH1
200
TOP2A
21
H3
p<0.05
TOP2A/H3
ΔIgG
ΔH1
D
Input
Beads
40 80 120 40 80 120 40
: NaCl (mM)
: H1.8
: Nucleosomes
kDa
200
TOP2A
45
H1.8
21
6
Histones
Streptavidin
p=0.006
TOP2A (a.u)
NaCl (mM)
Nucleosome
Nucleosome+H1.8

H1.8 limits chromosome individualization through suppressing topo II chromatin binding

Since TOP2A binding is suppressed by H1.8, I then wondered if this is responsible for the H1.8 mediated suppression of chromosome individualization (**Figure 3-3**). Since topo II activity is required for decondensing sperm nuclei (Shintomi et al., 2015), I performed a partial depletion of topo II. If individualization is sensitive to TOP2A levels, then I expected that a reduction of TOP2A should result in a partial loss of individualization (**Figure 3-6A, B**). Reduction of TOP2A to 25% of control levels in extract led to a reduction of TOP2A on chromosomes (**Figure 3-6C**). Since H1.8 depletion (ΔH1) results in an accumulation of TOP2A on chromatin, the TOP2A level on chromatin in partially depleted extracts was similar to control (ΔIgG-100%) levels (**Figure 3-6C**). To assess chromosome individualization, I sorted the observed chromosome masses into three categories (**Figure 3-6D**). In the presence of wildtype TOP2A levels (100%), there was no difference in the levels of chromosome individualization observed between mock (ΔIgG-100) and H1.8 depletion (ΔH1-100). However, when TOP2A was partially depleted, mock depletion (ΔIgG-25) resulted in the accumulation of unindividualized chromosomes, whereas H1.8 depletion (ΔH1-25) did not (**Figure 3-6E**). This data suggests that TOP2A is limiting for chromosome individualization and that H1.8 mediated suppression of topo II limits chromosome individualization.

Figure 3-6 H1.8 reduces sensitivity of chromosome individualization to TOP2A depletion

A) Schematic of partial TOP2A depletion to test sensitivity of chromosome individualization to TOP2A levels. B) Western blots of total extract samples in the indicated conditions showing the partial TOP2A depletions. C) Quantification of chromosome-associated TOP2A upon partial TOP2A depletion. Each dot represents the mean of TOP2A intensity normalized to DNA intensity of a single chromosome cluster (from one nucleus). The data plotted is median +/- 95 % C.I. >20 nuclei were quantified for each condition. D) Representative images of the categories used to sort the DNA masses resulting from a chromosome individualization experiment. E) Percent frequency of DNA clusters categorized as unindividualized nuclei upon partial TOP2A depletion. Mean and S.E.M from three independent experiments. >100 chromosomes/clusters were quantified for each condition in every experiment.

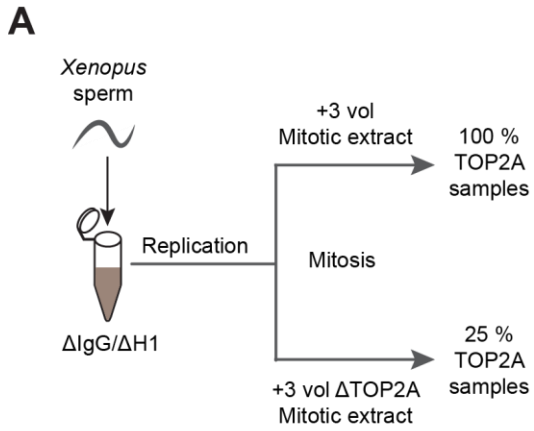
A
Xenopus
sperm
Replication
ΔIgG/ΔH1
+3 vol
Mitotic extract
100 %
TOP2A
samples
Mitosis
25 %
TOP2A
samples
+3 vol ΔTOP2A
Mitotic extract

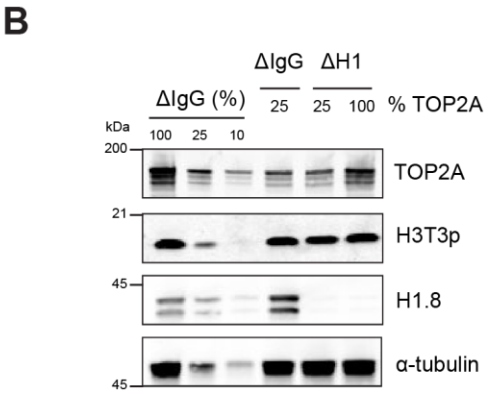
B
ΔIgG
ΔH1
ΔIgG (%)
25
25
100
% TOP2A
kDa
100
25
10
200
TOP2A
21
H3T3p
45
H1.8
45
α-tubulin

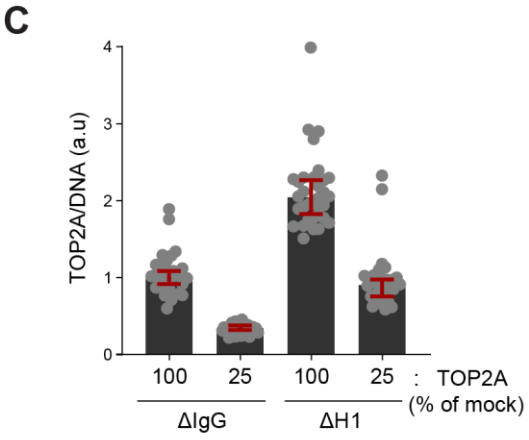
C
TOP2A/DNA (a.u)
4
3
2
1
0
100
25
100
25
: TOP2A
(% of mock)
ΔIgG
ΔH1

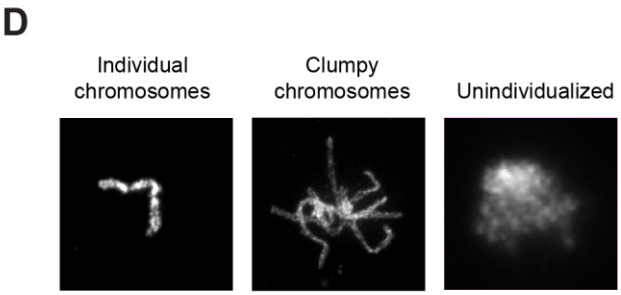
D
Individual
chromosomes
Clumpy
chromosomes
Unindividualized

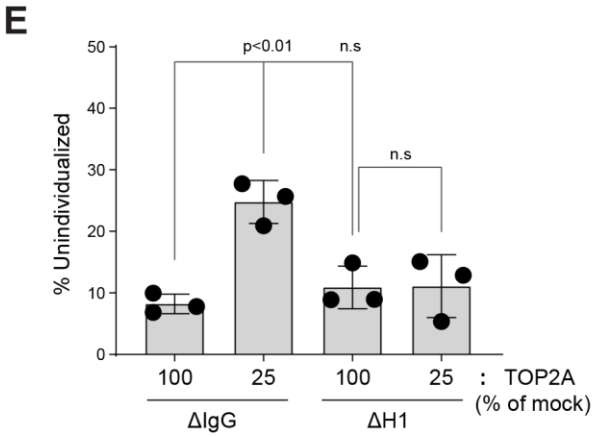
E
% Unindividualized
50
40
30
20
10
0
p<0.01
n.s
n.s
100
25
100
25
: TOP2A
(% of mock)
ΔIgG
ΔH1

TOP2A activity is enhanced by condensin I and suppressed by H1.8

Condensins promote topoisomerase activity to perform sister chromatid decatenation (Nagasaka et al., 2016; Piskadlo et al., 2017b) and resolve topological linkages (Baxter et al., 2011; Dyson et al., 2020). Since H1.8 appears to also suppress chromosome individualization through topo II and regulates chromatin binding of topo II, I wondered whether H1.8 directly regulates topo II. Firstly, I asked if the H1.8 mediated suppression of topo II chromatin binding is dependent on condensin I. To do this, I performed TOP2A immunofluorescence on metaphase chromosomes from H1.8, condensin I co-depleted (ΔH1ΔCAP-G) extracts (**Figure 3-7**). I observed no significant effect of condensin I depletion alone (ΔCAP-G) or condensin I co-depletion (ΔH1ΔCAP-G) on TOP2A levels on chromatin. This suggests that H1.8 regulates topo II enrichment on chromatin independent of condensin I. This is consistent with previous reports on the lack of a change in topo II binding in the absence of condensin I (Cuvier and Hirano, 2003).

However, the catalytic function of topo II may be regulated separately from its DNA binding. TOP2A shows a preference for certain supercoiling states (Baxter et al., 2011). Condensin loop extrusion activity can also enable decatenation by localizing preferred substrates (Orlandini et al., 2019). To verify if H1.8 and condensin I both show similar effects on TOP2A activity as their chromatin binding effects, I attempted to directly measure topo II activity on chromatin substrates.

Decatenation of highly catenated circular kinetoplast DNA is a well-established catalytic assay to measure topoisomerase activity (Marini et al., 1980). In this assay, catenated circular DNAs remain on the well while decatenated DNAs migrate as a supercoiled circular DNA in agarose gel electrophoresis. Since I am attempting to measure TOP2A activity on chromatin substrates, I first generated a chromatinized kinetoplast substrate by incubating

kinetoplast DNA with interphase *Xenopus* egg extracts (**Figure 3-8A**). Since TOP2A activity would decatenate kinetoplast DNA before the completion of chromatinization, I chromatinized the kinetoplast DNA in extracts depleted of topo II. To verify that nucleosomes can effectively assemble on circular DNAs in egg extracts depleted of H1.8 and TOP2A, I incubated pBlueScript DNA in ΔIgGΔTOP2A and ΔH1ΔTOP2A extracts and checked for nucleosome assembly on these plasmids. Nucleosome deposition results in supercoiling of the plasmid DNA and since supercoiling increases the migration speed in an agarose gel, the addition of each nucleosome results in an additional band in the agarose gel (Germond et al., 1975). I found that nucleosomes assembly at equal efficiency on the plasmid DNA after incubation in ΔIgGΔTOP2A and ΔH1ΔTOP2A for 150 min (**Figure 3-8B**). Note that I used plasmid DNA for this assay since highly catenated kinetoplast DNA would remain in the well in the absence of TOP2A, making it difficult to assess nucleosome assembly using this assay. Therefore, I followed this nucleosome assembly protocol and incubated kinetoplasmid DNA with ΔIgGΔTOP2A and ΔH1ΔTOP2A extracts for 180 min. To measure TOP2A activity on these chromatinized substrates, I then added fresh mitotic extracts with topo II and collected samples at different time points to quantify the catenation status of the kinetoplast DNA. H1.8 depletion did not result in increased decatenation of kinetoplast DNA chromatinized in ΔH1 extracts (**Figure 3-8C**), suggesting that H1.8 does not affect TOP2A activity. This suggests that H1.8 does not affect TOP2A decatenation activity even if it affects chromatin binding of TOP2A. Condensin I depletion (ΔCAP-G) also did not affect the rate of decatenation on chromatinized kinetoplast DNA (**Figure 3-8D**). This is consistent with previous reports from *Xenopus* egg extracts (Cuvier and Hirano, 2003) and suggests that kinetoplast decatenation activity is independent of both condensin I and H1.8.

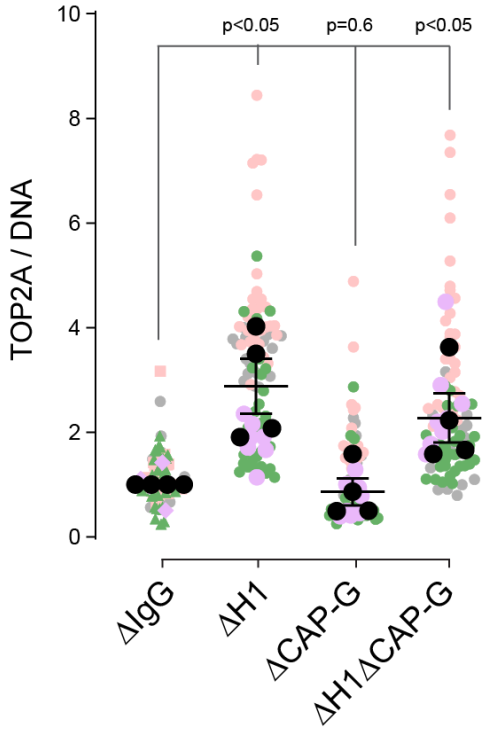

Figure 3-7 H1.8 regulates TOP2A loading independent of condensin I

Quantification of TOP2A immunofluorescence intensity normalized to the DNA signal for the indicated conditions. Each grey or magenta dot represents the average signal intensity of a single chromosome cluster (from one nucleus). Each grey, magenta, orange or grey dot represents the median signal intensity from a single experiment. Mean and S.E.M of the median of four independent experiments are also shown. >20 nuclei were quantified for each condition in every experiment.

Figure 3-8 Kinetoplast decatenation is not affected by H1.8 or condensin I depletion

A) Experimental scheme for decatenation assay on chromatinized kinetoplast DNA. Catenated kinetoplast DNA was incubated with indicated ΔTOP2A interphase egg extract for 180 min to assemble nucleosomes without TOP2A. Mitosis was induced with adding corresponding metaphase extracts containing TOP2A. At indicated time after mitotic induction, DNA samples were recovered to monitor decatenation. B) Chromatinization time course on relaxed circular pBlueScript DNA showing no difference in chromatinization upon H1.8 depletion in interphase extract. Nucleosome formation introduces negative supercoils. C) Chromatinized kinetoplast decatenation time course showing no difference in kinetics of decatenation upon H1 depletion. D) Chromatinized kinetoplast decatenation time course showing no difference in kinetics of decatenation upon CAP-G depletion.

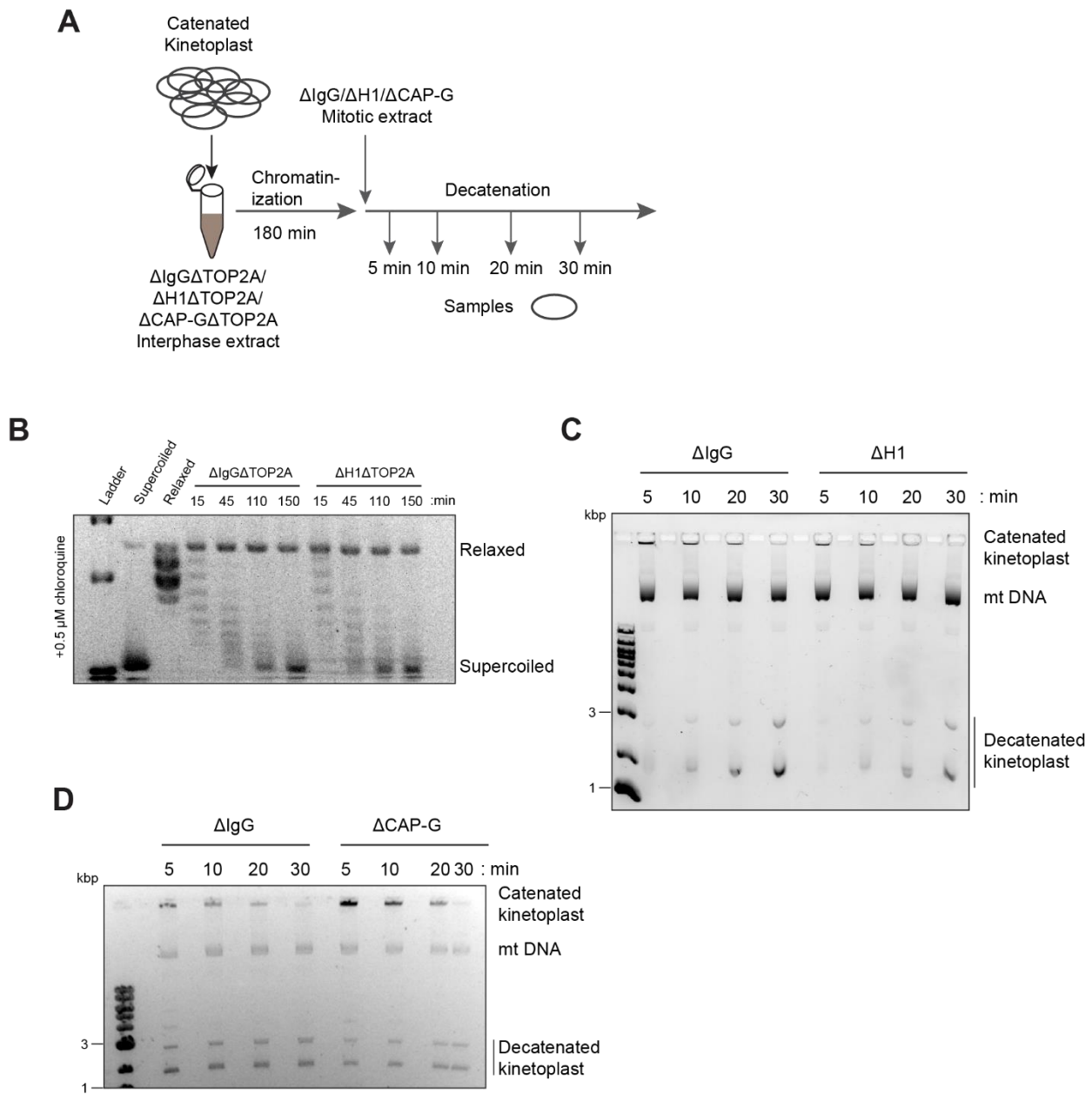
A
Catenated
Kinetoplast
ΔIgG/ΔH1/ΔCAP-G
Mitotic extract
Chromatin-
ization
180 min
Decatenation
5 min 10 min 20 min 30 min
Samples
ΔIgGΔTOP2A/
ΔH1ΔTOP2A/
ΔCAP-GΔTOP2A
Interphase extract
B
Ladder
Supercoiled
Relaxed
ΔIgGΔTOP2A
ΔH1ΔTOP2A
15 45 110 150 15 45 110 150 :min
+0.5 μM chloroquine
Relaxed
Supercoiled
C
ΔIgG
ΔH1
5 10 20 30 5 10 20 30 : min
kbp
Catenated
kinetoplast
mt DNA
3
1
Decatenated
kinetoplast
D
ΔIgG
ΔCAP-G
5 10 20 30 5 10 20 30 : min
kbp
Catenated
kinetoplast
mt DNA
3
1
Decatenated
kinetoplast

Since condensin I forms very large loops (Gibcus et al., 2018; Naumova et al., 2013; **Figure 2-16**), I wondered if kinetoplast decatenation fails to recapitulate the dynamics of topo II activity on longer chromatin substrates. To measure TOP2A activity on sperm chromatin, I developed a new assay. To do this, I arrested active TOP2A molecules using the topoisomerase drug teniposide (VM-26). VM-26 is a TOP2A poison that traps the decatenation reaction in a TOP2A-DNA covalent complex (TOP2cc) (Pommier et al., 2010). The enzyme TDP2 then processes these arrested complexes into a double strand break (DSB) (Ledesma et al., 2009; Schellenberg et al., 2017). I then detected these DSBs by the Ku70-Ku80 complex that localizes to free DNA ends (Mimori and Hardin, 1986-**Figure 3-9A**). To test if TOP2A activity can indeed be detected by this process, I asked if Ku70-Ku80 complex accumulates on sperm DNA in mitosis upon VM-26 addition in both undepleted and ΔTOP2A extracts. VM-26 addition resulted in a significant accumulation of Ku80 by immunofluorescence (**Figure 3-9B, C**). Consistent with the proposed mechanism, this Ku80 accumulation was largely abrogated in ΔTOP2A extracts. The Ku80 accumulation was also dosage dependent on VM-26 concentration (**Figure 3-9D**).

Using this assay, I then asked if H1.8 and condensin I affect TOP2A activity. To do this, I treated metaphase nuclei prepared in H1.8 depleted (ΔH1), condensin I depleted (ΔCAP-G) or H1.8, condensin I co-depleted (ΔH1ΔCAP-G) extracts and then treated them with DMSO or 20 μM VM-26. The nuclei were then fixed and stained with Ku80 antibody for immunofluorescence. Nuclei from control (ΔIgG) extracts showed a small amount of background double strand breaks (**Figure 3-10**, ΔIgG -), but showed increased Ku80 upon treatment with VM-26. If H1.8 depletion results in increased TOP2A activity, ΔH1 extracts should show increased accumulation of Ku80 upon VM-26 treatment. Consistent with this, H1.8 depletion (ΔH1) did not result in any increased double strand breaks in DMSO treatment but showed a large increase upon VM-26 treatment (ΔH1 +). This is also consistent with the

increased individualization observed upon H1.8 depletion. Surprisingly, CAP-G depletion resulted in increased background double strand breaks (ΔCAP-G -), but VM-26 addition did not result in any increased double strand breaks (ΔCAP-G +). This suggests that condensin I stimulates TOP2A activity and correlates with the failed individualization in ΔCAP-G extracts (**Figure 3-2**). As H1.8 co-depletion (ΔH1ΔCAP-G) rescued this chromosome individualization defect, I wondered if this is accompanied by a rescue of TOP2A activity. Indeed, H1.8 co-depletion (ΔH1ΔCAP-G) rescued Ku80 accumulation upon VM-26 treatment. These data taken together indicate that TOP2A activity is correlated with observed chromosome individualization. Higher TOP2A activity means more individualization and lower TOP2A activity means failed resolution.

The data in **Figure 3-10** show that H1.8 suppresses and condensin I promotes TOP2A activity. However, it is still unclear if the H1.8 mediated suppression of TOP2A activity is dependent on condensin activity as well. Chromosome individualization experiments show that loss of condensin I activity can be rescue by H1.8 depletion (**Figure 3-3**). This indicates that it may be possible to lose achieve proper chromosome compaction by losing both H1.8 and condensin I. However, the high background Ku80 levels observed upon condensin I depletion (**Figure 3-10,** ΔCAP-G-DMSO) and H1.8 co-depletion (**Figure 3-10,** ΔH1ΔCAP-G-DMSO) suggest that condensin I is required to suppress the accumulation of DNA damage. The source of this DNA damage is not immediately clear.

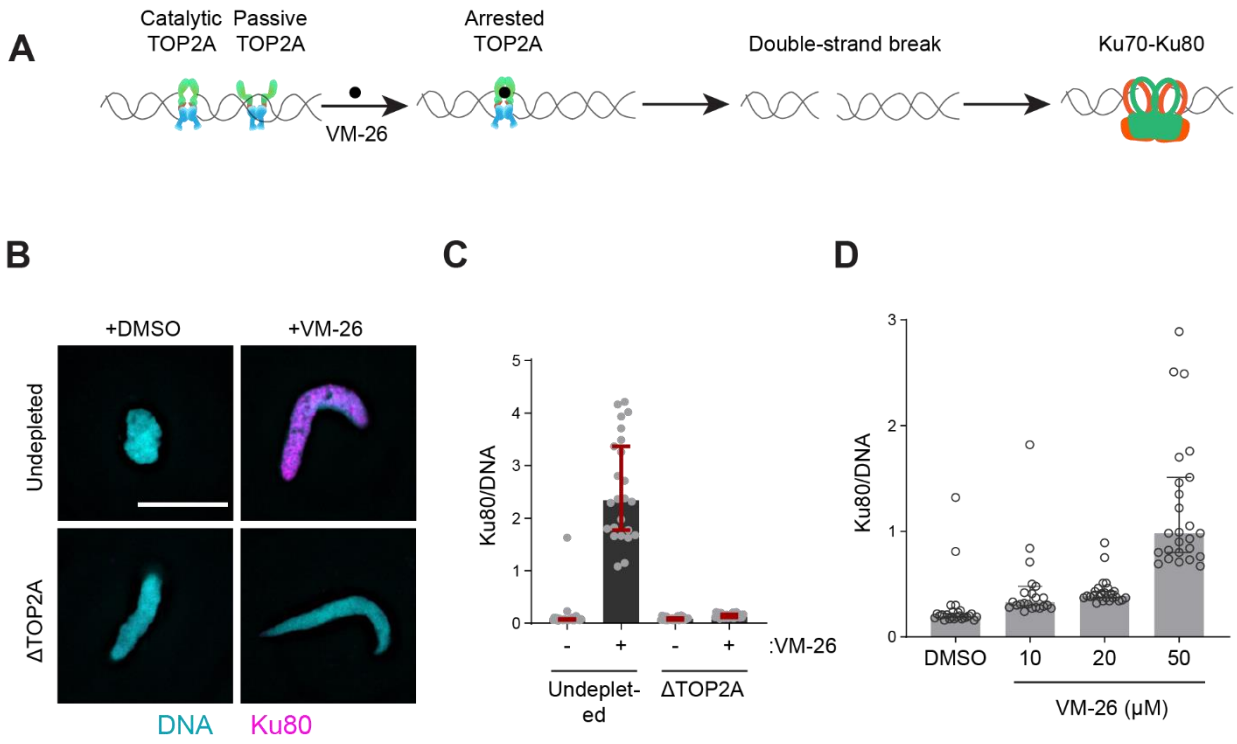

Figure 3-9 Novel assay to measure TOP2A activity on sperm chromatin

A) Schematic of VM-26 assay to detect topo II-dependent DNA breaks on chromatin using Ku80 immunofluorescence. B) Representative images of DNA and Ku80 immunofluorescence on sperm nucleus in indicated conditions. Bar, 10 μm. C) Quantification of Ku80 immunofluorescence signals on mitotic chromatin in B). Data is median and 95% C.I. >20 nuclei were quantified for each condition. D) Quantification of Ku80 immunofluorescence signal levels on chromosomes normalized to Hoechst (DNA) signals. Extracts containing metaphase chromosomes were treated with increasing VM-26 concentration for 60 min. Each dot represents the average signal intensities of a single chromosome cluster from a nucleus. Bars represent median and 95% C.I. >25 chromosome clusters were counted per each time point.

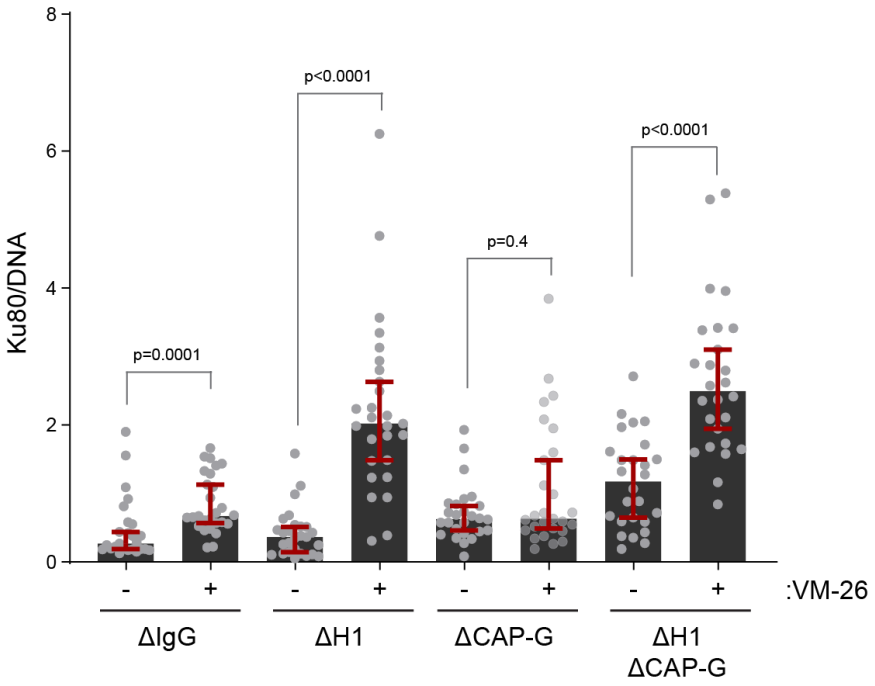

Figure 3-10 H1.8 suppresses and condensin I promotes TOP2A activity

VM-26-dependent Ku80 accumulation on mitotic chromatin under indicated conditions. Each dot is average of Ku80 immunofluorescence signal (normalized with DNA) of a single chromosome cluster (from one nucleus). Median and 95% C.I are shown. >20 nuclei were quantified for each condition.

H1.8 promotes chromosome clustering and spindle integrity

Mitotic chromosomes in HeLa cells treated with spindle disassembly cluster in the absence of Ki-67 (Cuylen et al., 2016). Chromosomes in *Xenopus* egg extracts treated with nocodazole also clustered (**Figure 2-1**). This suggests that chromosomes may be prone to increased interchromosomal interactions in the absence of an inhibiting factor. I have shown earlier that H1.8 suppresses chromosome individualization by enhancing interchromosomal interactions. This suggests that H1.8 should also promote chromosome clustering. To see if this is indeed true, I generated 3D surfaces by segmenting the chromosomal volume in nocodazole treated control and ΔH1 extracts. I then measured the surface area of these nuclei as a measure of how clustered the chromosomes are. Indeed, H1.8 depletion (ΔH1) resulted in a large increase in surface area of these nuclei, which was rescued by the addition of recombinant H1.8 (**Figure 3-11A, B**). This indicates that H1.8 promotes chromosome clustering.

Since H1.8 controls chromosome individualization through its suppression of condensins, I then asked if increased condensin I was required for this chromosome clustering. Condensin I depletion alone (ΔCAP-G) did not increase chromosome clustering as chromosomes are already tightly clustered in control (ΔIgG) (**Figure 3-11 C, D**). H1.8, condensin I co-depletion (ΔH1ΔCAP-G) chromosomes still showed increased surface area compared to control extracts, suggesting that condensin I may not be required for the decreased clustering observed due to H1.8 depletion. However, these nuclei did show some increased clustering compared to ΔH1 nuclei indicating that increased condensin I activity may play some role in this process.

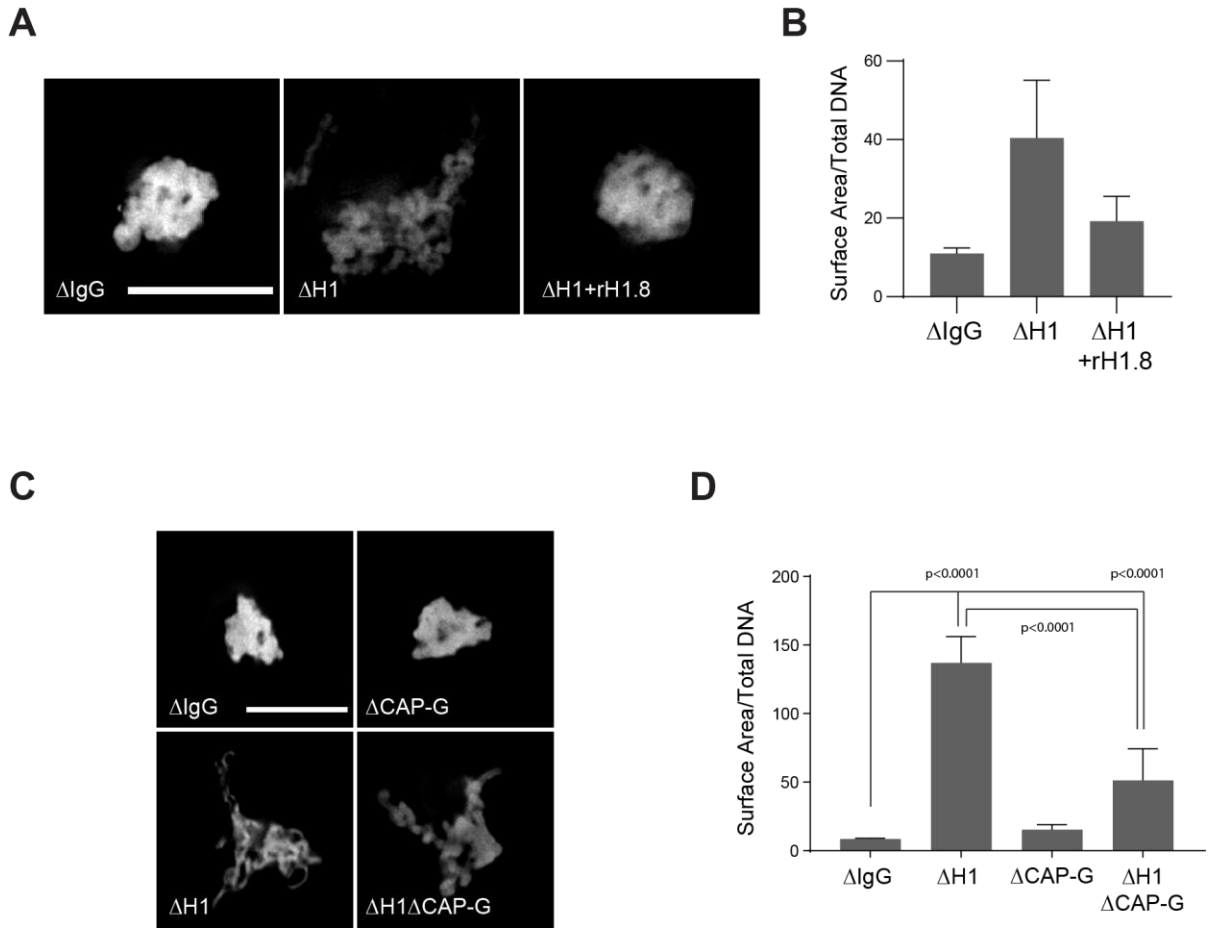

Figure 3-11 H1.8 depletion results in reduced chromosome clustering

A) Representative images of DNA (Hoechst 33342) upon H1.8 depletion and rescue using rH1.8. Bar, 10 μm. B) Quantification of the surface area normalized to the DNA amount by Hoechst staining. Data presented is median +/- 95 % C.I. > 20 nuclei were quantified in each condition. C) Representative images of DNA (Cy3-dUTP) in the indicated condition. Bar, 10 μm. D) Quantification of the surface area normalized to the DNA amount by Cy3-dUTP staining. Data presented is median +/- 95 % C.I. > 25 nuclei were quantified in each condition

Mitotic spindles in *Xenopus* egg extracts can be generated in the absence of centrosomes by DNA bound spindle assembly factors (Heald et al., 1996). This suggests that mitotic spindles in egg extracts are influenced by mitotic chromosome organization. Since H1.8 is required for chromosome clustering, I asked if it is also required to maintain spindle integrity. Spindles generated in *Xenopus* egg extracts in the different conditions were sorted into three categories: i) *bipolar aligned* - bipolar spindles with chromosomes aligned at the metaphase plate, ii) *bipolar misaligned* - bipolar spindles with misaligned chromosomes, iii) *abnormal misaligned* - monopolar or multipolar spindles (**Figure 3-12A**). If chromosome organization plays a significant role in maintaining spindle integrity, I expected that the loss of chromosome clustering would result in aberrant spindle assembly signaling and thus an increased number of abnormal spindles with defective chromosome organization.

Control extracts (ΔIgG) contained some bipolar misaligned spindles and a small number of abnormal spindles (**Figure 3-12B**). H1.8 depletion (ΔH1) however led to the accumulation of both bipolar, misaligned and abnormal spindles and this phenotype was rescued by the addition of recombinant H1.8. This may be expected due to the decreased chromosome clustering upon H1.8 depletion. This phenotype is more severe than those reported previously, where H1.8 depletion led only to chromosome alignment defects in metaphase (Maresca et al., 2005). The authors in this above cited study also proposed that the increased chromosome length may have caused this phenotype due to the inability of elongated chromosomes to fit in the mitotic spindle. To verify if increased chromosome length was indeed the cause of this phenotype, I asked if condensin I co-depletion (ΔH1ΔCAP-G) would rescue the spindle integrity. As noted previously, condensin I co-depletion led to the formation of very short chromosomes (**Figure 2-10**), which should rescue spindle integrity in ΔH1 extracts if the chromosome length was responsible for the phenotypes. Condensin I depletion alone (ΔCAP-G) resulted in the increased accumulation of abnormal spindles (**Figure 3-12C**). This appears

to be a milder phenotype than that observed upon depleting both condensin I and condensin II (Wignall et al., 2003). Contrary to the chromosome length model however, H1.8, condensin I co-depletion (ΔH1ΔCAP-G) did not lead to the formation of more normal spindles. In fact, these extracts accumulated slightly increased number of abnormal spindles. This suggests that the chromosome elongation is likely not responsible for the loss of spindle integrity upon H1.8 depletion.

This data however is consistent with the chromosome clustering in nocodazole, where H1.8, condensin I co-depletion did not rescue the reduced chromosome clustering observed upon H1.8 depletion alone (**Figure 3-11C, D**). I then asked if the decreased interchromosomal interactions in ΔH1 extracts may be responsible for this reduced chromosome clustering. Since TOP2A activity seems to be required to resolve these interchromosomal interactions (**Figure 3-4**), I asked if reduced TOP2A activity could rescue the spindle integrity in ΔH1 extracts. To do this, I treated control and ΔH1 extracts with DMSO or 20 μM ICRF-193, a TOP2A poison, and assessed the spindles. ICRF-193 addition to mock depleted extracts (ΔIgG) did not have a significant effect on spindle integrity, whereas ΔH1 depleted extracts showed a small rescue of abnormal spindles upon ICRF-193 addition (**Figure 3-12D**). However, this rescue was minimal and these extracts still contained a large fraction of abnormal spindles. This could be either due to incomplete inhibition of TOP2A activity by 20 μM ICRF-193 or could indicate that spindle integrity is dependent on factors other than interchromosomal contacts involved in chromosome individualization. Attempts at increasing ICRF-193 concentration to achieve a more complete TOP2A inhibition led to a complete collapse of spindles even in control extracts (data not shown). Thus, the mechanism for the loss of spindle integrity in ΔH1 extracts remains a mystery.

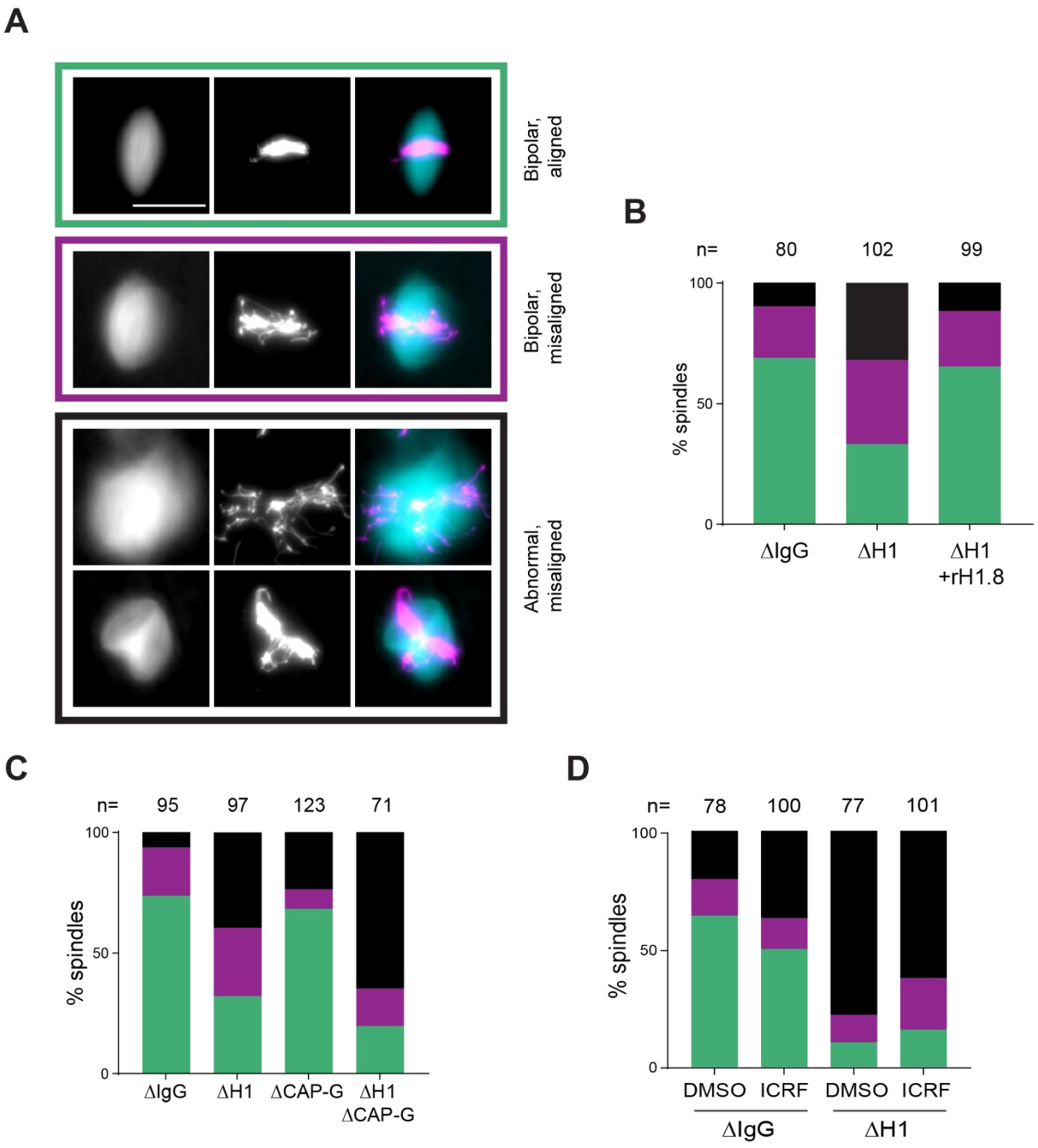

Figure 3-12 H1.8 maintains spindle integrity independent of chromosome length

A) Representative images of each spindle category using DNA (Cy3-dUTP) (left), Alexa647-tubulin (middle) and composite (right). Bar, 20 µm. B, C, D) Quantification of the number of spindles belonging to each category in the indicated condition. The n value above each bar represents the number of spindles counted in each condition.

Discussion and perspective

Chromosome individualization

The goal of mitotic DNA compaction is to effectively segregate the genomic material into the two daughter cells. To achieve this, mitotic compaction tries to achieve two things. The first one is to generate a mechanically rigid structure that can fit in and survive the forces generated in a mitotic spindle. The second one is to enable efficient decatenation in mitosis. Condensin activity organizes the rod-like mitotic chromosomes and is thus required for both these functions (Cuvier and Hirano, 2003). H1.8 mediated condensin suppression reduces the rod like organization of the chromosomes (**Figure 2-19**) and thus affects both role of mitotic chromosomes. I showed in the earlier chapter that H1.8 mediated suppression of condensin I prevents over-compaction of mitotic chromosomes laterally and increased chromosome length. In this chapter, I showed that H1.8 mediated suppression of condensins also prevents over individualization of mitotic chromosomes. I also then showed that this role of condensins is performed through directing topo II activity and that H1.8 suppresses topo II chromatin binding as well.

Most studies on mitotic decatenation discuss separation of sister chromatids. However, the significance and role of interchromosomal catenations is quite unclear. In interphase nuclei, chromosomes are largely segregated from each other into chromosome territories (Cremer and Cremer, 2010). However, chromosomes still do maintain a significant number of contacts. It is still unclear whether these contacts are just contacts or represent topological entanglements between the chromosomes. Recent reports suggest that at least in some cells in culture, chromosomes are largely unentangled (Goundaroulis et al., 2020; Tavares-Cadete et al., 2020). In *Xenopus* egg extracts, condensin I depletion appears to prevent separation of chromosomes from one another (**Figure 3-1**), however the nature of the forces preventing this separation is

not clear from this data. I then showed that continuous TOP2A activity (**Figure 3-4**) was required to individualize the chromosomes and that chromosome individualization is sensitive to TOP2A loading on chromatin (**Figure 3-6**). These data suggest that a substantial number of inter-chromosomal links remain in mitosis and that these links are likely to involve DNA catenations that need to be resolved through topo II.

Since topoisomerases can catalyze both catenation and decatenation of DNA (Krasnow and Cozzarelli, 1982), these reactions need to be actively driven towards decatenation in mitosis. Condensin activity is thought to drive resolution by driving the topoisomerase reaction equilibrium towards decatenation (Baxter et al., 2011; Dyson et al., 2020). Condensin driven loop organization can also play a role in maintaining this decatenated state (Piskadlo et al., 2017b). One possible mechanism for condensins to achieve this is by lowering the possibility of recatenation by maintaining a rigid rod like structure. In HeLa cells, condensin II activity is required to drive sister chromatid resolution (Nagasaka et al., 2016). Hi-C data indicates that both condensin I and condensin II contribute to chromosome rigidity and H1.8 mediated suppression of condensins also limits chromosome rigidity (**Figure 2-19**). Consistent with the reduced role of condensin II in maintaining the rigidity of *Xenopus* mitotic chromosomes, my data also show the normal levels of condensin II are also insufficient to drive individualization (**Figure 3-1, 3-3**). Releasing H1.8 mediated suppression of condensin II loading results in increased chromosomal rigidity (**Figure 2-18**) and also a rescue of individualization (**Figure 3-3**). This further supports the idea that interchromosomal links are topological catenations that need to be resolved by a combination of condensins and topo II. However, other factors such as Ki-67 (Cuylen et al., 2016) may also play a role in reducing interchromosomal contacts and the effect of H1.8 depletion on these factors is still unclear.

Topo II regulation in mitosis

The regulatory mechanisms of TOP2A recruitment to mitotic chromatin are less clear than those of condensins. TOP2A is a DNA binding protein that may also bind histone tails (Lane et al., 2013). Similar to condensin, both TOP2A and TOP2B preferentially localize at active and highly transcribed chromatin indicating a possible preference for nucleosome free regions (Canela et al., 2017; Thakurela et al., 2013; Yu et al., 2017). I showed that TOP2A levels on chromatin increase upon linker histone depletion in egg extracts and that linker histone inhibits TOP2A binding to nucleosome arrays *in vitro*, suggesting that a similar rheostat like mechanism for controlling TOP2A levels on mitotic chromatin by controlling H1 stoichiometry is possible. The preference of topo II for binding linker DNA may also explain the observation of well-spaced TOP2B binding peaks around the well-spaced nucleosomes around the CTCF- binding sites (Canela et al., 2017, 2019). If TOP2B also is similarly inhibited by linker histones, the lower linker histone stoichiometry in active regions (Izzo et al., 2013) of the genome may be necessary to resolve topological conflicts during transcription. Replication also creates topological conflicts which are resolved by topoisomerase activity (Heintzman et al., 2019). Coincidentally, replication dependent linker histone isoforms are partially phosphorylated in S-phase (Hergeth and Schneider, 2015). The functions of this phosphorylation are unclear, but a possible role in regulating TOP2B loading onto chromatin to resolve replication dependent topological conflicts presents an interesting possibility.

In mitosis, apart from driving topo II reaction equilibria towards decatenation, condensins may also play a role in enhancing topoisomerase activity. This may happen through creating more preferential substrates (Baxter et al., 2011) or through increasing the localizing substrates (Orlandini et al., 2019). This proposes a loading independent mechanism of regulating topo II activity on the chromatin. Previous studies using kinetoplast decatenation assays had shown no effect of condensin on TOP2A activity (Cuvier and Hirano, 2003). However, using a novel

assay, I showed that TOP2A activity on sperm chromatin is indeed promoted by condensin I and suppressed by H1.8 (**Figure 3-10**). This measured topo II activity is correlated with chromosome individualization indicating that condensin I may indeed positively affect topo II activity, not simply direct existing topo II activity. The exact mechanism of this activity enhancement is not clear from these data and remains an interesting area of study.

Mitotic spindle integrity

Chromosome clustering appears to be a phenotype connected to chromosome individualization. However, the exact mechanism of this clustering defect is still unclear. H1.8, condensin I co-depleted (ΔH1ΔCAP-G) extracts still show defective clustering (**Figure 3-11**) and defective spindles (**Figure 3-12C**). This appears to be correlated with the higher insulation in these chromosomes than control chromosomes (**Figure 2-19**). From the insulation score data, this would suggest that loss of both condensins should rescue this clustering phenotype and thus the spindle defects. However, loss of condensins appears to affect spindles in *Xenopus* egg extracts through disruption of kinetochore morphology. This complicates analysis of the role of chromosome clustering in maintaining spindle integrity. Other factors regulated by H1.8 may also play a role in maintaining spindle integrity.

Proper regulation of mitotic chromosome shape and individualization are both necessary to ensure efficient chromosome segregation in anaphase. Effective segregation also requires chromosome alignment in a bipolar mitotic spindle and effective topological resolution in anaphase. The presence of substantial interchromosomal contacts in mitosis (**Figure 3-4**) may thus be counterintuitive at first glance since chromosomes need to be independently segregated in anaphase. However, the loss of chromosome clustering upon loss of H1.8 led to the loss of spindle integrity. This suggests that clustering chromosomes through

incomplete individualization may also avoid generation of chromosomes that do not associate with the spindle.

Mammalian oocytes and early embryos are usually very large cells where the size of the spindle in meiotic metaphase II and early embryonic metaphases is much smaller compared to the size of the cells. This implies that mitotic spindle formation needs to be coupled to the DNA location. This suggests a need for chromosome clustering. This mechanism may be particularly important during early embryonic cell divisions when the spindle checkpoint cannot be activated by unattached chromosomes (Gerhart et al., 1984; Hara et al., 1980; Mara et al., 2019). Another possible reason for the suppressed individualization is related to the fact that oocyte chromosomes completely lose cohesion from arms at the end of meiosis I, while maintaining sister chromatid cohesion only at the centromeres (Lister et al., 2010). Normally, this centromeric cohesion is critical for supporting the kinetochore tension to establish bipolar attachment. During long natural arrest at meiotic metaphase II, these centromeres undergo cohesion fatigue, where centromeres prematurely separate. However, proper segregation may still be accomplished due to apparent inter-chromatids DNA linkages (Gruhn et al., 2019). Resolution of these DNA linkages may be prevented by H1.8-mediated suppression of condensin and TOP2A.

Chapter 4- Discussion and perspective

Linker histones regulate mitotic chromosome compaction through condensins and topo II

Linker histones were thought to be essential for mitotic compaction due to their central role in maintaining higher order compaction and their extensive mitotic phosphorylation (Roth and Allis, 1992). Experiments performed using *Xenopus* egg extracts showed that neither linker histones nor core histones are essential for the basic structure of the mitotic chromatid (Ohsumi et al., 1993; Shintomi et al., 2017). But, linker histones were shown to be essential for maintaining proper mitotic chromosome compaction through unknown mechanisms (Maresca et al., 2005). Our understanding of how the mitotic chromosomes are structured through condensin mediated loops has, in the past decade, shown us how mitotic compaction may be regulated (Gibcus et al., 2018; Kakui et al., 2017; Naumova et al., 2013).

I set out to tackle two questions at the beginning of my thesis. The first was to understand how linker histones regulate mitotic compaction and the second was to understand how condensins are regulated by local chromatin structure. In chapter 2, I showed that H1.8 competitively inhibits binding of condensins on mitotic chromatin and that H1.8 controls mitotic chromosome length solely through condensin I. In the course of answering these questions, I show in chapter 3 that H1.8 suppresses chromosome individualization through its regulation of both condensins and DNA topoisomerase, TOP2A. These results address both the questions I set out to tackle. Linker histone H1.8 controls mitotic compaction through both condensins and TOP2A and condensins are regulated by linker histones mediated compaction. As H1.8 controls condensin loading through competitive inhibition, I propose that changing linker histone stoichiometry on chromatin can tune both functions of the mitotic chromosome compaction, chromosome length and individualization (**Figure 4-1**).

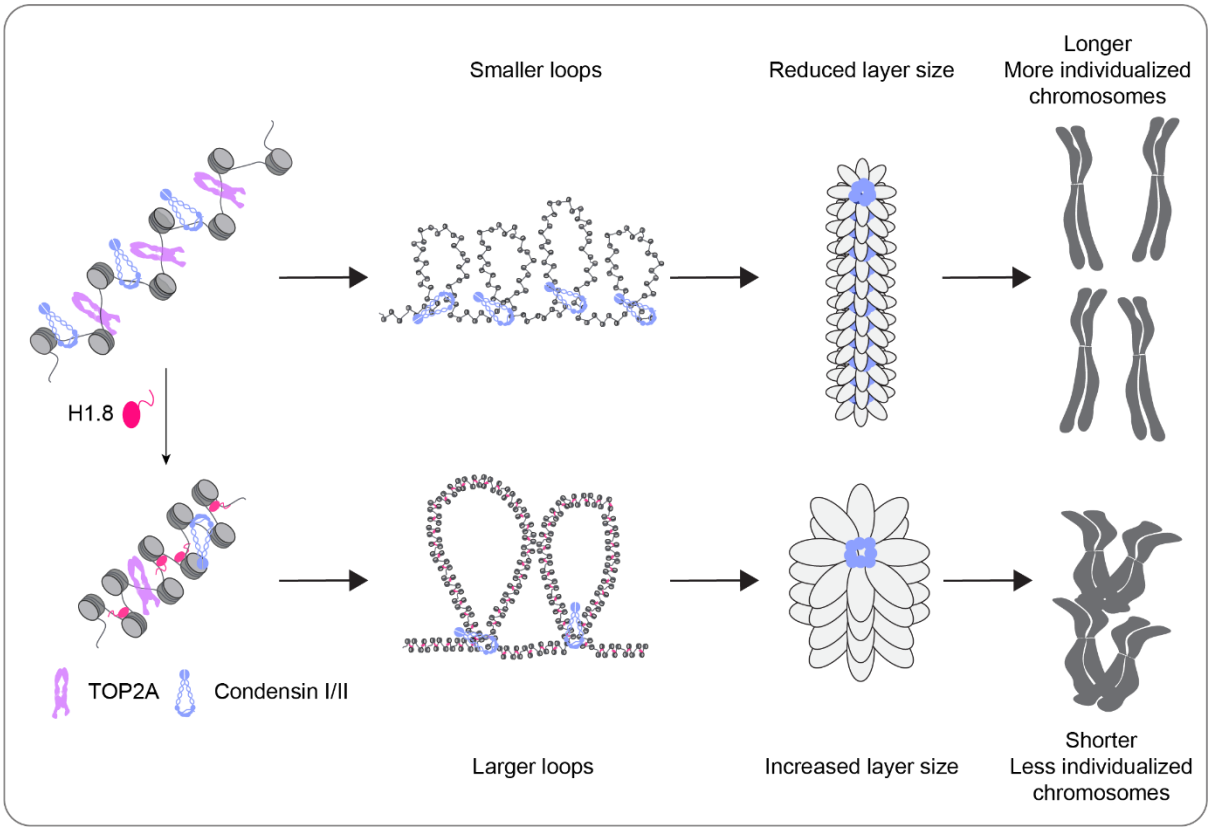

Figure 4-1 H1.8 controls mitotic chromosome compaction through condensins and topo II.

Proposed model showing how H1.8 regulates mitotic chromosome length through changing loop sizes and how it regulates chromosome individualization through both condensins and topo II.

Linker histone stoichiometry is quite variable (Woodcock et al., 2006) and linker histone binding in mitosis may be modulated by posttranslational modifications. This suggests a platform for regulating chromatin compaction by titrating linker histone availability. This model for linker histone regulation of mitotic compaction suggests that H1.8 prevents overcompaction of mitotic chromatin by restricting condensins. This is counterintuitive to the generally assumed role of linker histones in increasing compaction of chromatin and indicates that linker histones can serve two roles.

Linker histones induce chromatin compaction through their ability to constrain the DNA wrapping around a nucleosome (Bednar et al., 2017; Song et al., 2014). Since most of the chromatosome structures studied *in vitro* show similarly increased constraints on the nucleosomal DNA, it appears that the binding of linker histones is correlated to its compaction. However, a recent *in vitro* study has shown that chromatin compaction by different linker histone variants does not determine their chromatin binding affinity (Osunsade et al., 2019). This variance may be explained by differences in nucleosome structures due to the binding of different linker histone variants, some of which induce more constraints on nucleosomal DNA than others (Zhou et al., 2021). This suggests that it is useful to think of two different roles for linker histones, one as a highly abundant high affinity chromatin binding protein that blocks DNA binding proteins, and as a regulator of higher order chromosome (Izzo and Schneider, 2016). Since both these roles can result in similar phenotypes, blocking transcription factors competitively can perform the same role as silencing by enabling heterochromatinization, these roles are often difficult to tease apart (Healton et al., 2020).

Linker histones are gatekeepers of accessible DNA

80% of the genomic DNA in yeast is packaged in nucleosomes (Lee et al., 2007). Although it is difficult to estimate this number in human cells, most of the genomic DNA in human cells is also covered by nucleosomes (Chereji et al., 2019). With a nucleosome repeat length of 200 bp, this suggests that nucleosomes and linker DNA block access to up to 90 % of the genome. Since nucleosomes breathe (Li et al., 2005) and linker histones are dynamic (Misteli et al., 2000), this does not prevent access of transcription factors and other specific DNA binding proteins to their binding sites.

Some DNA binding proteins however, function through mass action, i.e their activity is related to the total amount of the protein on chromatin. Condensins are a classic example of such a DNA binding complex. My work here supports many previous observations that changing the average accessibility of genomic DNA changes the loading of such proteins on to DNA (Shintomi et al., 2017; Toselli-Mollereau et al., 2016b; Zierhut et al., 2014). Other mass action DNA binding proteins such as KIF22, KIF4A, Ki67 and the SMC5/6 complex have also been identified. If these proteins follow similar principles, linker histones can regulate the activities of these proteins through their accumulation on the DNA as well. Since most of the genomic DNA is protected by linker histones or nucleosomes, all these proteins compete with each other for a few binding sites (~ 10 % of the genome) (**Figure 4-2**). Since nucleosomes are more stable and serve many other purposes, dynamic linker histones serve as a great platform for cellular regulation of the chromatin abundance of these proteins.

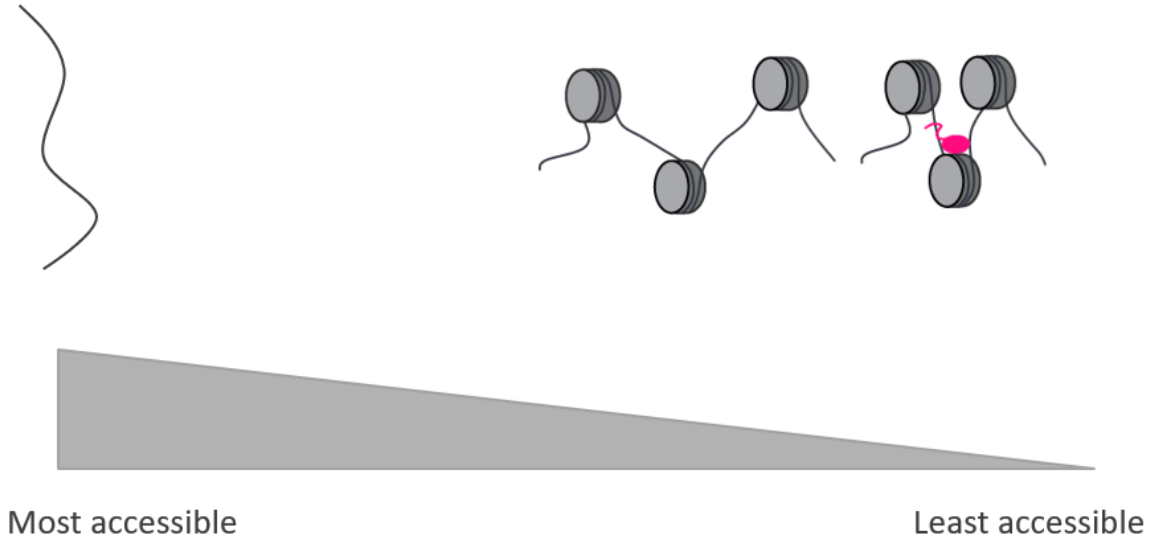

Figure 4-2 DNA accessibility is controlled by core and linker histones

Genomic DNA accessibility to DNA binding proteins is controlled by both nucleosomes and linker histones. Nucleosomes block access to a large majority of the genomic DNA but linker histones regulate access to a large fraction of the remaining linker DNA.

Outstanding questions

Linker histones variants and regulation in mitosis

There are many variants of the linker histones (Izzo et al., 2008). As discussed in Chapter 1, different tissues in humans express a different combination of the variants. This suggests functional specialization for the variants. Deleting single linker histone variants does result in variant specific gene expression changes (Alami et al., 2003), however these only represent a small fraction of the gene expression suggesting that variants share a lot of functional redundancy. Reducing the chromatin levels of linker histones to 50 %, by depletion of three of the five replication dependent H1s, in mice results in embryonic lethality showing that linker histones are essential for development (Fan et al., 2003). The triple knockout (TKO) mouse ES cell lines derived from these mice show specific gene expression changes but have no reported defects in mitosis (Fan et al., 2005). It is difficult to know whether this is due to a lack of careful analysis or due to changes in gene expression compensating for changes in mitotic compaction.

Somatic linker histones are unable to rescue H1.8 depletion in *Xenopus* egg extracts since they are sequestered by the importin β complex (Freedman and Heald, 2010). This is in contrast to the oocyte linker histone H1.8, which is stabilized on mitotic chromatin (Arimura et al., 2020). This suggests that, unlike somatic linker histones, H1.8 has been specialized to function in a mitotic role in oocytes. The reasons for this discrepancy in mitotic functions of the linker histone variants is not known. There are two easily identifiable differences between H1.8 and the C-terminal tails features shared by other somatic linker histone variants. The first is charge density. The C-terminal tail of linker histones is highly charged and is essential for its binding in cellular contexts (Misteli et al., 2000) (**Figure 4-3**). The C-tail of H1.8 is longer than those of somatic linker histones, but it has a lower total positive charge (~+40 somatic to +20 H1.8). This would result in a large difference to charge density of the oocyte linker

histones, which may explain the difference in importin β sequestration. Oocyte linker histone binding has been shown to result in higher mobility of nucleosomes and greater accessibility to transcription factors (Saeki et al., 2005). This suggests that oocyte linker histones, which show substantial divergence from somatic H1s, are specialized to perform mitotic roles in oocytes and early embryos.

Another large difference between oocyte linker histones and somatic H1s is the loss of Cdk1 phosphorylation sites on the C-terminal tail. Somatic linker histones have 3-4 well conserved Cdk consensus sites on the C-terminal tail (**Figure 4-3**), whereas oocyte linker histone variants have lost all such sites. Since oocyte H1s appear to have specialized functions, the role of this phosphorylation also appears to be an interesting avenue of research. This phosphorylation was thought to be important for the mitotic compaction (Roth and Allis, 1992). No evidence of such a role for this phosphorylation has yet been found. These sites are also partially phosphorylated in S-phase by S-phase cyclin dependent kinases and this has been shown to play in role in allowing replication in closed chromatin in some systems (Hergeth and Schneider, 2015).

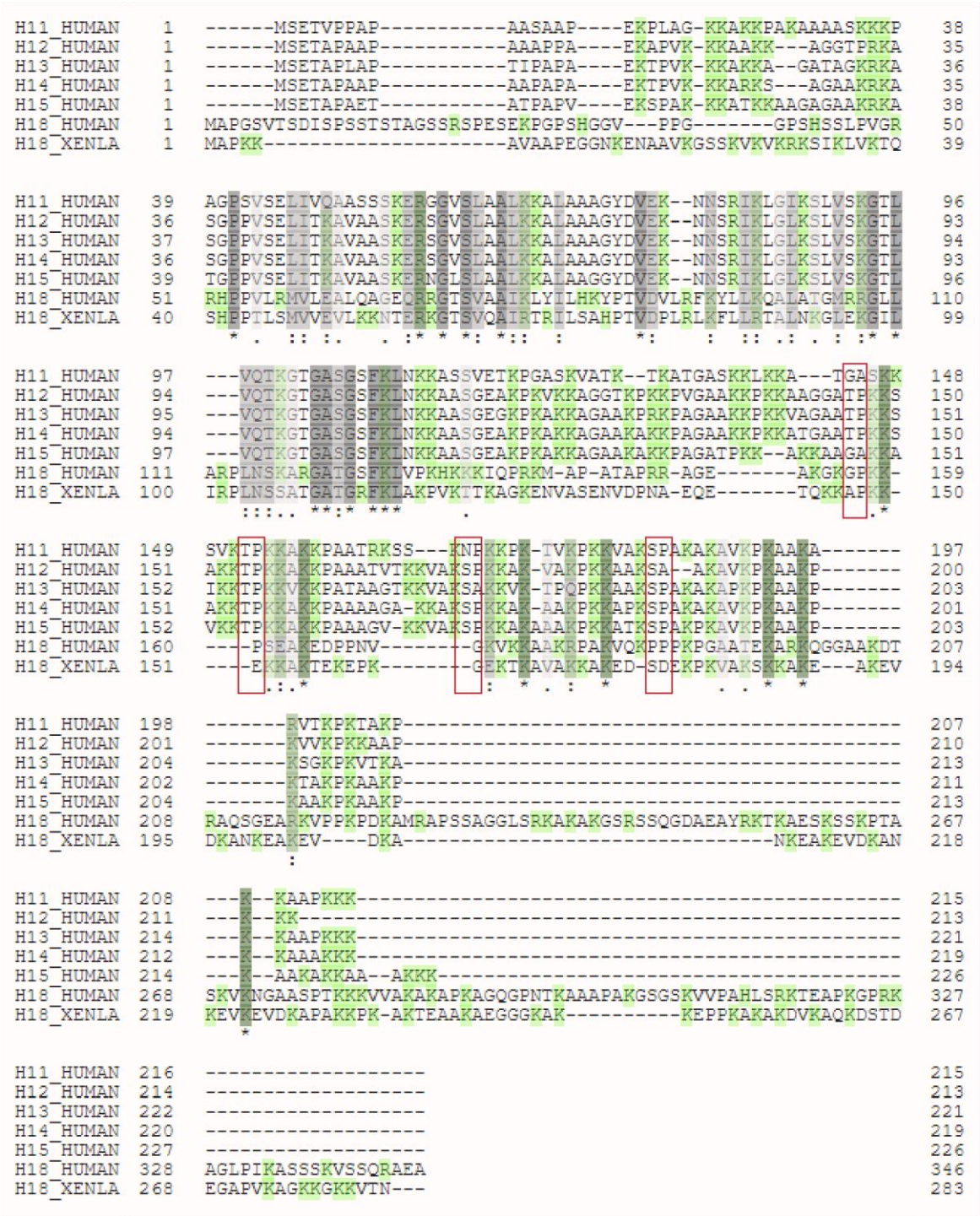

Figure 4-3 Somatic linker histones have conserved Cdk1 phosphorylation sites

Alignment of human H1 variants and frog H1.8. Gray coloring shows conserved residues, green coloring shows positively charged residues and the red boxes show conserved consensus Cdk1 sites.

Regulation of chromosome structure in development

As discussed earlier, changing linker histone stoichiometry can titrate access to a number of compaction factors and other mass action processes. Linker histone stoichiometry is highly variable between cell types and linker histones appear to be absent in at least some terminally differentiated cells (Woodcock et al., 2006). Cell size is also quite variable between these cells and changes during development (Ginzberg et al., 2015b). Since cells need to regulate chromosome size according to their cell size (Kieserman and Heald, 2011; Ladouceur et al., 2015; Schubert and Oud, 1997) and linker histone variants also show differential expression between tissues (Izzo et al., 2008) linker histone stoichiometry could be a useful rheostat for changing chromosome sizes in these cells.

This regulation of DNA accessibility may play a role in interphase functions as well. Linker histone loss appears to have some tissue specific affects similar to those observed due to cancer associated mutations in H1 variants (Willcockson et al., 2021; Yusufova et al., 2021). These studies find that H1 loss leads to specific changes in compartment and TAD structure in these cells and also gene expression changes. The mechanisms for these changes in genomic structure are unclear since local changes in chromatin fiber do not necessarily lead to changes in large genomic structures such as TADs. Similar tissue specific effects of linker histone mutations are likely to be found in other linker histone variants and tissues as well.

Chapter 5- Materials and methods

Table 5-1 List of primary antibodies used in this study

Antibody	Western blot concentration/dilution	IF concentration/ dilution	Immunodepletion condition	Reference
B4 (H1.8)	1 µg/ml	1 µg/ml	2 rounds- 2 volumes	Jenness et al., 2018
H3	1 µg/ml			Abcam-ab1791
H2B	1 µg/ml			Abcam-ab1790
α-tubulin	1:10000			Sigma-T9026
xKu80	2 µg/ml	4 µg/ml		Postow et al., 2008
xCAP-G	2 µg/ml	2 µg/ml	1.5 volumes	Zierhut et al., 2014
xCAP-G2	2 µg/ml	NA	NA	This study
xCAP-G2	2 µg/ml	4 µg/ml		OMRF195-Gift from S. Rankin
xCAP-D3	2 µg/ml	NA	1.5 volumes	This study
xCAP-C	2 µg/ml		NA	RU2045-This study
xTOP2A	2 µg/ml	1 µg/ml	1.2 volumes	Ryu et al., 2010-Gift from Y. Azuma
xCAP-D2	2 µg/ml	2 µg/ml		Hirano, Kobayashi and Hirano, 1997
xCENP-A	2 µg/ml	4 µg/ml		Wynne and Funabiki, 2015
H4K12AC		1 µg/ml		Gift from H.Kimura
H3S10P		1 µg/ml		Gift from H.Kimura

Table 5-2 List of custom antibodies generated in this study

Protein	Antigen	Western blot	Immuno depletion	Immuno fluorescence	Project number
xCAP-D3	CRQRISGKAPLKPSN	Yes	Yes	No	RU2042
xCAP-G2	CESSMRILNEMLHPS	Yes	No	No	RU2040
xCAP-C	CSKTKERRNRMEVDK	Yes	No	NA	RU2045

Table 5-3 List of plasmids used in this study

Plasmid name	Source
pET51-B4-His	Miller and Heald, 2015
pPIC3.5k CBP T7-Topo2a xl WT	Ryu et al., 2010

Xenopus egg extract protocols

Xenopus egg extract preparation

Cytostatic Factor (CSF) arrested *X. laevis* egg extracts were generated as previously described (Murray, 1991). To generate replicated mitotic chromosomes, 0.3 mM $CaCl_2$ was added to CSF arrested extracts containing *X. laevis* sperm to cycle the extracts into interphase at 20°C. Ninety minutes after adding $CaCl_2$, half the volume of fresh CSF extract and 40 nM of the non-degradable cyclin BΔ90 fragment were added to interphase extracts to induce mitotic entry (Glotzer et al., 1991; Holloway et al., 1993). After 60 min of incubation, extracts were processed for morphological and biochemical assessments. For all experiments involving immunofluorescence, 10 nM nocodazole was added along with the cyclin BΔ90.

Immunodepletion

For immunodepletions of 50-100 µl extracts, 250 µg/ml antibodies were conjugated to Protein-A coupled Dynabeads (Thermo Fisher Scientific) either at room temperature for 60 min or overnight at 4 ºC. Mock (IgG) and H1.8 (B4) antibody beads were crosslinked using 4 mM BS_3 (Thermo Fisher Scientific) at room temperature for 45 min and quenched using 10 mM Tris-HCl (Sigma). All antibody beads were washed extensively using Sperm Dilution Buffer (SDB; 10 mM HEPES, 1mM $MgCl_2$, 100 mM KCl, 150 mM Sucrose) and separated from the buffer using a magnet before addition of extract. H1.8 depletions (ΔH1) were performed with two 45 min rounds of depletion at 4 ºC using 2 volumes of antibody-coupled beads for each round. For double depletion of condensin I and II, a single round of depletion using 1.5 volume each of xCAP-G and xCAP-D3 antibody-coupled beads was performed. After the incubations, the beads were separated using a magnet.

Antibody production

xCAP-D3 C-terminal peptide (CRQRISGKAPLKPSN), xCAP-G2 C-terminal peptide (CESSMRILNEMLHPS) and xCAP-C C-terminal peptide (CSKTKERRNRMEVDK) were synthesized at The Rockefeller University Proteomics Resource Center). The peptide was then coupled to the keyhole limpet hemocyanin according to the manufacturer's protocol (Thermo-Fisher Scientific) and used to immunize rabbits (Cocalico Biologicals). Antibody was purified from the immunized rabbit sera using affinity purification against the same peptide coupled to SulfoLink resin (Thermo-Fisher Scientific). The antibody was dialyzed into PBS+ 50% glycerol and stored with the addition of 0.05% sodium azide.

Western blots

For total egg extract samples, 1 µl sample was added to 25 ul 1x sample buffer (50 mM Tris-HCl pH 6.8, 2 % SDS, 10% Glycerol, 2.5 % β-mercaptoethanol) and boiled for 10 min. Samples were spun at 8000 rpm for 3 min before gel electrophoresis and overnight transfer at 4 ºC. Blotting membranes were blocked with 4 % powdered skim-milk (Difco). Primary and secondary antibodies were diluted in LICOR Odyssey blocking buffer-PBS (LI-COR Biotechnology). Western blots were imaged on a LICOR Odyssey. Quantifications were done using Image-J.

IRDye 680LT Goat anti-Mouse IgG (H+L), IRDye 680LT Goat anti-Rabbit IgG (H+L), IRDye 800CW Goat anti-Mouse IgG (H+L) and IRDye 800CW Goat anti-Rabbit IgG (H+L) were used at 1:15000 (LI-COR Biosciences) dilution as secondaries for western blots.

Ku80 assay

For **Figures 3-9B, C** sperm nuclei were added along with DMSO/ 50 μM VM-26 to undepleted/ΔTOP2A CSF extract and incubated for 50 min at room temperature. The extract was then fixed and spun down onto coverslips for immunofluorescence. The coverslips were stained with xKu80 antibody to image Ku80 accumulation.

For **Figure 3-10**, sperm nuclei were replicated in extracts depleted of indicated proteins. The extracts were then cycled back into mitosis by the addition of fresh CSF extract and 40 nM cyclinBΔ90 (Glotzer et al., 1991; Holloway et al., 1993) and split into two. 5 min after cycling back, DMSO and 20 μM VM-26 were added to each of the two vials in each depletion condition. Samples were fixed for immunofluorescence after 20 min.

Kinetoplast decatenation assay

CSF extracts co-depleted with anti-TOP2A antibody and anti-IgG, anti-H1.8 or anti-CAP-G antibody were cycled into interphase by the addition of 0.3 mM $CaCl_2$. 100 μg/ml cycloheximide (Sigma) was also added to prevent translation of cyclin B. After 40 min at 21 ºC, 10 ng/μl kinetoplast DNA (TopoGEN) was added to the interphase extract and incubated for 150 min at 21 ºC. The extract was then cycled back into mitosis with the addition of 1 volume of CSF extract (ΔIgG/ΔH1/ΔCAP-G) containing TOP2A. 30 μl samples were taken at the indicated time points and added into a tube containing 270 μl Stop Buffer I (20 mM Tris-Cl pH 8, 20 mM EDTA, 0.5% SDS, 0.05 mg/ml RNase A) which stops the decatenation reaction and the tube was incubated at 37 ºC for 30 min. 300 μl Stop Buffer II (20 mM Tris-Cl pH 8, 20 mM EDTA, 0.5% SDS, 1 mg/ml Proteinase-K) was then added and the tube was incubated at 37 ºC for 60 min. The tubes were then extracted once with Phenol-Chloroform-Isoamylalcohol and once with Chloroform and precipitated with ethanol overnight. The pellet

after ethanol precipitation was resuspended in 1x TE with 0.05 mg/ml RNase A (Sigma) and incubated at 37 ^{o}C for 60 min to digest any remaining RNA. The samples were run on a 1% agarose gel and stained with SYBR-SAFE (Thermo-Fisher Scientific).

Plasmid supercoiling assay

CSF extracts depleted with anti-IgG, anti-H1.8 were cycled into interphase by the addition of 0.3 mM $CaCl_2$. 100 µg/ml cycloheximide (Sigma) was also added to prevent translation of cyclin B. After 40 min at 21 ^{o}C, 10 ng/µl relaxed circular pBlueScript DNA was added to the interphase extract. 30 µl samples were taken at the indicated time points and added into a tube containing 270 µl Stop Buffer I (20 mM Tris-Cl pH 8, 20 mM EDTA, 0.5% SDS, 0.05 mg/ml RNase A) which stops the decatenation reaction and the tube was incubated at 37 ^{o}C for 30 min. 300 µl Stop Buffer II (20 mM Tris-Cl pH 8, 20 mM EDTA, 0.5% SDS, 1 mg/ml Proteinase-K) was then added and the tube was incubated at 37 ^{o}C for 60 min. The tubes were then extracted once with phenol-chloroform-isoamylalcohol and once with Chloroform and precipitated with ethanol overnight. The pellet after ethanol precipitation was resuspended in 1x TE with 0.05 mg/ml RNaseA (Sigma) and incubated at 37 ^{o}C for 60 min to digest any remaining RNA. The samples were run on a 1% agarose gel in 1x TBE containing 0.5 µM chloroquine at 0.75 V/cm for 36 hours in 1x TBE containing 0.5 µM chloroquine. The gel was stained with SYBR-SAFE (Thermo-Fisher Scientific) and imaged.

Spindle assembly

0.3 mM $CaCl_2$ was added to CSF arrested extracts containing 500/µl *X. laevis* sperm to cycle the extracts into interphase. After replication, 5 µl interphase sample was mixed with 15 µl fresh CSF extract to cycle back into metaphase along with 0.2 µM Alexa 647 labelled tubulin.

After 60 min in metaphase, 1 µl sample was added to a 3 µl drop of Fix (5 mM K-HEPES pH 8, 0.1 mM EDTA, 100 mM NaCl, 2 mM KCl, 1 mM $MgCl_2$, 2 mM $CaCl_2$, 50 % glycerol, 10% formaldehyde, 0.5 µg/ml Hoechst 33342) and sealed with a square 18x18 mm coverslip.

Hi-C

Standard samples

10^6 *X. laevis* sperm nuclei were added to 150 µl interphase extract and allowed to replicate at 21 ^{0}C for 90 min. The extracts were cycled back into mitosis by adding 100 µl CSF extract, 40 nM of the non-degradable cyclin BΔ90 and 10 µM nocodazole (Sigma). After 60 min at metaphase, the samples were diluted into 12 ml of fixing solution (80 mM K-PIPES pH 6.8, 1 mM MgCl2, 1 mM EGTA, 30% glycerol, 0.1% Triton X-100, 1% formaldehyde) and incubated at room temperature with rocking for 10 min. The samples were then quenched with 690 µl 2.5 M glycine for 5 min at room temperature. The samples were then placed on ice for 15 min and then centrifuged at 6000 g at 4 ºC for 20 min. The pellet was then resuspended in 1 ml ice-cold DPBS. The tube was then centrifuged again at 13000 g for 20 min at 4 ºC. The buffer was aspirated, and the pellet was frozen in liquid nitrogen and then stored at -80 ºC.

Dispersed chromosome samples

The metaphase chromosome samples were prepared as above, but nocodazole was omitted. The metaphase extracts were diluted by adding 1.2 ml chromosome dilution buffer (10 mM K-HEPES pH 8, 200 mM KCl, 0.5 mM EGTA, 0.5 mM $MgCl_2$, 250 mM Sucrose) and incubated at room temperature for 8 min. 6 ml fixation buffer (5 mM K-HEPES pH 8, 0.1 mM EDTA, 100 mM NaCl, 2 mM KCl, 1 mM $MgCl_2$, 2 mM $CaCl_2$, 0.5% Triton X-100, 20% glycerol, 1% formaldehyde) was added to the tube, mixed by rotation 10 min at room temperature. 420 ul 2.5 M glycine was added to quench the formaldehyde and the mixture was incubated for 5 min

at room temperature. The samples were then placed on ice for 15 min and then centrifuged at 6500 g at 4 ºC for 20 min. The pellet was then resuspended in 1 ml ice-cold DPBS. The tube was then centrifuged again at 13000 g for 20 min at 4 ºC. The buffer was aspirated, and the pellet was frozen in liquid nitrogen and then stored at -80 ºC.

Library prep and sequencing (performed by Bastiaan Dekker)

Hi-C protocol was performed as previously described (Belaghzal et al., 2017), with exception that cell disruption by douncing was omitted. Briefly, pellets were digested by DpnII overnight at 37 °C prior to biotin fill-in with biotin-14-dATP for 4 h at 23 °C. After ligation at 16 °C for 4 h, crosslinking was reversed by proteinase K at 65°C overnight. Purified ligation products were sonicated with 200 bp average size, followed by 100-350 bp size selection. End repair was performed on size selected ligation products, prior to purifying biotin tagged DNA fragments with streptavidin beads. A-tailing was done on the purified DNA fragments followed by Illumina Truseq adapter ligation. Hi-C library was finished by PCR amplification and purification to remove PCR primers. Final library was sequenced on Illumina HiSeq 4000 with PE50.

Hi-C Data Processing (performed by Bastiaan Dekker)

Hi-C fastq files were mapped to the *Xenopus laevis* 9.2 genome with the distiller-nf pipeline (https://github.com/open2c/distiller-nf). The reads were aligned with bwa-mem, afterwards duplicate reads were filtered out. These valid pair reads were aggregated in genomic bins of 10, 25, 50, 100, 250, 500kb using the cooler format (Abdennur and Mirny, 2019). Cooler files were balanced using Iterative balancing correction (Imakaev et al., 2012), ignoring first two diagonals to avoid artifacts within the first bin such as re-ligation products. Contact heatmaps from balanced cooler files were viewed and exported with Higlass (Kerpedjiev et al., 2018).

Contact Probability (P(s)) and derivatives

Contact probability was calculated by contact frequency (*P)* as function of genomic distance (*s)*. Interaction pairs were selected for genomic distance from 1kb till 100mb binned at log-scale. Within each genomic bin observed number of interactions were divided by total possible number of interactions within the bin. Distance decay plots were normalized by total number interactions, derivative plots were made from corresponding *P(s)*.

Chromosome individualization

Chromosome dilution was performed as before with some modifications (Funabiki and Murray, 2000). 40 µl Chromosome Dilution Buffer (10 mM K-HEPES pH 8, 200 mM KCl, 0.5 mM EGTA, 0.5 mM $MgCl_2$, 250 mM Sucrose) was added to 10 µl metaphase extract containing chromosomes and incubated at room temperature for 8 min. 200 ul fixation buffer (5 mM K-HEPES pH 8, 0.1 mM EDTA, 100 mM NaCl, 2 mM KCl, 1 mM $MgCl_2$, 2 mM $CaCl_2$, 0.5% Triton X-100, 20% glycerol, 2% formaldehyde) was added to the tube and incubated for 10 min at room temperature. The samples were laid over a cushion (5 mM K-HEPES pH 8, 0.1 mM EDTA, 100 mM NaCl, 2 mM KCl, 1 mM $MgCl_2$, 2 mM $CaCl_2$, 50 % glycerol) with a coverslip placed under the cushion and centrifuged at 7000g for 20 min at 18 ^oC in a swinging bucket rotor. The coverslips were recovered and fixed with ice-cold methanol for 4 min, washed extensively and blocked overnight with antibody dilution buffer (50 mM Tris-Cl pH 7.5, 150 mM NaCl, 2% BSA).

For each extract, the optimal $MgCl_2$ concentration in the chromosome dilution buffer was assessed (0.5 mM to 2 mM range) in undepleted extracts by performing a titration with replicated metaphase chromosomes and visually inspecting the individualized chromosomes at high resolution (>1.25 NA).

Chromosome purification

One volume of metaphase extracts with ~3000/µl sperm nuclei was diluted into 3 volumes of DB2 (10 mM K-HEPES, 50 mM β-glycerophosphate, 50 mM NaF, 20 mM EGTA, 2 mM EDTA, 0.5 mM spermine, 1 mM phenylmethylsulfonyl fluoride, 200 mM sucrose) and laid over 1 ml cushion (DB2 with 50% sucrose). The tube was centrifuged in a swinging bucket rotor at 10,000g for 30 min at 4 ºC. Most of the cushion was aspirated and the pellet was resuspended in the remaining solution and transferred to a fresh tube. The sample was centrifuged again at 13000g for 15 min at 4 ºC. The pellet was then resuspended in 1x sample buffer and boiled for 10 min before being subject to gel electrophoresis.

Tissue culture protocols

Cell culture

HeLa cells were cultured in Dulbecco's Modified Eagle Medium (high glucose, with L-glutamine, pyruvate, Thermo-Fisher Scientific Cat no. 11995040) supplemented with 10% fetal bovine serum (Atlanta biologicals) and grown at 37 ºC, 5% CO_2. hTert-RPE1 cells were cultured in DMEM/F-12 (Thermo-Fisher Scientific) supplemented with 10% FBS and hTert-BJ fibroblast cells were cultured in 4:1 DMEM:Media 199 (Thermo-Fisher Scientific).

Microscopy protocols

Immunofluorescence

Immunofluorescence was performed according to previously published protocols (Desai et al., 1998). 10 µl metaphase extracts containing chromosomes were diluted into 2 ml of fixing solution (80 mM K-PIPES pH 6.8, 1 mM $MgCl_2$, 1 mM EGTA, 30% glycerol, 0.1% Triton X-

100, 2% formaldehyde) and incubated at room temperature for 7 min. The fixed chromosomes were then laid onto a cushion (80 mM K-PIPES pH 6.8, 1 mM $MgCl_2$, 1 mM EGTA, 50% glycerol) with a coverslip placed at the bottom of the tube and centrifuged at 5000g for 15 min at 18 ºC in a swinging bucket rotor. The coverslips were recovered and fixed with methanol (-20 ºC) for 4 min. The coverslips were then blocked overnight with antibody dilution buffer (50 mM Tris-Cl pH 7.5, 150 mM NaCl, 2% BSA). Primary and secondary antibodies were diluted in antibody dilution buffer and sealed in Prolong Gold AntiFade mounting media (Thermo-Fisher Scientific).

Alexa 488, Alexa 555 and Alexa 647 conjugated secondary antibodies (Jackson Immunoresearch) were used for IF. For expansion microscopy, only Alexa488 or Atto565 anti-rabbit secondary antibodies were used as they were not quenched during the oxidative step involved in the polymerization. Alternatively, biotin conjugated anti-rabbit secondary (Sigma-Aldrich) was used and stained post-expansion using Cy3-Streptavidin (Thermo-Fisher Scientific).

For coverslips stained with Alexa488-anti-CAP-G antibody (**Figure 2-1C, D, 2-4B, C, 52-10F**), coverslips stained with primary and secondary antibodies were washed three times with PBS-T (1x PBS +0.5% Tween-20). Then, they were blocked with 100 µg/ml rabbit IgG or 30 min and were incubated with Alexa488-anti-xCAP-G antibody without any washing steps in between. The coverslips were then washed three times with PBS-T and then sealed in Prolong Gold AntiFade mounting media (Thermo-Fisher Scientific).

Expansion microscopy

Expansion microscopy was performed as described on standard immonstained samples as described previously (Chozinski et al., 2016). *X. laevis* egg extract samples and human tissue

culture cell samples were prepared and stained using primary and secondary antibodies as described in the immunofluorescence section. Egg extract samples for expansion microscopy were not subjected to post-spindown fixation using methanol. The stained coverslips were then fixed using 0.25% glutaraldehyde (Electron Microscopy Sciences) in 1x PBS for 10 min at room temperature. These coverslips were then washed thrice in 1x PBS and once in monomer solution (1x PBS, 2M NaCl, 2.5% acrylamide, 0.15% N, N'-methylenebisacrylamide, 8.265 % sodium acrylate). A drop of 60 µl of gelation solution (1x monomer solution+0.2% ammonium persulfate+0.2% N,N,N′,N′-tetramethylethylenediamine (TEMED)) was placed on a parafilm coated dish and the coverslip was then inverted onto the drop. After 20-30 min at room temperature, the coverslip covered with the gel was moved to a 35 mm dish filled with 2 ml of proteinase solution (1x TAE, 0.5% Triton X-100, 0.8M guanidine hydrochloride, 8 U/ml Proteinase K (Roche)) and incubated at 37 ºC for 1 hour. This step usually loosens the gel from the coverslip. The gels were then expanded by incubating the gel in ddH_2O for three 30 min periods. This leads to a ~4-fold isotropic expansion of the gel. For post-staining labelling, the gel was incubated in Cy3-Streptavidin in ddH_2O for 30 min. The gels were then cut to fit on a 35 mm coverslip and then placed on a 35 mm glass bottom dish (MatTek) and sealed using low temperature agarose to immobilize the gel for imaging.

Image acquisition and analysis

All the quantitative immunofluorescence imaging and some of the spindle imaging was performed on a DeltaVision Image Restoration microscope (Applied Precision) which is a wide-field inverted microscope equipped with a pco.edge sCMOS camera (pco). The samples were imaged with z-sections of 200 nm width with a 100x (1.4 NA) objective and were

processed with a iterative processive deconvolution algorithm using the SoftWoRx (Applied Precision).

The maximum intensity single slice was selected, background subtraction was performed, and average intensities were calculated on a mask generated using the DNA signal. The analysis was performed using MATLAB (Mathworks) code.

For surface area measurements, images were interpolated into stacks of 67 nm width. A surface mask was built in three-dimensional space and surface area and DNA signal was calculated using the regionprops3 MATLAB function.

Chromosome length measurements were done on a single maximum intensity slice in ImageJ 1.52p.

Fluorescence lifetime imaging (FLIM)

Both *X. laevis* and human tissue culture samples, both fixed and live were stained with 1:1000 Picogreen (Thermo-Fisher Scientific) unless otherwise indicated. These samples were then imaged using a frequency domain Li-FLIM system (Lambert Instruments). The samples were imaged on a Nikon Eclipse Ti inverted microscope in a wide-field mode using a modulated 40MHz 445 nm LED. The images were captured using a LI2CAM intensified CCD camera (Lambert Instruments). The system was calibrated using a fluorescein solution (Lambert Instruments).

Biochemistry

Mononucleosomes and nucleosome array preparation

Nucleosome arrays were prepared as previously noted (Guse et al., 2011; Zierhut et al., 2014). The plasmid pAS696 which contains 19 repeats of the Widom 601 nucleosome position sequence (Lowary and Widom, 1998) was digested with EcoRI, XbaI, HaeII and DraI. The fragment containing the array was isolated using polyethylene glycol-based precipitation. The ends of the DNA fragment were filled in with dATP, dGTP, dCTP and Bio-16-dUTP (Chemcyte) using Klenow DNA polymerase (NEB) and purified using Sephadex G-50 Nick columns (Cytiva Biosciences).

Mononucleosomal DNA were prepared by digesting pAS696 using AvaI. The 196 bp fragment was isolated using polyethylene glycol-based precipitation. The ends of the fragment were filled in with dATP, dGTP, dTTP and Alexa647-aha-dCTP (Thermo-Fisher Scientific) using Klenow DNA polymerase (NEB) and purified using Sephadex G-50 Nick columns (Cytiva Biosciences).

For nucleosome deposition, 10 µg of DNA arrays or mononucleosomal DNA was mixed with equimolar amount of *X. laevis* H3-H4 tetramer and twice equimolar amount of *X. laevis* H2A-H2B dimers in 1x TE with 2 M NaCl. The mixture was added into in a Slide-A-Lyzer dialysis cassette (Thermo-Fisher Scientific) and placed into 500 ml High salt buffer (10 mM Tris-Cl pH 7.5 @ 4 ^{o}C, 2M NaCl, 1 mM EDTA, 5 mM β-mercaptoethanol, 0.01 % Triton X-100). Salt was reduced in a gradient by pumping in 2 L of Low salt buffer (10 mM Tris-Cl pH 7.5 at 4 ^{o}C, 100 mM NaCl, 1 mM EDTA, 5 mM β-mercaptoethanol, 0.01 % Triton X-100) at constant volume at 1 ml/min. The quality of the nucleosome arrays was ascertained by digesting the nucleosome arrays with AvaI overnight in low magnesium buffer (5 mM potassium acetate, 2 mM Tris-acetate, 0.5 mM magnesium acetate, 1 mM DTT, pH 7.9) and electrophoresed in a

5% polyacrylamide gel made in 0.5x TBE (45 mM Tris-borate, 1 mM EDTA). The mononucleosomes were assayed by direct electrophoresis.

Nucleosome binding assays

Nucleosome arrays were bound to M280 Streptavidin DynaBeads (Thermo-Fisher Scientific) in chromatin bead binding buffer (50 mM Tris-Cl pH 8, 150 mM NaCl, 0.25 mM EDTA, 0.05% Triton X-100, 2.5 % polyvinylalcohol) by shaking at 1300 rpm for 3.5 h. To block the Step tagged condensin complexes from binding the unconjugated streptavidin on the beads during the condensin pull downs, the beads were washed once in chromatin binding buffer and then incubated in 1 mM Biotin in chromatin binding buffer by shaking at 1300 rpm for 1 hour. The beads were then washed with chromatin binding buffer (50 mM Tris-Cl pH 8, 150 mM NaCl, 0.25 mM EDTA, 0.05% Triton X-100) three times, moved to a new tube, washed twice with SDB (10 mM HEPES, 1mM $MgCl_2$, 100 mM KCl, 150 mM Sucrose) and split into two tubes. SDB with 0.0008% poly-glutamic acid (Sigma)(Stein and Künzler, 1983) was mixed with 400 nM recombinant xH1.8 (buffer for control) and incubated for 5 min at room temperature. This mixture was incubated with the beads (half with buffer, half with xH1.8) with rotation at 16 ^{o}C. The beads were then washed 1x with SDB and 1x with binding buffer (10 mM HEPES pH 8, 40 mM NaCl, 2.5 mM $MgCl_2$, 0.5 mM DTT, 0.05% Triton X-100). Beads were washed 2x with binding buffer with indicated assay salt concentration and resuspended in binding buffer with 100 nM recombinant TOP2A, 380 nM human condensin I, condensin I Q loop mutant or 320 nM condensin II or condensin II Q loop mutant. The beads were rotated at room temperature for 30 min. Total reaction samples were taken and the beads were washed three times on a magnet in binding buffer and moved to a new tube. The beads were collected on a magnet and resuspended in 1x sample buffer (50 mM Tris-HCl pH 6.8, 2 % SDS, 10%

Glycerol, 2.5 % β-mercaptoethanol) and boiled for 5 min. Gel electrophoresis was performed and the gels were stained with GelCode Blue Stain reagent (Thermo-Fisher Scientific).

Condensin Gel Shift assays

200 nM Alexa 647 labelled 196 bp mononucleosomes were mixed with 0.0008% poly-glutamic acid (Sigma)(Stein and Künzler, 1983) and half was mixed with 400 nM recombinant xH1.8 in 1x binding buffer (10 mM HEPES pH 8, 50 mM NaCl, 2.5 mM $MgCl_2$, 5 mM ATP, 0.5 mM DTT, 0.05% Triton X-100) and incubated for 30 min at room temperature. 100 nM of the mononucleosomes with or H1.8 were mixed with the indicated concentration of condensin I in 1x binding buffer at 4 ^{0}C for 30 min and subject to electrophoresis onto a 5 % polyacrylamide gel in 0.5x TBE at room temperature. The gels were imaged on a LICOR Odyssey (LI-COR Biotechnology). The binding curves were fitted using Graphpad Prism 8.4.3 using the sigmoidal binding curve option of the non-linear curve fitting.

Protein purification

H1.8

A pET51b vector expressing *Xenopus laevis* H1.8 with an N-terminal Strep-Tag II and C-terminal 6x Histidine-tag was a gift from Rebecca Heald (UC Berkeley). *E. coli* Rosetta2 (DE3 pLysS) cells containing expression plasmids were grown in TBG-M9 media (15 g/l tryptone, 7.5 g/l yeast extract, 5 g/l NaCl, 0.15 g/l $MgSO_4$, 1.5 g/l NH_4Cl, 3 g/l KH_2PO_4, 6 g/l Na_2HPO_4; 0.4% glucose) at 37 ºC until they reach OD~0.6 and were supplemented with 1 mM isopropylthio-β-galactoside (IPTG) and grown at 18 ºC for 14 h. Cells were collected and resuspend in lysis buffer (1x PBS, 500 mM NaCl, 10% glycerol, 20 mM Imidazole, 0.1%

Triton X-100, 10 mM β-mercaptoethanol, 1 mM phenylmethylsulfonyl fluoride, 10 µg/ml leupeptin, 10 µg/ml pepstatin, 10 µg/ml chymostatin). All subsequent steps were carried out at 4 ºC. After 30 min incubation, the cell suspension was sonicated and centrifuged at 45000g for 45 min at 4 ºC. The supernatant was added to Ni-NTA beads (BioRad) and rotated for 60 min. The beads were then washed with Wash Buffer 1 (1x PBS, 20 mM imidazole, 500 mM NaCl, 4 mM β-mercaptoethanol, 10 mM ATP, 2.5 mM $MgCl_2$, cOmplete EDTA-free protease inhibitor cocktail-Roche). The beads were eluted with NTA elution buffer (1x PBS, 400 mM Imidazole, 500 mM NaCl). The correct fractions were collected and dialyzed into PBS supplement with 500 mM NaCl, concentrated using Amicon Ultra centrifugal filters (10k cutoff), flash frozen, aliquoted and stored at -80 ºC.

TopoIIα

X. laevis TOP2A tagged with calmodulin binding protein (CBP) was purified from *P. pastoris* yeast as reported (Ryu et al., 2010) with some modifications. *Pichia pastoris* integrated with a CBP tagged TOP2A cassette under the influence of an alcohol oxidase (AOX) promoter (a gift from Yoshiaki Azuma) were grown in BMGY media (1% Yeast Extract, 2% Peptone, 100 mM potassium phosphate pH 6, 1.34% Yeast Nitrogen Base, $4x10^{-5}$% biotin, 1% glycerol) containing 50 µg/ml G418 (Thermo-Fisher Scientific) at 30 ºC until OD~4.0. The cells were collected by centrifugation and split into BMMY media (1% Yeast Extract, 2% Peptone, 100 mM potassium phosphate pH 6, 1.34% Yeast Nitrogen Base, $4x10^{-5}$% biotin, 0.5% methanol) and grown at 22 ºC for 14 h. The cells were collected, packed into a syringe and extruded into liquid nitrogen in the form of noodles. These frozen noodles were lysed using a Retsch PM100 cryomill (Retsch) with continuous liquid nitrogen cooling. The cyromilled cells were then resuspended in Lysis Buffer (150mM NaCl, 18mM β-glycerophosphate, 1mM $MgCl_2$, 40mM

HEPES (pH 7.8), 5% glycerol, 0.1% Triton X-100, 1mM DTT, cOmplete EDTA-free protease inhibitor tablet) and sonicated on ice. The cells were centrifuged at 35,000g for 45 min at 4 ºC. 2 mM $CaCl_2$ was added to the supernatant along with Calmodulin-sepharose beads (Strategene) and the mixture was incubated at 4 ºC for 120 min. The beads were then washed with ATP-Wash Buffer (Lysis Buffer+ 5mM $MgCl_2$, 2mM $CaCl_2$, 1mM ATP), Wash Buffer 1 (Lysis Buffer + 2 mM $CaCl_2$), Wash Buffer 2 (300mM NaCl, 1mM $MgCl_2$, 2mM $CaCl_2$, 20mM HEPES (pH 7.8), 5% Glycerol, 1mM DTT) and then eluted into Elution Buffer (300mM NaCl, 1mM $MgCl_2$, 5mM EGTA, 20mM HEPES (pH 7.8), 5% glycerol, 1mM DTT).

The eluted protein was then passed through a MonoQ anion exchange column (Cytiva) on an AKTA-FPLC (Cytiva) to separate co-purified DNA. The flowthrough was then digested with TEV protease to cleave the CBP tag and then loaded on a HiTrap Heparin HP column (Cytiva) on an AKTA-FPLC and eluted using a salt gradient of 150 mM NaCl to 1 M NaCl. The selected fractions were then loaded on a Superose 6 gel filtration column (Cytiva) and eluted in Freezing buffer (250mM NaCl, 1mM $MgCl_2$, 20mM HEPES pH 7.8, 5% glycerol, 1mM DTT). The protein was then concentrated and frozen in aliquots at -80 ºC.

Condensins (performed by Dr. Erin Cutts)

Human condensin complexes were purified as described previously (Kong et al., 2020). Briefly, the five subunits of human condensin I and II, sub-complexes and Q-loop mutations and were assembled into biGBac vectors (Weissmann et al., 2016) to create baculovirus for protein expression in HighFive insect cells. Cell were lysed in condensin purification buffer (20 mM HEPES [pH 8], 300 mM KCl, 5 mM $MgCl_2$, 1 mM DTT, 10% glycerol) supplemented with Pierce protease inhibitor EDTA-free tablet (Thermo Scientific) and Benzonase (Sigma). Cleared lysate was loaded on to a StrepTrap HP (GE), washed with condensin purification buffer and eluted with condensin purification buffer supplemented with 5 mM Desthiobiotin

(Sigma). Protein containing fractions were pooled, diluted 2-fold with Buffer A (20 mM HEPES [pH 8], 5 mM $MgCl_2$, 5% glycerol, 1 mM DTT), loaded on to HiTrap Heparin HP column (GE), washed with Buffer A with 250 mM NaCl, then eluted with buffer A with 500 mM NaCl. Finally, size exclusion chromatography was performed using Condensin purification buffer and a Superose 6 16/70 or increase 10/300 column (GE).

Equilibrium model

The equilibrium binding ratio between nucleosomes with and without H1, after making the assumptions stated in text and applying the quasi-steady state approximation (Segel and Slemrod, 1989), yields a ratio predicted by equation 1. The predicted enrichments were then calculated using equation 1 at the indicated values of S and E. The plotting was done in Graphpad Prism.

$$\frac{([Cond-Nuc]+[Cond-H1-Nuc])\ in\ \Delta H1}{([Cond-Nuc]+[Cond-H1-Nuc]) in\ \Delta IgG} = \frac{1}{1-S+SE} \qquad \text{Eq 1}$$

Quantification and statistical analysis

All statistical analysis was performed using in-built functions in GraphPad Prism (v8.4.3). The significance analysis was performed using an unpaired students t-test in **Figures 2-1D, I; 2-3B; 2-4C, D; 2-10D; 3-3D; 3-4B, C, D; 3-6E; 3-7**. The data in **Figures 2-10E; 2-11 B, C; 3-10; 3-11D** were analyzed by a two-tailed Mann-Whitney test.

For the CENP-A foci counting in **Figures 3-2, 3-3**, DNA masses were identified using a DNA mask and CENP-A foci were identified in each DNA mask using an Otsu's thresholding algorithm.

For the categorization of unindividualized chromosomes in **Figure 3-6**, a large area of coverslip was imaged in panels and all the observed DNA masses were counted and categorized in an unblinded fashion.

Appendix

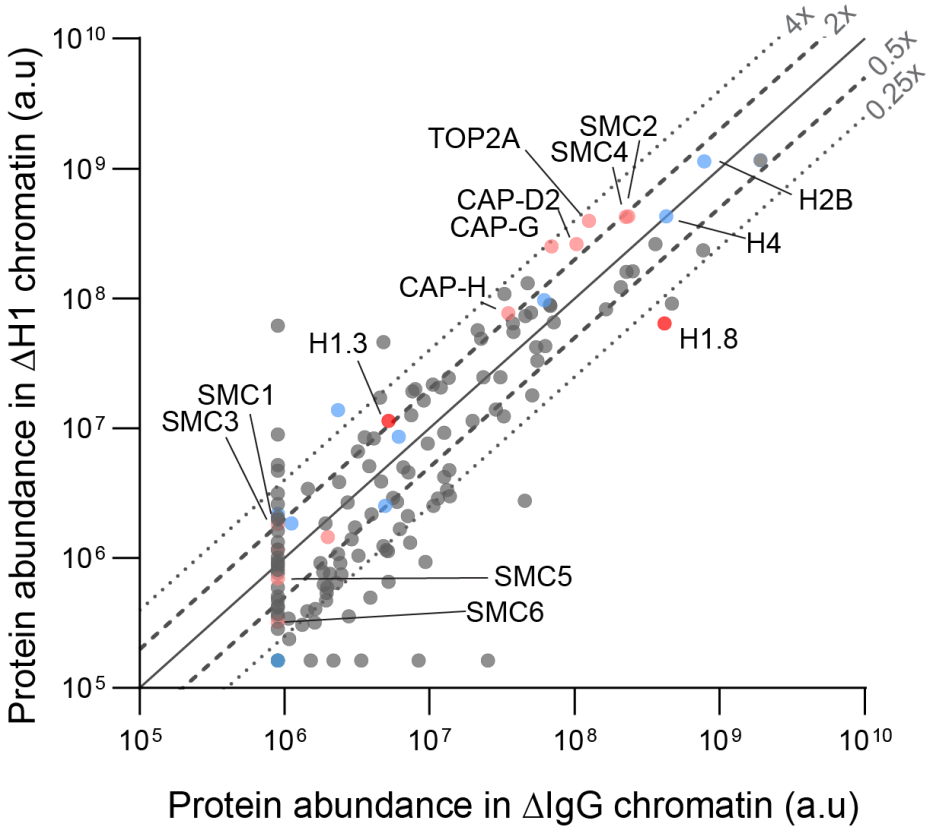

Figure A-1 Mass spectrometry data of metaphase chromatin from H1.8 depleted extracts

Metaphase chromatin proteins from mock and H1.8-depleted extracts were subjected to mass spectrometry. The abundances are plotted against each other. The solid line represents equal abundance and the dashed and dotted lines represent ½ and ¼ changes respectively. The significant ones are colored.

Table A-1 Mass spectrometry data of chromatin purified from mock, H1.8 depleted extracts

Description	Gene ID	Peptides	Unique Peptides	ΔIgG abundance (ion current)	ΔH1 abundance (ion current)	ΔH1/ ΔIgG
Histone H2A type 2-B	HIST2H2AB	7	4	1.92E+09	1.16E+09	0.60
Rep: Histone H2B 1.1 - Xenopus laevis (African clawed frog), complete	H2B 1.1	19	2	7.84E+08	1.14E+09	1.46
DNA damage-binding protein 1	DDB1	25	25	4.70E+08	9.14E+07	0.19
Histone H4	HIS1H4A	14	14	4.30E+08	4.30E+08	1.00
Histone H1oo	H1FOO	14	10	4.16E+08	6.43E+07	0.15
Aurora kinase B	AURKB	22	6	3.60E+08	2.62E+08	0.73
Borealin	CDCA8	18	18	2.51E+08	1.61E+08	0.64
Structural maintenance of chromosomes protein 4	SMC4	62	63	2.34E+08	4.28E+08	1.83
Inner centromere protein	INCENP	34	2	2.27E+08	1.60E+08	0.71
Structural maintenance of chromosomes protein 2	SMC2	64	64	2.26E+08	4.23E+08	1.87
Regulator of chromosome condensation - Xenopus laevis (African clawed frog), complete	RCC	17	12	2.08E+08	1.22E+08	0.59
GTP-binding nuclear protein Ran	RAN	8	8	1.65E+08	8.23E+07	0.50
DNA topoisomerase 2-alpha	TOP2A	62	48	1.26E+08	3.96E+08	3.13
Condensin complex subunit 3	NCAPG	43	43	1.03E+08	2.61E+08	2.54
Importin subunit alpha-2	KPNA2	13	4	7.16E+07	6.52E+07	0.91
Condensin complex subunit 1	NCAPD2	53	3	6.94E+07	2.53E+08	3.65
Transcriptional regulator ATRX	ATRX	41	41	6.78E+07	8.80E+07	1.30
DNA replication licensing factor MCM4	MCM4	34	33	6.76E+07	8.91E+07	1.32
Importin subunit beta-1	KPNB1	25	2	6.29E+07	4.30E+07	0.68
Histone H2A.J	H2AFJ	4	1	6.16E+07	9.71E+07	1.58
Protein CIP2A	KIAA1524	21	21	5.55E+07	3.32E+07	0.60
Replication protein A 70 kDa DNA-binding subunit	RPA1	24	24	5.44E+07	4.23E+07	0.78
Bromodomain and WD repeat-containing protein 3	BRWD3	29	29	5.10E+07	1.80E+07	0.35

Description	Gene ID	Peptides	Unique Peptides	ΔIgG abundance (ion current)	ΔH1 abundance (ion current)	ΔH1/ ΔIgG
Bromodomain adjacent to zinc finger domain protein 1A	BAZ1A	33	12	5.03E+07	7.76E+07	1.54
SWI/SNF-related matrix-associated actin-dependent regulator of chromatin subfamily A member 5	SMARCA5	39	8	4.76E+07	1.31E+08	2.75
DNA replication licensing factor MCM6	MCM6	28	27	4.57E+07	7.28E+07	1.59
DNA replication licensing factor MCM2	MCM2	23	23	3.80E+07	5.53E+07	1.46
MCM3 minichromosome maintenance deficient 3 (S. cerevisiae), isoform CRA_b	MCM3	27	27	3.75E+07	6.39E+07	1.70
Condensin complex subunit 2	NCAPH	17	8	3.48E+07	7.72E+07	2.22
Dopamine receptor interacting protein 4	DRIP4	18	18	3.29E+07	1.08E+08	3.29
Lymphoid-specific helicase	HELLS	4	4	3.25E+07	1.23E+07	0.38
Regulator of chromosome condensation	RCC1	11	6	3.09E+07	2.48E+07	0.80
DNA topoisomerase 2-binding protein 1	TOPBP1	19	19	2.87E+07	1.39E+07	0.49
Telomere-associated protein RIF1	RIF1	8	8	2.53E+07	1.62E+05	0.01
Protein HIRA	HIRA	14	14	2.35E+07	2.47E+07	1.05
DNA replication licensing factor MCM7	MCM7	26	26	2.26E+07	4.91E+07	2.17
DNA replication licensing factor MCM5	MCM5	25	25	2.15E+07	5.69E+07	2.64
Serine/threonine-protein phosphatase 2A 65 kDa regulatory subunit A alpha isoform	PPP2R1A	17	10	1.98E+07	1.14E+07	0.57
Exportin-2	CSE1L	7	7	1.38E+07	3.00E+06	0.22
Probable ATP-dependent RNA helicase DDX6	DDX6	5	1	1.37E+07	4.78E+06	0.35
FACT complex subunit SPT16	SUPT16H	18	18	1.35E+07	2.44E+07	1.80
Polyadenylate-binding protein 1	PABPC1	8	2	1.32E+07	3.35E+06	0.25
Baculoviral IAP repeat-containing protein 5	BIRC5	6	4	1.26E+07	9.26E+06	0.74
FACT complex subunit SSRP1	SSRP1	18	18	1.19E+07	2.06E+07	1.74

Description	Gene ID	Peptides	Unique Peptides	ΔIgG abundance (ion current)	ΔH1 abundance (ion current)	ΔH1/ ΔIgG
Rep: Importin alpha 5.1 protein - Xenopus laevis (African clawed frog), complete	Imp 5.1	4	4	1.14E+07	2.88E+06	0.25
Nuclear pore complex protein Nup98-Nup96	NUP98	19	19	1.06E+07	2.52E+06	0.24
Histone H2B type 1-J	HIST1H2BJ	18	1	1.05E+07	2.18E+07	2.07
ATPase family AAA domain-containing protein 2B	ATAD2B	19	11	9.71E+06	7.64E+06	0.79
Importin subunit beta-1	KPNB1	24	1	9.36E+06	9.32E+05	0.10
Shugoshin-like 1	SGOL1	17	17	9.09E+06	1.63E+07	1.79
RuvB-like 1	RUVBL1	7	7	8.41E+06	1.62E+05	0.02
Mediator of DNA damage checkpoint protein 1	MDC1	27	27	7.99E+06	2.00E+07	2.50
Fanconi anemia group I protein	FANCI	21	21	7.64E+06	1.93E+07	2.52
Ubinuclein-2	UBN2	12	10	7.49E+06	1.26E+07	1.68
Mitotic checkpoint protein BUB3	BUB3	3	3	7.34E+06	1.32E+06	0.18
Borealin	CDCA8	5	5	7.13E+06	4.57E+06	0.64
Importin subunit alpha-8	KPNA7	10	1	7.10E+06	2.12E+06	0.30
Replication protein A 32 kDa subunit	RPA2	5	5	6.60E+06	5.02E+06	0.76
14-3-3 protein zeta/delta	YWHAZ	3	3	6.23E+06	1.68E+06	0.27
Core histone macro-H2A.2	H2AFY2	8	8	6.13E+06	8.63E+06	1.41
Shugoshin-like 2	SGOL2	7	7	5.99E+06	2.70E+06	0.45
Nucleoprotein TPR	TPR	13	13	5.61E+06	2.92E+06	0.52
Nuclear pore complex protein Nup133	NUP133	6	5	5.22E+06	6.56E+05	0.13
Histone H1.3	HIST1H1D	4	2	5.19E+06	1.14E+07	2.20
Nuclear pore complex protein Nup214	NUP214	6	6	5.15E+06	1.13E+06	0.22
Histone chaperone ASF1A	ASF1A	1	1	5.04E+06	1.15E+06	0.23
Histone H2A.x	H2AFX	4	1	4.95E+06	2.54E+06	0.51
Tyrosine-protein kinase BAZ1B	BAZ1B	23	2	4.82E+06	4.60E+07	9.54
Heterogeneous nuclear ribonucleoprotein H	HNRNPH1	2	1	4.79E+06	1.24E+06	0.26
Bromodomain adjacent to zinc finger domain protein 1A	BAZ1A	23	2	4.62E+06	3.90E+06	0.84
Fanconi anemia group D2 protein	FANCD2	20	20	4.54E+06	1.72E+07	3.79

Description	Gene ID	Peptides	Unique Peptides	ΔIgG abundance (ion current)	ΔH1 abundance (ion current)	ΔH1/ ΔIgG
Condensin complex subunit 2	NCAPH	13	4	4.11E+06	8.32E+06	2.02
Nucleolar transcription factor 1	UBTF	17	2	3.97E+06	2.17E+06	0.55
Elongation factor 2	EEF2	3	3	3.89E+06	4.95E+05	0.13
Condensin complex subunit 1	NCAPD2	53	3	3.84E+06	5.12E+06	1.34
Histone-binding protein RBBP7	RBBP7	10	10	3.56E+06	8.52E+06	2.39
Protein LSM14 homolog B	LSM14B	2	2	3.37E+06	1.62E+05	0.05
X-ray repair cross-complementing protein 5	XRCC5	2	2	3.24E+06	1.04E+06	0.32
Metastasis-associated protein MTA2	MTA2	7	7	3.20E+06	6.60E+06	2.06
Ran GTPase-activating protein 1	RANGAP1	7	7	3.06E+06	1.73E+06	0.56
Guanine nucleotide-binding protein subunit beta-4	GNB4	2	2	2.90E+06	1.40E+06	0.48
Lamin-B1	LMNB1	6	3	2.77E+06	3.56E+05	0.13
Histone deacetylase 1	HDAC1	4	1	2.72E+06	2.69E+06	0.99
Cell division cycle-associated protein 7	CDCA7	5	5	2.46E+06	7.50E+05	0.31
Guanine nucleotide-binding protein G(i) subunit alpha-2	GNAI2	2	2	2.42E+06	9.13E+05	0.38
DNA excision repair protein ERCC-6-like	ERCC6L	14	13	2.37E+06	3.86E+06	1.63
Histone H2A.V	H2AFV	6	2	2.34E+06	1.38E+07	5.89
Nuclear pore complex protein Nup155	NUP155	5	5	2.33E+06	1.08E+06	0.46
Nuclear pore complex protein Nup85	NUP85	7	7	2.27E+06	6.43E+05	0.28
Kinesin-like protein KIF2C	KIF2C	4	4	2.17E+06	1.62E+05	0.07
Nuclear pore membrane glycoprotein 210	NUP210	8	8	2.05E+06	7.59E+05	0.37
Structural maintenance of chromosomes protein 6	SMC6	7	7	1.99E+06	1.45E+06	0.73
SWI/SNF complex subunit SMARCC1	SMARCC1	5	5	1.97E+06	5.94E+05	0.30
Nuclear pore complex protein Nup50	NUP50	4	4	1.95E+06	5.38E+05	0.28
Rep: Histone-binding protein N1/N2 - Xenopus	err	2	2	1.93E+06	4.73E+05	0.25

Description	Gene ID	Peptides	Unique Peptides	ΔIgG abundance (ion current)	ΔH1 abundance (ion current)	ΔH1/ ΔIgG
laevis (African clawed frog), partial (13%)						
Chromodomain-helicase-DNA-binding protein 4	CHD4	7	7	1.91E+06	1.86E+06	0.98
Nuclear pore complex protein Nup93	NUP93	13	13	1.86E+06	6.24E+05	0.34
Rep: Serine/threonine-protein kinase PLK1 - Xenopus laevis (African clawed frog), complete	err	3	3	1.85E+06	7.77E+05	0.42
Nucleoporin SEH1	SEH1L	2	2	1.76E+06	9.12E+05	0.52
Zinc finger protein 207	ZNF207	2	2	1.63E+06	4.06E+05	0.25
Centromere-associated protein E	CENPE	5	5	1.62E+06	3.20E+05	0.20
E3 SUMO-protein ligase RanBP2	RANBP2	10	10	1.51E+06	1.62E+05	0.11
Antigen KI-67	MKI67	5	5	1.45E+06	3.42E+06	2.35
Serine/threonine-protein phosphatase 2A 65 kDa regulatory subunit A alpha isoform	PPP2R1A	8	1	1.43E+06	3.92E+05	0.27
Nuclear pore complex protein Nup88	NUP88	4	4	1.32E+06	3.05E+05	0.23
Histone H3.3	H3F3A	8	1	1.12E+06	1.85E+06	1.66
Protein ELYS	AHCTF1	3	2	1.08E+06	2.39E+05	0.22
Zinc finger protein 638	ZNF638	2	1	1.07E+06	3.44E+05	0.32
Cullin-4A	CUL4A	9	6	9.00E+05	4.76E+05	0.53
Transcription termination factor 2	TTF2	13	12	9.00E+05	8.96E+06	9.95
Histone H1.3	HIST1H1D	3	1	9.00E+05	6.14E+07	68.20
E3 SUMO-protein ligase RanBP2	RANBP2	4	2	9.00E+05	5.09E+05	0.57
Nuclear pore complex protein Nup107	NUP107	9	9	9.00E+05	1.62E+05	0.18
Nucleoporin Nup43	NUP43	1	1	9.00E+05	1.62E+05	0.18
Nuclear pore complex protein Nup153	NUP153	4	1	9.00E+05	1.62E+05	0.18
Nucleoporin p58/p45	NUPL1	2	1	9.00E+05	1.62E+05	0.18
Nucleoporin NUP188 homolog	NUP188	4	4	9.00E+05	1.62E+05	0.18
Serine/threonine-protein kinase ATR	ATR	3	3	9.00E+05	5.96E+05	0.66
Structural maintenance of chromosomes protein 3	SMC3	11	11	9.00E+05	1.15E+06	1.28

Description	Gene ID	Peptides	Unique Peptides	ΔIgG abundance (ion current)	ΔH1 abundance (ion current)	ΔH1/ ΔIgG
E3 SUMO-protein ligase RanBP2	RANBP2	7	5	9.00E+05	9.47E+05	1.05
Lamin A/C	LMNA	23	8	9.00E+05	1.62E+05	0.18
Nucleoporin NUP53	NUP35	2	2	9.00E+05	1.62E+05	0.18
Nuclear pore complex protein Nup205	NUP205	12	12	9.00E+05	1.62E+05	0.18
NUP153 variant protein (Fragment)	NUP153 VARIANT PROTEIN	5	5	9.00E+05	1.62E+05	0.18
Transportin-1	TNPO1	2	2	9.00E+05	1.62E+05	0.18
POM121-like protein 2	POM121L2	5	5	9.00E+05	1.62E+05	0.18
Nucleoporin p54	NUP54	4	4	9.00E+05	1.62E+05	0.18
Nuclear pore complex protein Nup153	NUP153	7	4	9.00E+05	1.62E+05	0.18
Nuclear pore complex protein Nup160	NUP160	9	9	9.00E+05	9.11E+05	1.01
Putative GTP-binding protein 6	GTPBP6	1	1	9.00E+05	5.23E+06	5.81
Histone H2A type 2-B	HIST2H2AB	5	2	9.00E+05	2.19E+06	2.44
ATPase family AAA domain-containing protein 2	ATAD2	11	7	9.00E+05	1.62E+05	0.18
SWI/SNF-related matrix-associated actin-dependent regulator of chromatin subfamily A member 5	SMARCA5	35	4	9.00E+05	3.15E+06	3.50
Structural maintenance of chromosomes protein 1A	SMC1A	4	4	9.00E+05	1.84E+06	2.04
N-alpha acetyl transferase 40	NAA40	10	4	9.00E+05	8.72E+06	9.69
Keratin, type II cytoskeletal 8	KRT8	30	5	9.00E+05	2.60E+06	2.89
Zinc fingers and homeoboxes protein 3	ZHX3	11	11	9.00E+05	4.70E+06	5.22
ITLN2 protein	ITLN2	6	2	9.00E+05	1.62E+05	0.18
ATPase family AAA domain-containing protein 2B	ATAD2B	7	3	9.00E+05	3.52E+05	0.39
Tudor and KH domain-containing protein	TDRKH	1	1	9.00E+05	8.61E+05	0.96
RuvB-like 2	RUVBL2	4	4	9.00E+05	1.01E+06	1.13
Nucleosome assembly protein 1-like 1	NAP1L1	2	2	9.00E+05	1.62E+05	0.18
Cohesin subunit SA-1	STAG1	2	2	9.00E+05	3.22E+05	0.36
Lamin-B1	LMNB1	4	1	9.00E+05	1.62E+05	0.18

Description	Gene ID	Peptides	Unique Peptides	ΔIgG abundance (ion current)	ΔH1 abundance (ion current)	ΔH1/ ΔIgG
Lamina-associated polypeptide 2, isoforms beta/gamma	TMPO	3	3	9.00E+05	7.65E+05	0.85
Histone deacetylase 1	HDAC1	4	1	9.00E+05	8.30E+05	0.92
Replication factor C subunit 3	RFC3	3	3	9.00E+05	4.19E+05	0.47
Putative helicase MOV-10	MOV10	3	3	9.00E+05	4.15E+05	0.46
Chromodomain-helicase-DNA-binding protein 7	CHD7	2	2	9.00E+05	3.72E+05	0.41
Phenylalanine--tRNA ligase beta subunit	FARSB	4	4	9.00E+05	4.13E+05	0.46
Zona pellucida sperm-binding protein 4	ZP4	2	2	9.00E+05	4.25E+05	0.47
Poly [ADP-ribose] polymerase 1	PARP1	1	1	9.00E+05	1.62E+05	0.18
Leucyl-cystinyl aminopeptidase	LNPEP	1	1	9.00E+05	1.62E+05	0.18
Protein lunapark	LNP	1	1	9.00E+05	1.62E+05	0.18
Zinc finger protein 638	ZNF638	2	1	9.00E+05	1.62E+05	0.18
Bleomycin hydrolase	BLMH	1	1	9.00E+05	1.62E+05	0.18
Actin-related protein 2	ACTR2	2	2	9.00E+05	1.62E+05	0.18
Antigen KI-67	MKI67	1	1	9.00E+05	1.62E+05	0.18
Proteasome subunit beta type-6	PSMB6	1	1	9.00E+05	1.62E+05	0.18
Putative uncharacterized protein DKFZp686C24207	DKFZP686C24207	1	1	9.00E+05	1.62E+05	0.18
Signal recognition particle receptor subunit beta	SRPRB	1	1	9.00E+05	1.62E+05	0.18
ATP-dependent RNA helicase DDX1	DDX1	1	1	9.00E+05	1.62E+05	0.18
Proteasome subunit beta type-5	PSMB5	1	1	9.00E+05	1.62E+05	0.18
Proteasome subunit beta type-1	PSMB1	1	1	9.00E+05	1.62E+05	0.18
Remodeling and spacing factor 1	RSF1	1	1	9.00E+05	1.62E+05	0.18
Dual specificity mitogen-activated protein kinase kinase 1	MAP2K1	1	1	9.00E+05	1.62E+05	0.18
26S proteasome non-ATPase regulatory subunit 6	PSMD6	2	2	9.00E+05	1.62E+05	0.18
Transcriptional repressor p66-alpha	GATAD2A	2	2	9.00E+05	1.62E+05	0.18

Description	Gene ID	Peptides	Unique Peptides	ΔIgG abundance (ion current)	ΔH1 abundance (ion current)	ΔH1/ ΔIgG
Rep: MGC83068 protein - Xenopus laevis (African clawed frog), partial (34%)	err	1	1	9.00E+05	1.62E+05	0.18
Nicalin	NCLN	2	2	9.00E+05	1.62E+05	0.18
Rep: Non-structural maintenance of chromosomes element 1 homolog - Xenopus laevis (African clawed frog), partial (50%)	err	2	1	9.00E+05	1.62E+05	0.18
Transmembrane protein 199	TMEM199	1	1	9.00E+05	1.62E+05	0.18
NADH dehydrogenase [ubiquinone] 1 alpha subcomplex subunit 8	NDUFA8	2	2	9.00E+05	1.62E+05	0.18
Polypeptide N-acetylgalactosaminyltransferase 2	GALNT2	2	2	9.00E+05	1.62E+05	0.18
Rep: Peptidyl-prolyl cis-trans isomerase - Xenopus laevis (African clawed frog), partial (87%)	err	2	2	9.00E+05	1.62E+05	0.18
Importin subunit alpha-2	KPNA2	2	2	9.00E+05	1.62E+05	0.18
Non-structural maintenance of chromosomes element 4 homolog A	NSMCE4A	1	1	9.00E+05	1.62E+05	0.18
Rep: Cold-inducible RNA binding protein 2 - Xenopus laevis (African clawed frog), complete	err	2	2	9.00E+05	1.62E+05	0.18
Rep: Proliferating cell nuclear antigen - Xenopus laevis (African clawed frog), partial (57%)	err	2	2	9.00E+05	1.62E+05	0.18
Programmed cell death protein 4	PDCD4	2	2	9.00E+05	1.62E+05	0.18
Protein LYRIC	MTDH	2	1	9.00E+05	1.62E+05	0.18
Rep: MGC80186 protein - Xenopus laevis (African clawed frog), partial (78%)	err	2	1	9.00E+05	1.62E+05	0.18
Dynactin subunit 1	DCTN1	2	2	9.00E+05	1.62E+05	0.18
Delta-1-pyrroline-5-carboxylate synthase	ALDH18A1	2	2	9.00E+05	1.62E+05	0.18

Description	Gene ID	Peptides	Unique Peptides	ΔIgG abundance (ion current)	ΔH1 abundance (ion current)	ΔH1/ ΔIgG
Rep: LOC100037025 protein - Xenopus laevis (African clawed frog), partial (22%)	err	2	1	9.00E+05	1.62E+05	0.18
Isocitrate dehydrogenase [NAD] subunit gamma, mitochondrial	IDH3G	2	2	9.00E+05	1.62E+05	0.18
Oligosaccharyltransferase complex subunit OSTC	OSTC	1	1	9.00E+05	1.62E+05	0.18
Uroplakin-1a	UPK1A	1	1	9.00E+05	1.62E+05	0.18
Receptor expression-enhancing protein 6	REEP6	2	2	9.00E+05	1.62E+05	0.18
Cytoskeleton-associated protein 4	CKAP4	3	3	9.00E+05	1.62E+05	0.18
Rep: Myosin heavy chain - Rana catesbeiana (Bull frog), partial (19%)	err	1	1	9.00E+05	1.62E+05	0.18
Heterogeneous nuclear ribonucleoprotein H	HNRNPH1	2	1	9.00E+05	1.62E+05	0.18
Rep: RAP55 protein - Xenopus laevis (African clawed frog), partial (53%)	err	1	1	9.00E+05	1.62E+05	0.18
err	err	1	1	9.00E+05	1.62E+05	0.18
Annexin A1	ANXA1	1	1	9.00E+05	1.62E+05	0.18
Electron transfer flavoprotein subunit alpha, mitochondrial	ETFA	2	2	9.00E+05	1.62E+05	0.18
Rep: Vitellogenin-A2 precursor (VTG A2) [Contains: Lipovitellin I; Lipovitellin II; Phosvitin] - Xenopus laevis (African clawed frog), partial (6%)	err	2	1	9.00E+05	1.62E+05	0.18
Reticulon-3	RTN3	2	1	9.00E+05	1.62E+05	0.18
Rep: MGC84997 protein - Xenopus laevis (African clawed frog), partial (36%)	err	2	1	9.00E+05	1.62E+05	0.18
Methylcrotonoyl-CoA carboxylase beta chain, mitochondrial	MCCC2	2	2	9.00E+05	1.62E+05	0.18
Nucleoporin Nup37	NUP37	2	2	9.00E+05	1.62E+05	0.18
Desmoplakin	DSP	3	1	9.00E+05	1.62E+05	0.18
Long-chain specific acyl-CoA dehydrogenase, mitochondrial	ACADL	3	3	9.00E+05	1.62E+05	0.18

Description	Gene ID	Peptides	Unique Peptides	ΔIgG abundance (ion current)	ΔH1 abundance (ion current)	ΔH1/ ΔIgG
ATP synthase subunit delta, mitochondrial	ATP5D	1	1	9.00E+05	1.62E+05	0.18
Microtubule-associated protein RP/EB family member 1	MAPRE1	3	3	9.00E+05	1.62E+05	0.18
Mitochondrial carnitine/acylcarnitine carrier protein	SLC25A20	3	3	9.00E+05	1.62E+05	0.18
Rep: LOC100037109 protein - Xenopus laevis (African clawed frog), partial (84%)	err	2	2	9.00E+05	1.62E+05	0.18
Rep: 60S ribosomal protein L6 - Xenopus laevis (African clawed frog), partial (96%)	err	3	1	9.00E+05	1.62E+05	0.18
Pyruvate kinase isozymes M1/M2	PKM	4	2	9.00E+05	1.62E+05	0.18
60S ribosomal protein L7	RPL7	3	1	9.00E+05	1.62E+05	0.18
Protein disulfide-isomerase TMX3	TMX3	3	3	9.00E+05	1.62E+05	0.18
Rep: MGC81256 protein - Xenopus laevis (African clawed frog), partial (47%)	err	5	1	9.00E+05	1.62E+05	0.18
Aminoacyl tRNA synthase complex-interacting multifunctional protein 1	AIMP1	3	3	9.00E+05	1.62E+05	0.18
ITPR1 protein	ITPR1	5	5	9.00E+05	1.62E+05	0.18
Saccharopine dehydrogenase-like oxidoreductase	SCCPDH	4	4	9.00E+05	1.62E+05	0.18
Dolichyl-diphosphooligosaccharide--protein glycosyltransferase 48 kDa subunit	DDOST	2	1	9.00E+05	1.62E+05	0.18
Pyruvate dehydrogenase E1 component subunit beta, mitochondrial	PDHB	4	1	9.00E+05	1.62E+05	0.18
Long-chain-fatty-acid--CoA ligase 1	ACSL1	5	1	9.00E+05	1.62E+05	0.18
Rep: Nuclear pore complex protein Nup133 (Nucleoporin Nup133) (133 kDa nucleoporin). - Xenopus tropicalis, partial (22%)	err	2	1	9.00E+05	1.62E+05	0.18

Description	Gene ID	Peptides	Unique Peptides	ΔIgG abundance (ion current)	ΔH1 abundance (ion current)	ΔH1/ ΔIgG
Ras-related protein Rab-5C	RAB5C	3	1	9.00E+05	1.62E+05	0.18
Rep: Nuclear pore complex glycoprotein p62 - Xenopus laevis (African clawed frog), partial (49%)	err	2	2	9.00E+05	1.62E+05	0.18
ATP-dependent RNA helicase DDX3X	DDX3X	4	2	9.00E+05	1.62E+05	0.18
Filamin-A	FLNA	7	2	9.00E+05	1.62E+05	0.18
Rep: LOC494706 protein - Xenopus laevis (African clawed frog), partial (73%)	err	4	1	9.00E+05	1.62E+05	0.18
Rep: Rpl9-prov protein - Xenopus laevis (African clawed frog), complete	err	4	1	9.00E+05	1.62E+05	0.18
Rep: MGC52646 protein - Xenopus laevis (African clawed frog), partial (47%)	err	5	1	9.00E+05	1.62E+05	0.18
Eukaryotic translation initiation factor 3 subunit G	EIF3G	4	1	9.00E+05	1.62E+05	0.18
Sodium/potassium-transporting ATPase subunit alpha-3	ATP1A3	6	1	9.00E+05	1.62E+05	0.18
60S ribosomal protein L9	RPL9	4	1	9.00E+05	1.62E+05	0.18
Rep: Histone H2A.Z-like - Xenopus laevis (African clawed frog), complete	err	5	1	9.00E+05	1.62E+05	0.18
Tubulin alpha-8 chain (Fragment)	TUBA8	5	1	9.00E+05	1.62E+05	0.18
Aconitate hydratase, mitochondrial	ACO2	9	1	9.00E+05	1.62E+05	0.18
Probable ATP-dependent RNA helicase DDX6	DDX6	5	1	9.00E+05	1.62E+05	0.18
Polyadenylate-binding protein 1	PABPC1	8	2	9.00E+05	1.62E+05	0.18
T-complex protein 1 subunit epsilon	CCT5	9	2	9.00E+05	1.62E+05	0.18
SWI/SNF-related matrix-associated actin-dependent regulator of chromatin subfamily A member 5	SMARCA5	9	1	9.00E+05	1.62E+05	0.18
Tubulin alpha-4A chain	TUBA4A	10	0	9.00E+05	1.62E+05	0.18

Description	Gene ID	Peptides	Unique Peptides	ΔIgG abundance (ion current)	ΔH1 abundance (ion current)	ΔH1/ ΔIgG
Eukaryotic translation initiation factor 4 gamma 1	EIF4G1	11	2	9.00E+05	1.62E+05	0.18
Cytochrome b-c1 complex subunit 2, mitochondrial	UQCRC2	8	2	9.00E+05	1.62E+05	0.18
Tubulin alpha-3C/D chain	TUBA3C	10	1	9.00E+05	1.62E+05	0.18
Dolichyl-diphosphooligosaccharide--protein glycosyltransferase subunit 2	RPN2	9	1	9.00E+05	1.62E+05	0.18
Dolichyl-diphosphooligosaccharide--protein glycosyltransferase subunit 2	RPN2	8	2	9.00E+05	1.62E+05	0.18
YTH domain family protein 1	YTHDF1	9	1	9.00E+05	1.62E+05	0.18
Protein disulfide-isomerase	P4HB	13	6	9.00E+05	1.62E+05	0.18
Hsc70-interacting protein	ST13	7	0	9.00E+05	1.62E+05	0.18
Elongation factor 1-alpha 1	EEF1A1	9	2	9.00E+05	1.62E+05	0.18
Rep: ATP synthase subunit beta - Xenopus tropicalis (Western clawed frog) (Silurana tropicalis), partial (32%)	err	4	2	9.00E+05	1.62E+05	0.18
T-complex protein 1 subunit alpha	TCP1	16	1	9.00E+05	1.62E+05	0.18
Lamin A/C	LMNA	16	1	9.00E+05	1.62E+05	0.18
Tubulin beta chain	TUBB	13	2	9.00E+05	1.62E+05	0.18
Tyrosine-protein kinase BAZ1B	BAZ1B	22	1	9.00E+05	1.62E+05	0.18
DNA topoisomerase 2-beta	TOP2B	15	1	9.00E+05	1.62E+05	0.18
78 kDa glucose-regulated protein	HSPA5	29	2	9.00E+05	1.62E+05	0.18
Death domain-associated protein 6	DAXX	3	3	9.00E+05	1.62E+05	0.18
Rep: Pcbp2b protein - Xenopus laevis (African clawed frog), partial (92%)	err	3	3	9.00E+05	1.62E+05	0.18
Kinesin-like protein KIF22	KIF22	2	2	9.00E+05	1.62E+05	0.18
Checkpoint protein HUS1	HUS1	1	1	9.00E+05	1.62E+05	0.18

Description	Gene ID	Peptides	Unique Peptides	ΔIgG abundance (ion current)	ΔH1 abundance (ion current)	ΔH1/ ΔIgG
Cullin-4B	CUL4B	4	1	9.00E+05	1.62E+05	0.18
Cullin-associated NEDD8-dissociated protein 1	CAND1	2	2	9.00E+05	2.85E+05	0.32
ATP-dependent RNA helicase DDX3X	DDX3X	5	3	9.00E+05	1.62E+05	0.18
Non-structural maintenance of chromosomes element 1 homolog	NSMCE1	3	2	9.00E+05	9.58E+05	1.06
Serine/threonine-protein phosphatase 2A 56 kDa regulatory subunit gamma isoform	PPP2R5C	3	3	9.00E+05	4.16E+05	0.46
Structural maintenance of chromosomes protein 5	SMC5	4	4	9.00E+05	6.96E+05	0.77
Calcineurin-binding protein cabin-1	CABIN1	10	10	9.00E+05	2.08E+06	2.31
X-ray repair cross-complementing protein 6	XRCC6	3	3	9.00E+05	1.99E+06	2.21
RNA-binding protein 25	RBM25	6	5	9.00E+05	1.33E+06	1.48
Pre-mRNA-processing factor 40 homolog A	PRPF40A	1	1	9.00E+05	1.62E+06	1.80
DNA polymerase epsilon subunit 3	POLE3	2	2	9.00E+05	1.17E+06	1.30
Ubinuclein-2	UBN2	4	2	9.00E+05	7.71E+05	0.86
Interferon-inducible double stranded RNA-dependent protein kinase activator A	PRKRA	3	3	9.00E+05	8.11E+05	0.90
High mobility group protein B2	HMGB2	4	1	9.00E+05	1.15E+06	1.28

Local compaction by fluorescence lifetime imaging

During fluorescence, electrons of the fluorescent molecule in a lower energy state are excited into a higher energy state upon absorption of an incident photon. This excited electron loses

some energy and thus relaxes into a lower spin state of the higher energy level. These processes occur at a time scale of less than a few picoseconds. The electron can then spend a relatively extended amount of time in this state before relaxing back to the initial energy state by emitting a photon (**Figure A-1A**). This process, for most common fluorophores, usually takes place in the order of a few nanoseconds and is known as the fluorescence life time of the fluorophore (Lakowicz, 2006). Even when all the fluorophores in a population are excited at once with a short pulse of incident energy, the fluorophore molecules spend different amount of time in the excited state before returning to the ground state, resulting in an exponential decay in the emitted photons (**Figure A-1B**). The characteristic time constant of the exponential decay is the lifetime of the fluorophore. The lifetime of fluorophores can also be measured using the changes in amplitude and phase of fluorescence responses to an oscillating excitation wave (**Figure A-1C**). This method, known as frequency domain fluorescence lifetime imaging (FLIM), enables lifetime measurements without the use of sophisticated imaging setups (Engineering and Street, 2006; Lakowicz, 2006).

Fluorescence lifetimes have been used to measure DNA compaction in a variety of ways (Llères et al., 2009; Spagnol and Dahl, 2016). DNA intercalating dyes such as Hoechst and Picogreen appear to show compaction dependent fluorescence lifetimes (Spagnol and Dahl, 2016). To verify if this was indeed true, I immobilized compact demembranated sperm in a glass bottom dish, stained them with the dna dye Picogreen, and measured the lifetime with increasing magnesium concentration (**Figure A-2A**). Consistent with a magnesium dependent DNA compaction, this led to a monotonic decrease in fluorescence lifetime with magnesium concentration (**Figure A-2B**). To verify that this was due to a magnesium dependent compaction, I added EDTA to reverse the dna compaction, and this led to a consistent increase in fluorescence lifetime. The lifetimes during the recovery phase were lower than at the similar estimated magnesium concentration during the compaction phase,

but this may be due to a partial bleaching of the fluorophore during the imaging process. Similar compaction of DNA has also been noted using polycations such as spermine, and consistent with this, I observe lower lifetimes upon addition of spermine, which could be reversed by washing off the spermine in the buffer again (**Figure A-3A, B**). This confirms that fluorescence lifetime can report on salt dependent compaction of DNA.

I then wanted to verify if lifetimes can also serve as a reporter for a more physiological compaction process. Nucleosome deposition leads to a ~6-7 fold linear compaction of DNA and is a major step of DNA compaction in all eukaryotic cells (Luger et al., 1997). *Xenopus* egg extracts can deposit nucleosomes onto DNA substrates (Laskey et al., 1977). To check if the lifetime can report on this nucleosome deposition dependent compaction, I incubated beads coated with either DNA or *in vitro* salt dialysis generated nucleosome substrates with interphase egg extracts. I then collected samples at 20 min, which is not sufficient time for nucleosome deposition but allows enough time for binding of DNA binding proteins, as an initial time point and also at 2 hours, which allows for completion of nucleosome deposition (Zierhut et al., 2014) (**Figure A-4A**). The lifetime of *in vitro* generated nucleosome beads, which cannot deposit more nucleosomes, does not change from 20 min to 2 hours (**Figure A-4B**). However, the DNA beads which accumulate nucleosomes overtime, show a significant drop in fluorescence lifetime, consistent with the nucleosome dependent compaction. The lifetime of the DNA beads sample after 2 hours is also indistinguishable from that of the nucleosomes, consistent with the idea that nucleosome deposition controls the compaction reported by the fluorescence lifetime changes.

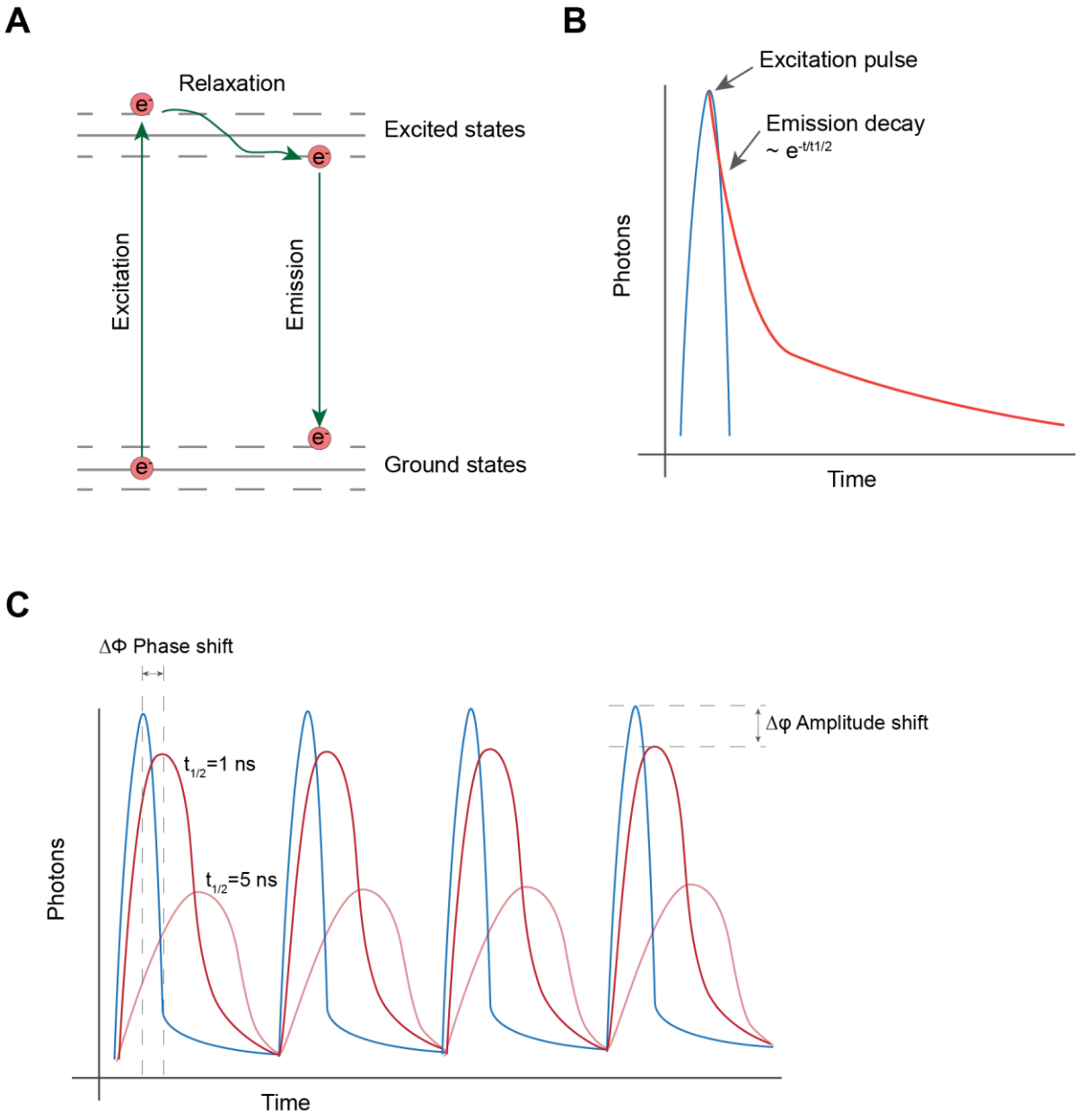

Figure A-2 Scheme for fluorescence lifetime measurement

A) Energy levels of electrons in fluorophores during fluorescence.

B) Exponential decay of fluorescence photon emission

C) Scheme for fluorescence domain fluorescence lifetime measurements using phase and amplitude shift of fluorescence response.

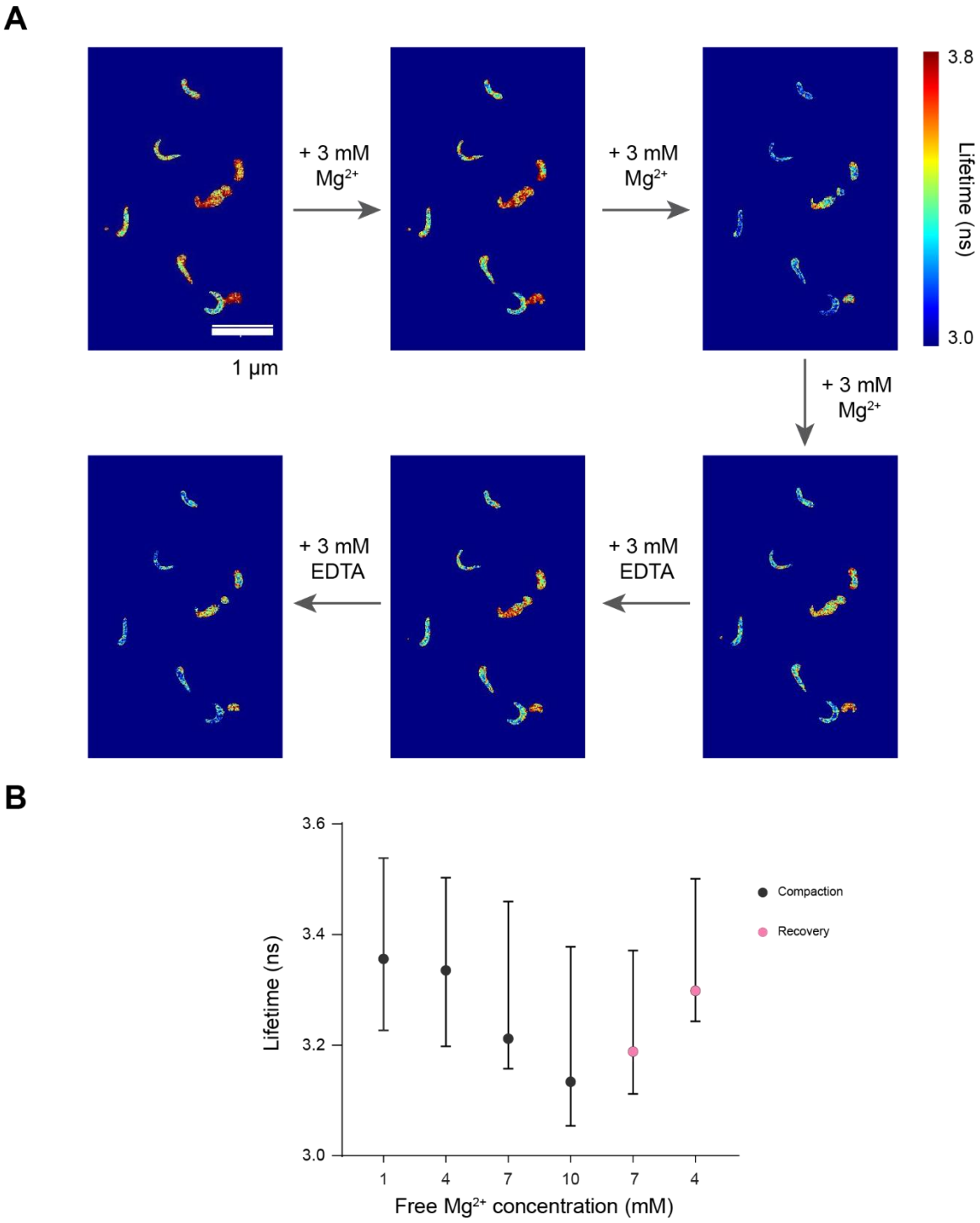

Figure A-3 Lifetime reports on magnesium dependent compaction

A) Images showing the changes in fluorescence lifetimes at the indicated free magnesium concentrations. Color map is shown on the right. B) The mean lifetime of each sperm nucleus in A) is plotted below. Error bars are 95% C.I.

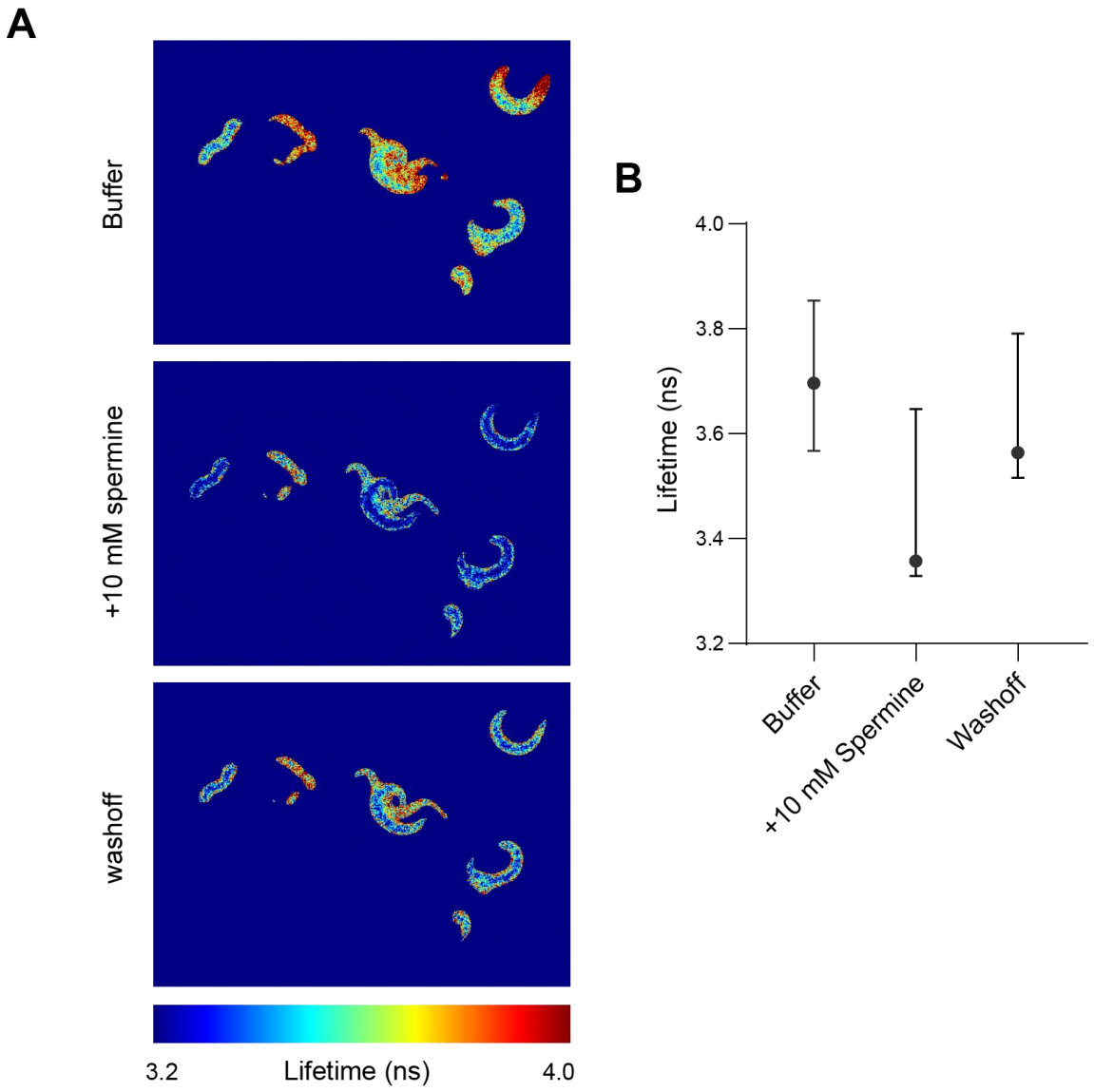

Figure A-4 Lifetime reports on spermine dependent compaction

A) Images showing the lifetimes of sperm nuclei upon addition of spermine and by wash off. Colormap is indicated below. B) The average of the average fluorescence lifetimes of each sperm nucleus in A) is plotted. Error bars are 95% C.I.

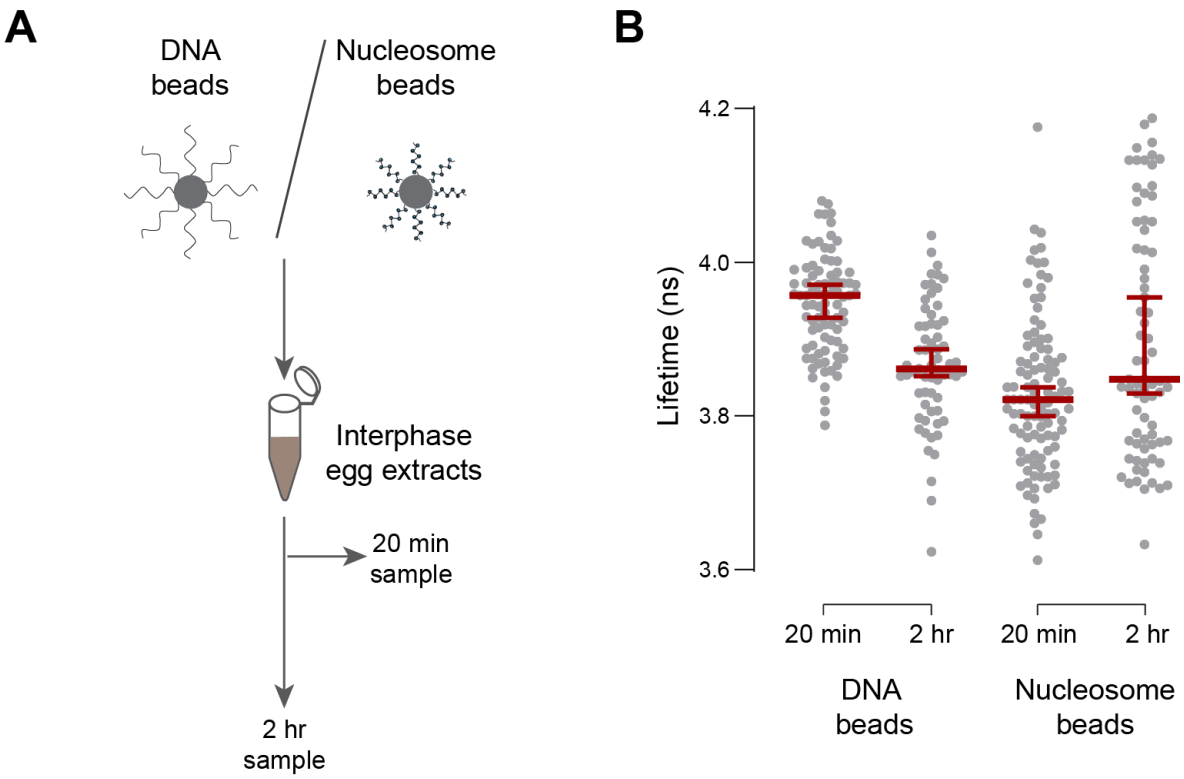

Figure A-5 Lifetime reports nucleosome dependent compaction

A) Protocol to measure the effect of nucleosome deposition on DNA compaction and the time points that the samples were collected at. B) Lifetimes of the DNA and nucleosome beads that were fixed and collected at the indicated time points. Each dot is the mean of a single cluster of beads. Data plotted is median and 95% C.I.

To verify if fluorescence lifetime can also report local compaction in other systems as well, I asked if hyperacetylation induced decompaction of the nucleosome fiber results in increased fluorescence lifetimes (Allahverdi et al., 2011; Shogren-Knaak et al., 2006). Trichostatin A (TSA) treatment of HeLa cells results in increased acetylation of histone H4 at lysine 12 in mitotic cells (**Figure A-5A**) and this also led to a reduction in fluorescence lifetime (**Figure A-5B**), consistent with previous reports on TSA induced decompaction (Llères et al., 2009). The lifetime also faithfully reports on chromatin compaction induced by ATP reduction induced by treating cells with 10 mM sodium azide and 2 mM 2-deoxyglucose (**Figure A-5C, D**). The data presented in the last few sections suggests that the fluorescence lifetime indeed reports on both DNA and chromatin compaction in a variety of *in vitro* and *in vivo* contexts. However the exact mechanism of this compaction is still unclear.

The lifetime of fluorophores is sensitive to many factors, including the chemical environment of the fluorophore, and processes such as quenching and Forster resonance energy transfer (FRET) (Lakowicz, 2006; Llères et al., 2009). An investigation of fluorescence lifetimes of intercalating DNA dyes suggested that the fluorophores show lower lifetimes when bound to more compacted DNA (Spagnol and Dahl, 2016). Although the authors suggested that this was due to quenching as a result of increased local fluorophore concentration, the exact mechanism of the reduced lifetimes was not established. To investigate the mechanism of this change in fluorescence lifetimes, I performed several tests. Since quenching occurs due to energy transfer between an excited fluorophore and a nearby unexcited fluorophore, quenching is sensitive to the concentration of fluorophore (Lakowicz, 2006). If quenching was playing a role in this compaction dependent lifetime change, I expected that the lifetime of the fluorophore would be increased at lower fluorophore concentrations where quenching is unlikely to occur. To measure this, I immobilized condensed and demembranated *X. laevis* sperm nuclei on coverslips and stained them with buffer containing decreasing amounts of

DNA intercalating dye Picogreen and measured the Picogreen lifetimes using a frequency domain FLIM microscope. Indeed, consistent with the quenching hypothesis, lower Picogreen concentrations showed increased lifetimes (**Figure A-6A**). However, intercalators also change the supercoiling state of the DNA (Shure et al., 1977). To test if a change in the supercoiling state was instead responsible for this change in fluorescence lifetime, I fixed the sperm nuclei before staining them with different concentrations of Picogreen dye. Surprisingly, the lifetime was not dependent on the Picogreen dye concentration (**Figure A-6B**). This suggested that the changes in fluorescence lifetime at higher Picogreen concentrations may be reporting changes in supercoiling state and not due to quenching. Lifetimes were also insensitive to potassium iodide concentration, suggesting that the intercalated dye is not accessible to the solvent (**Figure A-6C**)(Lakowicz, 2006).

I then asked if H1.8 and condensin I play a role in regulating local compaction of the chromatin fiber. To do this, I generated replicated metaphase sperm chromosomes from mock and H1.8 depleted extracts, fixed them and stained them with Picogreen to measure the fluorescence lifetime (**Figure A-7A, B**). H1.8 depletion led to an increase in fluorescence lifetime, suggesting that H1.8 compacts the nucleosome fiber. This is consistent with previous reports on the role of linker histones in nucleosome fiber compaction (Li et al., 2016; Song et al., 2014; Thoma et al., 1979b). Condensin I depletion (ΔCAP-G) also resulted in local decompaction. The exact mechanism of such decompaction is unclear, although a loss of condensin mediated supercoiling (Kimura and Hirano, 1997) could explain the observations. Interestingly, the co-depletion of H1.8 and condensin I (ΔH1ΔCAP-G) resulted in a further decompaction, suggesting that linker histones and condensin I may compact chromatin fiber by orthogonal mechanisms.

Figure A-6 Tissue culture chromatin compaction by lifetime measurements

A) Immunofluorescence data showing the increase in acetylation of mitotic cells upon treatment with histone deacetylase inhibitor Trichostatin A treatment. Each dot represents the mean of a single mitotic nucleus. Data plotted is median and error bars are 95% C.I. B) The lifetimes of mitotic nuclei treated with DMSO (control) or TSA (as in A)) are shown. Each dot is the average lifetime of a single nucleus. Data plotted is median and error bars are 95% C.I. C) Protocol to measure the local compaction upon depletion of ATP. D) The lifetimes of mitotic nuclei treated with DMSO (control) or TSA (as in A)) are shown. Each dot is the average lifetime of a single nucleus. Data plotted is median and error bars are 95% C.I.

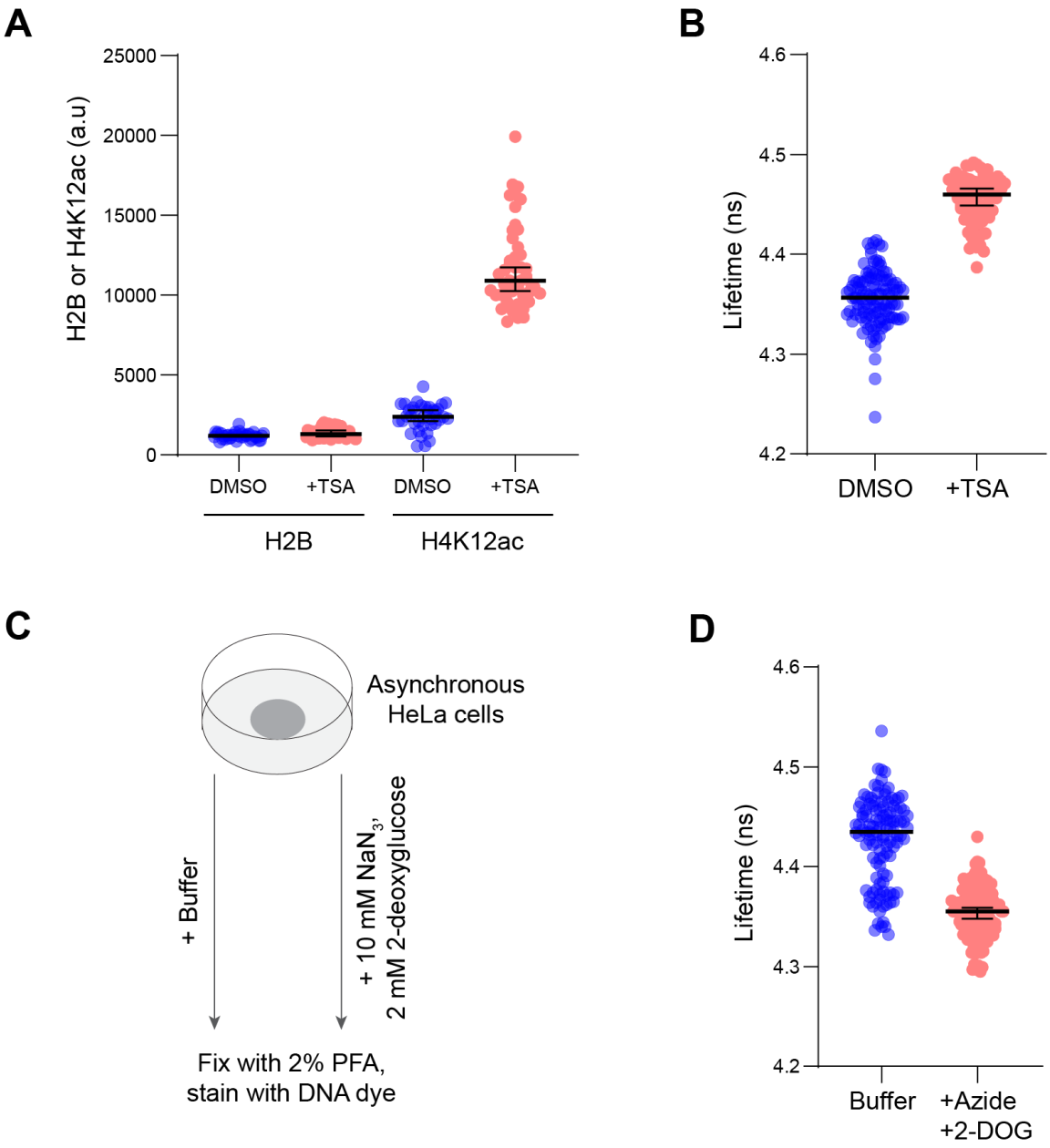
A
H2B or H4K12ac (a.u)
25000
20000
15000
10000
5000
0
DMSO
+TSA
DMSO
+TSA
H2B
H4K12ac
B
Lifetime (ns)
4.6
4.5
4.4
4.3
4.2
DMSO
+TSA
C
Asynchronous
HeLa cells
+ Buffer
+ 10 mM NaN3,
2 mM 2-deoxyglucose
Fix with 2% PFA,
stain with DNA dye
D
Lifetime (ns)
4.6
4.5
4.4
4.3
4.2
Buffer
+Azide
+2-DOG

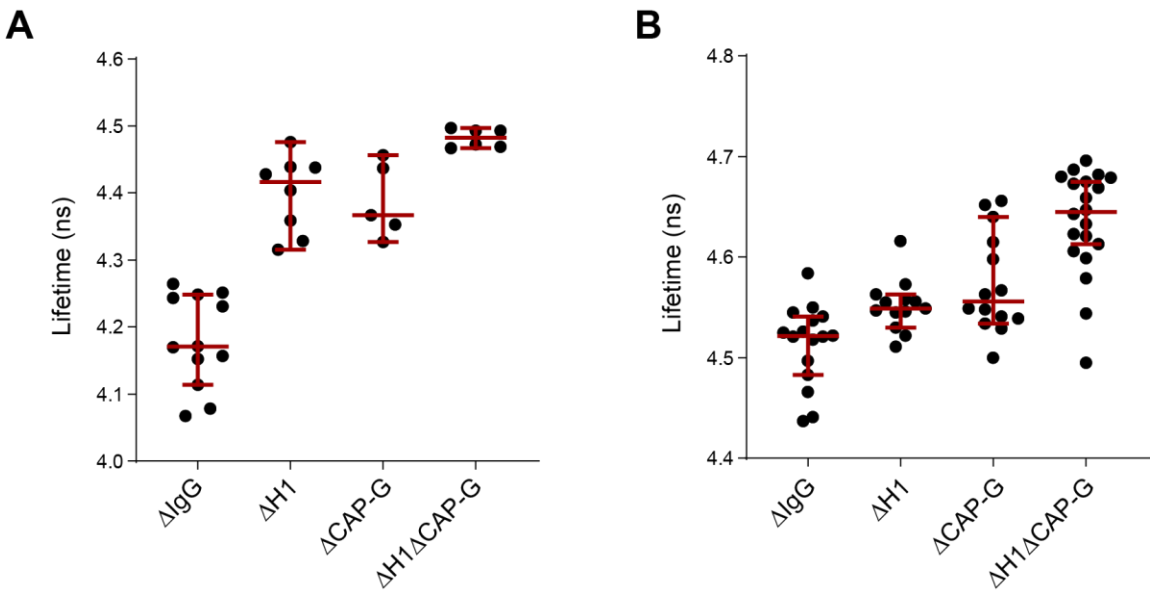

Figure A-7 H1.8 and condensin I both contribute to local compaction

A) Nocodazole treated metaphase sperm nuclei prepared in the extracts depleted of the indicated proteins were fixed and the lifetimes were measured of the nuclei. Each dot represents the average lifetime of a single nucleus in the indicated condition. Data plotted is median and 95% C.I. B) Same as in A) for a different experiment.

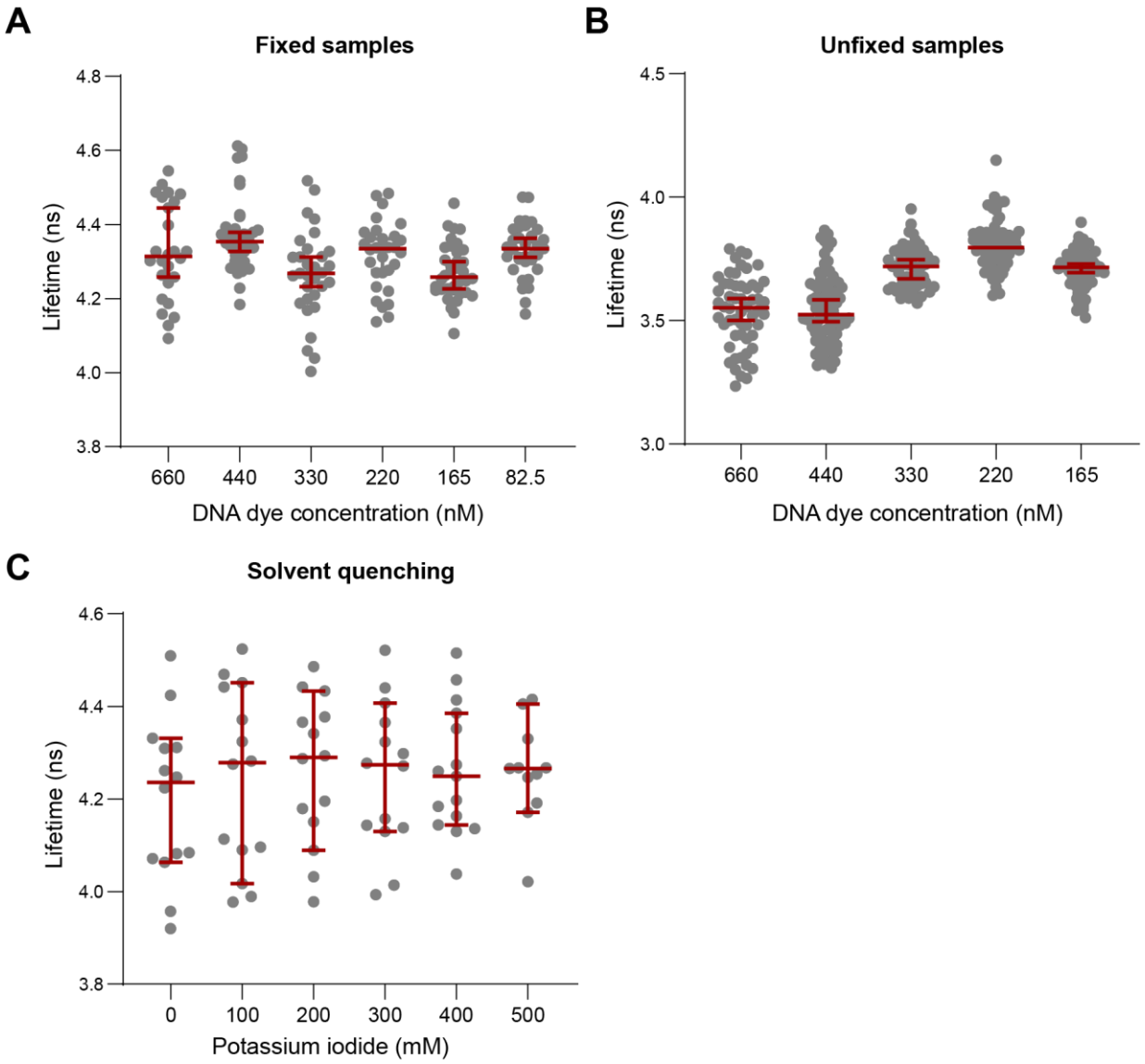

Figure A-8 Mechanism of fluorescence lifetime changes

A) Condensed demembranated sperm nuclei fixed using formaldehyde and then stained using the indicated concentration of DNA dye. B) As in A), but the nuclei were not fixed. C) Sperm nuclei stained with Picogreen were incubated in buffer containing the indicated potassium iodide concentration. A, B, C) Each dot represents the average lifetime of a single sperm nucleus. Data plotted is median and error bars are 95% C.I.

Expansion microscopy of chromosomal proteins

Condensins and topoisomerases were long thought to form a part of an independent protein scaffold that organizes the mitotic chromosome (Adolph et al., 1977; Adolphs et al., 1977; Paulson and Laemmli, 1977). The presence of an independent protein scaffold that mechanically organizes the mitotic chromosome was shown to be unlikely as restriction enzyme digestion abolished the mechanical integrity of chromosomes (Poirier and Marko, 2002). The absence of an independent scaffold was further supported by direct super-resolution imaging of condensin in HeLa chromosomes (Walther et al., 2018) and the observation of discrete foci of condensin on stretched chromosomes (Sun et al., 2018). Since H1.8 depletion led to an accumulation of condensin (**Chapter 2**) and longer chromosomes (Maresca et al., 2005), I wondered if H1.8 depletion also affected the organization of condensins on mitotic chromosomes.

Since the scaffold structures are smaller than the wavelength of light, observation of scaffold structure requires imaging the proteins using super-resolution imaging (Poonperm et al., 2015; Walther et al., 2018). To enable higher throughput three-dimensional imaging of the fine structure of the scaffold proteins, I instead performed expansion microscopy. Unlike other super-resolution techniques, expansion microscopy achieves higher effective resolution by performing diffraction limited imaging on physically expanded samples (Chen et al., 2015). During expansion microscopy, fixed samples labelled using antibody-based probes were then encased and crosslinked to an acrylamide-based gel (**Figure A-8A**). The protein mesh was then digested using a proteinase K digest to reduce the mechanical integrity of the sample. At this point, the locations of the scaffold proteins are marked by the antibody label. The gel is then expanded by hypotonic treatment and the antibody labels crosslinked to the gel also expand isotropically (Chozinski et al., 2016). This results in the generation of a 4-5-fold enlarged structure where only the relative locations of the labels is preserved from the

original sample (**Figure A-8A, B**). I could also verify that the expansion protocol preserved the morphology of well-studied tubulin structures in interphase and mitotic HeLa cells (**Figure A-9**).

I then asked whether the distribution of chromatin in the nucleus is uniform. To do this, I performed expansion microscopy on immortalized BJ fibroblast cells using an antibody against H4K12ac, which stains both interphase and mitotic chromosomes. The expanded interphase nuclei retain the DNA distribution of unexpanded nuclei and show accumulation of dense chromatin at the nuclear periphery, representative of lamin associated heterochromatin (**Figure A-10**). However, unlike the expanded nuclei, the chromatin in less dense regions shows a more punctate staining, suggesting that the distribution of nucleosomes is non-uniform even among euchromatic loci. This is consistent with super-resolution PALM microscopy on histones in other tissue culture cells (Ricci et al., 2015b) and data from the cryo-electron tomography technique ChromEMT (Ou et al., 2017). Similar punctate staining was also observed in mitotic cells, suggesting the nucleosome clusters may not be cell cycle dependent (**Figure A-10**). This data also indicated to me that expansion microscopy may be useful in capturing fine structural details of nuclear organization.

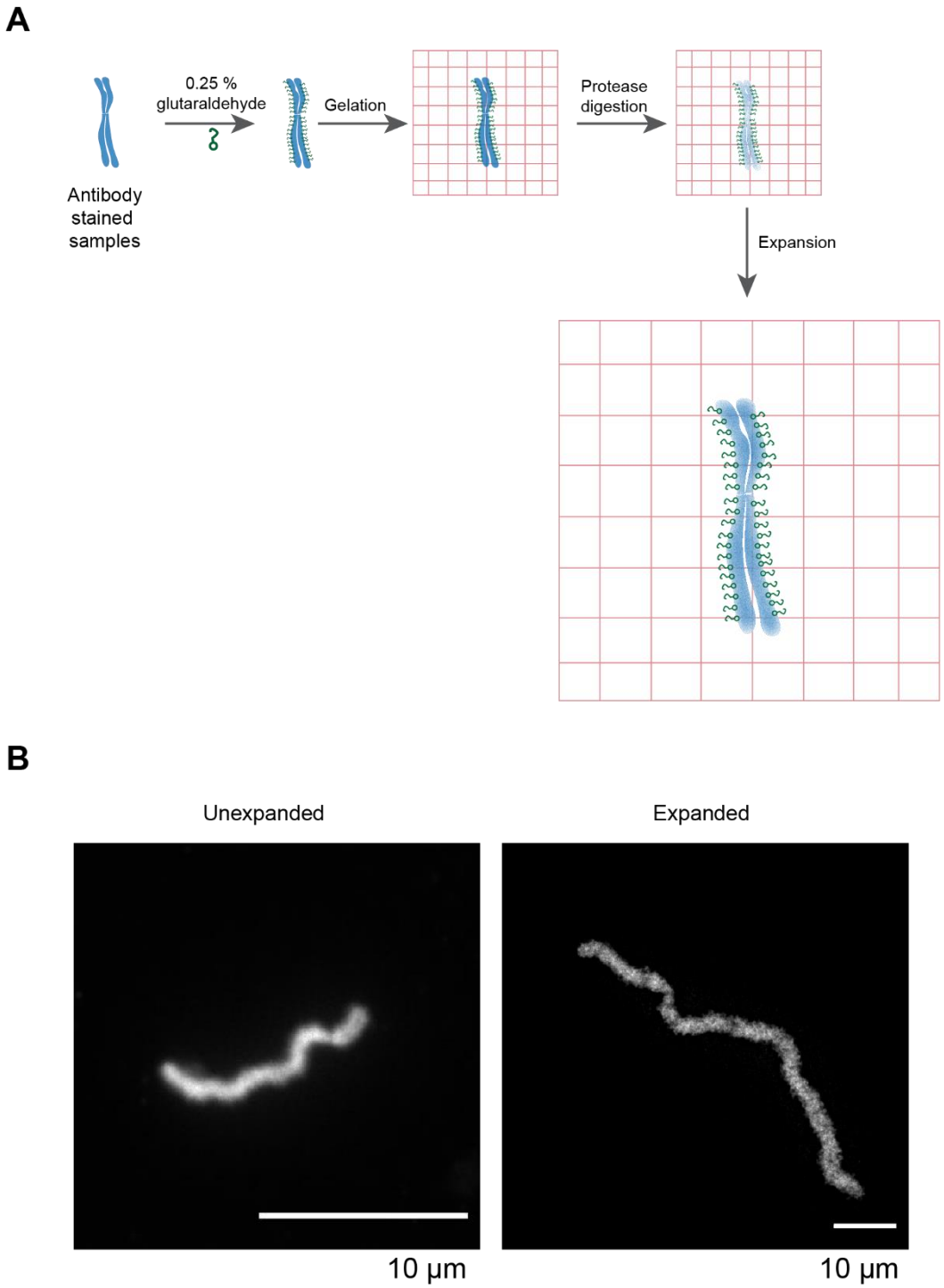

Figure A-9 Protocol for performing expansion microscopy

A) Samples were fixed and stained using immunofluorescence. They were then crosslinked to a gel, digested using a proteinase and expanded. B) A representative example of an egg extract chromosome sample expanded ~4-fold.

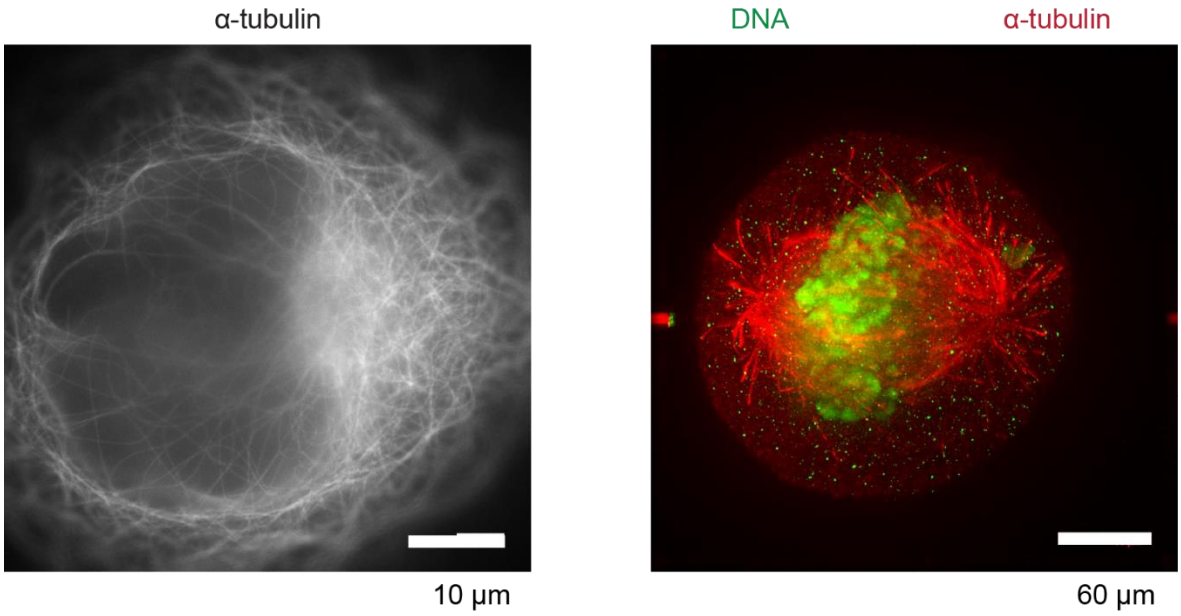

Figure A-10 Expansion microscopy preserves large-scale cellular structure

A representative expanded interphase cell (left) and mitotic cell (right) stained for α-tubulin and DNA (right only) showing the preservation of the tubulin and DNA structure of the cells in both interphase and mitosis.

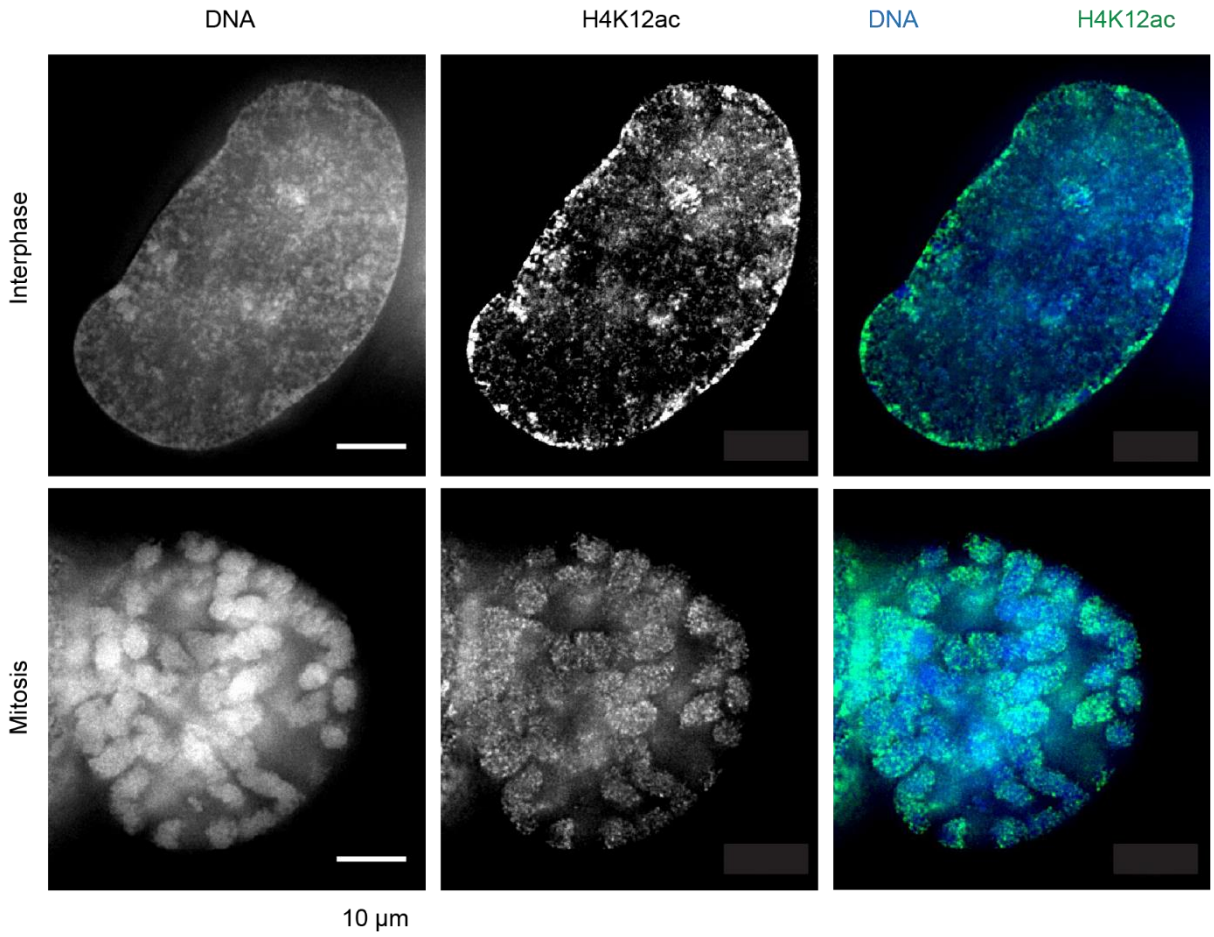

Figure A-11 Nucleosomes show local clustering in both interphase and mitosis

Representative expanded interphase cell (top) and mitotic cell (bottom) stained for DNA and acetylated lysine-12 of histone H4 showing the small clusters of nucleosomes stained with the H4K12ac antibody.

I then examined the substructures of the scaffold proteins in *X. laevis* egg extract metaphase chromosomes. As observed previously, at diffraction limited resolution, condensin I and TOP2A both form rod like structures that were thought to compose the protein scaffold of mitotic chromosomes (**Figure A-11A**)(Cuvier and Hirano, 2003). Upon expanding the samples, however, both condensin I and TOP2A show a much more discontinuous punctate staining structure (**Figure A-11B**). This is similar to the discontinuous condensin structures observed in HeLa cells (Walther et al., 2018) and bolsters the argument against an independent protein scaffold. These condensin I clusters were also localized all through the chromatids unlike the condensin I clusters in HeLa cells which show a preference for the outer edges of the chromatids (Walther et al., 2018). These clusters were also significantly larger and fewer in number than the nucleosome clusters observed and were estimated to be around 150 nm in diameter in unexpanded chromosomes (**Figure A-11B**). Such punctate staining is also not shared by other mitosis specific antibodies such as those against phosphorylated Serine-10 of histone H3 (H3S10p) and linker histone H1.8 (**Figure A-12**). I could also confirm that TOP2A in HeLa cells also shows similar punctate staining upon expansion, but not in unexpanded cells (**Figure A-13**).

Since condensins to accumulate at the base of the loops, I speculated that these discrete punctate structures may be the result of accumulations of condensins at the base of loops. It is however unclear why TOP2A accumulates at the base of these loops, though it appears possible that loop extrusion by condensins generates TOP2A substrates at the base of loops (Orlandini et al., 2019). Since this hypothesis suggests that the punctate staining of TOP2A is dependent on loop formation by condensins, I asked if depleting condensins would abolish the punctate staining. I thus performed expansion microscopy on nocodazole treated nuclei from extracts depleted of condensin I and/or condensin II (**Figure A-14-top**). Condensin I depletion (ΔCAP-G) resulted in a small change in the punctate nature of TOP2A

staining, which I measured using the standard deviation of TOP2A signal (**Figure A-14-bottom**). Condensin II depletion (ΔCAP-D3) resulted in a small increase in standard deviation of TOP2A staining, suggesting that condensin II may not play such a significant role in loop organization in egg extract chromosomes. This is consistent with the observations from the Hi-C data in chapter 2. Depleting both condensins (ΔCAP-GΔCAP-D3) however led to a large reduction in the punctate nature of TOP2A staining. This data confirms the possibility that the TOP2A puncta may indeed be the result of accumulation of TOP2A at condensin loop anchor sites. Since H1.8 suppresses loading of condensins and TOP2A, I then asked if H1.8 changes the organization of the condensins in the chromosome. Although there is increased condensin I on these chromosomes, condensin I still shows punctate staining in H1.8 depleted chromosomes (**Figure A-15**). This suggests that H1.8 only changes condensin loading on chromosomes and does not affect the scaffold organization, confirming observations from the Hi-C data (**Chapter 2**).

Figure A-12 Condensin I and TOP2A show punctate staining on mitotic chromosomes

A) Representative unexpanded replicated mitotic chromosomes from egg extracts stained using CAP-G (condensin I-top) and TOP2A (bottom) showing the rod-like structure of the scaffold components. B) Representative expanded mitotic chromosomes stained using antibodies against CAP-G (condensin I-bottom), TOP2A (top) and H4K12ac, showing the punctate nature of the staining upon expansion.

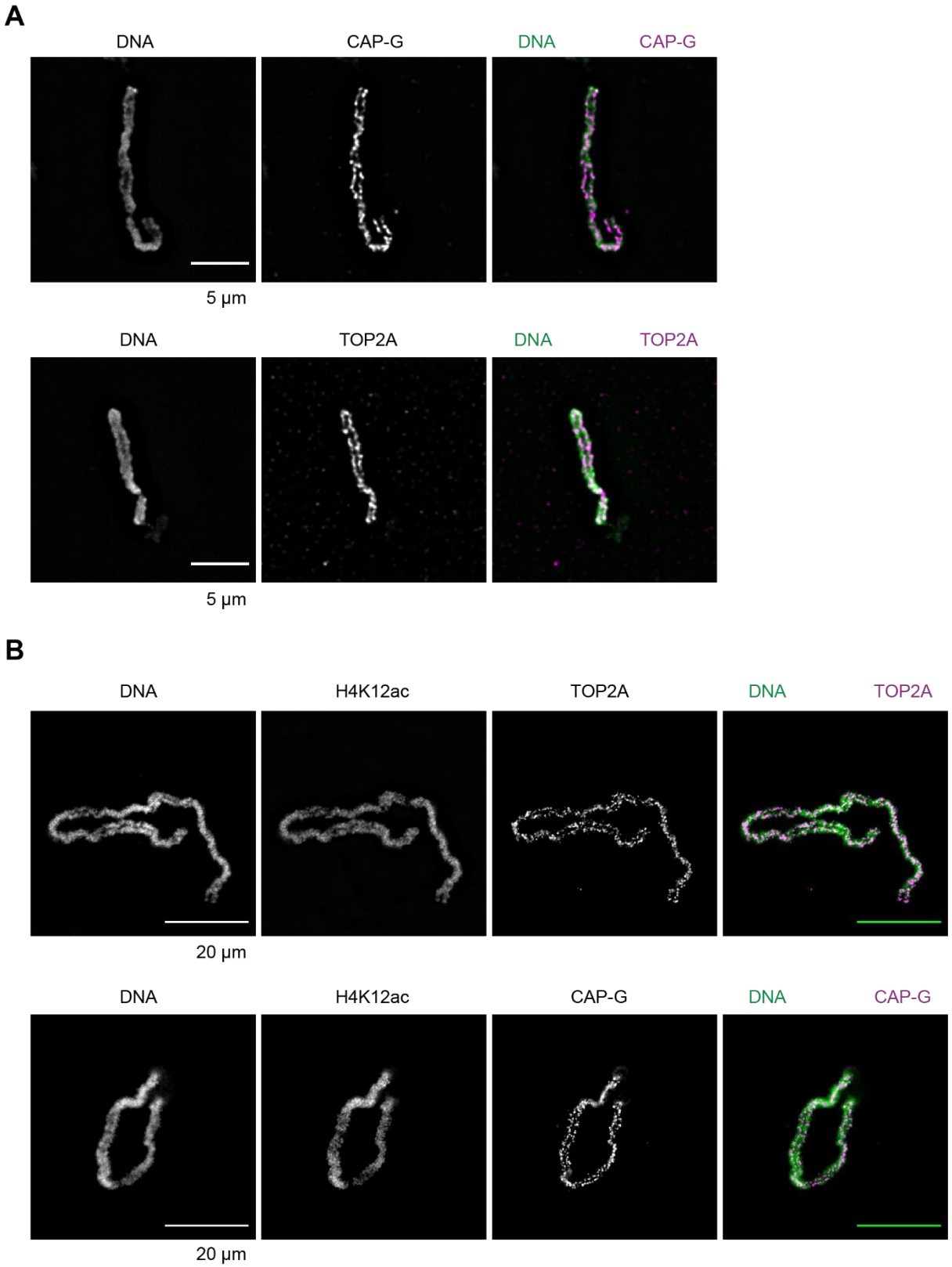
A
DNA
CAP-G
DNA
CAP-G
5 μm
DNA
TOP2A
DNA
TOP2A
5 μm
B
DNA
H4K12ac
TOP2A
DNA
TOP2A
20 μm
DNA
H4K12ac
CAP-G
DNA
CAP-G
20 μm

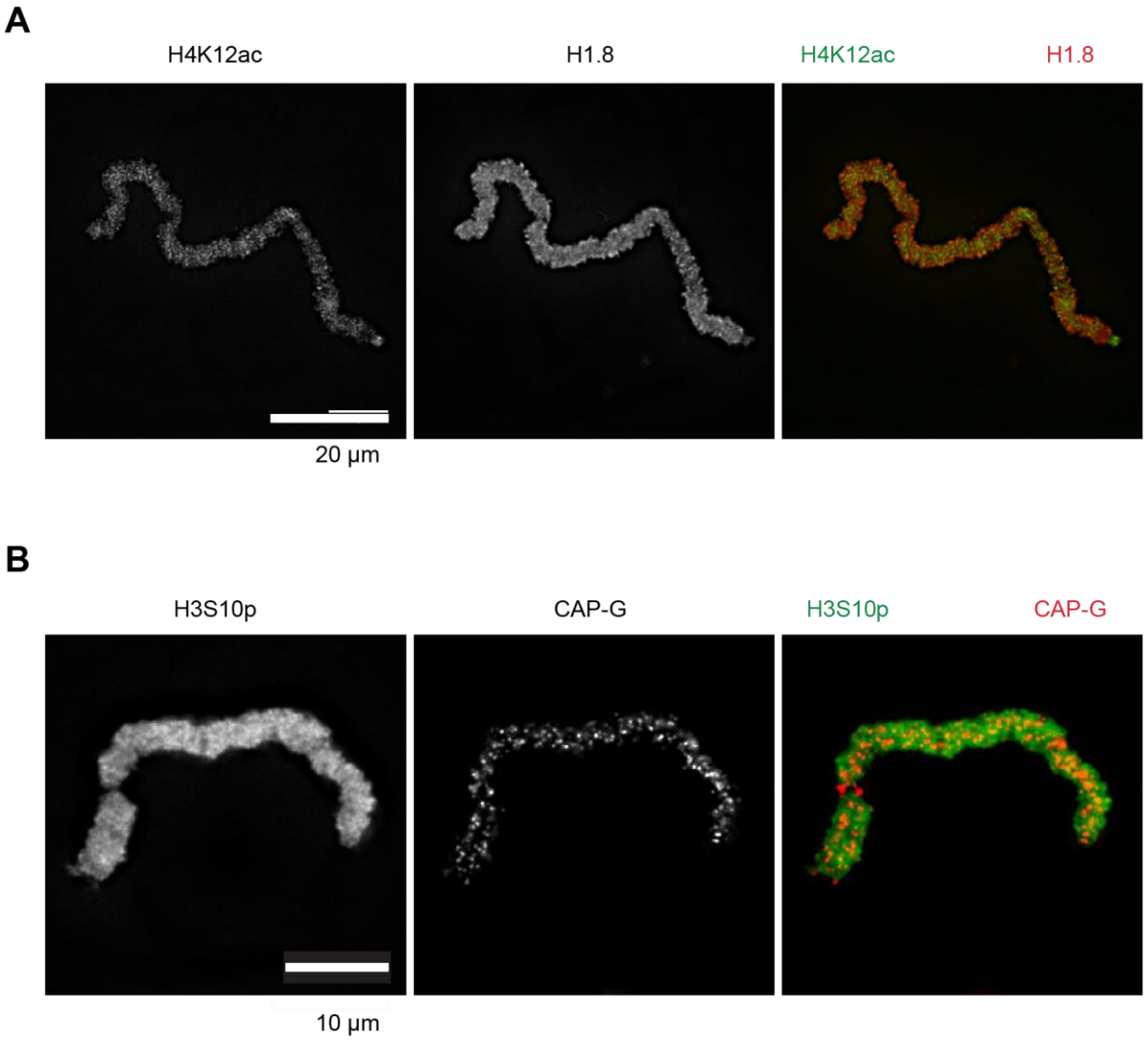

Figure A-13 Punctate staining is not ubiquitous for mitotic antibodies

A) Representative expanded chromosome stained for H4K12ac and H1.8 showing the more uniform staining of H1.8. B) As in A) but stained using antibodies against H3S10p and CAP-G (condensin I).

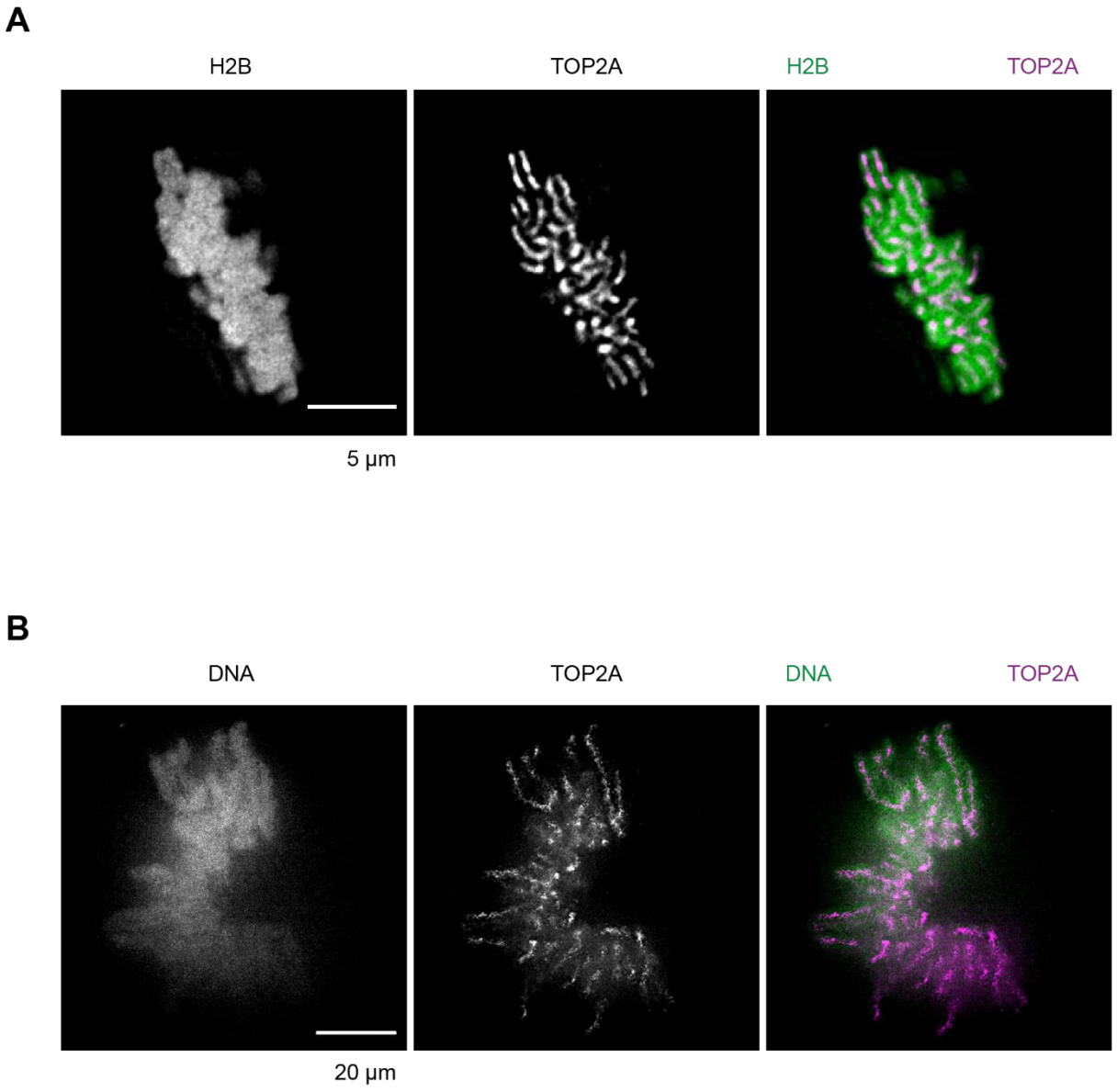

Figure A-14 TOP2A shows punctate staining in tissue culture cells

A) Representative unexpanded mitotic hTert-RPE1 cell stained for TOP2A and DNA showing the rod-like nature of staining of TOP2A. B) Representative expanded hTert-RPE1 mitotic cell stained for DNA and TOP2A showing the punctate staining upon expansion.

Figure A-15 Condensins are required for TOP2A puncta

Representative expanded TOP2A staining in chromosomes prepared from extracts depleted of the indicated proteins showing the punctate nature of TOP2A being reduced upon depletion of condensin I or both condensins (top). Quantification of the standard deviation of TOP2A signal in the images shown (bottom).

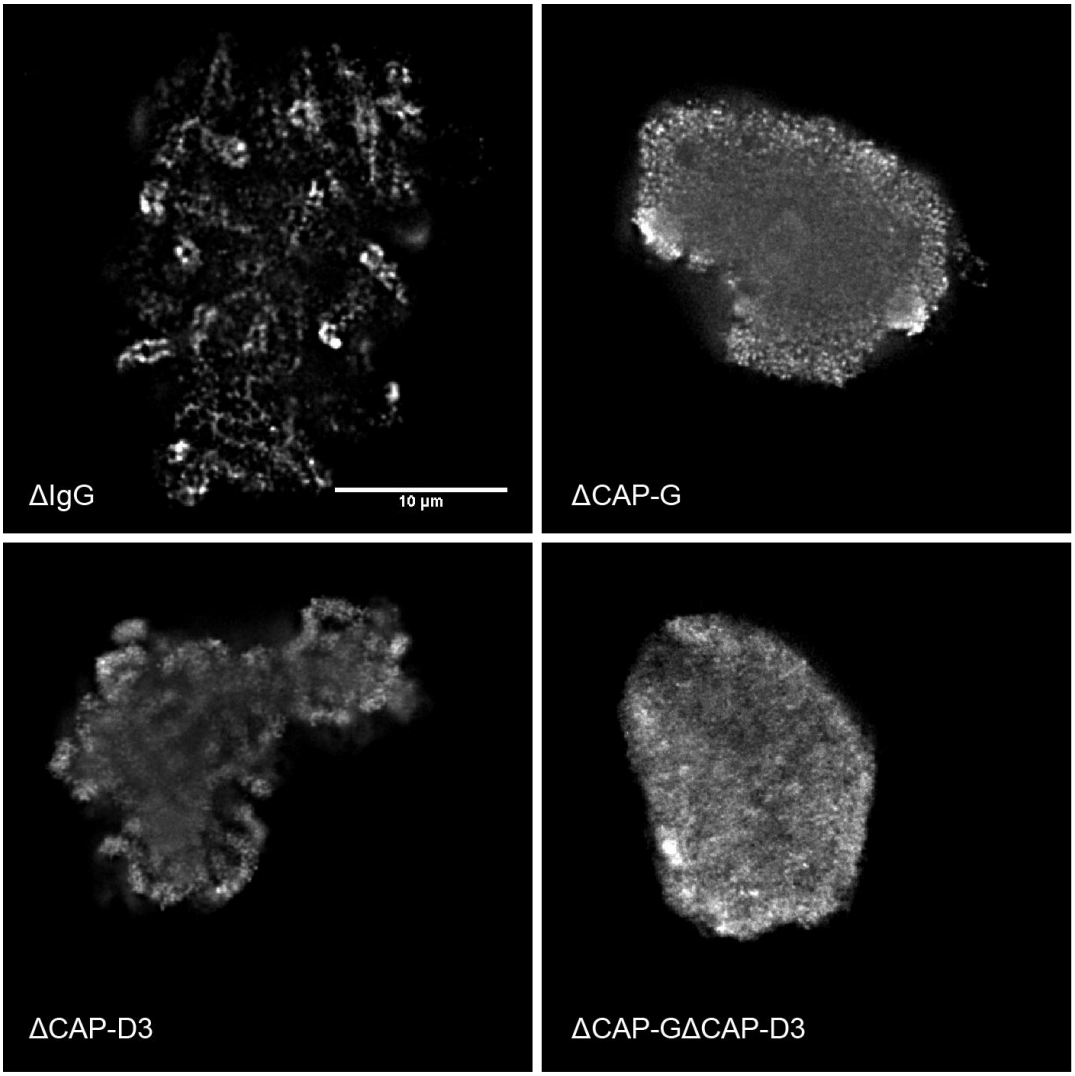
ΔIgG
10 μm
ΔCAP-G
ΔCAP-D3
ΔCAP-GΔCAP-D3

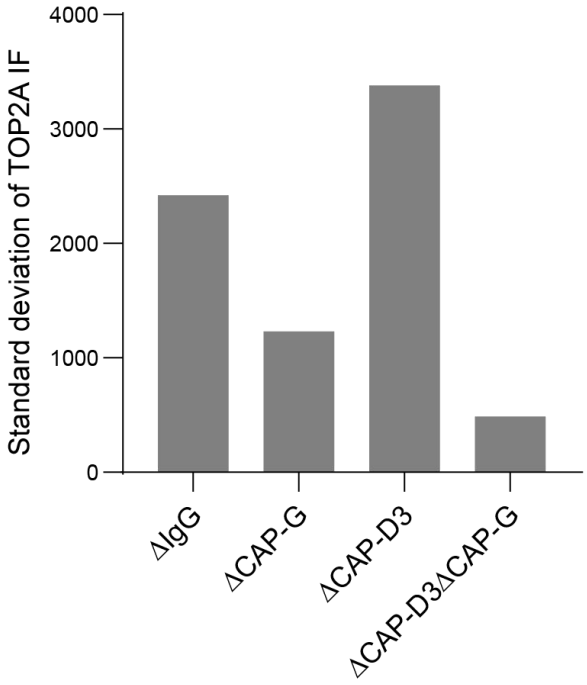
Standard deviation of TOP2A IF
4000
3000
2000
1000
0
ΔIgG
ΔCAP-G
ΔCAP-D3
ΔCAP-D3ΔCAP-G

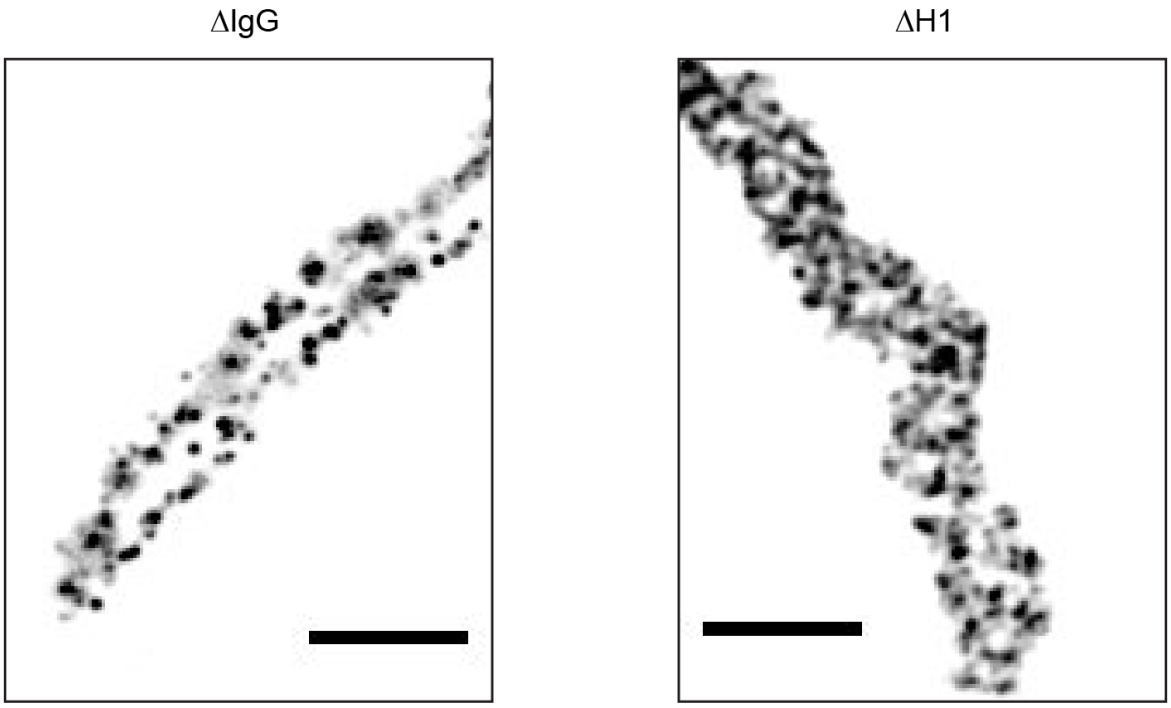

Figure A-16 H1.8 does not affect punctate staining of condensin I

Representative images of zoomed in metaphase chromosomes stained with CAP-G (condensin I) from mock (left) or H1.8-depleted (right) extracts. Scale bar is 5 μm.

References

Abdennur, N., and Mirny, L.A. (2019). Cooler: scalable storage for Hi-C data and other genomically labeled arrays. Bioinformatics *36*, 311–316.

Abe, S., Nagasaka, K., Hirayama, Y., Kozuka-Hata, H., Oyama, M., Aoyagi, Y., Obuse, C., and Hirota, T. (2011). The initial phase of chromosome condensation requires Cdk1-mediated phosphorylation of the CAP-D3 subunit of condensin II. Genes Dev. *25*, 863–874.

Abramo, K., Valton, A., Venev, S. V, Ozadam, H., Fox, A.N., and Dekker, J. (2019). A chromosome folding intermediate at the condensin-to-cohesin transition during telophase. Nat. Cell Biol. *21*, 1393–1402.

Adachi, Y., Luke, M., and Laemmli, U.K. (1991). Chromosome assembly in vitro: topoisomerase II is required for condensation. Cell *64*, 137–148.

Adolph, K.W., Cheng, S.M., and Laemmli, U.K. (1977). Role of Nonhistone Proteins Chromosome Structure in Metaphase. Cell *12*, 605–616.

Adolphs, K.W., Cheng, S.M., Paulson, J.R., and Laemmli, U.K. (1977). Isolation of a protein scaffold from mitotic HeLa cell chromosomes. Proc. Natl. Acad. Sci. U. S. A. *74*, 4937–4941.

Alami, R., Fan, Y., Pack, S., Sonbuchner, T.M., Besse, A., Lin, Q., Greally, J.M., Skoultchi, A.I., and Bouhassira, E.E. (2003). Mammalian linker-histone subtypes differentially affect gene expression in vivo. Proc. Natl. Acad. Sci. *100*, 5920–5925.

Alberts, B., Johnson, A., Lewis, J., Morgan, D., Raff, M., Roberts, K., and Walter, P. (2015). Molecular Biology of the Cell, Sixth Edition. In MOLECULAR BIOLOGY OF THE CELL, SIXTH EDITION, (270 MADISON AVENUE, NEW YORK, NY 10016 USA: GARLAND SCIENCE, TAYLOR & FRANCIS), pp. 1–1342.

Alipour, E., and Marko, J.F. (2012). Self-organization of domain structures by DNA-loop-extruding

enzymes. Nucleic Acids Res. *40*, 11202–11212.

Allahverdi, A., Yang, R., Korolev, N., Fan, Y., Davey, C.A., Liu, C.F., and Nordenskiöld, L. (2011). The effects of histone H4 tail acetylations on cation-induced chromatin folding and self-association. Nucleic Acids Res. *39*, 1680–1691.

Allan, J., Hartman, P.G., Crane-Robinson, C., and Aviles, F.X. (1980). The structure of histone H1 and its location in chromatin. Nature *288*, 675–679.

Amat, R., Böttcher, R., Le Dily, F., Vidal, E., Quilez, J., Cuartero, Y., Beato, M., De Nadal, E., and Posas, F. (2019). Rapid reversible changes in compartments and local chromatin organization revealed by hyperosmotic shock. Genome Res. *29*, 18–28.

Amodeo, A.A., Jukam, D., Straight, A.F., and Skotheim, J.M. (2015). Histone titration against the genome sets the DNA-to-cytoplasm threshold for the Xenopus midblastula transition . Proc. Natl. Acad. Sci. *112*, E1086–E1095.

Andreyeva, E.N., Bernardo, T.J., Kolesnikova, T.D., Lu, X., Yarinich, L.A., Bartholdy, B.A., Guo, X., Posukh, O. V., Healton, S., Willcockson, M.A., et al. (2017). Regulatory functions and chromatin loading dynamics of linker histone H1 during endoreplication in Drosophila. Genes Dev. *31*, 603–616.

Aono, N., Sutani, T., Tomonaga, T., Mochida, S., and Yanagida, M. (2002). Cnd2 has dual roles in mitotic condensation and interphase. Nature *417*, 197–202.

Aragón, L. (2018). The Smc5/6 complex: New and old functions of the enigmatic long-distance relative. Annu. Rev. Genet. *52*, 89–107.

Arimura, Y., Shih, R.M., Froom, R., and Funabiki, H. (2020). Nucleosome structural variations in interphase and metaphase chromosomes. BioRxiv 2020.11.12.380386.

Bakhrebah, M., Zhang, T., Mann, J.R., Kalitsis, P., and Hudson, D.F. (2015). Disruption of a conserved CAP-D3 threonine alters condensin loading on mitotic chromosomes leading to chromosome hypercondensation. J. Biol. Chem. *290*, 6156–6167.

Banigan, E.J., van den Berg, A.A., Brandão, H.B., Marko, J.F., and Mirny, L.A. (2020). Chromosome organization by one-sided and two-sided loop extrusion. Elife *9*, 1–46.

Bao, Y., Konesky, K., Park, Y.J., Rosu, S., Dyer, P.N., Rangasamy, D., Tremethick, D.J., Laybourn, P.J., and Luger, K. (2004). Nucleosomes containing the histone variant H2A.Bbd organize only 118 base pairs of DNA. EMBO J. *23*, 3314–3324.

Basu, A., Bobrovnikov, D.G., Qureshi, Z., Kayikcioglu, T., Ngo, T.T.M., Ranjan, A., Eustermann, S., Cieza, B., Morgan, M.T., Hejna, M., et al. (2021). Measuring DNA mechanics on the genome scale. Nature *589*, 462–467.

Bauer, C.R., Hartl, T.A., and Bosco, G. (2012). Condensin II Promotes the Formation of Chromosome Territories by Inducing Axial Compaction of Polyploid Interphase Chromosomes. PLoS Genet. *8*, 1–12.

Baxter, J., Sen, N., López Martínez, V., Monturus De Carandini, M.E., Schvartzman, J.B., Diffley, J.F.X.X., Aragón, L., Martínez, V.L., De Carandini, M.E.M., Schvartzman, J.B., et al. (2011). Positive supercoiling of mitotic DNA drives decatenation by topoisomerase II in eukaryotes. Science (80-.). *331*, 1328–1332.

Bazett-Jones, D.P., Kimura, K., and Hirano, T. (2002). Efficient Supercoiling of DNA by a Single Condensin Complex as Revealed by Electron Spectroscopic Imaging Figure 1. Stoichiometric Relationships between Protein and Nucleic Acid in the Condensin-DNA Complexes. Mol. Cell *9*, 1183–1190.

Beagrie, R.A., Scialdone, A., Schueler, M., Kraemer, D.C.A., Chotalia, M., Xie, S.Q., Barbieri, M., De Santiago, I., Lavitas, L.M., Branco, M.R., et al. (2017). Complex multi-enhancer contacts captured by genome architecture mapping. Nature *543*, 519–524.

Bednar, J., Horowitz, R.A., Dubochet, J., and Woodcock, C.L. (1995). Chromatin conformation and salt-induced compaction: Three-dimensional structural information from cryoelectron microscopy. J. Cell Biol. *131*, 1365–1376.

Bednar, J., Horowitz, R.A., Grigoryev, S.A., Carruthers, L.M., Hansen, J.C., Koster, A.J., and Woodcock, C.L. (1998). Nucleosomes, linker DNA, and linker histone form a unique structural motif that directs the higher-order folding and compaction of chromatin. Proc. Natl. Acad. Sci. U. S. A. *95*, 14173–14178.

Bednar, J., Garcia-Saez, I., Boopathi, R., Cutter, A.R., Papai, G., Reymer, A., Syed, S.H., Lone, I.N., Tonchev, O., Crucifix, C., et al. (2017). Structure and Dynamics of a 197 bp Nucleosome in Complex with Linker Histone H1. Mol. Cell *66*, 384-397.e8.

Belaghzal, H., Dekker, J., and Gibcus, J.H. (2017). Hi-C 2 . 0 : An optimized Hi-C procedure for high-resolution genome-wide mapping of chromosome conformation. Methods *123*, 56–65.

Belaghzal, H., Borrman, T., Stephens, A.D., Lafontaine, D.L., Venev, S. V, Weng, Z., Marko, J.F., and Dekker, J. (2021). Liquid chromatin Hi-C characterizes compartment-dependent chromatin interaction dynamics. Nat. Genet.

Belmont, A.S. (2006). Mitotic chromosome structure and condensation. Curr. Opin. Cell Biol. *18*, 632–638.

Belmont, A.S., and Bruce, K. (1994). Visualization of G1 chromosomes: A folded, twisted, supercoiled chromonema model of interphase chromatid structure. J. Cell Biol. *127*, 287–302.

Belton, J.M., McCord, R.P., Gibcus, J.H., Naumova, N., Zhan, Y., and Dekker, J. (2012). Hi-C: A comprehensive technique to capture the conformation of genomes. Methods *58*, 268–276.

Benedetti, F., Dorier, J., Burnier, Y., and Stasiak, A. (2014). Models that include supercoiling of topological domains reproduce several known features of interphase chromosomes. Nucleic Acids Res. *42*, 2848–2855.

Bennett, G.M., and Moran, N.A. (2013). Small, smaller, smallest: The origins and evolution of ancient dual symbioses in a phloem-feeding insect. Genome Biol. Evol. *5*, 1675–1688.

Berger, J.M., Gamblin, S.J., Harrison, S.C., and Wang, J.C. (1996). Structure and mechanism of DNA topoisomerase II. Nature *379*, 225–232.

Bernad, R., Sánchez, P., Rivera, T., Rodríguez-corsino, M., Boyarchuk, E., Vassias, I., Ray-gallet, D., Arnaoutov, A., Dasso, M., Almouzni, G., et al. (2011). HJURP and condensin II are required for CENP-A assembly. *192*, 569–582.

Bickmore, W.A., and Van Steensel, B. (2013). Genome architecture: Domain organization of interphase chromosomes. Cell *152*, 1270–1284.

Bintu, B., Mateo, L.J., Su, J.-H., Sinnott-Armstrong, N.A., Parker, M., Kinrot, S., Yamaya, K., Boettiger, A.N., and Zhuang, X. (2018). Super-resolution chromatin tracing reveals domains and cooperative interactions in single cells. Science (80-.). *362*, eaau1783.

Blow, J.J., and Laskey, R.A. (1986). Initiation of DNA replication in nuclei and purified DNA by a cell-free extract of Xenopus eggs. Cell *47*, 577–587.

Boehning, M., Dugast-Darzacq, C., Rankovic, M., Hansen, A.S., Yu, T., Marie-Nelly, H., McSwiggen, D.T., Kokic, G., Dailey, G.M., Cramer, P., et al. (2018). RNA polymerase II clustering through carboxy-terminal domain phase separation. Nat. Struct. Mol. Biol. *25*, 833–840.

Boettiger, A.N., and Murphy, S. (2020). Advances in Chromatin Imaging at Kilobase-Scale Resolution. Trends Genet. *36*, 273–287.

Boettiger, A.N., Bintu, B., Moffitt, J.R., Wang, S., Beliveau, B.J., Fudenberg, G., Imakaev, M., Mirny, L.A., Wu, C.T., and Zhuang, X. (2016). Super-resolution imaging reveals distinct chromatin folding for different epigenetic states. Nature *529*, 418–422.

Bonev, B., Mendelson Cohen, N., Szabo, Q., Fritsch, L., Papadopoulos, G.L., Lubling, Y., Xu, X., Lv, X., Hugnot, J.P., Tanay, A., et al. (2017). Multiscale 3D Genome Rewiring during Mouse Neural Development. Cell *171*, 557-572.e24.

Boveri, T. (1909). Die Blastomerenkerne von Ascaris megalocephala. Arch. Für Zellforsch. *3*, 181.

Brahmachari, S., and Marko, J.F. (2019). Chromosome disentanglement driven via optimal compaction of loop-extruded brush structures. Proc. Natl. Acad. Sci. U. S. A. *116*, 24956–24965.

Branco, M.R., Branco, T., Ramirez, F., and Pombo, A. (2008). Changes in chromosome organization during PHA-activation of resting human lymphocytes measured by cryo-FISH. Chromosom. Res. *16*, 413–426.

Brandão, H.B., Ren, Z., Karaboja, X., Mirny, L.A., and Wang, X. (2020). DNA-loop extruding SMC complexes can traverse one another in vivo doi: bioRxiv preprint. BioRxiv 2020.10.26.356329.

Cai, S., Böck, D., Pilhofer, M., and Gan, L. (2018a). The in situ structures of mono-, di-, and trinucleosomes in human heterochromatin. Mol. Biol. Cell *29*, 2450–2457.

Cai, S., Chen, C., Tan, Z.Y., Huang, Y., Shi, J., and Gan, L. (2018b). Cryo-ET reveals the macromolecular reorganization of S. pombe mitotic chromosomes in vivo. Proc. Natl. Acad. Sci. *115*, 10977–10982.

Canela, A., Maman, Y., Jung, S., Wong, N., Callen, E., Day, A., Kieffer-Kwon, K.R., Pekowska, A., Zhang, H., Rao, S.S.P., et al. (2017). Genome Organization Drives Chromosome Fragility. Cell *170*, 507-521.e18.

Canela, A., Maman, Y., Huang, S.N., Wutz, G., Tang, W., Zagnoli-Vieira, G., Callen, E., Wong, N., Day, A., Peters, J.-M., et al. (2019). Topoisomerase II-Induced Chromosome Breakage and Translocation Is Determined by Chromosome Architecture and Transcriptional Activity. Mol. Cell 1–15.

Cavalheiro, G.R., Pollex, T., and Furlong, E.E. (2021). To loop or not to loop: what is the role of TADs in enhancer function and gene regulation? Curr. Opin. Genet. Dev. *67*, 119–129.

Charbin, A., Bouchoux, C., and Uhlmann, F. (2014). Condensin aids sister chromatid decatenation by topoisomerase II. Nucleic Acids Res. *42*, 340–348.

Chen, F., Tillberg, P.W., and Boyden, E.S. (2015). Expansion microscopy. Science (80-.). *347*, 543–548.

Cheng, T.M.K., Heeger, S., Chaleil, R.A.G., Matthews, N., Stewart, A., Wright, J., Lim, C., Bates, P.A., and Uhlmann, F. (2015). A simple biophysical model emulates budding yeast chromosome

condensation. Elife *2015*, 1–22.

Chereji, R. V., Bryson, T.D., and Henikoff, S. (2019). Quantitative MNase-seq accurately maps nucleosome occupancy levels. Genome Biol. *20*, 198.

Chozinski, T.J., Halpern, A.R., Okawa, H., Kim, H.-J.J., Tremel, G.J., Wong, R.O.L.L., and Vaughan, J.C. (2016). Expansion microscopy with conventional antibodies and fluorescent proteins. Nat. Methods *13*, 485–488.

Christensen, M.O., Larsen, M.K., Barthelmes, H.U., Hock, R., Andersen, C.L., Kjeldsen, E., Knudsen, B.R., Westergaard, O., Boege, F., and Mielke, C. (2002). Dynamics of human DNA topoisomerases IIα and IIβ in living cells. J. Cell Biol. *157*, 31–44.

Christophorou, M.A., Castelo-Branco, G., Halley-Stott, R.P., Oliveira, C.S., Loos, R., Radzisheuskaya, A., Mowen, K.A., Bertone, P., Silva, J.C.R., Zernicka-Goetz, M., et al. (2014). Citrullination regulates pluripotency and histone H1 binding to chromatin. Nature *507*, 104–108.

Chu, L., Liang, Z., Mukhina, M., Fisher, J., Vincenten, N., Zhang, Z., Hutchinson, J., Zickler, D., and Kleckner, N. (2020). The 3D Topography of Mitotic Chromosomes. Mol. Cell *79*, 902-916.e6.

Ciosk, R., Zachariae, W., Michaelis, C., Shevchenko, A., Mann, M., and Nasmyth, K.A. (1998). An ESP1/PDS1 Complex Regulates Loss of Sister Chromatid Cohesion at the Metaphase to Anaphase Transition in Yeast. Cell *93*, 1067–1076.

Ciosk, R., Shirayama, M., Shevchenko, A., Tanaka, T., Toth, A., Shevchenko, A., and Nasmyth, K.A. (2000). Cohesin's binding to chromosomes depends on a separate complex consisting of Scc2 and Scc4 proteins. Mol. Cell *5*, 243–254.

Collepardo-Guevara, R., and Schlick, T. (2014). Chromatin fiber polymorphism triggered by variations of DNA linker lengths. Proc. Natl. Acad. Sci. *111*, 8061–8066.

Costantino, L., Hsieh, T.-H.S., Lamothe, R., Darzacq, X., and Koshland, D. (2020). Cohesin residency determines chromatin loop patterns. Elife *9*, 1–31.

Cremer, T., and Cremer, M. (2010). Chromosome territories. Cold Spring Harb. Perspect. Biol. *2*, 1–23.

Crosio, C., Fimia, G.M., Loury, R., Kimura, M., Okano, Y., Zhou, H., Sen, S., Allis, C.D., and Sassone-Corsi, P. (2002). Mitotic phosphorylation of histone H3: spatio-temporal regulation by mammalian Aurora kinases. Mol. Cell. Biol. *22*, 874–885.

Cutts, E.E., and Vannini, A. (2020). Condensin complexes: understanding loop extrusion one conformational change at a time. Biochem. Soc. Trans. *48*, 2089–2100.

Cuvier, O., and Hirano, T. (2003). A role of topoisomerase II in linking DNA replication to chromosome condensation. J. Cell Biol. *160*, 645–655.

Cuylen-Haering, S., Metz, J., and Haering, C.H. (2011). Condensin structures chromosomal DNA through topological links. Nat. Struct. Mol. Biol. *18*, 894–901.

Cuylen, S., Blaukopf, C., Politi, A.Z., Müller-Reichert, T., Neumann, B., Poser, I., Ellenberg, J., Hyman, A.A., and Gerlich, D.W. (2016). Ki-67 acts as a biological surfactant to disperse mitotic chromosomes. Nature *535*, 308–312.

Dai, J., Sultan, S., Taylor, S.S., and Higgins, J.M.G. (2005). The kinase haspin is required for mitotic histone H3 Thr 3 phosphorylation and normal metaphase chromosome alignment. Genes Dev. *19*, 472–488.

Dasso, M., Dimitrov, S., and Wolffe, A.P. (1994). Nuclear assembly is independent of linker histones. Proc. Natl. Acad. Sci. U. S. A. *91*, 12477–12481.

Datta, S., Lecomte, L., and Haering, C.H. (2020). Structural insights into DNA loop extrusion by SMC protein complexes. Curr. Opin. Struct. Biol. *65*, 102–109.

Daum, J.R., Potapova, T.A., Sivakumar, S., Daniel, J.J., Flynn, J.N., Rankin, S., and Gorbsky, G.J. (2011). Cohesion fatigue induces chromatid separation in cells delayed at metaphase. Curr. Biol. *21*, 1018–1024.

Davidson, I.F., Bauer, B., Goetz, D., Tang, W., Wutz, G., and Peters, J. (2019). DNA loop extrusion by human cohesin. Science (80-.). *366*, 1338–1345.

Dekker, J., and Heard, E. (2015). Structural and functional diversity of Topologically Associating Domains. FEBS Lett. *589*, 2877–2884.

Dekker, J., Rippe, K., Dekker, M., and Kleckner, N. (2002). Capturing chromosome conformation. Science *295*, 1306–1311.

Desai, A., Murray, A.W., Mitchison, T., and Walczak, C.E. (1998). Chapter 20 The Use of Xenopus Egg Extracts to Study Mitotic Spindle Assembly and Function in Vitro. Methods Cell Biol. *61*, 385–412.

Dixon, J.R., Selvaraj, S., Yue, F., Kim, A., Li, Y., Shen, Y., Hu, M., Liu, J.S., and Ren, B. (2012). Topological domains in mammalian genomes identified by analysis of chromatin interactions. Nature *485*, 376–380.

Dorigo, B., Schalch, T., Kulangara, A., Duda, S., Schroeder, R.R., and Richmond, T.J. (2004). Nucleosome arrays reveal the two-start organization of the chromatin fiber. Science *306*, 1571–1573.

Dou, Y., Bowen, J., Liu, Y., and Gorovsky, M.A. (2002). Phosphorylation and an ATP-dependent process increase the dynamic exchange of H1 in chromatin. J. Cell Biol. *158*, 1161–1170.

Downs, J.A., Kosmidou, E., Morgan, A., and Jackson, S.P. (2003). Suppression of homologous recombination by the Saccharomyces cerevisiae linker histone. Mol. Cell *11*, 1685–1692.

Du, Z., Zheng, H., Huang, B., Ma, R., Wu, J., Zhang, X., He, J., Xiang, Y., Wang, Q., Li, Y., et al. (2017). Allelic reprogramming of 3D chromatin architecture during early mammalian development. Nature *547*, 232–235.

Duan, Z., Andronescu, M., Schutz, K., McIlwain, S., Kim, Y.J., Lee, C., Shendure, J., Fields, S., Blau, C.A., and Noble, W.S. (2010). A three-dimensional model of the yeast genome. Nature *465*, 363–367.

Dworkin-Rastl, E., Kandolf, H., and Smith, R.C. (1994). The maternal histone H1 variant, H1M (B4

protein), is the predominant H1 histone in Xenopus pregastrula embryos. Dev. Biol. *161*, 425–439.

Dyson, S., Segura, J., Martínez-García, B., Valdés, A., and Roca, J. (2020). Condensin minimizes topoisomerase II-mediated entanglements of DNA in vivo. EMBO J. 1–14.

Earnshaw, W.C., and Laemmli, U.K. (1983). Architecture of metaphase chromosomes and chromosome scaffolds. J. Cell Biol. *96*, 84–93.

Eeftens, J.M., Bisht, S., Kerssemakers, J., Kschonsak, M., Haering, C.H., and Dekker, C. (2017). Real-time detection of condensin-driven DNA compaction reveals a multistep binding mechanism. EMBO J. e201797596.

Elbatsh, A.M.O., Kim, E., Eeftens, J.M., Raaijmakers, J.A., van der Weide, R.H., García-Nieto, A., Bravo, S., Ganji, M., uit de Bos, J., Teunissen, H., et al. (2019). Distinct Roles for Condensin's Two ATPase Sites in Chromosome Condensation. Mol. Cell *76*, 724-737.e5.

Eltsov, M., MacLellan, K.M., Maeshima, K., Frangakis, A.S., and Dubochet, J. (2008). Analysis of cryo-electron microscopy images does not support the existence of 30-nm chromatin fibers in mitotic chromosomes in situ. Proc. Natl. Acad. Sci. *105*, 19732–19737.

Engineering, C., and Street, P. (2006). Calibration of a wide-field frequency-domain fluorescence lifetime microscopy system using light emitting diodes as light sources. *224*, 166–180.

Erdel, F., Rademacher, A., Vlijm, R., Herten, D., Frank, L., and Weinmann, R. (2020). Mouse Heterochromatin Adopts Digital Compaction States without Showing Hallmarks of HP1-Driven Liquid-Liquid Phase Separation Article Mouse Heterochromatin Adopts Digital Compaction States without Showing Hallmarks of HP1-Driven Liquid-Liquid Phase Separa. 1–14.

Falk, M., Feodorova, Y., Naumova, N., Imakaev, M., Lajoie, B.R., Leonhardt, H., Joffe, B., Dekker, J., Fudenberg, G., Solovei, I., et al. (2019). Heterochromatin drives compartmentalization of inverted and conventional nuclei. Nature *570*, 395–399.

Fan, Y., Nikitina, T., Morin-Kensicki, E.M., Zhao, J., Magnuson, T.R., Woodcock, C.L., and Skoultchi, A.I. (2003). H1 Linker Histones Are Essential for Mouse Development and Affect

Nucleosome Spacing In Vivo. Mol. Cell. Biol. *23*, 4559–4572.

Fan, Y., Nikitina, T., Zhao, J., Fleury, T.J., Bhattacharyya, R., Bouhassira, E.E., Stein, A., Woodcock, C.L., and Skoultchi, A.I. (2005). Histone H1 depletion in mammals alters global chromatin structure but causes specific changes in gene regulation. Cell *123*, 1199–1212.

Fang, H., Clark, D.J., and Hayes, J.J. (2012). DNA and nucleosomes direct distinct folding of a linker histone H1 C-terminal domain. Nucleic Acids Res. *40*, 1475–1484.

Farcas, A., Uluocak, P., Helmhart, W., and Nasmyth, K.A. (2011). Cohesin's concatenation of sister DNAs maintains their intertwining. Mol. Cell *44*, 97–107.

Farr, C.J., Antoniou-Kourounioti, M., Mimmack, M.L., Volkov, A., and Porter, A.C.G. (2014). The α isoform of topoisomerase II is required for hypercompaction of mitotic chromosomes in human cells. Nucleic Acids Res. *42*, 4414–4426.

Finch, J.T., and Klug, A. (1976). Solenoidal model for superstructure in chromatin. Proc. Natl. Acad. Sci. *73*, 1897–1901.

Finn, E.H., Pegoraro, G., Brandão, H.B., Valton, A.-L., Oomen, M.E., Dekker, J., Mirny, L.A., and Misteli, T. (2019). Extensive Heterogeneity and Intrinsic Variation in Spatial Genome Organization. Cell *176*, 1502-1515.e10.

Fischle, W., Boo, S.T., Dormann, H.L., Ueberheide, B.M., Garcia, B.A., Shabanowitz, J., Hunt, D.F., Funabiki, H., and Allis, C.D. (2005). Regulation of HP1-chromatin binding by histone H3 methylation and phosphorylation. Nature *438*, 1116–1122.

Fitz-James, M.H., Tong, P., Pidoux, A.L., Ozadam, H., Yang, L., White, S.A., Dekker, J., and Allshire, R.C. (2020). Large domains of heterochromatin direct the formation of short mitotic chromosome loops. Elife *9*.

Flemming, W. (1882). Zellsubstanz, Kern und Zelltheilung / (Leipzig : F.C.W. Vogel,).

Freedman, B.S., and Heald, R. (2010). Functional comparison of H1 histones in Xenopus reveals

isoform-specific regulation by Cdk1 and RanGTP. Curr. Biol. *20*, 1048–1052.

Fry, C.J., Shogren-Knaak, M.A., and Peterson, C.L. (2004). Histone H3 amino-terminal tail phosphorylation and acetylation: Synergistic or independent transcriptional regulatory marks? Cold Spring Harb. Symp. Quant. Biol. *69*, 219–226.

Fudenberg, G., and Imakaev, M. (2017). FISH-ing for captured contacts: towards reconciling FISH and 3C. Nat. Methods *14*, 673–678.

Fudenberg, G., and Mirny, L.A. (2012). Higher order chromatin structure: bridging physics and biology. Curr. Opin. Genet. Dev. *22*, 115–124.

Fudenberg, G., Imakaev, M., Lu, C., Goloborodko, A., Abdennur, N., and Mirny, L.A. (2016). Formation of Chromosomal Domains by Loop Extrusion. Cell Rep. *15*, 2038–2049.

Funabiki, H. (2019). Correcting aberrant kinetochore microtubule attachments: a hidden regulation of Aurora B on microtubules. Curr. Opin. Cell Biol. *58*, 34–41.

Funabiki, H., and Murray, A.W. (2000). The Xenopus chromokinesin Xkid is essential for metaphase chromosome alignment and must be degraded to allow anaphase chromosome movement. Cell *102*, 411–424.

Funabiki, H., Yamano, H., Kumada, K., Nagao, K., Hunt, T., and Yanagida, M. (1996a). Cut2 proteolysis required for sister-chromatid seperation in fission yeast. Nature *381*, 438–441.

Funabiki, H., Kumada, K., and Yanagida, M. (1996b). Fission yeast Cut1 and Cut2 are essential for sister chromatid separation, concentrate along the metaphase spindle and form large complexes. EMBO J. *15*, 6617–6628.

Furlong, E.E.M., and Levine, M. (2018). Developmental enhancers and chromosome topology. *1345*, 1341–1345.

Furuya, M., Tanaka, M., Teranishi, T., Matsumoto, K., Hosoi, Y., Saeki, K., Ishimoto, H., Minegishi, K., Iritani, A., and Yoshimura, Y. (2007). H1foo is indispensable for meiotic maturation of the mouse

oocyte. J. Reprod. Dev. *53*, 895–902.

Fyodorov, D. V., Zhou, B., Skoultchi, A.I., and Bai, Y. (2018). Emerging roles of linker histones in regulating chromatin structure and function. Nat. Rev. Mol. Cell Biol. *19*, 192–206.

Gallego-Paez, L.M., Tanaka, H., Bando, M., Takahashi, M., Nozaki, N., Nakato, R., Shirahige, K., and Hirota, T. (2014). Smc5/6-mediated regulation of replication progression contributes to chromosome assembly during mitosis in human cells. Mol. Biol. Cell *25*, 302–317.

Gandhi, R., Gillespie, P.J., and Hirano, T. (2006). Human Wapl Is a Cohesin-Binding Protein that Promotes Sister-Chromatid Resolution in Mitotic Prophase. Curr. Biol. *16*, 2406–2417.

Ganji, M., Shaltiel, I.A., Bisht, S., Kim, E., Kalichava, A., Haering, C.H., and Dekker, C. (2018). Real-time imaging of DNA loop extrusion by condensin. Science (80-.). *360*, 102–105.

Gassler, J., Brandão, H.B., Imakaev, M., Flyamer, I.M., Ladstätter, S., Bickmore, W.A., Peters, J.-M., Mirny, L.A., and Tachibana, K. (2017). A mechanism of cohesin-dependent loop extrusion organizes zygotic genome architecture. EMBO J. *36*, 3600–3618.

Gerhart, J., Wu, M., and Kirschner, M. (1984). Cell cycle dynamics of an M-phase-specific cytoplasmic factor in Xenopus laevis oocytes and eggs. J. Cell Biol. *98*, 1247–1255.

Gerlich, D.W., Hirota, T., Koch, B., Peters, J.-M., and Ellenberg, J. (2006). Condensin I stabilizes chromosomes mechanically through a dynamic interaction in live cells. Curr. Biol. *16*, 333–344.

Germond, J.E., Hirt, B., Oudet, P., Gross-Bellark, M., and Chambon, P. (1975). Folding of the DNA double helix in chromatin-like structures from simian virus 40. Proc. Natl. Acad. Sci. *72*, 1843–1847.

Gibcus, J.H., Samejima, K., Goloborodko, A., Samejima, I., Naumova, N., Nuebler, J., Kanemaki, M.T., Xie, L., Paulson, J.R., Earnshaw, W.C., et al. (2018). A pathway for mitotic chromosome formation. Science (80-.). *359*.

Gibson, B.A., Doolittle, L.K., Schneider, M.W.G., Jensen, L.E., Gamarra, N., Henry, L., Gerlich, D.W., Redding, S., and Rosen, M.K. (2019). Organization of Chromatin by Intrinsic and Regulated

Phase Separation. Cell 1–15.

Giet, R., and Glover, D.M. (2001). Drosophila aurora B kinase is required for histone H3 phosphorylation and condensin recruitment during chromosome condensation and to organize the central spindle during cytokinesis. J. Cell Biol. *152*, 669–681.

Gillespie, P.J., Gambus, A., and Blow, J.J. (2012). Preparation and use of Xenopus egg extracts to study DNA replication and chromatin associated proteins. Methods *57*, 203–213.

Giménez-Abián, J.F., Sumara, I., Hirota, T., Hauf, S., Gerlich, D., de la Torre, C., Ellenberg, J., and Peters, J. (2004). Regulation of Sister Chromatid Cohesion between Chromosome Arms. Curr. Biol. *14*, 1187–1193.

Ginzberg, M.B., Kafri, R., and Kirschner, M. (2015a). On being the right (cell) size. Science (80-.). *348*.

Ginzberg, M.B., Kafri, R., and Kirschner, M. (2015b). On being the right (cell) size. Science (80-.). *348*, 1245075–1245075.

Glotzer, M., Murray, A.W., and Kirschner, M.W. (1991). Cyclin is degraded by the ubiquitin pathway. *349*.

Golfier, S., Quail, T., Kimura, H., and Brugués, J. (2020). Cohesin and condensin extrude DNA loops in a cell-cycle dependent manner. Elife *9*.

Goloborodko, A., Marko, J.F., and Mirny, L.A. (2016a). Chromosome Compaction by Active Loop Extrusion. Biophys. J. *110*, 2162–2168.

Goloborodko, A., Imakaev, M. V., Marko, J.F., and Mirny, L.A. (2016b). Compaction and segregation of sister chromatids via active loop extrusion. Elife *5*, 1–16.

Goundaroulis, D., Lieberman Aiden, E., and Stasiak, A. (2020). Chromatin Is Frequently Unknotted at the Megabase Scale. Biophys. J. *118*, 2268–2279.

Green, L.C., Kalitsis, P., Chang, T.M., Cipetic, M., Kim, J.H., Marshall, O., Turnbull, L., Whitchurch,

C.B., Vagnarelli, P., Samejima, K., et al. (2012). Contrasting roles of condensin I and condensin II in mitotic chromosome formation. J. Cell Sci. *125*, 1591–1604.

Grigoryev, S.A., Bascom, G., Buckwalter, J.M., Schubert, M.B., Woodcock, C.L., and Schlick, T. (2016). Hierarchical looping of zigzag nucleosome chains in metaphase chromosomes. Proc. Natl. Acad. Sci. *113*, 1238–1243.

Gruhn, J.R., Zielinska, A.P., Shukla, V., Blanshard, R., Capalbo, A., Cimadomo, D., Nikiforov, D., Chan, A.C.-H., Newnham, L.J., Vogel, I., et al. (2019). Chromosome errors in human eggs shape natural fertility over reproductive life span. Science (80-.). *365*, 1466–1469.

Guacci, V., Hogan, E., and Koshland, D. (1994). Chromosome condensation and sister chromatid pairing in budding yeast. J. Cell Biol. *125*, 517–530.

Guacci, V., Koshland, D., and Strunnikov, A. (1997). A direct link between sister chromatid cohesion and chromosome condensation revealed through the analysis of MCD1 in S. cerevisiae. Cell *91*, 47–57.

Guse, A., Carroll, C.W., Moree, B., Fuller, C.J., and Straight, A.F. (2011). In vitro centromere and kinetochore assembly on defined chromatin templates. Nature *477*, 354–358.

Gutierrez-Escribano, P., Newton, M.D., Llauró, A., Huber, J., Tanasie, L., Davy, J., Aly, I., Aramayo, R., Montoya, A., Kramer, H., et al. (2019). A conserved ATP- and Scc2/4-dependent activity for cohesin in tethering DNA molecules. Sci. Adv. *5*, eaay6804.

Gutierrez-Escribano, P., Hormeño, S., Madariaga-Marcos, J., Solé-Soler, R., O'Reilly, F.J., Morris, K., Aicart-Ramos, C., Aramayo, R., Montoya, A., Kramer, H., et al. (2020). Purified Smc5/6 Complex Exhibits DNA Substrate Recognition and Compaction. Mol. Cell *80*, 1039-1054.e6.

Gutierrez, N., Gallego, E., Papadopoulou, T., Vandoermel-Pournin, S., Dubois, A., Tachtsidi, A., Navarro, P., Owens, N., Cohen-Tannoudji, M., Festuccia, N., et al. (2019). Transcription factor activity and nucleosome organization in mitosis. Genome Res. *29*, 250–260.

Haering, C.H., Löwe, J., Hochwagen, A., and Nasmyth, K. (2002). Molecular architecture of SMC

proteins and the yeast cohesin complex. Mol. Cell *9*, 773–788.

Hansen, A.S., Hsieh, T.-H.S., Cattoglio, C., Pustova, I., Saldaña-Meyer, R., Reinberg, D., Darzacq, X., and Tjian, R. (2019). Distinct Classes of Chromatin Loops Revealed by Deletion of an RNA-Binding Region in CTCF. Mol. Cell *76*, 395-411.e13.

Hara, K., Tydeman, P., and Kirschner, M. (1980). A cytoplasmic clock with the same period as the division cycle in Xenopus eggs. Proc. Natl. Acad. Sci. U. S. A. *77*, 462–466.

Hara, K., Zheng, G., Qu, Q., Liu, H., Ouyang, Z., Chen, Z., Tomchick, D.R., and Yu, H. (2014). Structure of cohesin subcomplex pinpoints direct shugoshin-Wapl antagonism in centromeric cohesion. Nat. Struct. Mol. Biol. *21*, 864–870.

Hartl, T.A., Smith, H.F., and Bosco, G. (2008). Chromosome Alignment and Transvection Are Antagonized by Condensin II. Science (80-.). *322*, 1384–1387.

Hassler, M., Shaltiel, I.A., and Haering, C.H. (2018). Towards a Unified Model of SMC Complex Function. Curr. Biol. *28*, R1266–R1281.

Hayakawa, K., Ohgane, J., Tanaka, S., Yagi, S., and Shiota, K. (2012). Oocyte-specific linker histone H1foo is an epigenomic modulator that decondenses chromatin and impairs pluripotency. Epigenetics *7*, 1029–1036.

Heald, R., Tournebize, R., Blank, T., Sandaltzopoulos, R., Becker, P., Hyman, A., and Karsenti, E. (1996). Self-organization of microtubules into bipolar spindles around artificial chromosomes in Xenopus egg extracts. Nature *382*, 420–425.

Healton, S.E., Pinto, H.D., Mishra, L.N., Hamilton, G.A., Hamilton, G.A., Wheat, J.C., Swist-Rosowska, K., Shukeir, N., Dou, Y., Steidl, U., et al. (2020). H1 linker histones silence repetitive elements by promoting both histone H3K9 methylation and chromatin compaction. Proc. Natl. Acad. Sci. U. S. A. *117*, 14251–14258.

Heintzman, D.R., Campos, L. V., Byl, J.A.W., Osheroff, N., and Dewar, J.M. (2019). Topoisomerase II Is Crucial for Fork Convergence during Vertebrate Replication Termination. Cell Rep. *29*, 422-

436.e5.

Hendzel, M.J., Lever, M.A., Crawford, E., and Th'Ng, J.P.H. (2004). The C-terminal Domain Is the Primary Determinant of Histone H1 Binding to Chromatin in Vivo. J. Biol. Chem. *279*, 20028–20034.

Hergeth, S.P., and Schneider, R. (2015). The H1 linker histones: multifunctional proteins beyond the nucleosomal core particle. EMBO Rep. *16*, 1439–1453.

Herrera, J.E., West, K.L., Schiltz, R.L., Nakatani, Y., and Bustin, M. (2002). Histone H1 Is a Specific Repressor of Core Histone Acetylation in Chromatin. Mol. Cell. Biol. *20*, 523–529.

Hildebrand, E.M., and Dekker, J. (2020). Mechanisms and Functions of Chromosome Compartmentalization. Trends Biochem. Sci. *45*, 385–396.

Hirano, T. (2014). Condensins and the evolution of torsion-mediated genome organization. Trends Cell Biol. *24*, 727–733.

Hirano, T. (2016). Condensin-Based Chromosome Organization from Bacteria to Vertebrates. Cell *164*, 847–857.

Hirano, T., and Mitchison, T.J. (1991). Cell cycle control of higher-order chromatin assembly around naked DNA in vitro. J. Cell Biol. *115*, 1479–1489.

Hirano, T., and Mitchison, T.J. (1994). A heterodimeric coiled-coil protein required for mitotic chromosome condensation in vitro. Cell *79*, 449–458.

Hirota, T., Gerlich, D.W., Koch, B., Ellenberg, J., and Peters, J.-M. (2004). Distinct functions of condensin I and II in mitotic chromosome assembly. J. Cell Sci. *117*, 6435–6445.

Holloway, S.L., Glotzer, M., King, R.W., and Murray, A.W. (1993). Anaphase is initiated by proteolysis rather than by the inactivation of maturation-promoting factor. Cell *73*, 1393–1402.

Hoogenboom, W.S., Klein Douwel, D., and Knipscheer, P. (2017). Xenopus egg extract: A powerful tool to study genome maintenance mechanisms. Dev. Biol. *428*, 300–309.

Hopfner, K.P., Karcher, A., Shin, D.S., Craig, L., Arthur, L.M., Carney, J.P., and Tainer, J.A. (2000).

Structural biology of Rad50 ATPase: ATP-driven conformational control in DNA double-strand break repair and the ABC-ATPase superfamily. Cell *101*, 789–800.

Houlard, M., Godwin, J., Metson, J., Lee, J., Hirano, T., and Nasmyth, K.A. (2015). Condensin confers the longitudinal rigidity of chromosomes. Nat. Cell Biol. *17*, 771–781.

Hoyt, M.A., Totis, L., and Roberts, B.T. (1991). S. cerevisiae genes required for cell cycle arrest in response to loss of microtubule function. Cell *66*, 507–517.

Hsieh, T.-H.S., Weiner, A., Dekker, J., Friedman, N., Oliver, J., Lajoie, B., Rando, O.J., Dekker, J., Friedman, N., Rando, O.J., et al. (2015). Mapping Nucleosome Resolution Chromosome Folding in Yeast by Micro-C. Cell *162*, 108–119.

Hsieh, T.-H.S., Fudenberg, G., Goloborodko, A., and Rando, O.J. (2016). Micro-C XL: Assaying chromosome conformation from the nucleosome to the entire genome. Nat. Methods *13*, 1009–1011.

Hsieh, T.-H.S., Cattoglio, C., Slobodyanyuk, E., Hansen, A.S., Rando, O.J., Tjian, R., and Darzacq, X. (2020). Resolving the 3D Landscape of Transcription-Linked Mammalian Chromatin Folding. Mol. Cell *78*, 539-553.e8.

Hsu, J.Y., Sun, Z.W., Li, X., Reuben, M., Tatchell, K., Bishop, D.K., Grushcow, J.M., Brame, C.J., Caldwell, J.A., Hunt, D.F., et al. (2000). Mitotic phosphorylation of histone H3 is governed by Ipl1/aurora kinase and Glc7/PP1 phosphatase in budding yeast and nematodes. Cell *102*, 279–291.

Hug, C.B., Grimaldi, A.G., Kruse, K., and Vaquerizas, J.M. (2017). Chromatin Architecture Emerges during Zygotic Genome Activation Independent of Transcription. Cell *169*, 216-228.e19.

Imakaev, M., Fudenberg, G., McCord, R.P., Naumova, N., Goloborodko, A., Lajoie, B.R., Dekker, J., and Mirny, L.A. (2012). Iterative correction of Hi-C data reveals hallmarks of chromosome organization. Nat. Methods *9*, 999–1003.

Imakaev, M. V., Fudenberg, G., and Mirny, L.A. (2015). Modeling chromosomes: Beyond pretty pictures. FEBS Lett. *589*, 3031–3036.

International Human Genome Sequencing Consortium (2004). Finishing the euchromatic sequence of the human genome. Nature *431*, 931–945.

Iwasaki, Y.W., Murano, K., Ishizu, H., Shibuya, A., Iyoda, Y., Siomi, M.C., Siomi, H., and Saito, K. (2016). Piwi Modulates Chromatin Accessibility by Regulating Multiple Factors Including Histone H1 to Repress Transposons. Mol. Cell *63*, 408–419.

Izzo, A., and Schneider, R. (2016). The role of linker histone H1 modifications in the regulation of gene expression and chromatin dynamics. Biochim. Biophys. Acta - Gene Regul. Mech. *1859*, 486–495.

Izzo, A., Kamieniarz, K., and Schneider, R. (2008). The histone H1 family: Specific members, specific functions? Biol. Chem. *389*, 333–343.

Izzo, A., Kamieniarz-Gdula, K., Ramírez, F., Noureen, N., Kind, J., Manke, T., vanSteensel, B., and Schneider, R. (2013). The Genomic Landscape of the Somatic Linker Histone Subtypes H1.1 to H1.5 in Human Cells. Cell Rep. *3*, 2142–2154.

Izzo, A., Ziegler-Birling, C., Hill, P.W.S., Brondani, L., Hajkova, P., Torres-Padilla, M.-E., and Schneider, R. (2017). Dynamic changes in H1 subtype composition during epigenetic reprogramming. J. Cell Biol. *216*, 3017–3028.

Jans, J., Gladden, J.M., Ralston, E.J., Pickle, C.S., Michel, A.H., Pferdehirt, R.R., Eisen, M.B., and Meyer, B.J. (2009). A condensin-like dosage compensation complex acts at a distance to control expression throughout the genome. Genes Dev. *23*, 602–618.

Jenness, C., Giunta, S., Müller, M.M., Kimura, H., Muir, T.W., and Funabiki, H. (2018). HELLS and CDCA7 comprise a bipartite nucleosome remodeling complex defective in ICF syndrome. Proc. Natl. Acad. Sci. 201717509.

Jeppsson, K., Carlborg, K.K., Nakato, R., Berta, D.G., Lilienthal, I., Kanno, T., Lindqvist, A., Brink, M.C., Dantuma, N.P., Katou, Y., et al. (2014). The Chromosomal Association of the Smc5/6 Complex Depends on Cohesion and Predicts the Level of Sister Chromatid Entanglement. PLoS Genet. *10*.

Jiang, C., and Pugh, B.F. (2009). Nucleosome positioning and gene regulation: Advances through genomics. Nat. Rev. Genet. *10*, 161–172.

Kakui, Y., Rabinowitz, A., Barry, D.J., and Uhlmann, F. (2017). Condensin-mediated remodeling of the mitotic chromatin landscape in fission yeast. Nat. Genet. *49*, 1553–1557.

Kanaar, R., and Wyman, C. (2008). DNA Repair by the MRN Complex: Break It to Make It. Cell *135*, 14–16.

Ke, Y., Xu, Y., Chen, X., Feng, S., Liu, Z., Sun, Y., Yao, X., Li, F., Zhu, W., Gao, L., et al. (2017). 3D Chromatin Structures of Mature Gametes and Structural Reprogramming during Mammalian Embryogenesis. Cell *170*, 367-381.e20.

Kerpedjiev, P., Abdennur, N., Lekschas, F., McCallum, C., Dinkla, K., Strobelt, H., Luber, J.M., Ouellette, S.B., Azhir, A., Kumar, N., et al. (2018). HiGlass: web-based visual exploration and analysis of genome interaction maps. Genome Biol. *19*, 125.

Kieserman, E.K., and Heald, R. (2011). Mitotic chromosome size scaling in Xenopus. Cell Cycle *10*, 3863–3870.

Kim, H., and Loparo, J.J. (2016). Multistep assembly of DNA condensation clusters by SMC. Nat. Commun. *7*, 10200.

Kim, E., Kerssemakers, J., Shaltiel, I.A., Haering, C.H., and Dekker, C. (2020). DNA-loop extruding condensin complexes can traverse one another. Nature.

Kim, J.H., Zhang, T., Wong, N.C., Davidson, N., Maksimovic, J., Oshlack, A., Earnshaw, W.C., Kalitsis, P., and Hudson, D.F. (2013). Condensin i associates with structural and gene regulatory regions in vertebrate chromosomes. Nat. Commun. *4*, 1–14.

Kim, K.-D.D., Tanizawa, H., Iwasaki, O., and Noma, K.I. (2016). Transcription factors mediate condensin recruitment and global chromosomal organization in fission yeast. Nat. Genet. *48*, 1242–1252.

Kim, Y., Shi, Z., Zhang, H., Finkelstein, I.J., and Yu, H. (2019). Human cohesin compacts DNA by loop extrusion. Science (80-.). *366*, 1345–1349.

Kimura, H., and Cook, P.R. (2001). Kinetics of core histones in living human cells: little exchange of H3 and H4 and some rapid exchange of H2B. J. Cell Biol. *153*, 1341–1353.

Kimura, K., and Hirano, T. (1997). ATP-Dependent Positive Supercoiling of DNA by 13S Condensin: A Biochemical Implication for Chromosome Condensation. Cell *90*, 625–634.

Kimura, K., Rybenkov, V. V., Crisona, N.J., Hirano, T., and Cozzarelli, N.R. (1999). 13S condensin actively reconfigures DNA by introducing global positive writhe: Implications for chromosome condensation. Cell *98*, 239–248.

Kimura, K., Cuvier, O., and Hirano, T. (2001). Chromosome Condensation by a Human Condensin Complex in Xenopus Egg Extracts. J. Biol. Chem. *276*, 5417–5420.

Kireeva, N., Lakonishok, M., Kireev, I., Hirano, T., and Belmont, A.S. (2004). Visualization of early chromosome condensation: A hierarchical folding, axial glue model of chromosome structure. J. Cell Biol. *166*, 775–785.

Kitajima, T.S., Sakuno, T., Ishiguro, K.I., Iemura, S.I., Natsume, T., Kawashima, S.A., and Watanabe, Y. (2006). Shugoshin collaborates with protein phosphatase 2A to protect cohesin. Nature *441*, 46–52.

Kong, M., Cutts, E.E., Pan, D., Beuron, F., Kaliyappan, T., Xue, C., Morris, E.P., Musacchio, A., Vannini, A., and Greene, E.C. (2020). Human Condensin I and II Drive Extensive ATP-Dependent Compaction of Nucleosome-Bound DNA. Mol. Cell 683540.

Konishi, A., Shimizu, S., Hirota, J., Takao, T., Fan, Y., Matsuoka, Y., Zhang, L., Yoneda, Y., Fujii, Y., Skoultchi, A.I., et al. (2003). Involvement of histone H1.2 in apoptosis induced by DNA double-strand breaks. Cell *114*, 673–688.

Krasnow, M.A., and Cozzarelli, N.R. (1982). Catenation of DNA rings by topoisomerases. Mechanism of control by spermidine. J. Biol. Chem. *257*, 2687–2693.

Krietenstein, N., Abraham, S., Venev, S. V., Abdennur, N., Gibcus, J.H., Hsieh, T.-H.S., Parsi, K.M., Yang, L., Maehr, R., Mirny, L.A., et al. (2020). Ultrastructural Details of Mammalian Chromosome Architecture. Mol. Cell *78*, 554-565.e7.

Krishnan, S., Smits, A.H., Vermeulen, M., and Reinberg, D. (2017). Phospho-H1 Decorates the Inter-chromatid Axis and Is Evicted along with Shugoshin by SET during Mitosis. Mol. Cell *67*, 579-593.e6.

Kruhlak, M.J., Hendzel, M.J., Fischle, W., Bertos, N.R., Hameed, S., Yang, X.J., Verdin, E., and Bazett-Jones, D.P. (2001). Regulation of Global Acetylation in Mitosis through Loss of Histone Acetyltransferases and Deacetylases from Chromatin. J. Biol. Chem. *276*, 38307–38319.

Kschonsak, M., and Haering, C.H. (2015). Shaping mitotic chromosomes: From classical concepts to molecular mechanisms. BioEssays *37*, 755–766.

Kschonsak, M., Merkel, F., Bisht, S., Metz, J., Rybin, V., Hassler, M., and Haering, C.H. (2017). Structural Basis for a Safety-Belt Mechanism That Anchors Condensin to Chromosomes. Cell *171*, 588-600.e24.

Kurumizaka, H., Kujirai, T., and Takizawa, Y. (2020). Contributions of Histone Variants in Nucleosome Structure and Function. J. Mol. Biol. *433*, 166678.

Kuwada, Y. (1939). Chromosome Structure A critical review. Cytologia (Tokyo). *10*, 213–256.

Ladouceur, A.-M., Dorn, J.F., and Maddox, P.S. (2015). Mitotic chromosome length scales in response to both cell and nuclear size. J. Cell Biol. *209*, 645–652.

Laemmli, U.K., Cheng, S.M., Adolph, K.W., Paulson, J.R., Brown, J.A., and Baumbach, W.R. (1978). Metaphase Chromosome Structure: The Role of Nonhistone Proteins. Cold Spring Harb. Symp. Quant. Biol. *42*, 351–360.

Lafont, A.L., Song, J., and Rankin, S. (2010). Sororin cooperates with the acetyltransferase Eco2 to ensure DNA replication-dependent sister chromatid cohesion. Proc. Natl. Acad. Sci. U. S. A. *107*, 20364–20369.

Lakowicz, J.R. (2006). Principles of fluorescence spectroscopy (Springer).

Lane, A.B., Giménez-Abián, J.F., and Clarke, D.J. (2013). A novel chromatin tether domain controls topoisomerase IIα dynamics and mitotic chromosome formation. J. Cell Biol. *203*, 471–486.

Larionov, V.L., Karpova, T.S., Kouprina, N.Y., and Jouravleva, G.A. (1985). A mutant of Saccharomyces cerevisiae with impaired maintenance of centromeric plasmids. Curr. Genet. *10*, 15–20.

Larson, A.G., Elnatan, D., Keenen, M.M., Trnka, M.J., Johnston, J.B., Burlingame, A.L., Agard, D.A., Redding, S., and Narlikar, G.J. (2017). Liquid droplet formation by HP1α suggests a role for phase separation in heterochromatin. Nature *547*, 236–240.

Laskey, R.A., Mills, A.D., and Morris, N.R. (1977). Assembly of SV40 chromatin in a cell-free system from Xenopus eggs. Cell *10*, 237–243.

Lavoie, B.D., Tuffo, K.M., Oh, S., Koshland, D., and Holm, C. (2000). Mitotic chromosome condensation requires Brn1p, the yeast homologue of Barren. Mol. Biol. Cell *11*, 1293–1304.

Lavoie, B.D., Hogan, E., and Koshland, D. (2004). In vivo requirements for rDNA chromosome condensation reveal two cell-cycle-regulated pathways for mitotic chromosome folding. Genes Dev. *18*, 76–87.

Le, T.B.K., Imakaev, M. V, Mirny, L.A., and Laub, M.T. (2013). High-Resolution Mapping of the Spatial Organization of a Bacterial Chromosome. Science (80-.). *342*, 731–734.

Ledesma, F.C., El Khamisy, S.F., Zuma, M.C., Osborn, K., and Caldecott, K.W. (2009). A human 5′-tyrosyl DNA phosphodiesterase that repairs topoisomerase-mediated DNA damage. Nature *461*, 674–678.

Lee, W., Tillo, D., Bray, N., Morse, R.H., Davis, R.W., Hughes, T.R., and Nislow, C. (2007). A high-resolution atlas of nucleosome occupancy in yeast. Nat. Genet. *39*, 1235–1244.

Lengronne, A., Katou, Y., Mori, S., Yokabayashi, S., Kelly, G.P., Ito, T., Watanabe, Y., Shirahige,

K., and Uhlmann, F. (2004). Cohesin relocation from sites of chromosomal loading to places of convergent transcription. Nature *430*, 573–578.

Leonard, J., Sen, N., Torres, R., Sutani, T., Jarmuz, A., Shirahige, K., and Aragón, L. (2015). Condensin Relocalization from Centromeres to Chromosome Arms Promotes Top2 Recruitment during Anaphase. Cell Rep. *13*, 2336–2344.

Li, G., Levitus, M., Bustamante, C., and Widom, J. (2005). Rapid spontaneous accessibility of nucleosomal DNA. Nat. Struct. Mol. Biol. *12*, 46–53.

Li, L., Lyu, X., Hou, C., Takenaka, N., Nguyen, H.Q., Ong, C.-T., Cubeñas-Potts, C., Hu, M., Lei, E.P., Bosco, G., et al. (2015). Widespread Rearrangement of 3D Chromatin Organization Underlies Polycomb-Mediated Stress-Induced Silencing. Mol. Cell *58*, 216–231.

Li, W., Chen, P., Yu, J., Dong, L., Liang, D., Feng, J., Yan, J., Wang, P.Y., Li, Q., Zhang, Z., et al. (2016). FACT Remodels the Tetranucleosomal Unit of Chromatin Fibers for Gene Transcription. Mol. Cell *64*, 120–133.

Li, Y., Haarhuis, J.H.I., Sedeño Cacciatore, Á., Oldenkamp, R., van Ruiten, M.S., Willems, L., Teunissen, H., Muir, K.W., de Wit, E., Rowland, B.D., et al. (2020). The structural basis for cohesin–CTCF-anchored loops. Nature *578*, 472–476.

Lieberman-Aiden, E., van Berkum, N.L., Williams, L., Imakaev, M., Ragoczy, T., Telling, A., Amit, I., Lajoie, B.R., Sabo, P.J., Dorschner, M.O., et al. (2009). Comprehensive Mapping of Long-Range Interactions Reveals Folding Principles of the Human Genome. Science (80-.). *326*, 289–293.

Lipp, J.J., Hirota, T., Poser, I., and Peters, J.-M. (2007). Aurora B controls the association of condensin I but not condensin II with mitotic chromosomes. J. Cell Sci. *120*, 1245–1255.

Lister, L.M., Kouznetsova, A., Hyslop, L.A., Kalleas, D., Pace, S.L., Barel, J.C., Nathan, A., Floros, V., Adelfalk, C., Watanabe, Y., et al. (2010). Age-related meiotic segregation errors in mammalian oocytes are preceded by depletion of cohesin and Sgo2. Curr. Biol. *20*, 1511–1521.

Llères, D., James, J., Swift, S., Norman, D.G., and Lamond, A.I. (2009). Quantitative analysis of

chromatin compaction in living cells using FLIM-FRET. J. Cell Biol. *187*, 481–496.

Lohka, M.J., and Masui, Y. (1984). Roles of cytosol and cytoplasmic particles in nuclear envelope assembly and sperm pronuclear formation in cell-free preparations from amphibian eggs. J. Cell Biol. *98*, 1222–1230.

Longworth, M.S., Herr, A., Ji, J.Y., and Dyson, N.J. (2008). RBF1 promotes chromatin condensation through a conserved interaction with the Condensin II protein dCAP-D3. Genes Dev. *22*, 1011–1024.

Losada, A., Hirano, M., and Hirano, T. (1998). Identification of Xenopus SMC protein complexes required for sister chromatid cohesion. Genes Dev. *12*, 1986–1997.

Losada, A., Yokochi, T., Kobayashi, R., and Hirano, T. (2000). Identification and characterization of SA/Scc3p subunits in the Xenopus and human cohesin complexes. J. Cell Biol. *150*, 405–416.

Losada, A., Hirano, M., and Hirano, T. (2002). Cohesin release is required for sister chromatid resolution, but not for condensin-mediated compaction, at the onset of mitosis. Genes Dev. *16*, 3004–3016.

Lowary, P.., and Widom, J. (1997). Nucleosome packaging and nucleosome positioning of genomic DNA. Proc. Natl. Acad. Sci. U. S. A. *94*, 1183–1188.

Lowary, P.., and Widom, J. (1998). New DNA sequence rules for high affinity binding to histone octamer and sequence-directed nucleosome positioning. J. Mol. Biol. *276*, 19–42.

Löwe, J., Cordell, S.C., and Van Den Ent, F. (2001). Crystal structure of the SMC head domain: An ABC ATPase with 900 residues antiparallel coiled-coil inserted. J. Mol. Biol. *306*, 25–35.

Lu, X., Wontakal, S.N., Emelyanov, A. V., Morcillo, P., Konev, A.Y., Fyodorov, D. V., and Skoultchi, A.I. (2009). Linker histone H1 is essential for Drosophila development, the establishment of pericentric heterochromatin, and a normal polytene chromosome structure. Genes Dev. *23*, 452–465.

Lu, X., Wontakal, S.N., Kavi, H., Kim, B.J., Guzzardo, P.M., Emelyanov, A. V., Xu, N., Hannon,

G.J., Zavadil, J., Fyodorov, D. V., et al. (2013). Drosophila H1 Regulates the Genetic Activity of Heterochromatin by Recruitment of Su(var)3-9. Science (80-.). *340*, 78–81.

Luger, K., Mäder, A.W., Richmond, R.K., Sargent, D.F., and Richmond, T.J. (1997). Crystal structure of the nucleosome core particle at 2.8 Å resolution. Nature *389*, 251–260.

Luger, K., Dechassa, M.L., and Tremethick, D.J. (2012). New insights into nucleosome and chromatin structure: an ordered state or a disordered affair? Nat. Rev. Mol. Cell Biol. *13*, 436–447.

MacCallum, D.E., Losada, A., Kobayashi, R., and Hirano, T. (2002). ISWI remodeling complexes in Xenopus egg extracts: identification as major chromosomal components that are regulated by INCENP-aurora B. Mol. Biol. Cell *13*, 25–39.

Machida, S., Takizawa, Y., Ishimaru, M., Sugita, Y., Sekine, S., Nakayama, J. ichi, Wolf, M., and Kurumizaka, H. (2018). Structural Basis of Heterochromatin Formation by Human HP1. Mol. Cell *69*, 385-397.e8.

Maeshima, K., Hihara, S., and Eltsov, M. (2010). Chromatin structure: Does the 30-nm fibre exist in vivo? Curr. Opin. Cell Biol. *22*, 291–297.

Maeshima, K., Matsuda, T., Shindo, Y., Imamura, H., Tamura, S., Imai, R., Kawakami, S., Nagashima, R., Soga, T., Noji, H., et al. (2018). A Transient Rise in Free Mg2+Ions Released from ATP-Mg Hydrolysis Contributes to Mitotic Chromosome Condensation. Curr. Biol. *28*, 444-451.e6.

Manuelidis, L. (1985). Individual interphase chromosome domains revealed by in situ hybridization. Hum. Genet. *71*, 288–293.

Mara, L., Paim, G., and Fitzharris, G. (2019). Cell-Size-Independent Spindle Checkpoint Failure Underlies Chromosome Segregation Error in Mouse Report Cell-Size-Independent Spindle Checkpoint Failure Underlies Chromosome Segregation Error. 865–873.

Maresca, T.J., Freedman, B.S., and Heald, R. (2005). Histone H1 is essential for mitotic chromosome architecture and segregation in Xenopus laevis egg extracts. J. Cell Biol. *169*, 859–869.

Marini, J.C., Miller, K.G., and Englund, P.T. (1980). Decatenation of kinetoplast DNA by topoisomerases. J. Biol. Chem. *255*, 4976–4979.

Marko, J.F. (2008). Micromechanical studies of mitotic chromosomes. Chromosom. Res. *16*, 469–497.

Marko, J.F., Rios, P.D.L., Barducci, A., and Gruber, S. (2019). DNA-segment-capture model for loop extrusion by structural maintenance of chromosome (SMC) protein. *47*, 6956–6972.

Marshall, W.., Straight, A., Marko, J.F., Swedlow, J., Dernburg, A., Belmont, A., Murray, A.W., Agard, D.., and Sedat, J.. (1997). Interphase chromosomes undergo constrained diffusional motion in living cells. Curr. Biol. *7*, 930–939.

Mateescu, B., England, P., Halgand, F., Yaniv, M., and Muchardt, C. (2004). Tethering of HP1 proteins to chromatin is relieved by phospoacetylation of histone H3. EMBO Rep. *5*, 490–496.

Mateo, L.J., Murphy, S.E., Hafner, A., Cinquini, I.S., Walker, C.A., and Boettiger, A.N. (2019). Visualizing DNA folding and RNA in embryos at single-cell resolution. Nature *568*, 49–54.

Matsubara, K., Sano, N., Umehara, T., and Horikoshi, M. (2007). Global analysis of functional surfaces of core histones with comprehensive point mutants. Genes to Cells *12*, 13–33.

McCord, R.P., Kaplan, N., and Giorgetti, L. (2020). Chromosome Conformation Capture and Beyond: Toward an Integrative View of Chromosome Structure and Function. Mol. Cell *77*, 688–708.

McGuinness, B.E., Hirota, T., Kudo, N.R., Peters, J., and Nasmyth, K. (2005). Shugoshin Prevents Dissociation of Cohesin from Centromeres During Mitosis in Vertebrate Cells. PLoS Biol. *3*, e86.

Michaelis, C., Ciosk, R., and Nasmyth, K. (1997). Cohesins: chromosomal proteins that prevent premature separation of sister chromatids. Cell *91*, 35–45.

Mimori, T., and Hardin, J.A. (1986). Mechanism of interaction between Ku protein and DNA. J. Biol. Chem. *261*, 10375–10379.

Minshull, J., Sun, H., Tonks, N.K., and Murray, A.W. (1994). A MAP kinase-dependent spindle

assembly checkpoint in Xenopus egg extracts. Cell *79*, 475–486.

Mir, M., Bickmore, W., Furlong, E.E.M., and Narlikar, G. (2019). Chromatin topology, condensates and gene regulation: Shifting paradigms or just a phase? Dev. *146*, 1–6.

Misteli, T., Gunjan, a, Hock, R., Bustin, M., and Brown, D.T. (2000). Dynamic binding of histone H1 to chromatin in living cells. Nature *408*, 877–881.

Mitter, M., Gasser, C., Takacs, Z., Langer, C.C.H., Tang, W., Jessberger, G., Beales, C.T., Neuner, E., Ameres, S.L., Peters, J., et al. (2020). Conformation of sister chromatids in the replicated human genome. Nature *586*, 139–144.

Mizuguchi, T., Fudenberg, G., Mehta, S., Belton, J.M., Taneja, N., Folco, H.D., FitzGerald, P., Dekker, J., Mirny, L.A., Barrowman, J., et al. (2014). Cohesin-dependent globules and heterochromatin shape 3D genome architecture in S. pombe. Nature *516*, 432–435.

Mora-Bermúdez, F., and Ellenberg, J. (2007). Measuring structural dynamics of chromosomes in living cells by fluorescence microscopy. Methods *41*, 158–167.

Mora-Bermúdez, F., Gerlich, D.W., and Ellenberg, J. (2007). Maximal chromosome compaction occurs by axial shortening in anaphase and depends on Aurora kinase. Nat. Cell Biol. *9*, 822–831.

Murnion, M.E., Adams, R.R., Callister, D.M., Allis, C.D., Earnshaw, W.C., and Swedlow, J.R. (2001). Chromatin-associated Protein Phosphatase I Regulates Aurora-B and Histone H3 Phosphorylation. J. Biol. Chem. *276*, 26656–26665.

Murray, A.W. (1991). Chapter 30 Cell Cycle Extracts. In Methods in Cell Biology, pp. 581–605.

Nagano, T., Lubling, Y., Stevens, T.J., Schoenfelder, S., Yaffe, E., Dean, W., Laue, E.D., Tanay, A., and Fraser, P. (2013). Single-cell Hi-C reveals cell-to-cell variability in chromosome structure. Nature *502*, 59–64.

Nagasaka, K., Hossain, M.J., Roberti, M.J., Ellenberg, J., and Hirota, T. (2016). Sister chromatid resolution is an intrinsic part of chromosome organization in prophase. Nat. Cell Biol. *18*, 692–699.

Nasim, A., and Smith, B.P. (1975). Genetic control of radiation sensitivity in Schizosaccharomyces pombe. Genetics *79*, 573–582.

Nasmyth, K.A. (2001). Disseminating the Genome: Joining, Resolving, and Separating Sister Chromatids During Mitosis and Meiosis. Annu. Rev. Genet. *35*, 673–745.

Nasmyth, K.A., and Haering, C.H. (2005). THE STRUCTURE AND FUNCTION OF SMC AND KLEISIN COMPLEXES. Annu. Rev. Biochem. *74*, 595–648.

Naumova, N., Imakaev, M., Fudenberg, G., Zhan, Y.Y.Y., Lajoie, B.R., Mirny, L.A., and Dekker, J. (2013). Organization of the Mitotic Chromosome. Science (80-.). *342*, 948–953.

Newport, J., and Kirschner, M. (1982). A major developmental transition in early xenopus embryos: I. characterization and timing of cellular changes at the midblastula stage. Cell *30*, 675–686.

Nielsen, C.F., Zhang, T., Barisic, M., Kalitsis, P., and Hudson, D.F. (2020). Topoisomerase IIa is essential for maintenance of mitotic chromosome structure. Proc. Natl. Acad. Sci. U. S. A. *117*.

Niki, H., Jaffe, A., Imamura, R., Ogura, T., and Hiraga, S. (1991). The new gene mukB codes for a 177 kd protein with coiled-coil domains involved in chromosome partitioning of E. coli. EMBO J. *10*, 183–193.

Nishino, Y., Eltsov, M., Joti, Y., Ito, K., Takata, H., Takahashi, Y., Hihara, S., Frangakis, A.S., Imamoto, N., Ishikawa, T., et al. (2012). Human mitotic chromosomes consist predominantly of irregularly folded nucleosome fibres without a 30-nm chromatin structure. EMBO J. *31*, 1644–1653.

Nora, E.P., Lajoie, B.R., Schulz, E.G., Giorgetti, L., Okamoto, I., Servant, N., Piolot, T., Van Berkum, N.L., Meisig, J., Sedat, J., et al. (2012). Spatial partitioning of the regulatory landscape of the X-inactivation centre. Nature *485*, 381–385.

Nora, E.P., Goloborodko, A., Valton, A., Gibcus, J.H., Uebersohn, A., Abdennur, N., Dekker, J., Mirny, L.A., and Bruneau, B.G. (2017). Targeted Degradation of CTCF Decouples Local Insulation of Chromosome Domains from Genomic Compartmentalization. Cell *169*, 930-944.e22.

Ohsumi, K., Katagiri, C., and Kishimoto, T. (1993). Chromosome condensation in Xenopus mitotic extracts without histone H1. Science (80-.). *262*, 2033–2035.

Ono, T., Losada, A., Hirano, M., Myers, M.P., Neuwald, A.F., and Hirano, T. (2003). Differential contributions of condensin I and condensin II to mitotic chromosome architecture in vertebrate cells. Cell *115*, 109–121.

Ono, T., Fang, Y., Spector, D.L., and Hirano, T. (2004). Spatial and temporal regulation of condensins I and II in mitotic chromosome assembly in human cells. Mol. Biol. Cell *15*, 3296–3308.

Ono, T., Yamashita, D., and Hirano, T. (2013). Condensin II initiates sister chromatid resolution during S phase. J. Cell Biol. *200*, 429–441.

Orlandini, E., Marenduzzo, D., and Michieletto, D. (2019). Synergy of topoisomerase and structural-maintenance-of-chromosomes proteins creates a universal pathway to simplify genome topology. Proc. Natl. Acad. Sci. U. S. A. *116*, 8149–8154.

Osunsade, A., Prescott, N.A., Hebert, J.M., Ray, D.M., Jmeian, Y., Lorenz, I.C., and David, Y. (2019). A Robust Method for the Purification and Characterization of Recombinant Human Histone H1 Variants. Biochemistry *58*, 171–176.

Ou, H.D., Phan, S., Deerinck, T.J., Thor, A., Ellisman, M.H., and O'Shea, C.C. (2017). ChromEMT: Visualizing 3D chromatin structure and compaction in interphase and mitotic cells. Science (80-.). *357*, eaag0025.

Parelho, V., Hadjur, S., Spivakov, M., Leleu, M., Sauer, S., Gregson, H.C., Jarmuz, A., Canzonetta, C., Webster, Z., Nesterova, T., et al. (2008). Cohesins Functionally Associate with CTCF on Mammalian Chromosome Arms. Cell *132*, 422–433.

Passarge, E. (1979). Emil Heitz and the concept of heterochromatin: Longitudinal chromosome differentiation was recognized fifty years ago. Am. J. Hum. Genet. *31*, 106–115.

Patel, L., Kang, R., Rosenberg, S.C., Qiu, Y., Raviram, R., Chee, S., Hu, R., Ren, B., Cole, F., and Corbett, K.D. (2019). Dynamic reorganization of the genome shapes the recombination landscape in

meiotic prophase. Nat. Struct. Mol. Biol. *26*.

Paulson, J.R., and Laemmli, U.K. (1977). The structure of histone-depleted metaphase chromosomes. Cell *12*, 817–828.

Pellicer, J., Fay, M.F., and Leitch, I.J. (2010). The largest eukaryotic genome of them all? Bot. J. Linn. Soc. *164*, 10–15.

Pérez-Montero, S., Carbonell, A., Morán, T., Vaquero, A., and Azorín, F. (2013). The embryonic linker histone H1 variant of Drosophila, dBigH1, regulates zygotic genome activation. Dev. Cell *26*, 578–590.

Perišić, O., Collepardo-Guevara, R., and Schlick, T. (2010). Modeling studies of chromatin fiber structure as a function of DNA linker length. J. Mol. Biol. *403*, 777–802.

Phillips-Cremins, J.E., Sauria, M.E.G., Sanyal, A., Gerasimova, T.I., Lajoie, B.R., Bell, J.S.K., Ong, C.T., Hookway, T.A., Guo, C., Sun, Y., et al. (2013). Architectural protein subclasses shape 3D organization of genomes during lineage commitment. Cell *153*, 1281–1295.

Piskadlo, E., Tavares, A., and Oliveira, R.A. (2017a). Metaphase chromosome structure is dynamically maintained by condensin I-directed DNA (de)catenation. Elife *6*, 1–22.

Piskadlo, E., Tavares, A., and Oliveira, R.A. (2017b). Metaphase chromosome structure is dynamically maintained by condensin I-directed DNA (de)catenation. Elife *6*, 1–22.

Poepsel, S., Kasinath, V., and Nogales, E. (2018). Cryo-EM structures of PRC2 simultaneously engaged with two functionally distinct nucleosomes. Nat. Struct. Mol. Biol. *25*, 154–162.

Poirier, M.G., and Marko, J.F. (2002). Mitotic chromosomes are chromatin networks without a mechanically contiguous protein scaffold. Proc. Natl. Acad. Sci. U. S. A. *99*, 15393–15397.

Pommier, Y., Leo, E., Zhang, H., and Marchand, C. (2010). DNA topoisomerases and their poisoning by anticancer and antibacterial drugs. Chem. Biol. *17*, 421–433.

Poonperm, R., Takata, H., Hamano, T., Matsuda, A., Uchiyama, S., Hiraoka, Y., and Fukui, K.

(2015). Chromosome Scaffold is a Double-Stranded Assembly of Scaffold Proteins. Sci. Rep. *5*, 11916.

Pope, B.D., Ryba, T., Dileep, V., Yue, F., Wu, W., Denas, O., Vera, D.L., Wang, Y., Hansen, R.S., Canfield, T.K., et al. (2014). Topologically associating domains are stable units of replication-timing regulation. Nature *515*, 402–405.

Potapova, T.A., Unruh, J.R., Yu, Z., Rancati, G., Li, H., Stampfer, M.R., and Gerton, J.L. (2019). Superresolution microscopy reveals linkages between ribosomal DNA on heterologous chromosomes. J. Cell Biol. *218*, 2492–2513.

Potts, P.R., and Yu, H. (2005). Human MMS21/NSE2 Is a SUMO Ligase Required for DNA Repair. Mol. Cell. Biol. *25*, 7021–7032.

Potts, P.R., and Yu, H. (2007). The SMC5/6 complex maintains telomere length in ALT cancer cells through SUMOylation of telomere-binding proteins. Nat. Struct. Mol. Biol. *14*, 581–590.

Ramakrishnan, V., Finch, J.T., Graziano, V., Lee, P.L., and Sweet, R.M. (1993). Crystal structure of globular domain of histone H5 and its implications for nucleosome binding. Nature *362*, 219–223.

Rao, S.S.P., Huntley, M.H., Durand, N.C., Stamenova, E.K., Bochkov, I.D., Robinson, J.T., Sanborn, A.L., Machol, I., Omer, A.D., Lander, E.S., et al. (2014). A 3D map of the human genome at kilobase resolution reveals principles of chromatin looping. Cell *159*, 1665–1680.

Rao, S.S.P., Huang, S.C., Glenn St Hilaire, B., Engreitz, J.M., Perez, E.M., Kieffer-Kwon, K.R., Sanborn, A.L., Johnstone, S.E., Bascom, G.D., Bochkov, I.D., et al. (2017). Cohesin Loss Eliminates All Loop Domains. Cell *171*, 305-320.e24.

Redolfi, J., Zhan, Y., Valdes-Quezada, C., Kryzhanovska, M., Guerreiro, I., Iesmantavicius, V., Pollex, T., Grand, R.S., Mulugeta, E., Kind, J., et al. (2019). DamC reveals principles of chromatin folding in vivo without crosslinking and ligation. Nat. Struct. Mol. Biol. *26*, 471–480.

Renshaw, M.J., Ward, J.J., Kanemaki, M., Natsume, K., Nédélec, F.J., and Tanaka, T.U. (2010). Condensins Promote Chromosome Recoiling during Early Anaphase to Complete Sister Chromatid

Separation. Dev. Cell *19*, 232–244.

Ricci, M.A., Manzo, C., Garc??a-Parajo, M.F., Lakadamyali, M., and Cosma, M.P. (2015a). Chromatin fibers are formed by heterogeneous groups of nucleosomes in vivo. Cell *160*, 1145–1158.

Ricci, M.A., Manzo, C., García-Parajo, M.F., Lakadamyali, M., and Cosma, M.P. (2015b). Chromatin fibers are formed by heterogeneous groups of nucleosomes in vivo. Cell *160*, 1145–1158.

Riggs, A.D. (1990). DNA methylation and late replication probably aid cell memory, and type I DNA reeling could aid chromosome folding and enhancer function. Philos. Trans. R. Soc. Lond. B. Biol. Sci. *326*, 285–297.

Risca, V.I., Denny, S.K., Straight, A.F., and Greenleaf, W.J. (2016). Variable chromatin structure revealed by in situ spatially correlated DNA cleavage mapping. Nature *541*, 237–241.

Rosa, A., and Everaers, R. (2008). Structure and dynamics of interphase chromosomes. PLoS Comput. Biol. *4*.

Rosencrance, C.D., Ammouri, H.N., Yu, Q., Ge, T., Rendleman, E.J., Marshall, S.A., and Eagen, K.P. (2020). Chromatin Hyperacetylation Impacts Chromosome Folding by Forming a Nuclear Subcompartment. Mol. Cell *78*, 112-126.e12.

Rosin, L.F., Nguyen, S.C., and Joyce, E.F. (2018). Condensin II drives large-scale folding and spatial partitioning of interphase chromosomes in Drosophila nuclei. PLoS Genet. *14*, 1–26.

Rosin, L.F., Crocker, O., Isenhart, R.L., Nguyen, S.C., Xu, Z., and Joyce, E.F. (2019). Chromosome territory formation attenuates the translocation potential of cells. Elife *8*, 1–17.

Roth, Y.S., and Allis, D.C. (1992). Chromatin condensation:does histone H1 dephosphotylation play a role? Elsevier Sci. *0004*, 93–98.

Roulland, Y., Ouararhni, K., Naidenov, M., Ramos, L., Shuaib, M., Syed, S.H., Lone, I.N., Boopathi, R., Fontaine, E., Papai, G., et al. (2016). The Flexible Ends of CENP-A Nucleosome Are Required for Mitotic Fidelity. Mol. Cell *63*, 674–685.

Routh, A., Sandin, S., and Rhodes, D. (2008). Nucleosome repeat length and linker histone stoichiometry determine chromatin fiber structure. Proc. Natl. Acad. Sci. *105*, 8872–8877.

Rowley, M.J., Lyu, X., Rana, V., Ando-Kuri, M., Karns, R., Bosco, G., and Corces, V.G. (2019). Condensin II Counteracts Cohesin and RNA Polymerase II in the Establishment of 3D Chromatin Organization. Cell Rep. *26*, 2890-2903.e3.

Roy, M.A., Dhanaraman, T., and D'Amours, D. (2015). The Smc5-Smc6 heterodimer associates with DNA through several independent binding domains. Sci. Rep. *5*, 1–12.

Rydberg, B., Holley, W.R., Mian, I.S., and Chatterjee, A. (1998). Chromatin conformation in living cells: support for a zig-zag model of the 30 nm chromatin fiber 1 1Edited by T. Richmond. J. Mol. Biol. *284*, 71–84.

Ryu, H., Furuta, M., Kirkpatrick, D., Gygi, S.P., and Azuma, Y. (2010). PIASy-dependent SUMOylation regulates DNA topoisomerase IIα activity. J. Cell Biol. *191*, 783–784.

Saeki, H., Ohsumi, K., Aihara, H., Ito, T., Hirose, S., Ura, K., and Kaneda, Y. (2005). Linker histone variants control chromatin dynamics during early embryogenesis. Proc. Natl. Acad. Sci. U. S. A. *102*, 5697–5702.

Samejima, K., Samejima, I., Vagnarelli, P., Ogawa, H., Vargiu, G., Kelly, D.A., Alves, F. de L., Kerr, A., Green, L.C., Hudson, D.F., et al. (2012). Mitotic chromosomes are compacted laterally by KIF4 and condensin and axially by topoisomerase IIα. J. Cell Biol. *199*, 755–770.

Samejima, K., Booth, D.G., Ogawa, H., Paulson, J.R., Xie, L., Watson, C.A., Platani, M., Kanemaki, M.T., and Earnshaw, W.C. (2018). Functional analysis after rapid degradation of condensins and 3D-EM reveals chromatin volume is uncoupled from chromosome architecture in mitosis. *i*.

Sanborn, A.L., Rao, S.S.P., Huang, S.C., Durand, N.C., Huntley, M.H., Jewett, A.I., Bochkov, I.D., Chinnappan, D., Cutkosky, A., Li, J., et al. (2015). Chromatin extrusion explains key features of loop and domain formation in wild-type and engineered genomes. Proc. Natl. Acad. Sci. U. S. A. *112*, E6456–E6465.

Sanulli, S., Trnka, M.J., Dharmarajan, V., Tibble, R.W., Pascal, B.D., Burlingame, A.L., Griffin, P.R., Gross, J.D., and Narlikar, G.J. (2019). HP1 reshapes nucleosome core to promote phase separation of heterochromatin. Nature *575*, 390–394.

Sawin, K.E., and Mitchison, T.J. (1991). Mitotic spindle assembly by two different pathways in vitro. J. Cell Biol. *112*, 925–940.

Schalbetter, S.A., Goloborodko, A., Fudenberg, G., Belton, J.-M., Miles, C., Yu, M., Dekker, J., Mirny, L.A., and Baxter, J. (2017). SMC complexes differentially compact mitotic chromosomes according to genomic context. Nat. Cell Biol. *19*, 1071–1080.

Schardin, M., Cremer, T., Hager, H.D., and Lang, M. (1985). Specific staining of human chromosomes in Chinese hamster x man hybrid cell lines demonstrates interphase chromosome territories. Hum. Genet. *71*, 281–287.

Schellenberg, M.J., Schellenberg, M.J., Lieberman, J.A., Herrero-ruiz, A., Butler, L.R., Williams, J.G., Muñoz-cabello, A.M., Mueller, G.A., London, R.E., and Williams, R.S. (2017). ZATT (ZNF451)– mediated resolution of topoisomerase 2. Science (80-.). *6468*, 1–11.

Schubert, I., and Oud, J.L. (1997). There is an upper limit of chromosome size for normal development of an organism. Cell *88*, 515–520.

Schwarzer, W., Abdennur, N., Goloborodko, A., Pekowska, A., Fudenberg, G., Loe-Mie, Y., Fonseca, N.A., Huber, W., Haering, C.H., Mirny, L.A., et al. (2017). Two independent modes of chromatin organization revealed by cohesin removal. Nature *551*, 51–56.

Segel, L.A., and Slemrod, M. (1989). The Quasi-Steady-State Assumption: A Case Study in Perturbation. SIAM Rev. *31*, 446–477.

Serrano, D., Cordero, G., Kawamura, R., Sverzhinsky, A., Sarker, M., Roy, S., Malo, C., Pascal, J.M., Marko, J.F., and D'Amours, D. (2020). The Smc5/6 Core Complex Is a Structure-Specific DNA Binding and Compacting Machine. Mol. Cell *80*, 1025-1038.e5.

Sexton, T., Yaffe, E., Kenigsberg, E., Bantignies, F., Leblanc, B., Hoichman, M., Parrinello, H.,

Tanay, A., and Cavalli, G. (2012). Three-dimensional folding and functional organization principles of the Drosophila genome. Cell *148*, 458–472.

Shimada, M., Chen, W.-Y., Nakadai, T., Onikubo, T., Guermah, M., Rhodes, D., and Roeder, R.G. (2019). Gene-Specific H1 Eviction through a Transcriptional Activator→p300→NAP1→H1 Pathway. Mol. Cell 1–16.

Shintomi, K., and Hirano, T. (2009). Releasing cohesin from chromosome arms in early mitosis : opposing actions of Wapl – Pds5 and Sgo1. 2224–2236.

Shintomi, K., and Hirano, T. (2011). The relative ratio of condensin I to II determines chromosome shapes. Genes Dev. *25*, 1464–1469.

Shintomi, K., Takahashi, T.S., and Hirano, T. (2015). Reconstitution of mitotic chromatids with a minimum set of purified factors. Nat. Cell Biol. *17*, 1014–1023.

Shintomi, K., Inoue, F., Watanabe, H., Ohsumi, K., Ohsugi, M., and Hirano, T. (2017). Mitotic chromosome assembly despite nucleosome depletion in Xenopus egg extracts. Science (80-.). *356*, 1284–1287.

Shogren-Knaak, M., Ishii, H., Sun, J.-M., Pazin, M.J., Davie, J.R., and Peterson, C.L. (2006). Histone H4-K16 acetylation controls chromatin structure and protein interactions. Science *311*, 844–847.

Shukron, O., and Holcman, D. (2017). Statistics of randomly cross-linked polymer models to interpret chromatin conformation capture data. Phys. Rev. E *96*, 1–8.

Shure, M., Pulleyblank, D.E., and Vinograd, J. (1977). The problems of eukaryotic and prokaryotic DNA packaging and in vivo conformation posed by superhelix density heterogeneity. Nucleic Acids Res. *4*, 1183–1206.

Simpson, R.T. (1978). Structure of the Chromatosome, a Chromatin Particle Containing 160 Base Pairs of DNA and All the Histones. Biochemistry *17*, 5524–5531.

Sofueva, S., Yaffe, E., Chan, W.C., Georgopoulou, D., Vietri Rudan, M., Mira-Bontenbal, H., Pollard,

S.M., Schroth, G.P., Tanay, A., and Hadjur, S. (2013). Cohesin-mediated interactions organize chromosomal domain architecture. EMBO J. *32*, 3119–3129.

Song, F., Chen, P., Sun, D., Wang, M., Dong, L., Liang, D., Xu, R.-M., Zhu, P., and Li, G. (2014). Cryo-EM Study of the Chromatin Fiber Reveals a Double Helix Twisted by Tetranucleosomal Units. Science (80-.). *344*, 376–380.

Spagnol, S.T., and Dahl, K.N. (2016). Spatially resolved quantification of chromatin condensation through differential local rheology in cell nuclei fluorescence lifetime imaging. PLoS One *11*, 1–19.

St-Pierre, J., Douziech, M., Bazile, F., Pascariu, M., Bonneil, É., Sauvé, V., Ratsima, H., and D'Amours, D. (2009). Polo Kinase Regulates Mitotic Chromosome Condensation by Hyperactivation of Condensin DNA Supercoiling Activity. Mol. Cell *34*, 416–426.

Stein, A., and Künzler, P. (1983). Histone H5 can correctly align randomly arranged nucleosomes in a defined in vitro system. Nature *302*, 548–550.

Stephan, A.K., Kliszczak, M., Dodson, H., Cooley, C., and Morrison, C.G. (2011). Roles of Vertebrate Smc5 in Sister Chromatid Cohesion and Homologous Recombinational Repair. Mol. Cell. Biol. *31*, 1369–1381.

Stevens, T.J., Lando, D., Basu, S., Atkinson, L.P., Cao, Y., Lee, S.F., Leeb, M., Wohlfahrt, K.J., Boucher, W., O'Shaughnessy-Kirwan, A., et al. (2017). 3D structures of individual mammalian genomes studied by single-cell Hi-C. Nature *544*, 59–64.

Stigler, J., Çamdere, G., Koshland, D.E., and Greene, E.C. (2016). Single-Molecule Imaging Reveals a Collapsed Conformational State for DNA-Bound Cohesin. Cell Rep. *15*, 988–998.

Strom, A.R., Emelyanov, A. V., Mir, M., Fyodorov, D. V., Darzacq, X., and Karpen, G.H. (2017). Phase separation drives heterochromatin domain formation. Nature *547*, 241–245.

Sun, M., Biggs, R., Hornick, J., and Marko, J.F. (2018). Condensin controls mitotic chromosome stiffness and stability without forming a structurally contiguous scaffold. Chromosom. Res. *26*, 277–295.

Sundin, O., and Varshavsky, A. (1981). Arrest of Segregation Leads to Accumulation of Highly Intertwined Catenated Dimers : Dissection of the Final Stages of SV40 DNA Replication. Cell *25*, 659–669.

Sutani, T., Yuasa, T., Tomonaga, T., Dohmae, N., Takio, K., and Yanagida, M. (1999). Fission yeast condensin complex: Essential roles of non-SMC subunits for condensation and Cdc2 phosphorylation of Cut3/SMC4. Genes Dev. *13*, 2271–2283.

Sutani, T., Sakata, T., Nakato, R., Masuda, K., Ishibashi, M., Yamashita, D., Suzuki, Y., Hirano, T., Bando, M., and Shirahige, K. (2015). Condensin targets and reduces unwound DNA structures associated with transcription in mitotic chromosome condensation. Nat. Commun. *6*, 1–13.

Swedlow, J.R., and Hirano, T. (2003). The making of the mitotic chromosome: modern insights into classical questions. Mol. Cell *11*, 557–569.

Szabo, Q., Jost, D., Chang, J.M., Cattoni, D.I., Papadopoulos, G.L., Bonev, B., Sexton, T., Gurgo, J., Jacquier, C., Nollmann, M., et al. (2018). TADs are 3D structural units of higher-order chromosome organization in Drosophila. Sci. Adv. *4*, 1–14.

Szabo, Q., Donjon, A., Jerković, I., Papadopoulos, G.L., Cheutin, T., Bonev, B., Nora, E.P., Bruneau, B.G., Bantignies, F., and Cavalli, G. (2020). Regulation of single-cell genome organization into TADs and chromatin nanodomains. Nat. Genet. *52*, 1151–1157.

Takahashi, M., Wakai, T., and Hirota, T. (2016). Condensin I-mediated mitotic chromosome assembly requires association with chromokinesin KIF4A. Genes Dev. *30*, 1931–1936.

Takata, H., Madung, M., Katoh, K., and Fukui, K. (2018). Cdk1-dependent phosphorylation of KIF4A at S1186 triggers lateral chromosome compaction during early mitosis. PLoS One *13*, 1–15.

Takemata, N., Samson, R.Y., and Bell, S.D. (2019). Physical and Functional Compartmentalization of Archaeal Chromosomes. Cell *179*, 165-179.e18.

Takemoto, A., Maeshima, K., Ikehara, T., Yamaguchi, K., Murayama, A., Imamura, S., Imamoto, N., Yokoyama, S., Hirano, T., Watanabe, Y., et al. (2009). The chromosomal association of condensin II

is regulated by a noncatalytic function of PP2A. Nat. Struct. Mol. Biol. *16*, 1302–1308.

Tavares-Cadete, F., Norouzi, D., Dekker, B., Liu, Y., and Dekker, J. (2020). Multi-contact 3C reveals that the human genome during interphase is largely not entangled. Nat. Struct. Mol. Biol. *27*, 1105–1114.

Tedeschi, A., Wutz, G., Huet, S., Jaritz, M., Wuensche, A., Schirghuber, E., Davidson, I.F., Tang, W., Cisneros, D.A., Bhaskara, V., et al. (2013). Wapl is an essential regulator of chromatin structure and chromosome segregation. Nature *501*, 564–568.

Terakawa, T., Bisht, S., Eeftens, J.M., Dekker, C., Haering, C.H., and Greene, E.C. (2017). The condensin complex is a mechanochemical motor that translocates along DNA. Science *358*, 672–676.

Terme, J.M., Sesé, B., Millán-Ariño, L., Mayor, R., Belmonte, J.C.I., Barrero, M.J., and Jordan, A. (2011). Histone H1 variants are differentially expressed and incorporated into chromatin during differentiation and reprogramming to pluripotency. J. Biol. Chem. *286*, 35347–35357.

Teves, S.S., An, L., Hansen, A.S., Xie, L., Darzacq, X., and Tjian, R. (2016). A dynamic mode of mitotic bookmarking by transcription factors. Elife *5*, 1–24.

Th'ng, J.P.H., Sung, R., Ye, M., and Hendzel, M.J. (2005). H1 Family Histones in the Nucleus. J. Biol. Chem. *280*, 27809–27814.

Thadani, R., Kamenz, J., Heeger, S., Muñoz, S., and Uhlmann, F. (2018). Cell-Cycle Regulation of Dynamic Chromosome Association of the Condensin Complex. Cell Rep. *23*, 2308–2317.

Thakurela, S., Garding, A., Jung, J., Schübeler, D., Burger, L., and Tiwari, V.K. (2013). Gene regulation and priming by topoisomerase IIα in embryonic stem cells. Nat. Commun. *4*.

Thiriet, C., and Hayes, J.J. (2009). Linker histone phosphorylation regulates global timing of replication origin firing. J. Biol. Chem. *284*, 2823–2829.

Thoma, F., Koller, T., and Klug, A. (1979a). Involvement of histone H1 in the organization of the nucleosome and of the salt-dependent superstructures of chromatin. J. Cell Biol. *83*, 403–427.

Thoma, F., Koller, T., and Klug, A. (1979b). Involvement of histone H1 in the organization of the nucleosome and of the salt-dependent superstructures of chromatin. J. Cell Biol. *83*, 403–427.

Toselli-Mollereau, E., Robellet, X., Fauque, L., Lemaire, S., Schiklenk, C., Klein, C., Hocquet, C., Legros, P., N'Guyen, L., Mouillard, L., et al. (2016a). Nucleosome eviction in mitosis assists condensin loading and chromosome condensation. EMBO J. *35*, 1565–1581.

Toselli-Mollereau, E., Robellet, X., Fauque, L., Lemaire, S., Schiklenk, C., Klein, C., Hocquet, C., Legros, P., N'Guyen, L., Mouillard, L., et al. (2016b). Nucleosome eviction in mitosis assists condensin loading and chromosome condensation. EMBO J. *35*, 1565–1581.

Tremethick, D.J. (2007). Higher-Order Structures of Chromatin: The Elusive 30 nm Fiber. Cell *128*, 651–654.

Uemura, T., Ohkura, H., Adachi, Y., Morino, K., Shiozaki, K., and Yanagida, M. (1987). DNA topoisomerase II is required for condensation and separation of mitotic chromosomes in S. pombe. Cell *50*, 917–925.

Uhlmann, F., Wernic, D., Poupart, M.-A., Koonin, E. V, and Nasmyth, K.A. (2000). Cleavage of Cohesin by the CD Clan Protease Separin Triggers Anaphase in Yeast. Cell *103*, 375–386.

Vagnarelli, P., Hudson, D.F., Ribeiro, S.A., Trinkle-Mulcahy, L., Spence, J.M., Lai, F., Farr, C.J., Lamond, A.I., and Earnshaw, W.C. (2006). Condensin and Repo-Man–PP1 co-operate in the regulation of chromosome architecture during mitosis. Nat. Cell Biol. *8*, 1133–1142.

Vian, L., Pękowska, A., Rao, S.S.P., Kieffer-Kwon, K.R., Jung, S., Baranello, L., Huang, S.C., El Khattabi, L., Dose, M., Pruett, N., et al. (2018). The Energetics and Physiological Impact of Cohesin Extrusion. Cell *173*, 1165-1178.e20.

Waizenegger, I.C., Hauf, S., Meinke, A., and Peters, J.M. (2000). Two distinct pathways remove mammalian cohesin from chromosome arms in prophase and from centromeres in anaphase. Cell *103*, 399–410.

Walther, N., Hossain, M.J., Politi, A.Z., Koch, B., Kueblbeck, M., Ødegård-Fougner, Ø., Lampe, M.,

and Ellenberg, J. (2018). A quantitative map of human Condensins provides new insights into mitotic chromosome architecture. J. Cell Biol. *217*, 2309–2328.

Wang, X., Llopis, P.M., and Rudner, D.Z. (2013). Organization and segregation of bacterial chromosomes. Nat. Rev. Genet. *14*, 191–203.

Wang, X., Le, T.B.K., Lajoie, B.R., Dekker, J., Laub, M.T., and Rudner, D.Z. (2015). Condensin promotes the juxtaposition of dna flanking its loading site in Bacillus subtilis. Genes Dev. *29*, 1661–1675.

Wang, X., Brandão, H.B., Le, T.B.K., Laub, M.T., and Rudner, D.Z. (2017). Bacillus subtilis SMC complexes juxtapose chromosome arms as they travel from origin to terminus. Science *355*, 524–527.

Wang, X., Hughes, A.C., Brandão, H.B., Walker, B., Lierz, C., Cochran, J.C., Oakley, M.G., Kruse, A.C., and Rudner, D.Z. (2018). In Vivo Evidence for ATPase-Dependent DNA Translocation by the Bacillus subtilis SMC Condensin Complex. Mol. Cell 841–847.

Watanabe, K., Pacher, M., Dukowic, S., Schubert, V., Puchta, H., and Schubert, I. (2009). The STRUCTURAL MAINTENANCE of CHROMOSOMES 5/6 complex promotes sister chromatid alignment and homologous recombination after DNA damage in Arabidopsis thaliana. Plant Cell *21*, 2688–2699.

Weissmann, F., Petzold, G., VanderLinden, R., Huis in 't Veld, P.J., Brown, N.G., Lampert, F., Westermann, S., Stark, H., Schulman, B.A., and Peters, J.-M. (2016). biGBac enables rapid gene assembly for the expression of large multisubunit protein complexes. Proc. Natl. Acad. Sci. *113*, E2564–E2569.

Wendt, K.S., Yoshida, K., Itoh, T., Bando, M., Koch, B., Schirghuber, E., Tsutsumi, S., Nagae, G., Ishihara, K., Mishiro, T., et al. (2008). Cohesin mediates transcriptional insulation by CCCTC-binding factor. Nature *451*, 796–801.

White, A.E., Hieb, A.R., and Luger, K. (2016). A quantitative investigation of linker histone interactions with nucleosomes and chromatin. Sci. Rep. *6*, 1–14.

Wignall, S.M., Deehan, R., Maresca, T.J., and Heald, R. (2003). The condensin complex is required for proper spindle assembly and chromosome segregation in Xenopus egg extracts. J. Cell Biol. *161*, 1041–1051.

Wilkins, B.J., Rall, N. a, Ostwal, Y., Kruitwagen, T., Hiragami-Hamada, K., Winkler, M., Barral, Y., Fischle, W., and Neumann, H. (2014). A Cascade of Histone Modifications Induces Chromatin Condensation in Mitosis. Science (80-.). *343*, 77–80.

Willcockson, M.A., Healton, S.E., Weiss, C.N., Bartholdy, B.A., Botbol, Y., Mishra, L.N., Sidhwani, D.S., Wilson, T.J., Pinto, H.B., Maron, M.I., et al. (2021). H1 histones control the epigenetic landscape by local chromatin compaction. Nature *589*, 293–298.

Woodcock, C.L., Skoultchi, A.I., and Fan, Y. (2006). Role of linker histone in chromatin structure and function: H1 stoichiometry and nucleosome repeat length. Chromosom. Res. *14*, 17–25.

Wühr, M., Freeman, R.M., Presler, M., Horb, M.E., Peshkin, L., Gygi, S., and Kirschner, M.W. (2014). Deep proteomics of the Xenopus laevis egg using an mRNA-derived reference database. Curr. Biol. *24*, 1467–1475.

Wutz, G., Várnai, C., Nagasaka, K., Cisneros, D.A., Stocsits, R.R., Tang, W., Schoenfelder, S., Jessberger, G., Muhar, M., Hossain, M.J., et al. (2017). Topologically associating domains and chromatin loops depend on cohesin and are regulated by CTCF, WAPL, and PDS5 proteins. EMBO J. *36*, 3573–3599.

Yamashita, D., Shintomi, K., Ono, T., Gavvovidis, I., Schindler, D., Neitzel, H., Trimborn, M., and Hirano, T. (2011). MCPH1 regulates chromosome condensation and shaping as a composite modulator of condensin II. J. Cell Biol. *194*, 841–854.

Yatskevich, S., Rhodes, J., and Nasmyth, K.A. (2019). Organization of Chromosomal DNA by SMC Complexes. Annu. Rev. Genet. *53*.

Yu, X., Davenport, J.W., Urtishak, K.A., Carillo, M.L., Gosai, S.J., Kolaris, C.P., Byl, J.A.W., Rappaport, E.F., Osheroff, N., Gregory, B.D., et al. (2017). Genome-wide TOP2A DNA cleavage is

biased toward translocated and highly transcribed loci. Genome Res. *27*, 1238–1249.

Yuen, K.C., Slaughter, B.D., and Gerton, J.L. (2017). Condensin II is anchored by TFIIIC and H3K4me3 in the mammalian genome and supports the expression of active dense gene clusters. Sci. Adv. *3*.

Yun, Y., An, P., Ning, J., Zhao, G.M., Yang, W.L., and Lei, A.M. (2014). H1foo is essential for in vitro meiotic maturation of bovine oocytes. Zygote *23*, 416–425.

Yusufova, N., Kloetgen, A., Teater, M., Osunsade, A., Camarillo, J.M., Chin, C.R., Doane, A.S., Venters, B.J., Portillo-Ledesma, S., Conway, J., et al. (2021). Histone H1 loss drives lymphoma by disrupting 3D chromatin architecture. Nature *589*, 299–305.

Zhang, Q., Giebler, H.A., Isaacson, M.K., and Nyborg, J.K. (2015). Eviction of linker histone H1 by NAP - family histone chaperones enhances activated transcription. Epigenetics Chromatin 1–17.

Zhao, X., and Blobel, G. (2005). A SUMO ligase is part of a nuclear multiprotein complex that affects DNA repair and chromosomal organization. Proc. Natl. Acad. Sci. U. S. A. *102*, 4777–4782.

Zhou, B., Jiang, J., Feng, H., Ghirlando, R., Xiao, S., Bai, Y., Zhou, B., Jiang, J., Feng, H., Ghirlando, R., et al. (2015). Structural Mechanisms of Nucleosome Recognition by Linker Histones Article Structural Mechanisms of Nucleosome Recognition by Linker Histones. Mol. Cell *59*, 628–638.

Zhou, B., Feng, H., Ghirlando, R., Li, S., Schwieters, C.D., and Bai, Y. (2016). A Small Number of Residues Can Determine if Linker Histones Are Bound On or Off Dyad in the Chromatosome. J. Mol. Biol. *428*, 3948–3959.

Zhou, B., Feng, H., Kale, S., Fox, T., Khant, H., de Val, N., Ghirlando, R., Panchenko, A.R., and Bai, Y. (2021). Distinct Structures and Dynamics of Chromatosomes with Different Human Linker Histone Isoforms. Mol. Cell *81*, 166-182.e6.

Zhou, J., Fan, J.Y., Rangasamy, D., and Tremethick, D.J. (2007). The nucleosome surface regulates chromatin compaction and couples it with transcriptional repression. Nat. Struct. Mol. Biol. *14*, 1070–1076.

Zierhut, C., Jenness, C., Kimura, H., and Funabiki, H. (2014). Nucleosomal regulation of chromatin composition and nuclear assembly revealed by histone depletion. Nat. Struct. Mol. Biol. *21*, 617–625.